TESIS DE LA UNIVERSIDAD DE ZARAGOZA

2020

138

Iván Lizaga Villuendas

Assessing soil redistribution and sediment apportionment from different land uses: geospatial analysis and modelling in a mountain agroecosystem

Departamento
Ciencias de la Tierra

Director/es
Navas Izquierdo, Ana María

http://zaguan.unizar.es/collection/Tesis

ISSN 2254-7606

Prensas de la Universidad
Universidad Zaragoza

© Universidad de Zaragoza
Servicio de Publicaciones

ISSN 2254-7606

Universidad Zaragoza
1542

Tesis Doctoral

ASSESSING SOIL REDISTRIBUTION AND SEDIMENT APPORTATIONMENT FROM DIFFERENT LAND USES: GEOSPATIAL ANALYSIS AND MODELLING IN A MOUNTAIN AGROECOSYSTEM

Autor

Iván Lizaga Villuendas

Director/es

Navas Izquierdo, Ana María

UNIVERSIDAD DE ZARAGOZA

Ciencias de la Tierra

2020

Repositorio de la Universidad de Zaragoza – Zaguan http://zaguan.unizar.es

Assessing soil redistribution and sediment apportionment from different land uses

Geospatial analysis and modelling in a mountain agroecosystem

Iván Lizaga Villuendas

Supervisor: Ana Navas Izquierdo

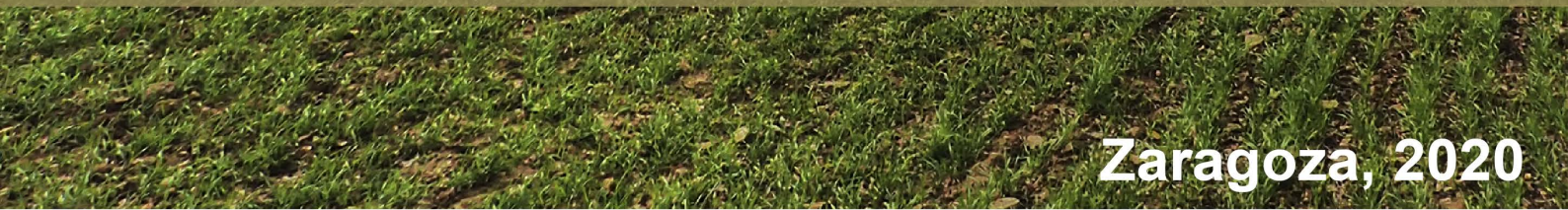

Zaragoza, 2020

Assessing soil redistribution and sediment apportionment from different land uses: geospatial analysis and modelling in a mountain agroecosystem

Thesis presented by

Ivan Lizaga Villuendas

Geologist in fulfilment of the requirements to obtain the degree

of Doctor Philosophiae from the University of Zaragoza

Supervisor: Prof. Ana Navas Izquierdo

Zaragoza, April 2020

Cover photograph: Barley cropland in a stormy day, photograph by Ivan Lizaga

Preface and acknowledgements

This dissertation was prepared for the degree of Doctor Philosophiae (PhD) at the Department of Earth Sciences in the Science Faculty of the University of Zaragoza, Spain.

The work for this doctoral project was done in the research group Erosion and Soil and Water Evaluation at the Department of Soil and Water in the Experimental Station of Aula Dei, Spanish National Research Council (EEAD-CSIC) in Zaragoza, Spain. Three research stays were carried out during the PhD period: In 2016 one month research stay at the Scripps Institution of Oceanography, University of California, San Diego under the supervision of Prof. Brice Semmens. In 2018 and 2019 two month stays, each were done at the University of Ghent in the ISOFYS lab under the supervision of Prof. Pascal Boeckx in 2018 and 2019.

This research was financially supported by the project CGL2014-52986-R and the aid of a predoctoral contract (BES-2015-071780), funded by the Spanish Ministry of Science.

First of all, I would like to express my special thanks and appreciations to my thesis supervisor Prof. Ana Navas Izquierdo, head of the Erosion and Soil and Water Evaluation Research group and of the laboratory of Radiometry at the EEAD-CSIC for giving me the opportunity to accomplish this investigation and discover the research world. I would like to thank your guidance, encouragement and advice throughout my time as a PhD student. I have been fortunate to have a supervisor who brings professional integrity, passion and enthusiasm to assist me in each step to complete this thesis and respond to my queries promptly. Thank you for your constructive comments, inspiration and support during the entire time of this thesis and providing me with the skills to enrich my understanding of science.

Many people have participated and contributed to the development of this thesis in one or another way whom I want to show my gratitude: I would like to thank to Dr Borja Latorre (EEAD-CSIC), who encouraged me to improve my programming skills and helped me with the modelling included in this research. Without his support in this area of knowledge, an important part of the thesis would not have been achieved. For his continuous support during fieldwork campaigns and qualified guidance, especially on soil science and soil mapping, I would like to thank Dr. Javier Machín Gayarre. I would also like to thank Teresa Lopez Bello who taught me everything I know about lab analysis, and without her knowledge and wisdom, I wouldn't be able to extract my data and to understand the importance of the hard and meticulous lab work. My appreciation also extends to my colleague Leticia Gaspar Ferrer for her support, advice and constructive comments, especially during the last years of my thesis.

I am grateful to the rest of the team that helped me in multiple ways: Santiago Beguería Portugués, Laura Quijano Gaudes, Leticia Palazón Tabuenca, Miquel Tomás Burguera, Roberto Serrano Notivolí, Teresa Guillamón Padilla, Ángela Manrique Alba and David Haro Monteagudo and the staff of the Department of Soil and Water for giving me all necessary assistance during my research.

I would like to express my gratitude to all the institutions that have supported this research: the Experimental Station of Aula Dei, the University of Zaragoza and the University of Ghent (Belgium), especially the ISOFYS lab for giving me the opportunity to perform the isotopic analyses and the assistance provided by Prof Pascal Boeckx and Dr Samuel Bodé. Finally, but not less important, I would like to thank my family, girlfriend and friends who have been the source of my strength throughout my life and especially during the hard last months of my PhD.

List of publications included in the thesis

The present thesis is a compendium of five research papers published in JCR scientific journals, one manuscript under review and another to be submitted (JCR journal) as well as an R package published in CRAN.

***Paper I**:*
Lizaga, I., Quijano, L., Palazón, L., Gaspar, L., Navas, A., 2017. Enhancing Connectivity Index to Assess the Effects of Land Use Changes in a Mediterranean Catchment. *Land Degradation & Development*. 663–675. https://doi.org/10.1002/ldr.2676

***Paper II**:*
Lizaga, I., Quijano, L., Gaspar, L., Navas, A., 2018. Estimating soil redistribution patterns with 137Cs measurements in a Mediterranean mountain catchment affected by land abandonment. *Land Degradation & Development* 29, 105–117. https://doi.org/10.1002/ldr.2843

***Paper III**:*
Lizaga, I., Quijano, L., Gaspar, L., Ramos, M.C., Navas, A., 2019. Linking land use changes to variation in soil properties in a Mediterranean mountain agroecosystem. *Catena* 172, 516–527. https://doi.org/10.1016/j.catena.2018.09.019

***Paper IV**:*
Lizaga, I., Gaspar, L., Blake, W., Latorre, B., Navas, A., 2019. Fingerprinting changes of source apportionments from mixed land uses in stream sediments before and after an exceptional rainstorm event. *Geomorphology* 341, 216-229. https://doi.org/10.1016/j.geomorph.2019.05.015

***Paper V**:*
Lizaga, I., Latorre, B., Gaspar, L., Navas, A., 2020. Consensus ranking as a method to identify non-conservative and dissenting tracers in fingerprinting studies. *Science of The Total Environment* 720, 137537. https://doi.org/10.1016/j.scitotenv.2020.137537

***Paper VI**:*
Lizaga, I., Gaspar, L., Latorre, B., Navas, A., 2020. Variations in transport of fine sediment and associated elements induced by rainfall and agricultural cycle in a Mediterranean agroforestry catchment. *Journal of Environmental Management* (first revision).

***Paper VII**:*
CSSI for tracking the provenance of sediments in a mediterranean agroecosystem under intense land cover changes (to be submitted)

***R Package**:*
Lizaga, I., Latorre, B., Gaspar, L., Navas, A., 2018b. fingerPro: an R Package for Sediment Source Tracing. https://cran.r-project.org/web/packages/fingerPro/index.html. https://doi.org/10.5281/zenodo.1402029

CONTENTS

CHAPTER 1

General introduction

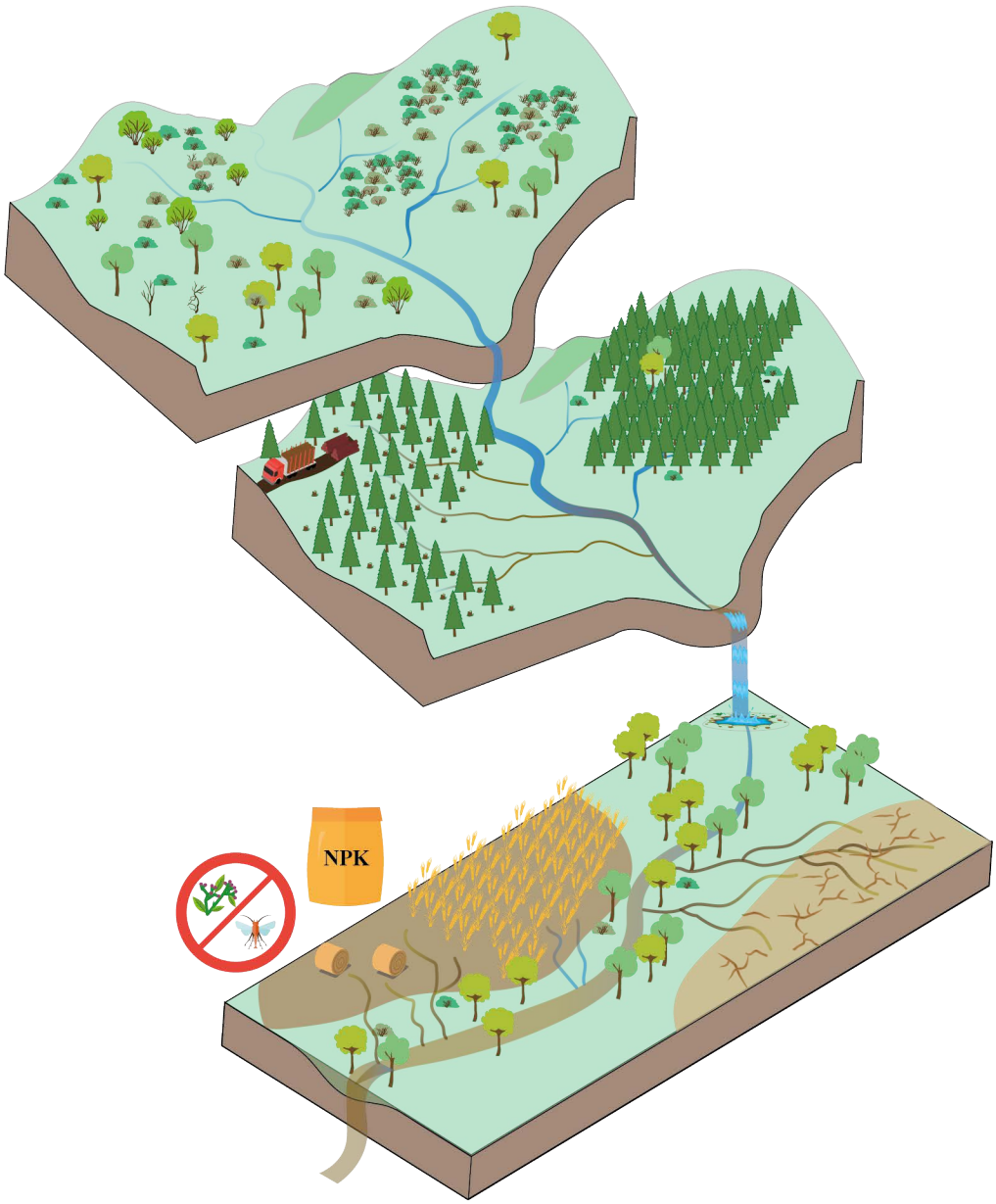

1. General introduction

A goal of present and future agriculture is to meet the food need for the growing global population. The world's population has doubled over the past five decades, from 3.7 billion people in 1970 to almost 7.8 billion in 2020 (Worldometer, 2020). Thus, the global demand for agricultural commodities has grown rapidly since the mid-20th century with a subsequent increase in crop production. To fulfil food needs, human activities have been the main drivers of ecosystem transformations through the transformation of natural landscapes into agricultural land (Chauchard et al., 2007). The conversion of rangeland into cropland is a local and global environmental issue (Foley et al., 2005), resulting in changes of soil properties including infiltration rates that eventually increase soil erosion through increased runoff (Li et al., 2007). These changes led to losses of soil nutrients and reduced long-term soil productivity that could rapidly deteriorate vast areas of land becoming a major threat to rural subsistence in many countries (Chauchard et al., 2007). Most of the past and recent research has pinpoint soil erosion as the main factor leading to soil degradation in most areas of the world. Nevertheless, despite almost a century of erosion research, the effect of this phenomenon continues to be the greatest threat to soil health, soil ecosystem services and subsequently, cropland productivity in many regions (Pennock, 2019). The impact and the effects of soil erosion on crop production have been estimated at a 0.4 per cent reduction in global crop yields.

In the past century the industrialization of Europe and the ensuing policies applied (CAP), lead the expansion of certain management systems focused on more fertile and accessible land. Since the 1960s, these changes promoted the abandonment of marginal areas, generally situated in the mountains, where traditional land uses became progressively economically nonviable (Debussche et al., 1999). In Europe, the Southern Mediterranean region underwent substantial landscape changes as the ones affecting Pre-Pyrenean mountain areas (Lasanta et al., 2016; Navas et al., 2005; Quijano et al., 2016a). This is particularly noticeable in Mediterranean mountain agroecosystems where these changes have caused considerable weakening in traditional farming methods leading to abandonment of the countryside and the decline of the traditional land use system. The first stages of land abandonment led to large surfaces of bare soil areas prone to erosion produced by unfavourable climatic conditions characterised by irregular space-time distribution of convective rainfall events (Mariani and Parisi, 2014).

High-intensity rainfall has been identified as one of the main drivers increasing soil erosion rates (Martínez-Casasnovas et al., 2002). Very intense rainstorms after dry periods are relatively frequent in the Mediterranean region (Serrano-Notivoli et al., 2017). The importance of these exceptional rainstorms is emphasized as it has been found to be responsible for major geomorphological changes including piping, gully formation, landslides and important soil loss (Grodek et al., 2012; Nadal-Romero et al., 2013). Thus, fragile soils with low nutrient contents as the ones existing in Mediterranean mountain agroecosystems, along with the absence of dense vegetation cover due to deforestation in the past century, have created large areas prone to erosion (Navas et al., 2017). Soils without plant cover are easily erodible during exceptional storm events such as the three-day long exceptional rainstorm event that occurred in 2012 in north-eastern Spain greatly affecting the central South Pyrenean agrosystems (Serrano-Muela et al., 2015).

Exceptional rainfall events accelerate soil and bedrock erosion on hillslopes, which commonly results in higher sediment mobilisation and variations in sediment sources released to water courses. The exported fine sediment produces important indirect impacts such as the rapid siltation of downstream water bodies that reached

a maximum in the Mediterranean mountains due to land abandonment in the mid-1950s (Navas et al., 2009). Furthermore, the higher frequency of droughts and extreme storm events projected under climate change will likely produce critical scenarios in these fragile environments. To this respect, Palazón et al. (2016) simulated in a large South Pyrenean catchment a scenario with a temperature increase of 2 ºC recording different responses in specific sediment yields for different types of plant covers with large increases for scrubland.

The anthropogenic pressure on mountain soil systems through farming and grazing reached a maximum during the nineteen century also affecting the south Pyrenean region. To overcome the low crop production due to the absence of machinery, fertilisers and soil conservation techniques, the cropland areas were increased. As a consequence, the natural forest was progressively cleared and replaced by croplands (Alonso-Sarría et al., 2016). In the region, the natural vegetated areas have high biodiversity and rich organic soils with high contents of soil organic carbon and total nitrogen (Navas et al., 2008; Lizaga et al., 2019a). However, due to vegetation removal, these areas experienced higher runoff and the subsequent surface soil removal that depleted soil carbon and nitrogen contents (Navas et al., 2012; Quijano et al., 2016b; Gaspar et al., 2019a).

Since land abandonment during the 1960s the natural vegetation regrowth and afforestation produced a large effect on reducing slope-channel coupling and runoff due to an increase in plant cover (Buendia et al., 2016; Cavalli et al., 2013; Heckmann et al., 2018; Lizaga et al., 2018a; Estrany et al., 2019; Llena et al., 2019). Thus, Mediterranean agricultural soils suffered significant modifications due to land use/land cover changes (Navas et al., 2008; Romanyà and Rovira, 2011). Among the most important effects of continuous conventional tillage practices and deforestation during past decades in the Mediterranean region are changes in the soil organic carbon content (Bruce et al., 1999; Martínez-Mena et al., 2002; Novara et al., 2016; Parras-Alcántara et al., 2015; Boix-Fayos et al., 2017). Recent research hypothesised that changes in agricultural management from conventional to conservation tillage practices along with increases in vegetation due to natural revegetation after abandonment of cultivated land will reduce soil erosion leading to increase SOC stocks (Lizaga et al., 2019a).

It is widely known that conventional tillage practices disturb and erode the soil surface and expose the less fertile deeper soil layers, which affects the physical, chemical and biological soil properties. The problems that these practices have created are particularly striking in mountainous areas and in regions where agricultural land is accompanied by adverse physiographic conditions, such as high elevations, steep slopes, shallow soils and dry climatic conditions with heavy rainfall events (MacDonald et al., 2000).

The need for improved knowledge on soil redistribution rates and sediment related problems have necessarily directed attention to the development of new techniques for assessing erosion and deposition rates in the landscape. In this regard, nuclear techniques deliver empirical evidences of soil redistribution rates by the use of fallout radionuclides, including ^{137}Cs, $^{210}Pb_{ex}$, and ^{7}Be (Porto et al., 2014; Taylor et al., 2019). These techniques provide an essentially unique means of assembling retrospective, spatially distributed information on soil redistribution rates within the landscape over different timescales, without the need for long-term monitoring.

In Mediterranean mountain landscapes research aimed to quantify soil redistribution rates has been successfully carried out by applying ^{137}Cs (Navas & Walling, 1992; Quine et al., 1994; Estrany et al., 2010) and later applied at catchment scales (Porto et al., 2003; Navas et al., 2005; Navas et al., 2013). However, few studies have investigated the impact of recent land use changes on soil erosion (Evrard et al., 2010; Gaspar and Navas, 2013; Gharibreza et al., 2013). As a consequence of land use changes along with intensive agricultural use, cultivated Mediterranean fields show large variability in soil redistribution rates with averages between -30 and

15 Mg ha^{-1} yr^{-1}, while in other land uses that offer protection to soil surface, such as scrubland or Mediterranean open forest, rates are more moderate, varying from -3 to 5 Mg ha^{-1} yr^{-1} (Navas et al., 2014; Lizaga et al., 2018b).

From another point of view, remote sensing enables the comparison of landscape evolution such as recent land use changes on a multitemporal scale and has potential to assess geomorphological variations, allowing the calculation of ecological indices. This technology permits monitoring large areas within a short period of time. Satellite images providing information about soil properties, crop management, human activities and modifications of the vegetation cover are of value to relate the variations in sediment export rates with the susceptibility of specific areas to be eroded (Schillaci et al., 2017; Lizaga et al., 2019a; Useya and Chen, 2019; Wang et al., 2019). The most frequently used vegetation index is the normalised difference vegetation index (NDVI) as described by Rouse et al. (1974). Furthermore, satellite imagery is a convenient tool for studying land use changes, allowing users to conduct research over large and otherwise remote areas (König et al. 2001). Furthermore, the analysis of NDVI variations allows deriving information on the degree of soil development and the evolution of the vegetation (Johansen and Tømmervik 2014). Several studies have tried to predict different soil properties and soil quality using remote sensing and soil sampling data (Ben-Dor and Banin 1995; Winowiecki et al. 2016). Most of these studies have included large continental or Mediterranean agricultural areas, but few of them have considered mountain agroecosystems.

Other important indirect impacts of land abandonment are the rapid siltation of water bodies at the first stages of land abandonment before the natural revegetation growth, which decreased reservoir storage capacities. The water storage capacity reduction of reservoirs has received increasing attention in Mediterranean regions due to the water scarcity projected scenario. Furthermore, rainfall decrease and air temperature increase can cause a reduction in crop yields of rainfed agriculture in Southern Mediterranean countries what will likely increase water demand (Saadi et al., 2015; Valverde et al., 2015). Previous investigations in sediment records accumulated during the last decades in reservoirs (Valero-Garcés et al., 1997; Navas et al., 2004) identified increases in sediment yields related to land abandonment followed by a decline since the 1980's in Pyrenean reservoirs. The subsequent afforestation carried out in the 1960s and the 1980s reduced significantly runoff and sediment connectivity due to vegetation regrowth that protects soil from erosion (Buendia et al., 2016; Lizaga et al., 2018a). However, worldwide soil erosion is an estimated 10–40 times greater than soil formation rates (Pimentel, 2006; Verheijen et al., 2009). Besides, high erosion rates and soil losses are associated with the export of agricultural pollutants (Liu et al., 2018). The relevance of the problem of sediment export is due to the associated pollutants delivery to streams such as excess of nutrients (i.e., phosphorus) degrading freshwater and marine systems worldwide (Carpenter et al., 1998; Kruk et al., 2020).

The large increase in fine grain sediment mobilised during exceptional storm events has been demonstrated to be one of the most widespread contaminants in aquatic ecosystems, compromising water quality and causing reservoir siltation (Navas et al., 2004). However, erosion processes are mostly influenced by a variety of driving forces such as slope, land management, altitude, vegetation cover, land use, soil type and changing weather patterns and extremes under current climate (Gómez et al., 2009; Renard et al., 2011; Lana-Renault et al., 2013; Lecce, 2013; Buendia et al., 2016; Nadal-Romero et al., 2019; Shang et al., 2019). For this reason, various approaches have been suggested for sediment yield monitoring (Favis-Mortlock et al., 2008; Walling and Collins, 2008; Dutta, 2016; Wynants et al., 2018) and a general consensus on the need to control soil erosion has been achieved. To this aim, it is important to evaluate what areas, soils or land uses exposed to erosion together

with agricultural practices and land management, are causing land degradation as these processes lead to the loss of soil quality.

To prevent future loss of fertile topsoil and the subsequent export of agricultural pollutants, it is crucial to understand the recent history of the sediment dynamics. However, there is still limited knowledge about the specific sources of sediments and associated pollutants and their variations in the last decades. Therefore, defining the sources of eroded fine-grained sediment is a fundamental requirement for catchment management as well as for understanding the evolution of landscapes and delineating the most sensitive areas to soil loss.

Tracking the sources of sediment and its associated contaminants is a vital step towards mitigation (Walling and Collins, 2008; Quesada et al., 2014). It is necessary to identify the areas most vulnerable to soil erosion in order to preserve soil nutrients and land as vital resources (Quijano et al., 2016c; Lloyd et al., 2019; Gaspar et al., 2019a). However, determining the sediment provenance in catchments using conventional monitoring techniques is often challenging and expensive. To evaluate this problem, several tools have been developed to quantify the effects of different erosion mechanisms, such as connectivity (Lizaga et al., 2018a; Llena et al., 2019), the spatiotemporal dynamics of erosion (Owens et al., 2011; Rovira et al., 2012; Wynants et al., 2020) and wind erosion (Schmidt et al., 2017; Zhang et al., 2018). Thus, some preliminary work carried out in the early 1980s showed fingerprinting techniques as key for addressing the sediment delivery from sources to sink (Klages and Hsieh, 1975). The procedure identifies sediment provenance and estimates the relative contribution of each potential sediment source, using a variety of selected tracer properties.

Initial fingerprinting studies were performed based on a single tracer (Walling et al., 1979). However, the inclusion of quantitative mixing models enabled to discriminate more than two sources with the subsequent increase in the number of tracers (Walling et al., 1993; Zhang and Liu, 2016). To date, sediment fingerprinting is becoming a widely used tool to tackle erosion problems, allowing identifying the sources of sediments and contaminants in catchments (Klages and Hsieh, 1975; Walling et al., 1979; Yu and Oldfield, 1989; Collins et al., 1996; Evrard et al., 2013; Schuller et al., 2013; Palazón et al., 2015a; Henry et al., 2016; Owens et al., 2016; Meusburger et al., 2018; Upadhayay et al., 2018) and, evaluating the effect of extreme flood events (Gaspar et al., 2019; Lizaga et al., 2019).

Nowadays, several studies use fingerprinting techniques to examine specific management problems in catchments (Schuller et al., 2013; Palazón et al., 2015b), and contamination in rivers and coastal waters (McCarthy et al., 2017; Evrard et al., 2019a). Research has been conducted to involve different sets of tracers such as geochemistry, magnetic properties and radiotracers as fingerprints to identify the primary source of sediments by applying unmixing models (Martínez-Carreras et al., 2010; Evrard et al., 2013; Laceby and Olley, 2015; Pulley et al., 2015; Meusburger et al., 2018; Gaspar et al., 2019a; Evrard et al., 2019). In this context, recent studies have proposed plant-specific organic molecules that exist in sediment as a new effective isotopic fingerprinting approach for land-use-specific sediment source identification (Gibbs, 2008; Gibbs, 2013). Thus, the use of compound-specific stable isotope (CSSI) techniques has emerged as a suitable alternative to previously analysed tracers (Reiffarth et al., 2016, 2019). Recent research has used CSSI signatures of soil organic biomarkers such as natural fatty acids to obtain the sediment export apportionments from various land uses (Blake et al., 2012; Alewell et al., 2016; Upadhayay et al., 2017; Mabit et al., 2018; Bravo-Linares et al., 2018; Lavrieux et al., 2019;).

The growing interest in recent years on sediment fingerprinting has led to different implementation approaches. The differences of the proposals mainly focus on three aspects: (a) different fingerprinting models (e.g. SourceTracker, IsoSource, SIFT, MixSIAR, FingerPro); (b) the use of correction factors (Koiter et al., 2018); and (c) tracer selection methodologies (Haddadchi et al., 2013; Smith and Blake, 2014; Owens et al., 2016; Collins et al., 2017).

The concern about tracer selection methodologies, including different statistical methods, has been discussed by several authors (Palazón et al., 2015b; Pulley et al., 2015). The tracer selection methods rely on the information of the sources to determine the tracer's ability to differentiate sediment sources. The most widespread methodology consisted of an initial mass conservation test, usually termed as range test (RT), followed by the two-step statistical procedure proposed by Collins and Walling (2002) that uses the Kruskal–Wallis (KW) and discriminant function analysis (DFA) tests. This procedure tests the ability of individual tracers to differentiate between sources and identifies the best combination of tracers that provides the maximum discrimination of the source classes. The main limitation of this widely used two-step statistical procedure is that it does not incorporate the information of the sediment mixtures in the analysis. Phillips and Gregg (2003) established that in a linear mixing model, the mixture sample must be within a polygon bounding the signatures of the sources as a requirement of conservativeness. More recently, following this hypothesis, Smith et al. (2013) created an R code to assess the geometry of the mixing space and to ensure that the mixture samples fit inside the sources. If a mixture sample is outside this polygon, then no physical solution exists for that mixture as one or more tracers are non-conservative. In this context, some researchers have implemented the biplot test that displays the mixture samples versus two tracers as a more restrictive condition than the traditional range test (Pulley et al., 2015).

Overall, the fingerprinting approach and the application of unmixing models and tracer selection methodologies have been proved necessary to understand source-tracer relationships and are of value in identifying sediment sources to inform best management practices. Furthermore, its implementation in conjunction with topography-based indexes and soil redistribution rates estimates would contribute to a clear understanding of soil mobilisation for further development of soil redistribution models and predict the future evolution of catchments.

Sediment connectivity indexes could represent a reasonable estimate of the temporal connectivity variation in Mediterranean agricultural catchments. Despite the potential of the index, empirical measurements are needed to confirm and compare connectivity index results. To this purpose, ^{137}Cs measurements to quantify and spatialize soil redistribution rates offer great potential to obtain ground truth data on soil mobilisation. The ^{137}Cs derived estimates could allow identifying and discriminating the main erosion and deposition areas and its effect on soil physico-chemical properties. Both techniques refer to delineate the areas where soil or sediment is mobilised, however, they do not identify the sources of sediment delivery to streams and water bodies. For this reason, the implementation of a third technique is necessary to ascertain the main sediment provenance areas and to understand the processes leading to increased sediment load.

During the last decades, changes in land use and land cover have influenced soil erosion and soil properties in Mediterranean mountain agroecosystems. Therefore there is an increasing need for reliable information in these landscapes to analyse the spatial redistribution of soil and sediments at catchment scale. The evaluation of the relations between the spatial distribution patterns of soil properties, soil redistribution processes and exported

sediment together with remote sensing information will allow a greater knowledge on the soil conservation status to tackle soil degradation and the export of sediment and pollutants to downstream water bodies. This knowledge is central to ensure the sustainability of fragile Mediterranean environments and in this context the Pre-Pyrenean agroecosystems are optimal to perform these types of studies. To this purpose, a representative catchment of the south Pyrenees has been selected to conduct this research and assess the impacts of recent land use and land cover changes. The study catchment has been subjected to centuries of rainfed agriculture, conventional tillage and posterior land abandonment followed by natural revegetation and afforestation that at present coexist with conservation agriculture. Such context of successive transformations is key to provide sound information to understand the dynamic of processes affecting Mediterranean agroforestry landscapes.

1.1 Objectives

This thesis aims to assess the impacts of land use and land covers changes (LU/LC), agricultural practices and climate factors such as extreme storm events on soil loss and export of sediment and associated elements in a mountain agroforestry catchment. As representative of Mediterranean mountain agroecosystems, the Barués catchment located in the central part of the Ebro basin was selected to assess the effects of human and environmental impacts in highly modified South Pyrenean landscapes. The area is affected by convective weather events, especially heavy rains, which are frequent during autumn with high soil erosion potential. At the start of the twentieth century, most of Barués catchment was agricultural land. In the 1960s, nearly 60% of its surface was cultivated. However, during the next decade, 75% of the agricultural land was abandoned. For this reason, the conditions of the study catchment represent a unique opportunity to track variations in soil and sediment dynamics associated with land use and land cover changes.

Information on the influence of these changes in soil properties and on the soil and associated nutrients losses is required to concentrate future efforts in the most affected areas. The erodible areas may increase export rates during extreme storm events and release pollutants to water bodies. Besides, human impacts such as clearcutting or inappropriate agricultural practices could further amplify the erosive impact by modifying the protection capacity of the plant cover with subsequent increase of sediment export. Knowledge on the effect of extreme storm events, the agricultural cycle and human activities such as harvesting, fertilising and clearcutting is necessary to understand patterns of sediment sources contribution, and the functioning of processes supplying fine sediment and associated pollutants to water bodies.

This crucial knowledge can be effectively achieved by the implementation of fingerprinting techniques with the combination of connectivity indexes, soil redistribution rates measurements and the use of remote sensing. Furthermore, developing open-source fingerprinting models and additional tools to strengthen the application of the fingerprinting technique are essential to tackle the detrimental impact of sediment supply to waters.

In an attempt to achieve these main goals, the research carried out has been structured in three major outlines:

Soil erosion and soil redistribution processes

To gain knowledge on the main drivers affecting the vegetation cover, sediment connectivity and soil redistribution rates and their effect on the spatial distribution of soil properties and nutrients, the following objectives have been established:

- to assess the variation of connectivity produced by recent LU/LC changes.
- to model how connectivity varies in pine-afforested areas using total aerial biomass data (TAB) for improving the understanding on the functioning of the hydrological network in afforested areas.
- to estimate the variation in the percentage of vegetation cover during the successional stages of the natural revegetation using the NDVI derived from remote sensed data.
- to compare the NDVI with the distribution of soil nutrients for assessing the impact of the revegetation recovery after land abandonment.
- to identify the spatial patterns of main soil properties and the differences between land uses.
- to quantify soil redistribution rates by using fallout ^{137}Cs and GIS and evaluate if the patterns of soil redistribution are influenced by the LU/LC changes in recent decades.

Software developing

Methods in fingerprinting techniques are still under discussion with tracer selection at the centre of the debate. In order to efficiently implement the fingerprinting technique, further knowledge is required on different statistical methods needed to select an optimum set of tracers to introduce in models. To this aim and for refining the current techniques, a new development has been defined:

- to further develop and improve an existing frequentist unmixing model.
- to create a complete package for facilitating the application of the sediment fingerprinting technique.
- to develop, test and verify a new methodology to identify non-conservative tracers and select those with a conservative and coherent message.

Sediment source fingerprinting

In order to establish effective control practices to prevent the release of sediments and pollutants from agriculture, the loss of fertile soil and detect the areas prone to erosion, the following objectives have been proposed:

- to evaluate how exceptional storm events can modify the properties of channel bed deposits and asses how the contributions from sediment sources might change.
- to determine which is the primary source of sediment and associated pollutants and analyse the links of sediment export with the agricultural cycle by using magnetic susceptibility, geochemistry and radiotracers at seasonal scale during two hydrological years.
- to evaluate the capability of plant-specific biomarkers such as CSSI to be used as fingerprinting tracers in areas affected by intense LU/LC changes.
- to implement δ^{13}C-FAs fingerprints to increase the discrimination of fully and partially covered year-round vegetated areas in Mediterranean agroecosystems.

1.2 Research contributions

In this thesis, a detailed assessment of the impact of land use changes, the agricultural cycle and extreme storm events on soil redistribution and mobilisation of soil particles has been fulfilled through an exhaustive field work, a variety of soil and sediment analyses and interpretation of the results supported by sound computer programing, software development and modelling.

Paper I contributes to further knowledge on the implementation of sediment connectivity and its variation with the land use changes together with the completion of the total aerial biomass (TAB) estimate to introduce forest density variability in the connectivity model.

Paper II evaluates the influences of recent LU/LC changes in ^{137}Cs derived soil redistribution rates to identify which are the LU/LC with high erosion and deposition rates as indicative of the intensity of soil mobilisation. Besides, this research explores the spatial distribution of the main erosion and deposition areas and its effect on main soil properties and on the distribution of soil organic matter.

Paper III compares changes in the main soil properties between areas that have remained unchanged vs abandoned ones, identifies different patterns of the spatial distribution of soil properties and pinpoint the land use as leading factor of such variations. The analysis of multitemporal satellite data was successful to estimate the natural live green vegetation during the successional stages of the natural revegetation after land abandonment. By combining ground truth data with remote sensing a positive correlation between soil nutrients, SOC and TN, with NDVI values is obtained, which can be extrapolated to other similar agroecosystems.

FingerPro R package comprises a methodological development and the publication of an open-source tool to quantify the provenance of sediments published in the CRAN platform. FingerPro is a low time-consuming and open-source mixing model that provides the users with tools to: i) characterise different sediment sources, establish correlations between the tracers and assist the selection of optimum tracers; ii) graph the results, using the state of the art of R packages; and iii) unmix sediment samples to estimate apportionments of sediment sources.

Paper IV exploits the opportunity offered by the occurrence of an exceptional storm event to track the changes in sediment provenance and the variation of sediment properties in streambed sediments under a 100 year return period storm event. In this research, we addressed the variations of sediment source contributions and the variation of sediment properties for three scenarios; ordinary water level, regular high discharge events and high discharge events produced by the extreme storm event.

Paper V provides a new method to extract individual tracer information that takes into account the mixture and aims to find a solution for the tracer selection in fingerprinting studies. We have devised an innovative methodology to identify non-conservative and dissenting tracers that enables to understand datasets and, likewise, the effect of each tracer. This new method represents a ground-breaking alternative that can fill the gaps of previous tracer selection methods.

Paper VI successfully assesses the variations in transport of fine sediment and associated pollutants directly produced by agricultural practices. For the first time, the combination of remote sensing data and the fingerprinting technique is applied to estimate the impact of the agricultural cycle and especially the effect of bare agricultural soils in the exported sediment and its provenance.

Paper VII implements for the first time in Mediterranean environments the use of plant-specific tracers such as CSSI for fingerprinting studies. In this research, it has been successfully tested the ability of CSSI based fingerprinting to efficiently discriminate LU/LC and identify the different sediment contributing sources in Mediterranean agroecosystems. Furthermore, the influence of informative priors is successfully assayed with information obtained from previous geochemical fingerprinting evaluation together with a geomorphological assessment pursued during field surveys.

CHAPTER 2

Material and Methods

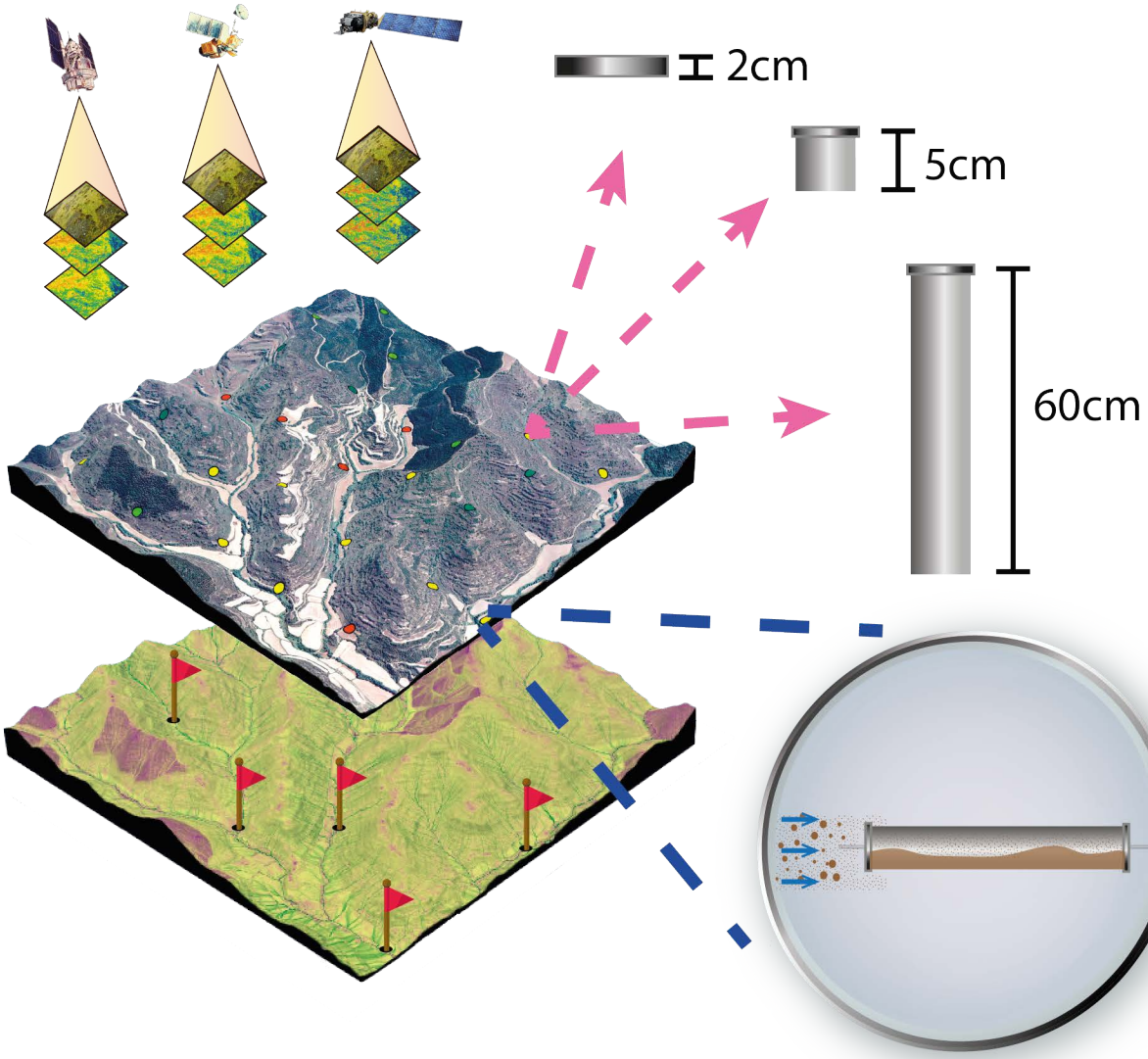

2. Materials and methods

2.1 Study area

The study catchment (23 km^2) is located in Barués in the middle part of the Ebro Basin (Fig. 1). From the geological perspective, it lies in the distal part of the Pre-Pyrenean range with characteristically south – southwest low angle strata dipping between 5° and 8°. Rock outcrops in the catchment include two conformable Oligo - Miocene lithostratigraphic units of the Uncastillo Formation, mainly composed of sandstone (Tirapu and Arenas, 1996). The lower eastern part of the catchment is dominated by the presence of a Quaternary glacis. The upper part of the Quaternary glacis is dissected by the La Reina tributary, an ephemeral stream with documented exceptional discharges under heavy rainfalls. Valley floors are infilled by eroded sediment from the slopes and are deeply incised by streams, especially in the middle part of the catchment where the stream talus deep reach its maximum. The stream channel banks composed of loess type material have steep talus without vegetation cover. The channel banks are characterised by deep straight walls due to flow incision by high water energy during heavy rainfalls. Rangelands occupy the highest altitudes, and the revegetated abandoned fields are mostly located at intermediate altitudes where most of the old cultivated fields were located. Interspersed patches of highly degraded areas, including bare soil (subsoil), are dispersed all over the catchment, although they are more abundant in the middle part on south-facing slopes.

The climate is characterised by cold winters and hot and dry summers. The mean annual rainfall is about 500 mm and rainfall periods concentrate in spring and autumn while the droughts take place between these two humid periods. The area is affected by very intense though localised storms and is drained by an ephemeral stream tributary of the Arba River. The maximum and minimum annual temperatures are 30°C and -6°C, respectively. The main soil types, classified (IUSS Working Group WRB, 2015) and mapped in 2016 by Machín (EEAD-CSIC, personal communication) are Calcisols and Cambisols.

At the start of the twentieth century, most of the catchment was agricultural land. In the 1960s, nearly 60% of the catchment was croplands. However, during the next 10 yr, 75% of the agricultural land was abandoned. Currently, ~16% of the catchment is still cultivated while open forest and pine occupy the remaining 83.5 % (Lizaga et al., 2017). Since the mid-1950s a decrease in agricultural land and a transition to naturally revegetated cover and pine afforestation has been documented (Fig. 1). There has also been a decrease in the number of individual cultivated fields, along with an increase in their size, in an attempt by farmers to increase the efficiency of production and cost recovery. The main land use/land covers are agricultural, open forest, scrubland and pine afforestation, occupying 16%, 50% and 19% of the catchment area, respectively. In addition, most of the agricultural land is located on the Quaternary glacis and on the fluvial terraces with gentle slopes occupying the valley floors. The main crops are winter cereals (*Triticum aestivum* L. and *Hordeum vulgare* L.). The pine forest mainly composed of *Pinus halepensis* Mill. has a mean tree cover density of 70%. The natural forest (*Quercux ilex* L., *Quercus coccifera L.*, and *Juniperus communis* L.) and the scrubland (*Rosmarinus officinalis* L., *Thymus vulgaris L.*, *Santolina chamaecyparissus L.*, *Genista scorpium* (L.) DC., *Macrochloa tenacissima* (L.) Kunth / *Stipa tenacissima* L., and *Lygeum spartum* (L.) Kunth are typically Mediterranean and in many areas are intermixed. The scrubland is the early phase of the successional stages of natural revegetation, in the transition to Mediterranean forest.

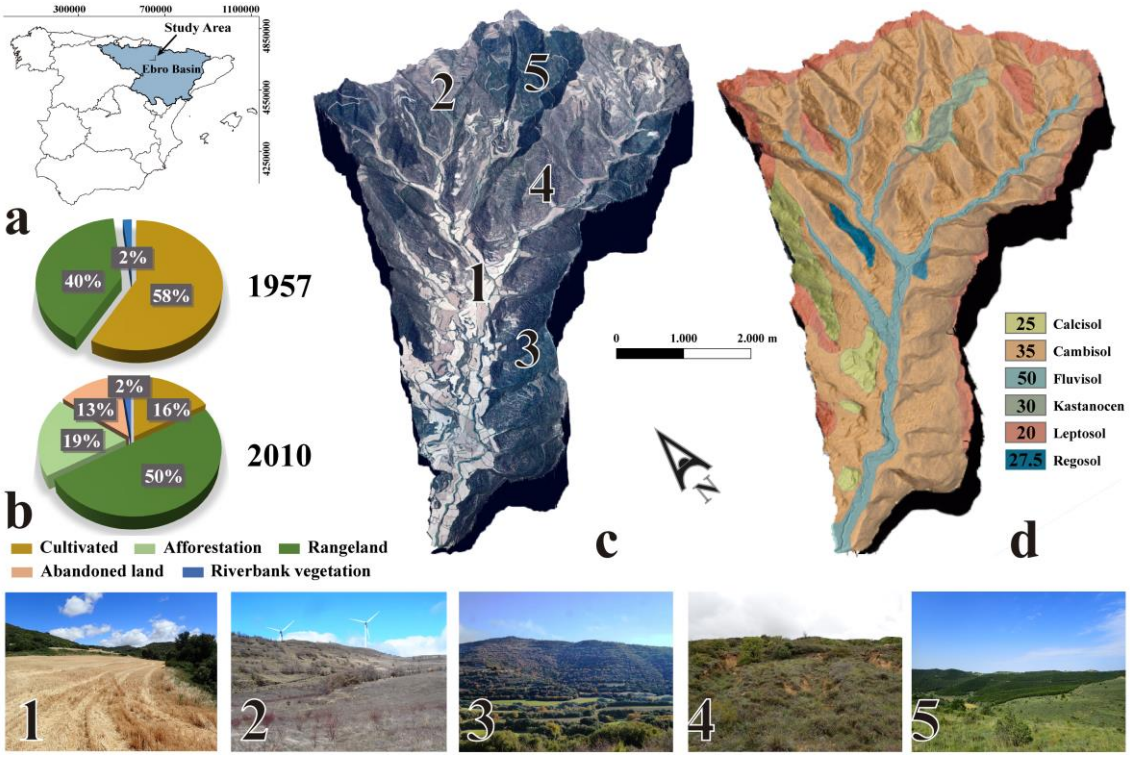

Fig. 1. a) Location of the Barués catchment in the central part of the Ebro Basin (NE Spain). b) Percentage of the different land uses in 1957 and 2010. c) 3D image of Barués catchment created with a DEM and an orthophoto (National Plan of Aerial Orthophotography, IGN). The numbers represent the main land uses shown in the photographs. d) 3D Map of soil types in the catchment (IUSS Working Group WRB, 2015). The number in the legend represents the average depth of each soil type.

2.2 Multi-temporal analysis of sediment connectivity

The assessment of the sediment connectivity was carried out by applying a topography-based index in two different scenarios using two land use maps for 1957 and 2010. The first map was created by orthorectification of the 1957 American army aerial photographs using a supervised classification in ERDAS after photographic enhancement. The actual map was digitised over 2010 PNOA (National Plan of Aerial Orthophotography) orthophotography and fieldwork maps. Nowadays, the most popular connectivity index from Borselli et al. (2008), the modified version by Cavalli et al. (2013) as well as geomorphological studies related to slopes or erosion (Kawabata & Bandibas, 2009; Gutiérrez & Lizaga, 2016; Masselink et al., 2016) are based on DEMs. Because accuracy of model results is fully dependent on DEM quality and resolution it is needed to apply and develop a correct topography-based index such as IC. Therefore, developing a model based on LIDAR data was necessary to refine the existing LIDAR points to create a high-resolution DEM (1 x 1 m). Accordingly, we used IGN (Spanish National Geographic Institute) raw LIDAR data points following Montealegre et al. (2013) methodology. First, we removed the noise of the data, deleting LIDAR points classified as noise using ArcGIS. Secondly, we proceeded to filter our LIDAR data in order to generate a bare ground 1 x 1 m raster DEM using MCC-LIDAR, a command-line tool for processing discrete-return LIDAR points in forested environments based on the Multiscale Curvature Classification algorithm developed by Evans & Hudak (2007). The root mean square error (RMSE) was calculated for both DEMs using a cross-validation method.

LIDAR data represent a tool that supports the calculation of forest inventories and allows the vegetation to be measured in three dimensions (Ruiz, 2012; Reyes & Delia, 2014). Total aerial biomass (TAB) was calculated for the afforestation forests using Equation (1) developed by Domingo et al., (2016) and the software FUSION. This equation was created and optimised in a nearby afforested area with *Pinus halepensis* Mill that had similar forest dendrometry characteristics as the pine afforestation in the study catchment. Equation (1) is a good complement to understand the change produced by the pine afforestation.

$$TAB\left(\frac{\text{kg}}{\text{ha}}\right) = e^{(0{,}0158*A2m)} * e^{(0{,}0713*P40)} \quad (1)$$

where *e* refers to the Euler's number, *A2m* is the percentage of the first LIDAR laser return above 2 m ground height, produced by the reflectance of the treetop canopy, and *P40* is the 40th percentile of LIDAR data. A 25 m x 25 m/pixel size was selected to create a raster image comparable to the study plots accomplished by Domingo et al. (2016) to obtain such an equation.

To analyse the variation of connectivity between the two stages, the sediment connectivity was estimated using a geomorphometric approach to simulate how connectivity changes due to different land covers. Hence, it is very important to determine how the system connectivity responds to human-induced cover changes (Harvey, 2002). For this reason, we applied the connectivity index (1) proposed by Borselli et al. (2008) using the C-factor from RUSLE (Revised Universal Soil Loss Equation) as a weight factor (W) in the index.

$$IC = log_{10}\frac{D_{up}}{D_{dn}} \quad (2)$$

where D_{up} and D_{dn} are the upslope and downslope components, defined by:

$$D_{up} = \overline{WS}\sqrt{A} \quad (3)$$

where W is the average weighting factor of the upslope contributing area, S is the average slope gradient of the upslope contributing area (m/m) and A is the upslope contributing area (m^2).

$$D_{dn} = \sum_i \frac{d_i}{W_i S_i} \quad (4)$$

where d_i is the length of the flow path along each i cell according to the steepest downslope direction (m), and W_i and S_i are the weighting factor and the slope gradient of the i cell, respectively.

Borselli et al. (2008) proposed $S = \sin\alpha + 0.005$ including 0.005 as the minimum slope value to avoid infinite values in Equation (4). Thus, we preserved the original values of our 1 x 1 m DEM to obtain more realistic results after checking the absence of 0 slope values. Besides calculating the contributing area, we used the procedure of multiple flow D-infinity approach (Tarboton, 1997) instead of the single flow direction algorithm (O'Callaghan & Mark, 1984) used in the hydrology ArcGIS toolbox as proposed in Cavalli et al. (2013). Using D-Infinity allows calculating the flow accumulation of converging and diverging flow directions to create a more realistic topographic index.

In addition, the connectivity index was improved by using a terrain roughness index as a weight factor. Cavalli and Marchi (2008) and Cavalli et al. (2013) developed and later implemented a roughness index (RI) in the connectivity index. RI was calculated as the standard deviation of the residual topography using the mean of the 25 neighbourhood cells values as a 5 x 5 moving window. However, for our index, we created a new roughness index (SdRI; Equation 5) calculated as the standard deviation of the slope as recommended by

Grohmann et al. (2011). SdRI was also applied using a 3 x 3 moving window to accentuate steep slope terrace characteristics of the low strata bedding preserved and modified by agricultural practices in our study catchment.

$$\sigma = \sqrt{\frac{\sum_{i=1}^{9}(x_i - x_m)^2}{9}} \quad (5)$$

Where x_i is the pixel value and x_m is the average of the 3 x 3 moving window.

Furthermore, in Equations (2) and (3), we also used our two land use maps (C-factor) as weighting factor to show the differences between both land uses (1957 and 2010) and how the connectivity index changed over time. The C-factor values assigned to our land uses are 0.0011, 0.0010, 0.06, 0.2 and 0.26 for pine afforestation, Mediterranean forest, abandoned land, cultivated land and trails respectively extracted from Panagos et al. (2015). Combining both approximations, a weighting factor was applied as the link between the C-Factor and SdRI index, trying to develop a better adjustment to reality. The model was tested in the entire catchment to facilitate visualisation at a more detailed scale in an area where the four land uses occur. We selected the same area as the red square of Fig. 1 to show how connectivity changed over 50 years due to land use and cover variations.

To introduce the probable variations of forest density in our model, the TAB layer created in the previous section was implemented inside the C-factor layer using it as the inverse of TAB to produce lower C-Factor in the areas with higher densities, and higher C-Factor in the areas with lower densities. Even with a 1 m resolution DEM, it was impossible to implement the same methodology for the other land covers: it was only used on afforested areas by creating a mask layer.

$$W = (C * \frac{1}{TAB}) * SdRI \quad (6)$$

where *W* is the weighting factor, C is the C-factor of the different land covers, TAB is the variance of the total aerial biomass (only used over pine afforestation) and SdRI is the roughness index. The data are normalised by scaling them between 0 and 1. The normalisation is needed because the weight factor is a dimensionless factor and should range from 0 to 1 to be weighted equally to slope in the index. For this reason, the W factor was normalised using unity-based normalisation Equation (7):

$$z_i = \frac{x_i - \min(x_i)}{\max(x_i) - \min(x_i)} \quad (7)$$

Where x_i is the pixel value and min/max x_i are the minimum and maximum values, respectively, of the moving window.

2.3 Remote sensing and GIS

Satellite imagery data were analysed with digital image processing methods and spatial analysis techniques to detect spatial and temporal changes in vegetation and land use. A multitemporal Landsat satellite dataset formed the basis for the change detection procedure. A series of twenty four Landsat images were acquired by the different multispectral sensors on board Landsat satellites. Image series were selected with different temporal resolutions to analyse the forest and scrubland variability or to assess the bare soil agriculture surface during the agricultural cycle. The digital image processing procedure, which included pre-processing of satellite multispectral images to ensure temporal comparability between scenes, was carried out by the Earth Resources Observation and Science Center (EROS) (USGS) for the Landsat 8-OLI and Landsat 5-TM sensors. Furthermore, following the methodology proposed by Fan and Liu (2016), a total of 220 vegetation spectra were downloaded from the USGS spectral library (Kokaly et al., 2017). Comparing these spectra, a linear

interpolation was pursued to determine reflectance values at given wavelengths for both Landsat 5 TM and Landsat 8 OLI and quantify the spectral band adjustment factor (Fan and Liu, 2017). In addition, the Landsat 8 values were corrected to ensure temporal comparability between images from different sensors. To calculate the bare soil areas an unsupervised classification was pursued together with the visual mapping. NDVI layers were created for the selected Landsat images. These transformations can provide information about the current state of the vegetation represented in a pixel and can be used to determine if the study area changes from one date to another and to follow its evolution.

The NDVI (Rousse et al. 1974) is formulated as:

$$NDVI = \frac{(\rho NIR - \rho RED)}{(\rho NIR + \rho RED)} \quad (8)$$

Where ρNIR is the reflectance of the near infrared spectral band and ρRED is the reflectance of the red spectral band. The NDVI images for each date were then compared with the previous temporal image to assess the evolution of the NDVI for each time interval. The NDVI values for these areas were extracted and the percentage variation in the vegetation index was calculated to evaluate the evolution of the vegetation recovery.

2.4 Soil and sediment sampling

The sample collection comprises three different samplings protocols: i) bulk soil samples collected with a motorised percussion corer to characterise the soils, and calculate the soil redistribution rates and its effect on the main soil properties; ii) For the appropriate characterisation of the sediment eroded by exceptional rainfall events, 5cm depth source sediment samples were collected on the basis that these events can produce deep rilling and remove up to 5cm of surface soil. Besides, two different sediment mixtures types have been sampled to address the effect of extreme storm events: 1) a set of channel bed sediment mixtures collected in the channel bed along the main streams from the headwaters to the outlet before and after the 2012 extreme storm event; 2) floodplain sediment mixtures. These different sampling methods were aimed to provide a close replication of sediments deposited before and after the exceptional discharge event and the sediment deposited in floodplains that corresponds to regular high discharge events. iii) For time-integrated studies, 2cm depth source samples are assumed to represent the material mobilized by regular erosion processes and delivered to stream channels. To capture the spatiotemporal variation in sediment mixtures, suspended sediment mixtures (SSM) were collected every three months from three sampling stations located along the catchment streams to analyse the seasonal variability in the exported sediment and assess the effects of contemporary land use/ land cover changes and agricultural practices.

2.5 Soil and sediment sample analysis

2.5.1 Soil properties and soil redistribution rates estimates

All the samples were air-dried, grinded, homogenised and sieved to <2mm. The bulk samples were analysed to obtain: Particle size, soil organic matter (SOM), soil organic carbon (SOC), TN, pH, $CaCO_3$, electrical conductivity (EC), wilting point, field capacity, magnetic properties (low-frequency magnetic susceptibility (LF) and frequency dependence (FD)) and ^{137}Cs specific massic activity.

The following methodologies were applied as follows:

To analyse the soil redistribution rates, the fraction > 2 mm was weighed to account for the stone content. Particle size, soil organic matter (SOM) and ^{137}Cs were analysed in the ≤ 2 mm fraction for 98 bulk soil samples. A Beckman Coulter LS 13320 laser diffraction particle size analyser was used for grain size analysis. Prior to particle size measurements, the organic fraction was removed by H_2O_2 (10%) heated to 80 ^{o}C. Samples were then chemically dispersed with 2 mL of sodium hexametaphosphate (40%), stirred for 2 h and sonicated for a few minutes to facilitate dispersion.

The methodology for ^{137}Cs analysis is widely described in the literature (Walling & Quine, 1991, Navas et al., 2005). The massic activity of ^{137}Cs was measured at the gamma lab of the EEAD-CSIC using a high resolution, low energy background, coaxial high-purity germanium (HPGe) gamma-ray detector coupled to an amplifier and multichannel analyser. The detector had an efficiency of 50% and a 1.9 keV resolution at 1.33 MeV (60Co) (shielded to reduce background) and was calibrated using standard soil samples placed in containers of the same geometry as the measured samples. Gamma emission of ^{137}Cs was measured at the 661.6 keV photopeak and counted for 86400s. The analytical precision of the measurements was approximately ± 3-5% at the 95% level of confidence, with a detection limit of 0.3 Bq kg^{-1}. The content of ^{137}Cs was expressed as a concentration or massic activity (Bq kg^{-1}) and as activity per unit area or inventory (Bq m^{-2}). The inventory was calculated using the mass of the fine fraction and the cross section of the core sampler. The values of the ^{137}Cs inventory associated with the 98 individual sampling points were converted into estimates of soil redistribution rates (Mg ha^{-1} yr^{-1}) by using Soto & Navas (2004) and Soto & Navas (2008) conversion models for uncultivated and cultivated soils, respectively. The models compare the measured inventory with the local reference inventory and determine the erosion or deposition rate required to account for the depletion or increase of the measured inventory, relative to the reference inventory.

In addition to the previously described analyses, the soil salinity was measured in a conductivity cell (Orion 013605MD) and expressed as the electrical conductivity of a 1:5 soil:water extract (EC 1:5) at 25 ^{o}C in dS m^{-1}. Soil pH was measured in a 1:2.5 soil:water extract with a pH electrode (Orion 9157BNMD). Total carbonate content (%) was analysed using a calcimeter (CSIC, 1976). SOC and TN were analysed by the dry combustion method using a LECO RC-612 multiphase carbon analyser and a LECO CN TruSpec carbon and nitrogen analyser, respectively. SOM was estimated by multiplying SOC content by the Van Bemmelen conversion factor (1.724), assuming that organic matter contains 58 % organic carbon. Mass specific magnetic susceptibility was measured in 10 ml topsoil and bulk soil samples at both low (0.47 kHz; χlf) and high (4.7 kHz; χhf) frequencies, using a Bartington Instruments dual-frequency MS2B sensor that operates with an alternating current and produces an alternating magnetic field at 80 A m^{-1} (Bartington Instruments Ltd. 2000). Mass specific magnetic susceptibility measurements at low and high frequency were expressed in units of 10^{-8} m^3 kg^{-1}. The results are the mean values of three measurements for each sample. Both allow determining absolute mass specific dual frequency-dependent susceptibility (χfd), defined as the difference between the measure at low and high frequencies (χfd = χlf – χhf). Alternatively, this parameter is commonly expressed as a percentage, that is the percentage frequency-dependent susceptibility (χfd%) using the following equation:

$$\chi fd\% = [(\chi lf - \chi hf)/\chi lf) \times 100] \quad (9)$$

2.5.2 Sediment source fingerprinting

Sediment source and mixture samples used for fingerprinting were sieved to <0.063mm to isolate a comparable grain size fraction between source and sediment materials and related to the predominant silt texture of soils in the catchment. The implementation of the technique requires *n* tracers to determine the contributions of *n* + 1 sources to the mixture. Due to the inherent complexity of the catchment characteristics, with large variations in climate, Geology, land use, vegetation, soil, and management practices, commonly, no unique tracer can discriminate between multiple sediment sources. Furthermore, from the analysed tracers, only those with conservative behaviour can be used for implementing the technique. Thus, additional analyses were implemented to obtain the necessary number of tracers to fulfil the basics of the technique. The analyses implemented for fingerprinting studies comprise: i) Magnetic properties; ii) stable elements; iii) radionuclides and iv) δ^{13}C-FAs.

Two different methodologies were used for the analysis of stable elements: X- Ray Fluorescence performed at the Consolidated Radio-isotope Facility (CORIF, University of Plymouth) using a Thermo Fisher Scientific Niton XL3T 950 He GOLDD+ XRF analyser, equipped with different excitation filters (main, low and high range) that optimize the analyser's sensitivity for various elements. Helium was used to allow measurement of light elements. All sources and mixtures (n=19) were packed into XRF sample cups with a 38.2-mm exposure diameter in which the laser pulse (3-mm diameter) strikes the surface of the sample. During analysis, sample cups were moved ten times to change the position of the laser, thereby obtaining ten different measures per sample to produce a dataset of 190 measurements. To assess the accuracy of the analysis and the XRF analyser drift three repetitions were obtained for each measurement, recording a very low drift of <1%. A total of 18 elements returned measurements above the limit of detection: Ba, Nb, Zr, Sr, Rb, Pb, Zn, Fe, Mn, Cr, Ti, Ca, K, Al, P, Si, Mg and V.

On the other hand, the total elemental composition was analysed by ICP-OES after total acid digestion pursued in two cycles with HF (48 %), HNO_3 and H_2O_2 and a second cycle with HNO_3, HCL, and Milli-Q water in a microwave oven (Navas and Machín, 2002). In this second procedure the following 28 elements were analysed: Al, As, Be, Bi, B, Ca, Cd, Co, Cr, Cu, Fe, K, Li, Mg, Mn, Na, Ni, Pb, P, Rb, Sb, Se, S, Sr, Ti, Tl, V, Zn. The resulting concentration was expressed in milligrams per kilogram (mg kg^{-1}).

Gamma emissions of ^{137}Cs, ^{210}Pb, ^{226}Ra, ^{238}U, ^{232}Th and ^{40}K were analysed at the gamma lab of the Experimental station of Aula-Dei (EEAD-CSIC, Spain) described in the "Soil properties and soil redistribution estimates" section. The radionuclide activities are expressed as massic activity in Bq kg^{-1} dry soil and counted for 43,200 s and 86000 s for the 5cm depth source and channel bed and flood plain mixture samples and for the 2cm depth source and suspended sediment mixture samples, respectively. Considering the appropriate corrections for laboratory background, ^{137}Cs activity was determined from the 661.6-keV photopeak; ^{210}Pb was measured at 46.5 keV. ^{226}Ra was determined from the 351.9-keV line of ^{214}Pb, a short-lived daughter of ^{226}Ra, after equilibrium was reached. ^{238}U was determined from the 63-keV line of ^{234}Th; ^{232}Th was estimated using the 911-keV photopeak of ^{228}Ac, and ^{40}K was determined from the 1461-keV photopeak.

Compound specific stable isotopes (CSSI) analyses were carried out at the Isotope Bioscience Laboratory (ISOFYS, University of Ghent). Lipids were extracted from the soil (source) and sediment (sink mixture) samples using accelerated solvent extraction (Dionex ASE 350, Thermo Scientific, Bremen Germany) with dichloromethane (DCM): MeOH (9:1 v/v) at 100ºC and 13 MPa for three cycles of 5 min (30 mL cells, 60%

flush volume). For this c.a. 3 g of dried (x °C, y h) and 0.063 mm sieved sample was weighed in 22 mL stainless steel cells to which a recovery standard was added (12.5 ng C17:0FA, dissolved in 50 µL ethyl acetate). The lipid extract was dried using rotary evaporation (CentriVap, Labconco, Kansas City, USA) at 60ºC and 20 mbar. Lipid fraction was re-dissolved in DCM/Isopropanol (2:1 v/v) before being separated in neutral and acid fraction using aminopropyl solid-phase extraction columns (Bond Elute, 500mg, 6mL, Agilent Technologies) according to Blake et al. (2012). Neutral fraction was removed with DCM/Isopropanol after which the acid fraction was eluted using 2 % acetic acid in diethyl ether (Russell and Werne, 2007). After taking the acid fraction to dryness by rotary evaporation, the Fatty acids were methylated using Methanolic BF_3 (14%, 20min at 60°C).

The obtained fatty acid methyl esters (FAME) were quantified, after addition of an internal standard (C19:0 FAME), using capillary gas chromatography (GC Trace Ultra, Thermo scientific) with flame ionisation detection (FID) equipped with a 5% Phenyl Polysilphenylene-siloxane column (BPX5, 30 m x 0.25 mm x 0.25 µm, Trajan). After adapting the solvent volume for optimal concentration for compound-specific stable isotope (CSSI) analysis, the ^{13}C abundance of the individual FAME was determined using GC-isotope ratio mass spectroscopy (GC-IRMS). The GC-IRMS system used consisted out of a Trace 1310 GC equipped with the same GC column as for GC-FID connected to an ISOLINK II through a CongFlo IV to a Delta-V advantage IRMS detector (All Thermo scientific). Normalisation of the ^{13}C signal on the Vienna Pee Dee belemnite (VPDB) scale was performed by injecting a mixture of C14:0, C16:0, C18:0 C20:0 and C30 FAME, and C14:0, C16:0, C18:0 C20:0 Fatty acid ethyl ester provided by Arndt Schimmelmann (Indiana University), calibrated using NBS 19, and L-SVEC defined as exactly +1.95 and -46.6 ‰, on the VPDB scale, respectively, every five samples. Additionally, mixtures of Fatty acids (C16, C17, C19 and C20) were methylated together with the samples to correct for the contribution of the methyl group of the FAME in order to obtain the $\delta^{13}C$ of the FA.

Following the methodology described in the previous section, particle size analyses were implemented for the fingerprinting studies to assess the grain size differences between sediment source and sediment mixture samples. Besides, to analyse the impact of extreme storm events in particle size and SOC exports, particle size analyses and SOC fractions (active carbon fraction (ACF) and stable carbon fraction (SCF)) were analysed. The decomposition of the most thermally labile components of SOC, the active carbon fraction (ACF) is released at approximately 300–350 ºC whereas decomposition of more refractory and stable carbon (SCF) occurs at higher temperatures (420–550 ºC) (López-Capel et al., 2008). The characterisation of active carbon and stable carbon fractions was carried out using LECO, RC-612 multiphase carbon analyser (Quijano et al., 2014a). The temperature of the furnace was stepped at 350 ºC and 550 ºC to oxidize the ACF and SCF, respectively.

2.6 Fingerprinting technique, models and tracer selection techniques

2.6.1 FingerPro model: A step by step fingerprinting procedure

We developed a new tool to quantify the provenance of sediments in agroforestry catchments. For the first time, the procedure for selection of the best combination of sediment tracers was included in the tool package together with an unmixing model algorithm in order to estimate the contribution of each possible source. Application of the functions in the package allows to: i) characterise the different tracer properties and select the relevant variables; ii) unmix the sediment samples and quantify the different source apportionment; iii) assess the effect of the source variability; and iv) visualise and export the results. One of the advantages of the FingerPro package is that it allows analysing and comparing different tracer properties, using the state of the art of R

packages. Thus, different graphs through the use of different functions are included in the package: a) box and whisker plots; b) correlation matrix; c) Principal Component Analysis (PCA) and d) Linear Discriminant Analysis (LDA).

The tracer selection methods implemented in the package are: i) Range test; ii) Kruskal-Wallis H test and iii) Discriminant Function Analysis.

The relative contribution of each potential sediment source is determined using a standard linear multivariate mixing model:

$$\sum_{j=1}^{m} a_{i,j} \cdot \omega_j = b_i \tag{10}$$

which satisfies:

$$\sum_{j=1}^{m} \omega_j = 1 \tag{11}$$

$$0 \leq \omega_j \leq 1$$

where b_i is the tracer property i (i =1 to n) of the sediment mixture, $a_{i,j}$ represents the tracer property i in the source type j (j =1 to m), ω_j is the unknown relative contribution of the source type j, m represents the number of potential sediment sources and n is the number of tracer properties selected.

This system of equations is mathematically determined if the number of tracers is greater than or equal to the number of potential sources minus one ($n \geq m - 1$). The procedure tries to find the source proportions that conserve the mass balance for all tracers. All possible combinations of each source contribution (0-100%) are examined in small increments, using Latin hypercube sampling (LHS) (McKay et al., 1979). The quality of each candidate is measured using the following function or goodness of fit (GOF), based on the sum of squares of the relative error:

$$GOF = 1 - \frac{1}{n} \times \left(\sum_{i=1}^{n} \frac{\left| b_i - \sum_{j=1}^{m} \omega_j a_{i,j} \right|}{\Delta_i} \right) \tag{12}$$

where Δ_i is the range of the tracer property i, used as a normalisation factor. The combinations that reproduce the observed sediment mixture with the maximum GOF is selected as the solution.

Variability analysis is assessed following classical frequentist inference by means of a Monte-Carlo method (Helton, 1994). A succession of deterministic calculations is executed, each with different input values sampled from their respective distributions, to obtain probability distributions of the targeted outcomes.

The heterogeneity of each source is considered as a t-distribution for each property. The fingerprinting analysis of each sediment mixture is repeated by randomly sampling the source probability distributions. For the first iteration, the central value of the source distributions is used as a reference result. The corresponding output values are gathered to infer the probability distribution of the potential source contributions. Several samples must be collected for characterising each source in order to compute the mean and standard deviation of the analysed tracer properties.

2.6.2 Consensus Ranking method

In order to investigate and select the best tracers for each fingerprinting study, a novel ensemble technique is developed. The novel routine, termed as consensus method combines the predictions of single-tracer models to identify non-conservative and dissenting tracers. Based on these results, a conservativeness index (CI) is presented along with a clustering method to identify groups of tracers with similar information and to analyse their correlations. Besides, a scoring function based on several random debates between tracers, in which the tracer that prevents consensus is discarded, is implemented as a decision support ranking (CR).

Thus, to quantify the predictions of each individual tracer, we propose to use the determined mass balance equations and fabricate the remaining required tracers using two different procedures. The first procedure consists in designing random virtual tracers (RVT). In the second one, the required tracers are randomly chosen (RCT) from the remaining ones. The set of solutions obtained in this case is a subset of that obtained with RVT, resulting in all the possible predictions of each tracer in the context defined by the experimental dataset. The propagation of errors in this framework is assessed using a simple Monte Carlo iterative technique (Sherriff et al., 2015) to quantify the effect of the dispersion of the sources and the mixture on the predictions of each individual tracer. The results from the single-tracer model can be used to define a conservativeness index (CI). The set of possible predictions from each tracer is sorted according to the Euclidian distance to the perfectly balanced mix where all contributions are equal:

$$d_i = \sqrt{\sum_{j=1}^{3}\left(w_{i,j} - \frac{1}{3}\right)^2} \qquad (13)$$

A percentile of the sorted solutions is chosen to compute the CI as the root mean square error (RMSE) of the non-conservative part (nc) of the apportionments from the selected solution:

$$CI = -\sqrt{\sum_{j=1}^{3}\left(nc\left(w_{i,j}\right)\right)^2}, \qquad nc(x) = \begin{cases} -x, & \text{if } x < 0 \\ 0, & \text{if } 0 \le x \le 1 \\ x - 1, & \text{if } x > 1 \end{cases} \qquad (14)$$

Consensus ranking (CR) is implemented combining the predictions of single-tracer models in several random debates. In each debate, a random subset of the tracers is selected. Its number corresponds to the minimum number of equations to overdetermine the system plus one. For example, with three potential sources four random tracers are needed. In each debate, several rounds are held excluding one tracer at a time. The consensus of each round is measured through the mathematical compatibility of the resulting system of equations. The tracer whose exclusion produces a higher consensus is marked as dissenting. Repeating this process through several debates, each tracer obtains a number of participations and a number of lost debates. The consensus is simply defined as the ratio of these two numbers with possible outcomes between 0 and 100. A low consensus indicates that a tracer is often in conflict with the opinion of other groups, while a high consensus represents a frequent agreement with the group.

CHAPTER 3

Enhancing connectivity index to assess the effects of land use changes in a Mediterranean catchment

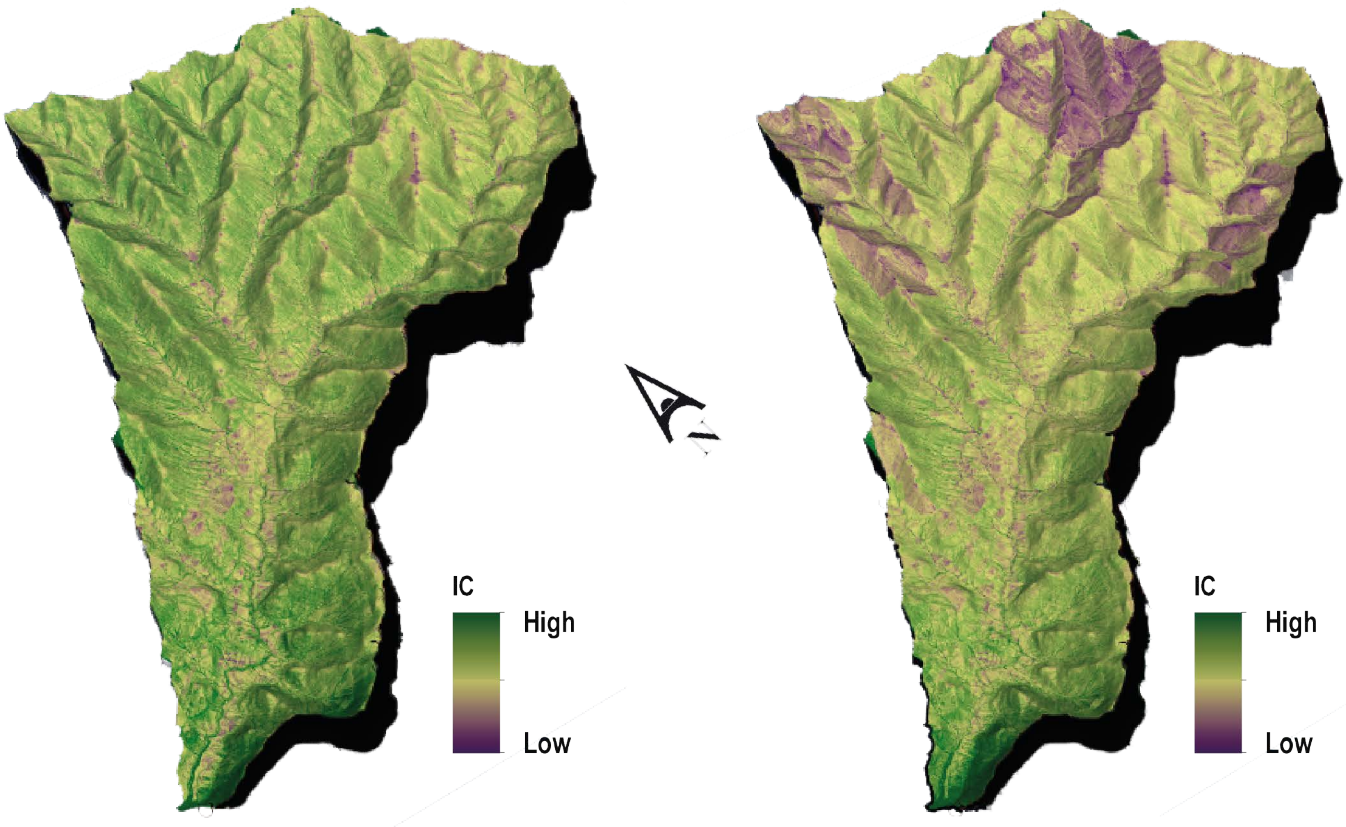

LAND DEGRADATION & DEVELOPMENT
Land Degrad. Develop. (2017)
Published online in Wiley Online Library (wileyonlinelibrary.com) **DOI**: 10.1002/ldr.2676

ENHANCING CONNECTIVITY INDEX TO ASSESS THE EFFECTS OF LAND USE CHANGES IN A MEDITERRANEAN CATCHMENT

Ivan Lizaga[1]*, Laura Quijano[1], Leticia Palazón[1], Leticia Gaspar[2], Ana Navas[1]

[1]*Soil and Water Department, Experimental Station of Aula Dei, CSIC, Avenida Montañana 1005, 50059 Zaragoza, Spain*
[2]*National Museum of Natural Sciences, CSIC, José Gutiérrez-Abascal 2, 28006 Madrid, Spain*

Received 9 August 2016; Revised 27 November 2016; Accepted 27 November 2016

ABSTRACT

In the Mediterranean region, the long history of cultivation is associated with significant changes in the original landscape. Agricultural intensification and subsequent land abandonment and reforestation have significantly affected the hydrological behaviour and connectivity patterns of hydrological systems. Thus, information on the spatial distribution of land use/cover is essential for monitoring the runoff response to interpret catchment hydrology. A medium-sized catchment of the central part of the Ebro Basin (NE Spain), representative of Mediterranean mountain agroecosystems, was selected to assess the effect of land use/cover changes during the last few decades on the hydrological network of the catchment. To this end, a topography-based index, the 'index of connectivity', was applied to assess the effects of land use changes from 1957 to 2010. The sediment connectivity was estimated by using a geomorphometric approach to simulate how connectivity changes due to the different land covers. To improve this index, we used a combination of C-factor, rugosity index and the novel application of a total aerial biomass equation over pine-reforested areas as a weighting factor. A high-resolution (1 × 1 m) digital elevation model was created by filtering and applying a multiscale curvature classification algorithm. The connectivity values show a decrease directly related to ~71% decrease of agricultural land. Understanding landscape patterns, changes and interactions of human activities is essential for land management in Mediterranean agroecosystems. Copyright © 2016 John Wiley & Sons, Ltd.

KEY WORDS: land abandonment; natural revegetation; connectivity; digital techniques; Mediterranean agroecosystems

INTRODUCTION

Sediment connectivity is the connected transfer of sediment from a source to a sink in a system via sediment detachment and sediment transport, controlled by how the sediment moves between all geomorphic zones in a landscape (Bracken *et al*., 2015). Sediment connectivity has an important effect on the development of morphological landform features, being one of the greatest conditioning factors on the development of hydrological networks. Sediment connectivity has a major influence on how sediment is moved and relocated, modifying the current landscape and determining the spatial distribution of sources and sinks of water (Puigdefabregas *et al*., 1999).

Highly linked to hydrological and sediment connectivity are the terms geomorphic or landscape sensitivity and coupling, introduced by Brunsden & Thornes (1979) and recently recovered by Fryirs (2016). Geomorphic or landscape sensitivity refers to how geomorphic systems respond to environmental change, that is, the ability of the system faced with external interference to withstand the change. This term is suitable to categorise how agricultural activities disturb the system and how it reacts over subsequent decades. Furthermore, coupling is used within the context of the effectiveness of the transfer of sediment between the components of a fluvial system (Harvey, 2001) at a relatively small scale (Faulkner, 2008).

Studies have devoted increasing attention to the connection between areas with different hydrological behaviour and land use, with particular focus on the connection between hillslopes and channels (Borselli *et al*., 2008; Vigiak *et al*., 2012) and modelling the different processes of hillslope instability (Heckmann & Schwanghart, 2013). In addition, an interpretation of sediment transport by runoff and the associated soil erosion processes requires a background knowledge and the determination of water pathways to determine the location of the most probable sources and targets/sinks in the catchment.

Since the 1950s, agriculture in European Mediterranean agroecosystems was commercialised through technological developments and the European Union common agricultural policy. There is a main environmental issue behind these policies, which favours the rapid expansion of certain management systems; crops have increased productivity, and the agricultural activity has become more focused on more fertile and accessible land.

This resulted in a transformation of traditional agricultural practices towards intensive farming. In many areas, this produced a major decline in traditional labour intensive practices, becoming mountain agriculture catchments in marginal agricultural land (Lasanta *et al*., 2016). The problems that these trends have created are particularly marked in mountainous areas and in regions where agricultural land

*Correspondence to: Ivan Lizaga, Soil and Water Department, Experimental Station of Aula Dei, CSIC, Avenida Montañana 1005, 50059 Zaragoza, Spain.
E-mail: ilizaga@eead.csic.es; lizaga.ivan10@gmail.com

Copyright © 2016 John Wiley & Sons, Ltd.

is generally found under unfavourable environmental conditions, such as high elevations, steep slopes, shallow soils and dry climatic conditions (MacDonald *et al*., 2000). In Spain, land abandonment has notably increased since the 1960s as a consequence of complex socioeconomic and environmental changes, leading to depopulation of rural areas and the impossibility of mechanisation in steep terrain (Quijano *et al*., 2016). In addition, subsequent reforestation during the 1970s and 1980s not only caused a large impact on runoff and connectivity reduction due to vegetation growth (Buendia *et al*., 2016) but also increased forest fires (Royo *et al*., 2015). At present, the loss of steep slope agriculture and the search for more propitious agricultural lands are not only reducing runoff in mountain catchments but also leading to abandonment of rural communities.

Over the last few centuries, steep slope areas in the Mediterranean region have been gradually transformed into terraced arable lands with an intensive impact both on the original soil and landscape. As a consequence of these changes, agricultural soils have been modified: At present, they have different soil properties compared with their previous and original conditions (Romanyà & Rovira, 2011).

Soil erosion and hydrological connectivity are greatly responsive to land use (García-Ruiz, 2010; Mohammad & Adam, 2010; Nunes *et al*., 2011; Mohawesh *et al*., 2015; Keesstra *et al*., 2016). Mankind, rather than natural forces, is the source of most contemporary changes in land cover (Meyer & Turner, 1994). Agricultural deforestation and most land use changes have generally been considered as a local environmental issue, but at present, they are becoming an important global problem (Foley *et al*., 2005). Soil erosion is directly related to the loss of soil nutrients in the topsoil resulting in soil degradation, which in turn leads to reduced soil productivity and increased soil erodibility (Novara *et al*., 2016; Quijano *et al*., 2016). Moreover, depletion of soil depth in agroecosystems can be a serious threat to agricultural sustainability (Fornes *et al*., 2005).

Steep slope agriculture has changed connectivity and erosion rates during the last few centuries in Mediterranean landscapes. Both coupling and sediment connectivity have to be viewed with regard to the temporal scale, ranging from the event timescale for hillslopes and channel coupling to geological timescales for morphological changes in large basins (Heckmann & Schwanghart, 2013). Together with land abandonment, the subsequent continuous expansion of natural forest and revegetated areas is clearly affecting runoff amount and streamflow yield (López-Moreno *et al*., 2011). It has also been suggested that during vegetation development, soil heterogeneity increases, thus playing an important role in infiltration processes (Cammeraat *et al*., 2010). Furthermore, changes in water yield are associated with an increase in continuous temperature due to global warming and the subsequent increase in evapotranspiration rates from natural vegetation (Martínez-Fernández *et al*., 2013).

A temporal approximation is essential to quantify the vegetation increase induced by the abandonment of agricultural lands, the introduction of reforestation with pines and the loss of extensive farming over the hillsides. Our objective is to assess the variation of connectivity produced by land cover changes during the last 50 years over a Mediterranean catchment representative of mountain agroecosystems that have experienced intensive land abandonment and reforestation during the past century. The innovative characteristic of this investigation is quantifying the connectivity changes over time, as Foerster *et al*. (2014) tested with remotely sensed data, and adapting a connectivity index (IC) in the study area. This adjustment could be extrapolated to most steep slope agriculture areas. Moreover, we also try to model how connectivity varies in pine-reforested areas by using total aerial biomass data (TAB) for a better understanding of the hydrological network functioning within reforested areas. A clear understanding of connectivity is essential for further development of soil redistribution models and to predict the future evolution of catchments.

MATERIALS AND METHODS

Study Area

The study area is included in the Arba river drainage catchment. The Barués catchment (23 km^2) is an ephemeral stream catchment located in the central part of the Ebro Basin in northeast Spain (Figure 1). From a geological point of view, it is situated on the distal part of the pre-Pyrenean range with characteristically S–SW low bedding between 5 and 8°. The rock outcrops include two concordant Oligomiocene lithostratigraphic units of the Uncastillo Formation composed of sandstones, claystones and siltstones (Sole *et al*., 1972; Teixel *et al*., 1992; Pardo & Arenas, 1996). The geomorphological setting is clearly conditioned by the low bedding of the strata. This sets up the path of the streams following the strata dip.

The climate is continental Mediterranean, characterised by cold winters and hot and dry summers. Rainfall events mainly occur in spring (April and May) and autumn (September and October) and a summer drought between the two humid periods. The mean annual temperature is 13·4 °C, and the mean annual rainfall is about 500 mm. Most abundant soils were classified during field surveys as Calcisols and Cambisols (FAO, 2014). The soils developed on Quaternary deposits are mainly formed by alluvial deposits and have basic pH, low soil organic carbon contents (between 0·13 and 5·65%) and the secondary accumulation of carbonates.

Multitemporal Analysis

The assessment of sediment connectivity was carried out by applying a topography-based index in two different scenarios by using two land use maps for 1957 and 2010. The first map was created by orthorectification of the 1957 American army aerial photographs by using a supervised classification in ERDAS after photographic enhancement. The actual map was digitised over 2010 National Plan of Aerial Orthophotography and fieldwork maps.

Copyright © 2016 John Wiley & Sons, Ltd.

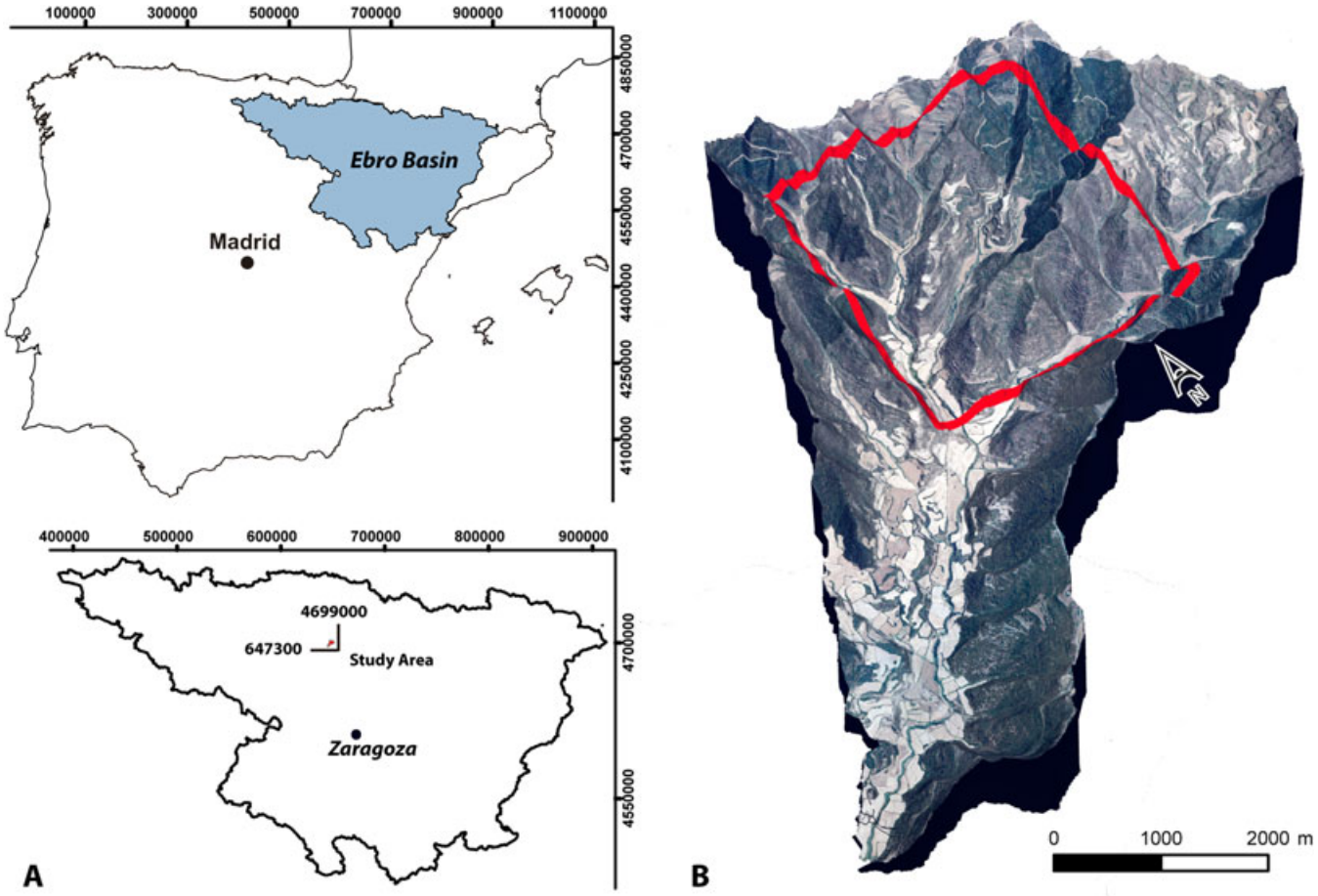

Figure 1. (A) Location of the study catchment in the central part of the Ebro Basin (NE Spain). (B) Detailed orthophotography of Barués catchment. Red square delimits visualisation of Figures 5 and 8. [Colour figure can be viewed at wileyonlinelibrary.com]

The streams with higher connectivity ratios were digitised over 2010 orthophotography, and the IC was created with the 2010 digital elevation model (DEM) and compared with the 1957 aerial photography drainage net to visualise whether a remarkable displacement or modification in the slopes occurred between both periods (Figure 2).

Stream displacement and topographic changes between the periods can only be measured for what it is visible in the multitemporal aerial photography due to the absence of the 1957 DEM. Figure 2 shows the near absence of displacement or modification of the secondary slope streams in a highly degraded area of the catchment. Most visible differences between both streams in Figure 2 are produced for the aerial stereoscopic photography deformation. These low grades of displacement in the secondary streams imply that most changes in the topography are below the detection limit of our DEM.

However, the main channel has variations in its morphology, being higher in the medium and lower parts where sections are deeper and surrounded by crop fields, and nearly insignificant in the upper parts of the catchment. Due to the impossibility of obtaining a 1957 DEM and after checking the absence of substantial modifications to the

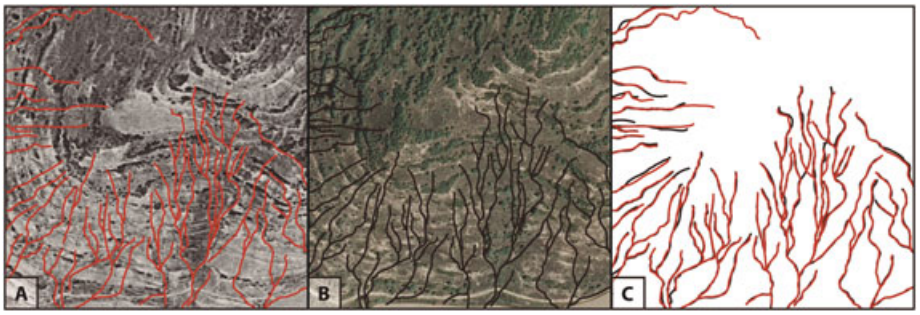

Figure 2. Comparison of stream variations between the aerial photography 1957 (A) and 2010 National Plan of Aerial Orthophotography (B) to compare the variation ratio. [Colour figure can be viewed at wileyonlinelibrary.com]

Copyright © 2016 John Wiley & Sons, Ltd.

topography between 1957 and 2010, it was decided to use a 2010 DEM with a low grade of uncertainty.

Digital Elevation Model Refinement

Nowadays, the most popular IC from Borselli *et al*. (2008), the modified version by Cavalli *et al*. (2013) and geomorphological studies related to slopes or erosion (Kawabata & Bandibas, 2009; Gutiérrez & Lizaga, 2016; Masselink *et al*., 2016) are based on DEMs. Thus, the accuracy of model results is fully dependent on DEM quality and resolution: It is needed to apply and develop a topography-based index such as IC correctly. Therefore, developing a model based on LIDAR data was necessary to refine the existing LIDAR points to create a high-resolution DEM (1 × 1 m). Accordingly, we used Spanish National Geographic Institute (IGN) raw LIDAR data points following Montealegre *et al*. (2013) methodology. First, we deleted the noise of the data, deleting LIDAR points classified as noise by using ArcGIS. Second, we proceeded to filter our LIDAR data in order to generate a bare ground 1 × 1 m raster DEM by using MCC–LIDAR, a command-line tool for processing discrete-return LIDAR points in forested environments based on the multiscale curvature classification algorithm developed by Evans & Hudak (2007). The root mean square error (RMSE) was calculated for both DEMs by using a cross-validation method (Table I).

Total Aerial Biomass

LIDAR data represent a tool that supports the calculation of forest inventories and allows the vegetation to be measured in three dimensions (Ruiz, 2012; Reyes & Delia, 2014). TAB was calculated for the reforestation forests (Rfs) by using Equation 1, developed by Domingo *et al*. (2016), and the software FUSION. This equation was created and optimised in a nearby reforested area with *Pinus halepensis* Mill that had similar forest dasymetric characteristics as the pine reforestation in the study catchment. Equation 1 is a good complement to understand the change produced by pine reforestation.

$$TAB\left(\frac{kg}{ha}\right) = e^{(0{\cdot}0158 * A2m)} * e^{(0{\cdot}0713 * P40)} \quad (1)$$

Where: *e* refers to the Euler's number, *A*2*m* is the percentage of the first LIDAR laser return above 2 m ground height, produced by the reflectance of the treetop canopy, and *P*40 is the 40th percentile of LIDAR data. A 25 × 25 m per pixel size was selected to create a raster image comparable with the study plots accomplished by Domingo *et al*. (2016) to obtain such an equation.

Connectivity Index and Adaptation to Steep Slope Agriculture

In headwater fluvial catchments, the more relevant aspect of coupling is the connection between hillslope and channel, that is, hillslope–channel coupling (Harvey, 2002). Sediment connectivity was estimated by using a geomorphometric approach to simulate how connectivity changes due to different land covers. Hence, it is very important to determine how the system connectivity responds to human-induced cover changes (Harvey, 2002). For this reason, we applied the IC (Equation 1) proposed by Borselli *et al*. (2008) by using the C-factor from Revised Universal Soil Loss Equation as a weighting factor (*W*) in the index.

$$IC = log_{10}\frac{D_{up}}{D_{dn}} \quad (2)$$

Where: D_{up} and D_{dn} are the upslope and downslope components, defined by:

$$D_{up} = \overline{WS}\sqrt{A} \quad (3)$$

Where: *W* is the average weighting factor of the upslope contributing area, *S* is the average slope gradient of the upslope contributing area (m/m), and *A* is the upslope contributing area (m^2).

$$D_{dn} = \sum_i \frac{d_i}{W_i S_i} \quad (4)$$

Where: d_i is the length of the flow path along each *i* cell according to the steepest downslope direction (m) and W_i and S_i are the weighting factor and the slope gradient of the *i* cell respectively.

Borselli *et al*. (2008) proposed $S = \sin\alpha + 0 \cdot 005$ including 0·005 as the minimum slope value to avoid infinite values in Equation 4. Thus, we preserved the original values of our 1 × 1 m DEM to obtain more realistic results after checking the absence of 0 slope values. Besides calculating the contributing area, we used the procedure of multiple flow D-infinity approach (Tarboton, 1997) instead of the single flow direction algorithm (O'Callaghan & Mark, 1984) used in the hydrology ArcGIS toolbox as

Table I. Root mean square error (RMSE) calculated for both digital elevation models (DEMs) over the entire study area and over the different land uses: MCC (calculated using MCC algorithm) and no MCC (regular filtered algorithm)

	Agricultural		Forest		Pine		All catchment	
	MCC	No MCC	MCC	No MCC	MCC	No MCC	MCC	No MCC
Mean	0·062	0·177	0·151	0·390	0·235	0·424	0·132	0·312
Max	0·643	1·210	0·860	1·572	0·350	1·630	0·671	1·439
Min	0·002	0·001	0·005	0·001	0·012	0·022	0·005	0·005
SD	0·100	0·130	0·218	0·137	0·325	0·681	0·192	0·243

Copyright © 2016 John Wiley & Sons, Ltd.

proposed in Cavalli *et al.* (2013). Using D-infinity allows us to calculate the flow accumulation of converging and diverging flow directions to create a more realistic topographic index.

In addition, the IC was improved by using a terrain roughness index (RI) as a W. Cavalli & Marchi (2008) and Cavalli *et al.* (2013) developed and later implemented in the IC. RI was calculated as the standard deviation of the residual topography by using the mean of the 25 neighbourhood cells values as a 5 × 5 moving window. However, for our index, we created a new roughness index (SdRI; Equation 5) calculated as the standard deviation of the slope as recommended by Grohmann *et al.* (2011). SdRI was also applied by using a 3 × 3 moving window to accentuate steep slope terrace characteristics of the low strata bedding preserved and modified by agricultural practices in our study catchment.

$$\sigma = \sqrt{\frac{\sum_{i=1}^{9} (x_i - x_m)^2}{9}} \tag{5}$$

Where: x_i is the pixel value and x_m is the average of the 3 × 3 moving window.

Figure 4 shows the good adjustment of the SdRI to the steep slope terraces compared with the RI, which also shows a good fit but appears to be better for larger terraces than those present in our study area.

Furthermore, in Equations 2 and 3, we also used our two land use maps (C-factor) as weighting factor to show the differences between both land uses (1957 and 2010) and how the IC changed over time. The C-factor values assigned to our land uses are 0·0011, 0·0010, 0·06, 0·2 and 0·26 for reforestation forest, Mediterranean forest, abandoned land, cultivated land and trails respectively extracted from Panagos *et al.* (2015). Combining both approximations, a weighting factor was applied as the link between the C-Factor and SdRI index, trying to develop a better adjustment to reality. The model was tested in the entire catchment to facilitate visualisation at a more detailed scale in an area where the four land uses occur. We selected the same area as the red square of Figure 1 to show how connectivity changed over 50 years due to land use and cover variations.

To introduce the probable variations of forest density in our model, the TAB layer created in the previous section was implemented inside the C-factor layer by using it as the inverse of TAB to produce lower C-Factor in the areas with higher densities and higher C-Factor in the areas with lower densities. Even with a 1-m resolution DEM, it was impossible to implement the same methodology for the other land covers: It was only used on reforested areas by creating a mask layer.

$$W = \left(C^* \frac{1}{TAB}\right) * SdRI \tag{6}$$

Where: W is the weighting factor, C is the C-factor of the different land covers, TAB is the variance of the total aerial biomass (only used over pine reforestation), and SdRI is the roughness index. These data are normalised by scaling them between 0 and 1. This normalisation is needed because the W is a dimensionless factor and should range from 0 to 1 to be weighted equally to slope in the index. For this reason, the W factor was normalised by using unity-based normalisation (Equation 7):

$$z_i = \frac{x_i - min(x_i)}{max(x_i) - min(x_i)} \tag{7}$$

Where: x_i is the pixel value and min/max x_i are the minimum and maximum values respectively, of the moving window.

RESULTS AND DISCUSSION

Digital Elevation Model

Increasing DEM quality allowed a significant improvement in the accuracy of the connectivity model. Without a good enhancement and a high-resolution digital terrain model, the possibilities of terrain error or the lack of reality adjustment increase exponentially (Li & Wong, 2010; Vaze *et al.*, 2010), therefore increasing the error of the IC. Thus, enhanced LIDAR data over regular IGN filtered LIDAR data allowed us to create a more accurate 1 × 1 m high-resolution DEM instead of the 5 × 5 m resolution IGN DEM. Figure 3 compares the hillshade created by using IGN and MCC-filtered data, both compared after increasing resolution to 1 × 1 m. Table I shows the RMSE reduction in MCC DEM and also how RMSE increases with higher vegetation canopy density and height.

Even increasing the resolution of the IGN DEM with their filtered data, there was a high adjustment error regarding the vegetation, but this error was greater in scrubland and riparian vegetation than in forests. In the Figure 3 LIDAR profiles, it is clearly visible how the MCC filter DEM (Figure 3B) successfully removed the scrubland points situated in the upper part and in the middle part of the profile, unlike the IGN DEM (Figure 3A), which is clearly visible in the hillshade image. For this reason, the DEM optimised with MCC-filtered data was selected (Figure 4).

Land Use Distribution Maps

Numerous studies in a variety of environments have demonstrated the significant effects of the vegetation cover increase on the reduction of runoff connectivity and water erosion (Elwell & Stocking, 1976; Zuazo & Pleguezuelo, 2008; Mohammad & Adam, 2010; Sandercock & Hooke, 2011; Fox *et al.*, 2012). The importance of land cover can be summarised in two main effects: the direct physical protection of the soil surface by the canopy and leaf cover preventing rainfall impact and soil detachment particles and the indirect improvement of the soil resistance and quality (García-Ruiz *et al.*, 1995; Boix-Fayos *et al.*, 1998; Dunjó *et al.*, 2004; Navas *et al.*, 2008).

The high variation in total runoff and consequently in transported sediment reflects the major importance of total land cover and land use type on runoff generation and soil

Copyright © 2016 John Wiley & Sons, Ltd.

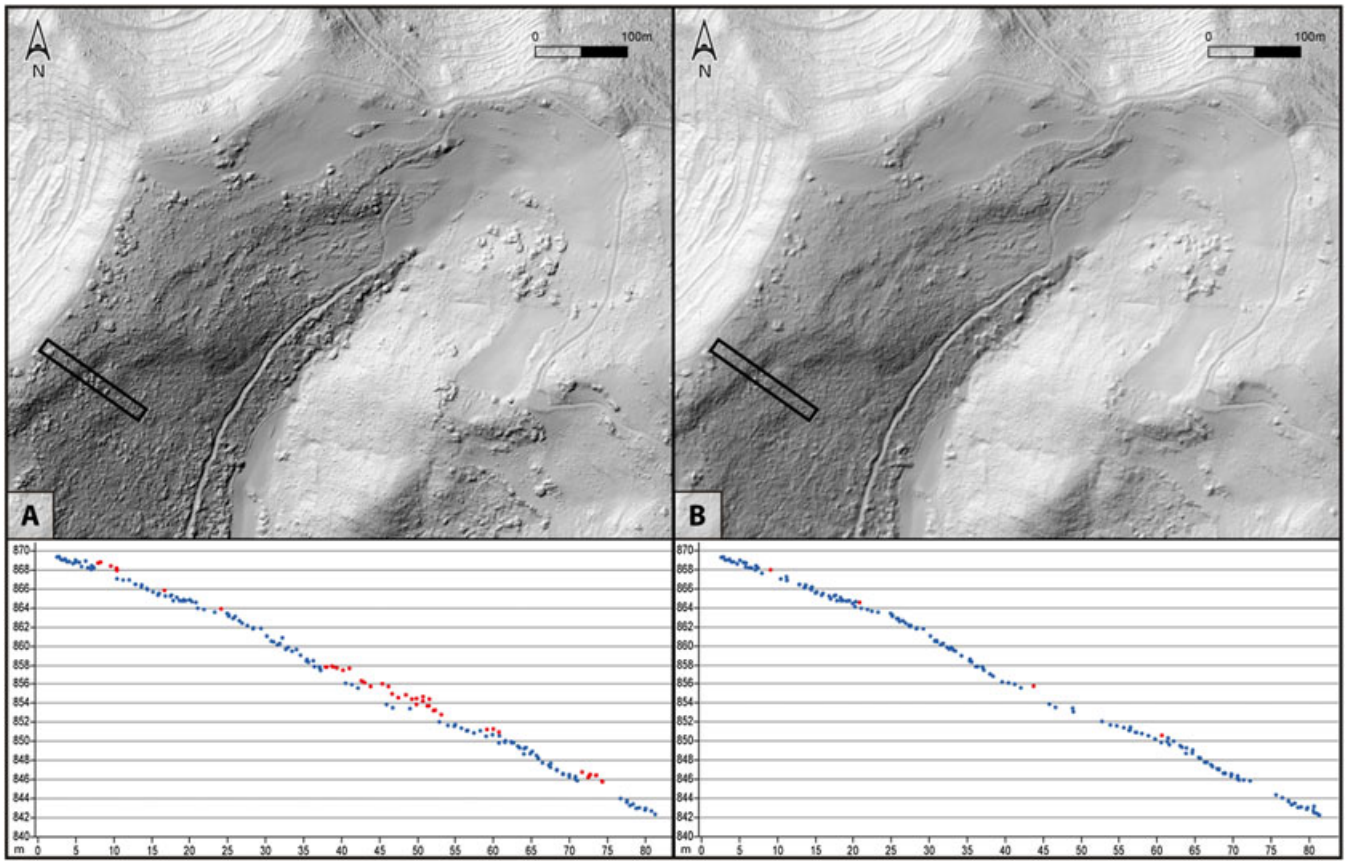

Figure 3. Hillshades created based on Spanish National Geographic Institute (IGN) LIDAR filter points with a LIDAR point profile extracted from the black rectangle situated in the SW. (A) No MCC filtering. (B) IGN LIDAR points filtered by MCC software. [Colour figure can be viewed at wileyonlinelibrary.com]

loss; these have significant implications on soil erosion (Kosmas *et al*., 1997). The results obtained for the 1957 and 2010 land cover maps reveal the major variation that took place during the last five decades in the study area.

Our results showed that Mediterranean forest and grassland have been the main land uses in the catchment over the years, together accounting for more than 50% of the total catchment surface area. A decrease in cultivated land was observed between 1957 and present, when the area dedicated to agriculture decreased from 13·4 to 3·8 km^2 (corresponding to a decrease of ~71%; Table II). On the other hand, forested areas increased from 9·2 km^2 in 1957 to 15·8 km^2 at present. Vegetation and land use are important factors on the catchment hydrology, as indicated by Bryan & Campbell (1986); both are key controls on the intensity and frequency of runoff and surface sheet erosion.

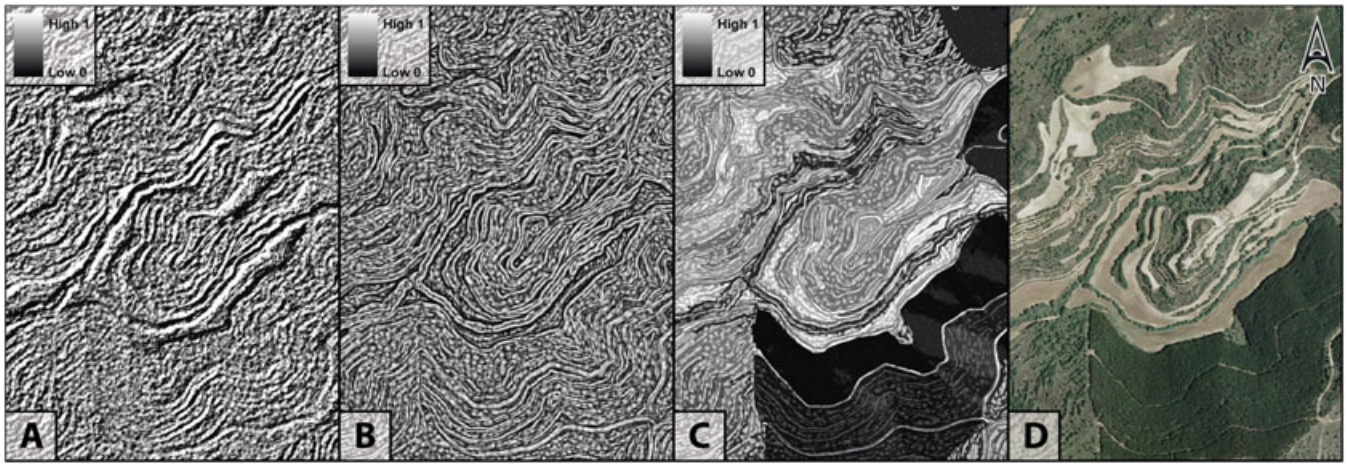

Figure 4. Comparison between Cavalli roughness index normalised (A), standard deviation roughness index normalised (B), weighting factor used in the connectivity index (C) and the orthophotography (D) to facilitate comparison and the location.

Copyright © 2016 John Wiley & Sons, Ltd.

Table II. 1957 and present land use/land cover measures and their representative percentages of the total catchment area

	1957 land use map		2010 land use map	
Land use/land cover	Square kilometres	% of the total area	Square kilometres	% of the total area
Cultivated	13·42	58·2	3·81	16·5
Mediterranean forest	9·23	40·0	11·49	49·8
Reforestation forest	–	–	4·36	18·9
Abandonment agriculture	–	–	2·93	12·7
Riverbank vegetation	0·40	1·8	0·46	2·0

Figure 5A shows a classic example of steep slope agriculture with almost 70% of the slopes and stream terraces cultivated. Conversely, Figure 5B shows an important modification caused by natural revegetation and reforestation over steep slopes. It has been shown in a nearby large mountain catchment that badlands and severely eroded areas have higher connectivity values than agricultural, forest and scrubland land uses/covers (Palazón & Navas, 2014).

Steep slope terraces are common in Mediterranean mountain agroecosystems for rudimentary agriculture. The near absence of tectonics in the Barués catchment determined the low-dip strata, resulting in an easily farmable terrain. Steep slope agriculture not only increases erosion and runoff ratios on the hillslopes but also produces slope instability, fostering the probability of mass movements due to the absence of vegetation cover that protects the soil from erosion

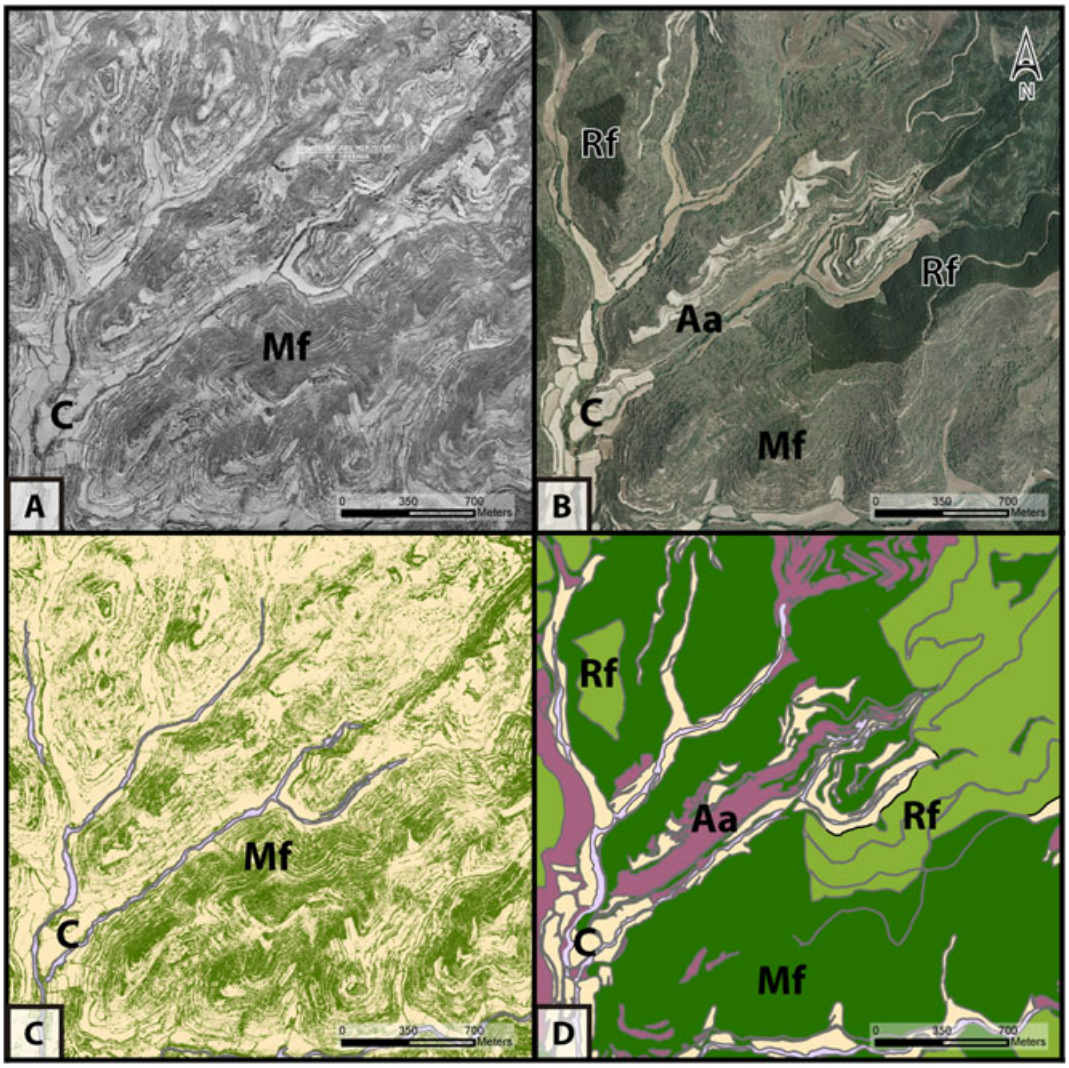

Figure 5. (A) 1957 aerial photograph. (B) 2010 orthophotography. (C) Land cover map developed using a supervised classification of (A). (D) 2010 land cover map. Cultivated land (C), Mediterranean forest (Mf), reforestation forest (Rf) and abandoned agriculture (Aa). [Colour figure can be viewed at wileyonlinelibrary.com]

Copyright © 2016 John Wiley & Sons, Ltd.

Figure 6. Slide movements located in the Barués downstream area surrounded by cultivated fields. Every stream without riverbank vegetation in the study area has this type of landslide, caused by the loss of sediment at the toe of stream walls. [Colour figure can be viewed at wileyonlinelibrary.com]

and prevents its displacement. This can be seen in Figure 6, which shows a typical rotational stream-bank failure movement. These types of landslide are usually developed during storm events on poorly cohesive materials favoured by the absence of vegetation cover, high slope and dryland crops situated on the top of the hills of the catchment. These small slide movements are developed on stream walls induced by erosion at the toe of the stream bank walls.

Quantification of riparian vegetation over time was difficult due to image resolution, but a minimum 10% increment was detected. The presence of riparian forest and the reinforcement of bank soils by herbaceous riparian vegetation significantly reduce the likelihood of erosion by mass failure, in agreement with the observations of Hubble *et al.* (2010). Moreover, riparian vegetation increases the apparent cohesion through root reinforcement of bank soils reducing bank migration rates, increasing bank strength and reducing bank failure frequency (Micheli & Kirchner, 2002).

Total Aerial Biomass

The Barués catchment TAB was divided into three major groups with distinctive ranges of TAB values (Figure 7). These three groups coincided with the three different reforestation forests periods (MOP-CHE, 1976; Ortigosa *et al.*, 1990) that conditioned the greater or lesser development of trees and forest. The three groups reported distinctive ranges of TAB values; thus, higher values were found on north faces and lower ones appeared on south-facing slopes (Figure 7). Nevertheless, younger reforestation was too minor as to test this assumption with TAB values. Table III shows major differences among the three different pine forests (Rf 1, Rf 2 and Rf 3). The oldest (Rf 1) nearly doubled the mean value of the TAB, while Rf 2 doubled the youngest one (Rf 3). The TAB mean values of the north-sloping faces (WNW–ENE, 292·5–67·5°) in contrast to the mean values of the south-sloping faces (WSW–ESE, 112·5–247·5°) calculated for each pine reforestation showed substantial differences. The solar angular ranges, being higher on the south-facing slopes, increasing temperature and reducing the accumulation of moisture, regulate this effect. Hence, the less developed soil biological activity and the lower organic matter content probably affect tree growth (Cerdà, 1998).

The TAB equation is a good complement in the model to understand the change produced by pine reforestation, not only related to coupling and connectivity but also to the increment of the vegetation volume. This increment probably reduced greenhouse environmental effects, as Fang *et al.* (2001) observed in China, suggesting that carbon sequestration through forest management practices could help offset carbon dioxide emissions.

Connectivity Index

With the modification in land cover, mostly in reforested areas, the decrease of runoff might interfere, reducing sediment displacement and probably concentrating highest connectivity and erosion areas in streams that remain coupled, as can be seen in the yellow–green streams within the reforested areas in Figure 8.

The IC with different land covers as a W gives an approximation of the effect of human activity over the study area. In Figure 8, the decrease in water and sediment fluxes can easily be recognised due to new covers such as natural revegetation, abandoned fields and the great variation induced by reforestation (Table IV).

Copyright © 2016 John Wiley & Sons, Ltd.

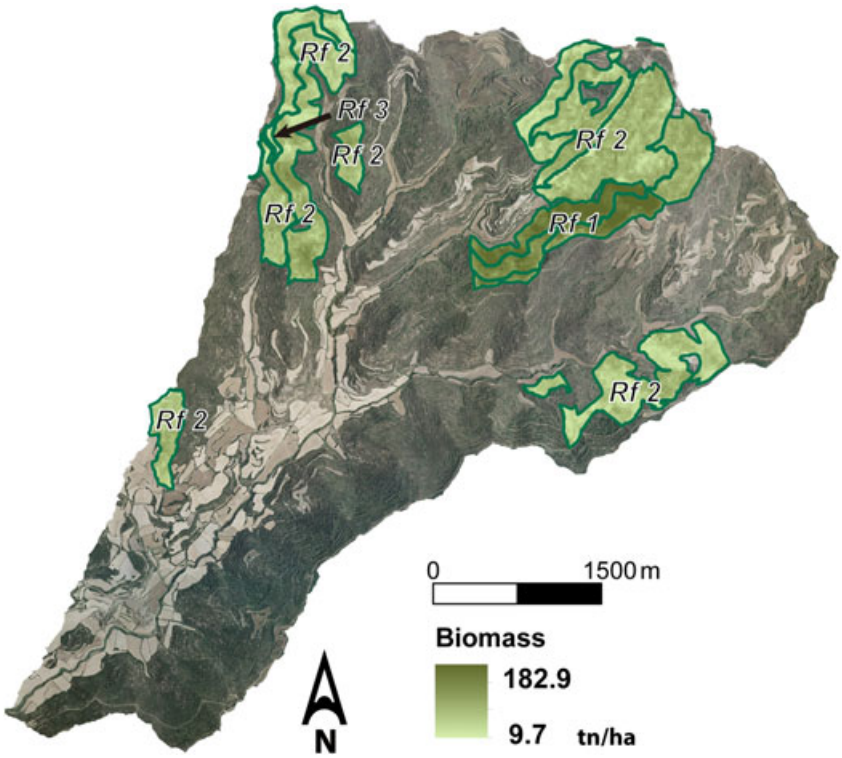

Figure 7. Total aerial biomass calculated over reforestation forest, where its variation inside the forest is clearly visible. Reforestation forest (Rf) 1 is the oldest reforestated forest; Rf 3 the youngest. [Colour figure can be viewed at wileyonlinelibrary.com]

The decrease of IC values could be related to the increase in trees and vegetation cover, which minimises the kinetic energy of the raindrops preventing soil detachment (Llorens, 1997; De Luna *et al*., 2000). Hence, vegetation cover probably improves soil quality by favouring infiltration and preventing runoff. On the contrary, high erosion rates and low slope resistance could easily produce topless and landslides as the most frequent mass movements (Figure 6). These feed large volumes of sediment into the stream system, as topless and bank failures are found in most stream banks along the principal streams in the catchment.

Implementation of SdRI gives greater relevance to the steep slope terrain adapting IC model to Mediterranean mountain agroecosystems. This is clearly visible on the top hills and also produces little decentralisation of the hydrological network caused by the alternating flat-steep slopes produced by the combination of ancient agriculture terraces and the strata (Figure 8). In addition, the TAB layer provides a real variation inside the pine reforestation, showing the difference between biomass and also proving that vegetated soils situated on the north-facing slopes had greater biomass. Higher proportions of biomass surely result in more developed soils and probably lower sediment yield, runoff and erosion, while bare soils on the south-facing slopes might have higher runoff rates.

The implementation of different land uses (C-factor) in the model shows the relevance of reforestation areas to the development of hydrological connectivity. Reforestation seems to be homogenous but has variations in above-ground biomass density inside reforested areas due to different factors such as topography, solar radiation and organic matter among others. Figure 4C shows the variation produced for the inclusion of the C-factor and TAB layer in the *W* factor over the roughness index, including the variation of the vegetation cover.

Figure 9 shows the zoomed biomass variation introduced into the IC with the TAB layer. The connectivity decline is clearly visible on the north faces in relation to the other orientations. This is probably due to the distribution of soil

Table III. Reforestation forest (Rf) 1, 2 and 3 show Min, Max and Mean values of tons per hectare, total total aerial biomass (TAB) and area of three different forest ages

	Pixel (25 × 25 m) value tons/ha			Mean pixel values		Total area	
	Min	Max	Mean	N, NW and NE faces	S, SW and SE faces	BT value	ha
Rf 1	35·1	182·9	109·4	110·7	94·5	104,151·8	70
Rf 2	13·7	121·5	52·0	56·6	49·1	287,201·5	358
Rf 3	9·7	33·6	21·9	36·6	26·7	1,434·7	5
						392,788	433

Copyright © 2016 John Wiley & Sons, Ltd.

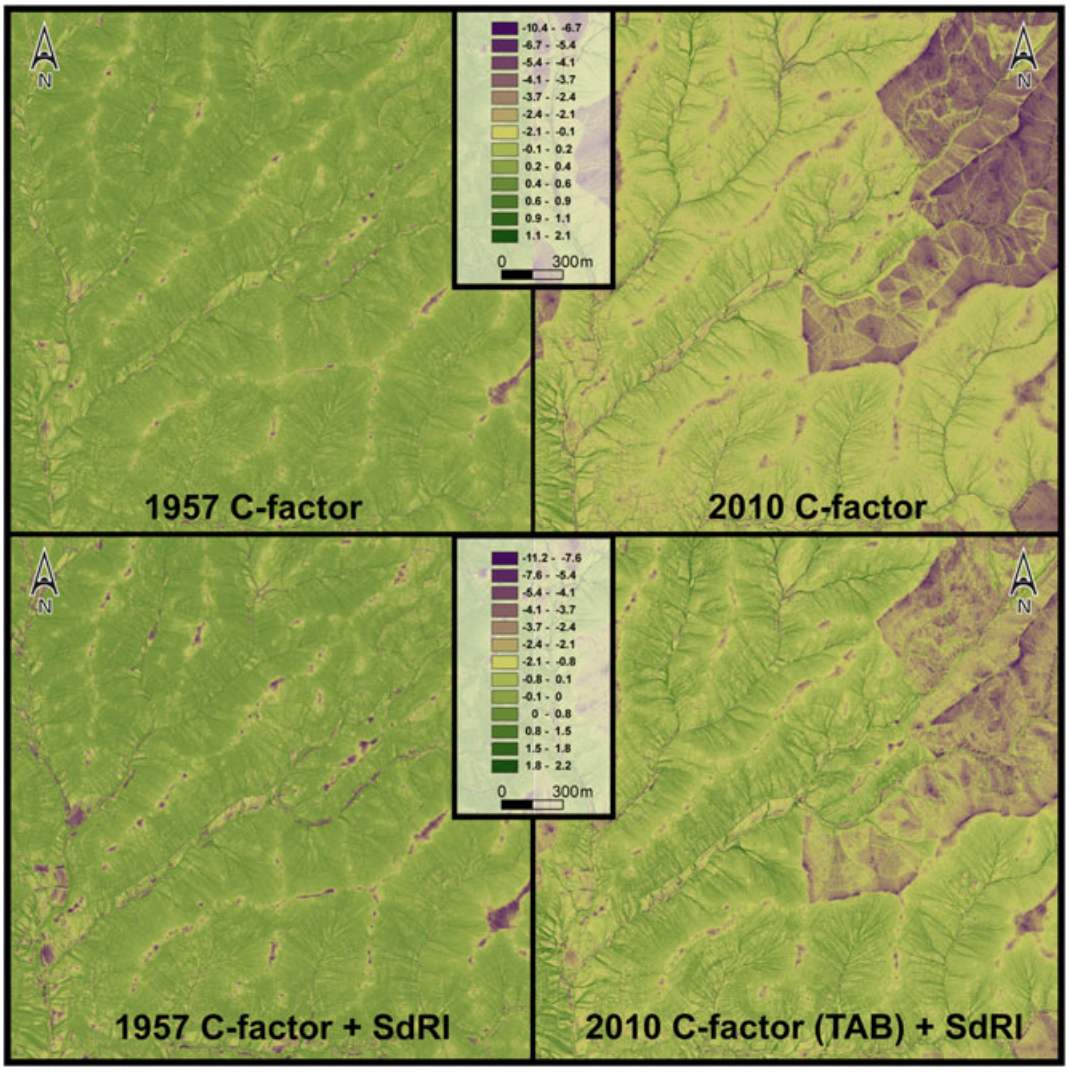

Figure 8. Connectivity index for 1957 and 2010 with only C-Factor (A and B) and adding standard deviation roughness index and total aerial biomass (C and D). These figures correspond to the red square on Figure 1 to improve visualisation of a representative part of the catchment affected by changes in land cover. [Colour figure can be viewed at wileyonlinelibrary.com]

moisture not only in the reforested areas but also in other areas because of the patchy vegetation structure (Marchamalo *et al*., 2015).

Comparing both IC output maps, land cover maps (Figures 5 and 8) and IC values (Table IV), the importance of land cover for preventing runoff and the benefits of landscape restoration can be seen. Strong changes in reforestation cover, land abandonment, natural revegetation and especially the reversal to Mediterranean forest probably have major effects on the loss of coupling and, as a consequence, on the decrease of discharge, as Navas *et al*. (2011) observed in the Yesa reservoir and probably also the streamflow reduction, as observed by many authors across the Iberian Peninsula (Morán-Tejeda *et al*., 2010; Lorenzo-Lacruz *et al*., 2012). Other authors have also reported runoff reduction as a consequence of the increase of

Table IV. Connectivity values over land uses in 2010

2010 Land use	Agricultural	Forest	Pine	Abandonment	Global
		1957			
Min	−9·6	−9·6	−9·5	−9·59	−9·578
Max	2·31	2·25	1·95	2·29	2·254
Mean	0·2	0·11	0·16	0·11	0·1
		2010			
Min	−10·6	−10·4	−11	−10·1	−10·496
Max	1·8	1·9	1·6	1·76	2·08
Mean	−0·17	−0·35	−0·96	−0·26	−0·322

Copyright © 2016 John Wiley & Sons, Ltd.

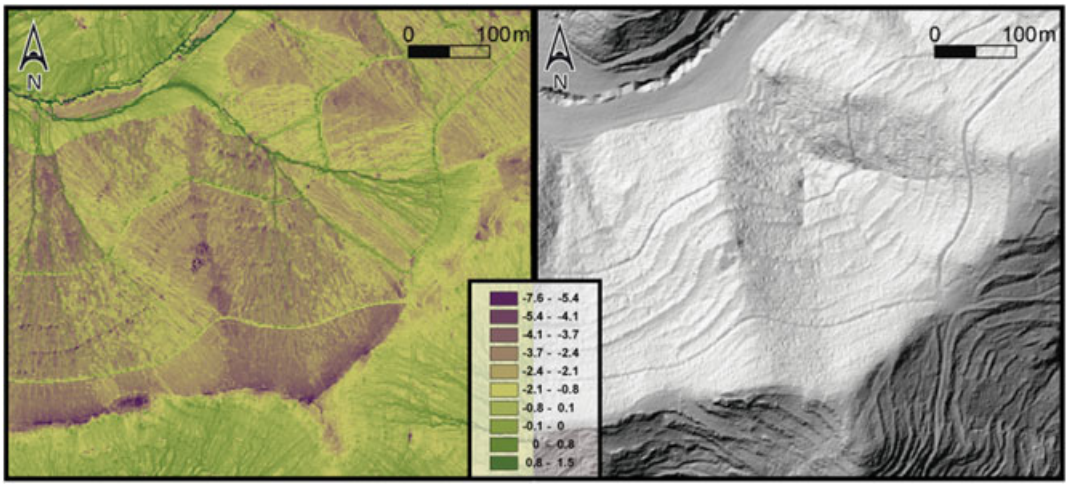

Figure 9. Zoomed-in portion of Figure 8. It is clearly visible how the connectivity changes due to the trails and also how it decreases in the north faces due to the variation introduced by the total aerial biomass layer. [Colour figure can be viewed at wileyonlinelibrary.com]

infiltration, interception and evapotranspiration rates. Furthermore, Table IV confirms that the highest connectivity changes are produced between the actual pine forest and the same area in 1957; this also occurs, though to a lesser extent, over the natural revegetated forest.

CONCLUSIONS

Land use/cover changes by human intervention during the 1960s, mostly due to tillage, have increased connectivity, thus intensifying natural geomorphological processes such as landsliding, gullying, incised streams and severe soil erosion.

The revegetated abandoned lands and reforested areas have been shown to be very efficient in reducing connectivity. Naturally revegetated areas have decreased the connectivity, thus probably limiting soil erosion. Pine reforestation has produced a clear increase over aerial biomass, probably enriching soil organic matter in the reforested areas of the catchment. The increase in biomass could be extrapolated to the other land covers in the catchment. Despite other naturally revegetated areas being likely to experience similar gain in biomass than reforested areas, it has not been possible to estimate it by using LIDAR techniques, because at present, the equation has still not yet been developed for such vegetation covers.

Soil maps with a high level of accuracy are a good approximation; yet, even improving DEM quality to 1 × 1 m and aerial photograph enhancement was not enough to show changes in the riparian vegetation between study dates. In future research, it will be necessary to estimate the channel variation to assess at lower scales how this variation has affected changes in connectivity. The implementation of SdRI and TAB improved both topography and vegetation cover features, increasing the quality and adjustment of the IC. Model enhancement with a 1 × 1 m high-resolution DEM, D-infinity, SdRI and TAB is important to understand the hydrological behaviour of agricultural mountain catchments.

The IC developed here is probably a good approximation to the reality in this area, emphasising that anthropogenic activities are nowadays the greatest landscape modifiers. Moreover, this index represents a good approximation to the temporal connectivity variation in Mediterranean agricultural catchments and has the potential to be used for ecological purposes, future soil management and for field survey studies.

ACKNOWLEDGEMENTS

We would like to thank Lorenzo Borselli and other anonymous referees for their useful comments and suggestions and also Dario Domingo for his help with the TAB application.

This research was financially supported by the project TRAZESCAR (CGL2014-52986R) and the aid of a predoctoral contract (BES-2015-071780) funded by the Spanish Ministry of Economy and Competition.

REFERENCES

Boix-Fayos C, Calvo-Cases A, Imeson AC, Soriano-Soto MD, Tiemessen IR. 1998. Spatial and short-term temporal variations in runoff, soil aggregation and other soil properties along a Mediterranean climatological gradient. *Catena* **33**: 123–138. https://doi.org/10.1016/S0341-8162(98)00048-4.

Borselli L, Cassi P, Torri D. 2008. Prolegomena to sediment and flow connectivity in the landscape: a GIS and field numerical assessment. *Catena* **75**: 268–277. https://doi.org/10.1016/j.catena.2008.07.006.

Bracken LJ, Turnbull L, Wainwright J, Bogaart P. 2015. Sediment connectivity: a framework for understanding sediment transfer at multiple scales. *Earth Surface Processes and Landforms* **40**: 177–188. https://doi.org/10.1002/esp.3635.

Brunsden D, Thornes J. 1979. Landscape sensitivity and change. *Transactions of the Institute of British Geographers* **4**: 463–484. Bryan RB, Campbell IA. 1986

Bryan RB, Campbell IA. 1986. Runoff and sediment discharge in a semi-arid drainage basin. *Zeitschrift für Geomorphologie* **58**: 121–143.

Buendia C, Batalla RJ, Sabater S, Palau A, Marcé R. 2016. Runoff trends driven by climate and afforestation in a Pyrenean Basin. *Land Degradation & Development* **27**: 823–838. https://doi.org/10.1002/ldr.2384.

Copyright © 2016 John Wiley & Sons, Ltd.

Cammeraat ELH, Cerdà A, Imeson AC. 2010. Ecohydrological adaptation of soils following land abandonment in a semi-arid environment. *Ecohydrology* **34**: 421–430. https://doi.org/10.1002/eco.161.

Cavalli M, Marchi L. 2008. Characterisation of the surface morphology of an alpine alluvial fan using airborne LiDAR. *Natural Hazards and Earth System Sciences* **8**: 323–333.

Cavalli M, Trevisani S, Comiti F, Marchi L. 2013. Geomorphometric assessment of spatial sediment connectivity in small Alpine catchments. *Geomorphology* **188**: 31–41. https://doi.org/10.1016/j.geomorph.2012.05.007.

Cerdà A. 1998. The influence of aspect and vegetation on seasonal changes in erosion under rainfall simulation on a clay soil in Spain. *Canadian Journal of Soil Science* **78**: 321–330. https://doi.org/10.4141/S97-060.

De Luna E, Laguna A, Giráldez JV. 2000. The role of olive trees in rainfall erosivity and runoff and sediment yield in the soil beneath. *Hydrology and Earth System Sciences* **4**: 141–153.

Domingo D, Lamelas MT, Montealegre AL, de la Riva J. 2016. Estimación de la pérdida de biomasa y de las emisiones de CO2 generadas por la combustión de masas forestales de *Pinus halepensis* Mill. en el incendio del municipio de Luna (Aragón), mediante datos LiDAR-PNOA. *Aplicaciones de las tecnologías de la información geográfica (TIG) para el desarrollo económico sostenible, Málaga, XVII Congreso Nacional TIG* **1**: 83–88.

Dunjó G, Pardini G, Gispert M. 2004. The role of land use–land cover on runoff generation and sediment yield at a microplot scale, in a small Mediterranean catchment. *Journal of Arid Environments* **57**: 239–256. https://doi.org/10.1016/S0140-1963(03)00097-1.

Elwell HA, Stocking MA. 1976. Vegetal cover to estimate soil erosion hazard in Rhodesia. *Geoderma* **15**: 61–70. https://doi.org/10.1016/0016-7061(76)90071-9.

Evans JS, Hudak AT. 2007. A multiscale curvature algorithm for classifying discrete return LiDAR in forested environments. *IEEE Transactions on Geoscience and Remote Sensing* **45**: 1029–1038.

Fang J, Chen A, Peng C, Zhao S, Ci L. 2001. Changes in forest biomass carbon storage in China between 1949 and 1998. *Science* **292**: 2320–2322. https://doi.org/10.1126/science.1058629.

Faulkner H. 2008. Connectivity as a crucial determinant of badland morphology and evolution. *Geomorphology*. Fluvial Systems: Dynamics, Morphology and the Sedimentary Record Special Issue in honour of Adrian Harvey **100**: 91–103. https://doi.org/10.1016/j.geomorph.2007.04.039.

Foerster S, Wilczok C, Brosinsky A, Segl K. 2014. Assessment of sediment connectivity from vegetation cover and topography using remotely sensed data in a dryland catchment in the Spanish Pyrenees. *Journal of Soils Sediments* **14**: 1982–2000. https://doi.org/10.1007/s11368-014-0992-3.

Foley JA, DeFries R, Asner GP, Barford C, Bonan G, Carpenter SR, Chapin FS, Coe MT, Daily GC, Gibbs HK, Helkowski JH, Holloway T, Howard EA, Kucharik CJ, Monfreda C, Patz JA, Prentice IC, Ramankutty N, Snyder PK. 2005. Global consequences of land use. *Science* **309**: 570–574. https://doi.org/10.1126/science.1111772.

Fornes WL, Whiting PJ, Wilson CG, Matisoff G. 2005. Caesium-137-derived erosion rates in an agricultural setting: the effects of model assumptions and management practices. *Earth Surface Processes and Landforms* **30**: 1181–1189. https://doi.org/10.1002/esp.1269.

Fox DM, Witz E, Blanc V, Soulié C, Penalver-Navarro M, Dervieux A. 2012. A case study of land cover change (1950–2003) and runoff in a Mediterranean catchment. *Applied Geography* **32**: 810–821. https://doi.org/10.1016/j.apgeog.2011.07.007.

Fryirs KA. 2016. River sensitivity: a lost foundation concept in fluvial geomorphology. *Earth Surf. Process*. https://doi.org/10.1002/esp.3940.

García-Ruiz JM. 2010. The effects of land uses on soil erosion in Spain: a review. *Catena* **81**: 1–11. https://doi.org/10.1016/j.catena.2010.01.001.

García-Ruiz JM, Lasanta T, Ortigosa L, Ruiz-Flaño P, Martí C, González C. 1995. Sediment yield under different land uses in the Spanish pyrenees. *Mountain Research and Development* **15**: 229–240. https://doi.org/10.2307/3673930.

Grohmann CH, Smith MJ, Riccomini C. 2011. Multiscale analysis of topographic surface roughness in the Midland Valley, Scotland. *IEEE Transactions on Geoscience and Remote Sensing* **49**: 1200–1213. https://doi.org/10.1109/TGRS.2010.2053546.

Gutiérrez F, Lizaga I. 2016. Sinkholes, collapse structures and large landslides in an active salt dome submerged by a reservoir: the unique case of the Ambal ridge in the Karun River, Zagros Mountains, Iran. *Geomorphology* **254**: 88–103. https://doi.org/10.1016/j.geomorph.2015.11.020.

Harvey AM. 2001. Coupling between hillslopes and channels in upland fluvial systems: implications for landscape sensitivity, illustrated from the Howgill Fells, northwest England. *Catena* **42**: 225–250. https://doi.org/10.1016/S0341-8162(00)00139-9.

Harvey AM. 2002. Effective timescales of coupling within fluvial systems. *Geomorphology* **44**: 175–201. https://doi.org/10.1016/S0169-555X(01)00174-X.

Heckmann T, Schwanghart W. 2013. Geomorphic coupling and sediment connectivity in an alpine catchment — exploring sediment cascades using graph theory. *Geomorphology* **182**: 89–103. https://doi.org/10.1016/j.geomorph.2012.10.033.

Hubble TCT, Docker BB, Rutherfurd ID. 2010. The role of riparian trees in maintaining riverbank stability: a review of Australian experience and practice. *Ecological Engineering* **36**: 292–304. https://doi.org/10.1016/j.ecoleng.2009.04.006.

Kawabata D, Bandibas J. 2009. Landslide susceptibility mapping using geological data, a DEM from ASTER images and an artificial neural network (ANN). *Geomorphology* **113**: 97–109. https://doi.org/10.1016/j.geomorph.2009.06.006.

Keesstra S, Pereira P, Novara A, Brevik EC, Azorin-Molina C, Parras-Alcántara L, Jordán A, Cerdà A. 2016. Effects of soil management techniques on soil water erosion in apricot orchards. *Science of the Total Environment* **551-552**: 357–366. https://doi.org/10.1016/j.scitotenv.2016.01.182.

Kosmas C, Danalatos N, Cammeraat LH, Chabart M, Diamantopoulos J, Farand R, Gutierrez L, Jacob A, Marques H, Martinez-Fernandez J, Mizara A, Moustakas N, Nicolau JM, Oliveros C, Pinna G, Puddu R, Puigdefabregas J, Roxo M, Simao A, Stamou G, Tomasi N, Usai D, Vacca A. 1997. The effect of land use on runoff and soil erosion rates under Mediterranean conditions. *Catena* **29**: 45–59. https://doi.org/10.1016/S0341-8162(96)00062-8.

Lasanta T, Nadal-Romero E, Errea P, Arnáez J. 2016. The effect of landscape conservation measures in changing landscape patterns: a case study in Mediterranean mountains. *Land Degradation and Development* **27**: 373–386. https://doi.org/10.1002/ldr.2359.

Li J, Wong DWS. 2010. Effects of DEM sources on hydrologic applications. *Computers, Environment and Urban Systems* **34**: 251–261. https://doi.org/10.1016/j.compenvurbsys.2009.11.002.

Llorens P. 1997. Rainfall interception by a *Pinus sylvestris* forest patch overgrown in a Mediterranean mountainous abandoned area II. Assessment of the applicability of Gash's analytical model. *Journal of Hydrology* **199**: 346–359. https://doi.org/10.1016/S0022-1694(96)03335-5.

López-Moreno JI, Vicente-Serrano SM, Moran-Tejeda E, Zabalza J, Lorenzo-Lacruz J, García-Ruiz JM. 2011. Impact of climate evolution and land use changes on water yield in the Ebro basin. *Hydrology and Earth Systems Sciences* **15**: 311–322. https://doi.org/10.5194/hess-15-311-2011.

Lorenzo-Lacruz J, Vicente-Serrano SM, López-Moreno JI, Morán-Tejeda E, Zabalza J. 2012. Recent trends in Iberian streamflows (1945–2005). *Journal of Hydrology* : 414–415. https://doi.org/10.1016/j.jhydrol.2011.11.023.

Marchamalo M, Hooke JM, Sandercock PJ. 2015. Flow and sediment connectivity in semi-arid landscapes in SE Spain: patterns and controls. *Land Degradation and Development* **27**: 1032–1044. https://doi.org/10.1002/ldr.2352.

Masselink RJH, Keesstra SD, Temme AJAM, Seeger M, Giménez R, Casalí J. 2016. Modelling discharge and sediment yield at catchment scale using connectivity components. *Land Degradation & Development* **27**: 933–945. https://doi.org/10.1002/ldr.2512.

MacDonald D, Crabtree JR, Wiesinger G, Dax T, Stamou N, Fleury P, Gutierrez Lazpita J, Gibon A. 2000. Agricultural abandonment in mountain areas of Europe: environmental consequences and policy response. *Journal of Environmental Management* **59**: 47–69. https://doi.org/10.1006/jema.1999.0335.

Martínez-Fernández J, Sánchez N, Herrero-Jiménez CM. 2013. Recent trends in rivers with near-natural flow regime: the case of the river headwaters in Spain. *Progress in Physical Geography* **37**: 685–700. https://doi.org/10.1177/0309133313496834.

Meyer WB, Turner BL, II (eds). 1994. Changes in land use and land cover: a global perspective. Cambridge University Press; 537.

Micheli ER, Kirchner JW. 2002. Effects of wet meadow riparian vegetation on streambank erosion. 2. Measurements of vegetated bank strength and consequences for failure mechanics. *Earth Surface Processes and Landforms* **27**: 687–697. https://doi.org/10.1002/esp.340.

Mohammad AG, Adam MA. 2010. The impact of vegetative cover type on runoff and soil erosion under different land uses. *Catena* **81**: 97–103. https://doi.org/10.1016/j.catena.2010.01.008.

Mohawesh Y, Taimeh A, Ziadat F. 2015. Effects of land use changes and soil conservation intervention on soil properties as indicators for land

Copyright © 2016 John Wiley & Sons, Ltd.

degradation under a Mediterranean climate. *Solid Earth* **6**: 857–868. https://doi.org/10.5194/se-6-857-2015.

Montealegre A, Lamelas T, de la Riva J, Fernández-Renau González-Anleo A, de Miguel Llanes E. 2013. Evaluación de Métodos de Filtrado Para la Clasificación de la Nube de Puntos del Vuelo LiDAR PNOA. *Teledetección. Sistemas Operacionales de Observación de la Tierra* : 184–187.

MOP-CHE. 1976. Memoria 1946–1975. Zaragoza, Ministerio de Obras públicas (DGOH) y Confederación Hidrográfica del Ebro.

Morán-Tejeda E, Ceballos-Barbancho A, Llorente-Pinto JM. 2010. Hydrological response of Mediterranean headwaters to climate oscillations and land-cover changes: the mountains of Duero River basin (Central Spain). *Global and Planetary Change* **72**: 39–49. https://doi.org/10.1016/j.gloplacha.2010.03.003.

Navas A, Machín J, Beguería S, López-Vicente M, Gaspar L. 2008. Soil properties and physiographic factors controlling the natural vegetation re-growth in a disturbed catchment of the Central Spanish Pyrenees. *Agroforestry Systems* **72**: 173–185. https://doi.org/10.1007/s10457-007-9085-2.

Navas A, Valero-Garcés B, Gaspar L, Palazón L. 2011. Radionuclides and stable elements in the sediments of the Yesa Reservoir, Central Spanish Pyrenees. *Journal of Soils and Sediments* **11**: 1082. https://doi.org/10.1007/s11368-011-0401-0.

Novara A, Keesstra S, Cerdà A, Pereira P, Gristina L. 2016. Understanding the role of soil erosion on co2-c loss using 13c isotopic signatures in abandoned Mediterranean agricultural land. *Science of the Total Environment.* **550**: 330–336. https://doi.org/10.1016/j.scitotenv.2016.01.0952016.

Nunes AN, de Almeida AC, Coelho COA. 2011. Impacts of land use and cover type on runoff and soil erosion in a marginal area of Portugal. *Applied Geography* **31**: 687–699. https://doi.org/10.1016/j.apgeog.2010.12.006.

O'Callaghan JF, Mark DM. 1984. The extraction of drainage networks from digital elevation data. *Computer Vision, Graphics, and Image Processing* **28**: 323–344. https://doi.org/10.1016/S0734-189X(84)80011-0.

Ortigosa LM, Garcia-Ruiz JM, Gil E. 1990. Land reclamation by reforestation in the Central Pyrenees. *Mountain Research and Development* **10**: 281–288. https://doi.org/10.2307/3673607.

Palazón L, Navas A. 2014. Modeling sediment sources and yields in a Pyrenean catchment draining to a large reservoir (Ésera River, Ebro Basin). *Journal of Soils and Sediments* **14**: 1612–1625. https://doi.org/10.1007/s11368-014-0911-7.

Panagos P, Borrelli P, Meusburger C, Alewell C, Lugato E, Montanarella L. 2015. Estimating the soil erosion cover-management factor at European scale. *Land Use Policy* **48C**: 38–50. https://doi.org/10.1016/j.landusepol.2015.05.021.

Pardo G, Arenas C. 1996. Late Oligocene-Early Miocene syntectonk fluvial sedimentation in the Aragonese Pyrenean domain of the Ebro basin: facies models and structural controls. *Journal of iberian geology: an international publication of earth sciences* **21**: 277–298.

Puigdefabregas J, Sole A, Gutierrez L, del Barrio G, Boer M. 1999. Scales and processes of water and sediment redistribution in drylands: results from the Rambla Honda field site in Southeast Spain. *Earth-Science Reviews* **48**: 39–70. https://doi.org/10.1016/S0012-8252(99)00046-X.

Quijano L, Gaspar L, Navas A. 2016. Spatial patterns of SOC, SON, 137Cs and soil properties as affected by redistribution processes in a Mediterranean cultivated field (Central Ebro Basin). *Soil and Tillage Research* **155**: 318–328. https://doi.org/10.1016/j.still.2015.09.007.

Reyes O, Delia A. 2014. Estimación de variables dasométricas mediante tecnología LiDAR. In: Tésis doctoral. Montecillo.Texcoco, Edo de Mexico.

Romanyà J, Rovira P. 2011. An appraisal of soil organic C content in Mediterranean agricultural soils. *Soil Use and Management* **27**: 321–332. https://doi.org/10.1111/j.1475-2743.2011.00346.x.

Royo M, Longares LA, de Luis M. 2015. Efecto de la gestión forestal post-incendio en la dinámica regenerativa de *Quercus ilex subsp. ballota* en la Sierra del Moncayo. XXIV Congreso de la Asociación de Geógrafos Españoles: Análisis espacial y representación geográfica: innovación y aplicación. Zaragoza 2015.

Ruiz LA. 2012. Assessment of factors affecting shrub volume estimations using airborne discrete-return LiDAR data in Mediterranean areas. *Journal of Applied Remote Sensing* **6**: 63544. https://doi.org/10.1117/1.JRS.6.063544.

Sandercock PJ, Hooke JM. 2011. Vegetation effects on sediment connectivity and processes in an ephemeral channel in SE Spain. *Journal of Arid Environments* **75**: 239–254. https://doi.org/10.1016/j.jaridenv.2010.10.005.

Sole J, Del Valle J, Ramírez J. 1972. Mapa Geológico de España escala 1:50,000. Instituto Geologico y Minero. Hoja MAGNA 207 26-10 Sos del Rey Católico.

Tarboton DG. 1997. A new method for the determination of flow directions and upslope areas in grid digital elevation models. *Water Resources Research* **33**: 309–319. https://doi.org/10.1029/96WR03137.

Teixel A, Montes M, Arenas C, Garrido E. 1992. Mapa Geológico de España escala 1:50,000. Instituto Geologico y Minero. Hoja MAGNA 207 27-10 Uncastillo.

Vaze J, Teng J, Spencer G. 2010. Impact of DEM accuracy and resolution on topographic indices. *Environmental Modelling & Software* **25**: 1086–1098. https://doi.org/10.1016/j.envsoft.2010.03.014.

Vigiak O, Borselli L, Newham L, McInnes J, Roberts A. 2012. Comparison of conceptual landscape metrics to define hillslope-scale sediment delivery ratio. *Geomorphology* **138**: 74–88.

Zuazo VHD, Pleguezuelo CRR. 2008. Soil-erosion and runoff prevention by plant covers. A review. *Agronomy for Sustainable Development* **28**: 65–86. https://doi.org/10.1051/agro:2007062.

Copyright © 2016 John Wiley & Sons, Ltd.

CHAPTER 4

Estimating soil redistribution patterns with ^{137}Cs measurements in a Mediterranean mountain catchment

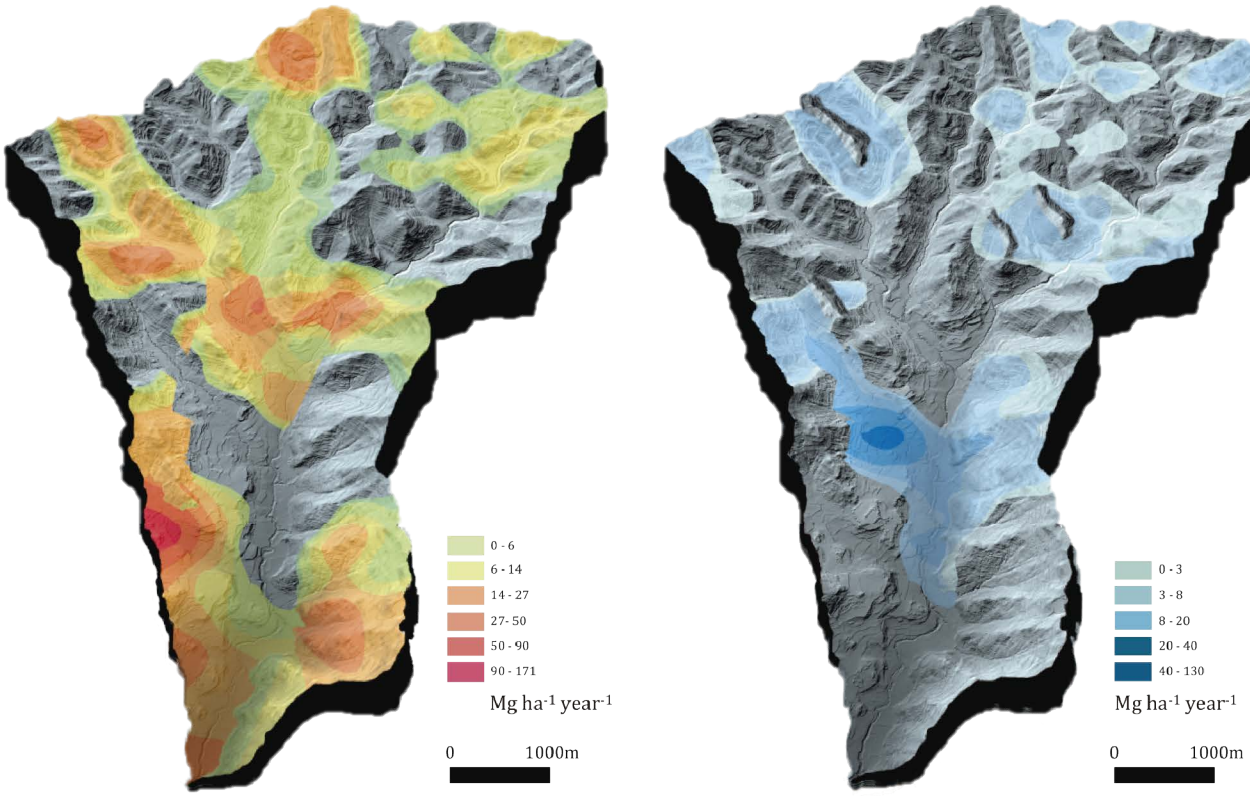

Received: 31 January 2017 | Revised: 18 October 2017 | Accepted: 26 October 2017

DOI: 10.1002/ldr.2843

WILEY

RESEARCH ARTICLE

Estimating soil redistribution patterns with ^{137}Cs measurements in a Mediterranean mountain catchment affected by land abandonment

Ivan Lizaga | Laura Quijano | Leticia Gaspar | Ana Navas

Departamento Suelo y Agua, Estación Experimental de Aula Dei, CSIC, Avenida Montañana, 1005, 50059 Zaragoza, Spain

Correspondence
A. Navas, Departamento Suelo y Agua, Estación Experimental de Aula Dei, CSIC, Avenida Montañana, 1005, 50059 Zaragoza, Spain.
Email: anavas@eead.csic.es

Funding information
Spanish Ministry of Economy and Competitiveness; TRAZESCAR, Grant/Award Number: CGL2014-52986-R; predoctoral contract, Grant/Award Number: BES-2015-071780

Abstract

In Mediterranean mountainous environments, the removal of natural vegetation for developing agriculture increased the surface areas prone to erosion in the past centuries. In Southern Pre-Pyrenees, the process was inverted during the middle of the 20th century. This work aims to assess how land use changes after widespread land abandonment affect soil redistribution. For this purpose, ^{137}Cs was used in a 23 km^2 catchment that was mostly cultivated at the beginning of the past century. After land abandonment, 16.5% of croplands persisted but afforestation and natural revegetation occupy 83.5% of the catchment area. ^{137}Cs massic activity and related soil properties—stoniness, grain size, and organic matter contents—were analysed in 98 bulk core samples. Physiographic characteristics—slope, altitude, and solar radiation—at the sampling points were determined by using Geographic Information Systems. Soil erosion and deposition rates were derived from ^{137}Cs measurements after applying conversion models and were spatially interpolated to estimate the amount of net soil loss. In cropland soils, mean erosion (62.6 Mg ha^{-1} yr^{-1}) and deposition rates (55.2 Mg ha^{-1} yr^{-1}) were significantly higher than in the other land uses. The lowest mean erosion rates (2.4 Mg ha^{-1} yr^{-1}) were found in natural forests and the lowest mean deposition (2.6 Mg ha^{-1} yr^{-1}) in pine afforestation evidencing the soil stabilization achieved in the last decades due to revegetation. A sediment budget with the interpolated rates, result in a specific sediment yield of 4.15 Mg ha^{-1} yr^{-1}. These results outline the impact of land use changes on soil redistribution in fragile mountain agroecosystems.

KEYWORDS

^{137}Cs measurements, catchment scale, erosion and deposition rates, land use changes, soil and physiographic properties

1 | INTRODUCTION

Over the past centuries human activities have been the main drivers of transformations in ecosystems by converting natural landscapes into agriculture lands (Chauchard, Carcaillet, & Guibal, 2007; Ellis et al., 2013; Ellis, Klein Goldewijk, Siebert, Lightman, & Ramankutty, 2010). The steep Mediterranean hillslopes provide a good example of such gradual transformation into terraced arable lands. Agricultural deforestation is a local and global environmental issue (Foley et al., 2005). These problems are exacerbated in fragile environments, such as the Mediterranean mountainous regions. These types of sensitive agroecosystems are prone to erosion due not only to climatic conditions but also because of the strong anthropogenic pressure exerted in these areas during the past centuries and their conversion to agriculture land (Bruun, Elberling, de Neergaard, & Magid, 2015; Colazo & Buschiazzo, 2015; Romanyà & Rovira, 2011).

The anthropogenic pressure on the soil system through farming and grazing has existed for several centuries in the central mountains of the Spanish Pyrenees. As a consequence, the natural forest was progressively cleared and replaced by croplands (Alonso-Sarría, Martínez-Hernández, Romero-Díaz, Cánovas-García, & Gomariz-Castillo, 2016). The problems that these practices have created are particularly striking in mountainous areas and in regions where agricultural land is found accompanying adverse environmental

 Copyright © 2017 John Wiley & Sons, Ltd.

conditions ı elevations, steep slopes, shallow soils and dry climatic conditions with heavy rainfall events (MacDonald et al., 2000). Conventional tillage practices disturb and erode the soil surface and expose the less fertile subsoil, which affects physical, chemical and biological soil properties. These changes can then induce loss of soil nutrients that may, over the long term, decrease the soil productivity. Furthermore, the Mediterranean climate is characterized by irregular spatial and temporal distribution of rainfall events along the year of short duration with the occurrence of very intense rainfall followed by long dry periods (Mariani & Parisi, 2014). These high intensity rainfalls have been identified as one of the main drivers causing soil loss (Martinez-Casasnovas, Ramos, & Ribes-Dasi, 2002) and increasing the erosion rates relative to tillage erosion (Quijano et al., 2017). Higher frequency of droughts and extreme storm events projected under climate change will likely produce a critical scenario in these fragile environments. Palazón and Navas (2016) simulated a scenario in a South Pyrenean catchment with a temperature increase of 2 °C. The simulations showed different responses for the different types of vegetation covers with increases in specific sediment yields for scrubland.

In the past century, the industrialization of Europe and the Common Agricultural Policy (CAP) applied, triggered socio-economic changes such as a rural exodus, the decline of traditional small-scale agriculture and pastoralism. Since the 1960s, these changes were characterised by an abandonment of marginal areas, generally situated in the mountains, where traditional land uses became progressively economically nonviable (Debussche, Lepart, & Dervieux, 1999) that leads to substantial landscape changes in the Pre-Pyrenean mountain areas (Lasanta, Nadal-Romero, Errea, & Arnáez, 2016; Quijano, Gaspar, & Navas, 2016; Navas et al., 2017). Other important indirect impacts of land abandonment are the rapid siltation of water bodies at the first stages of the abandonment before the natural revegetation growth, which decreased reservoir storage capacities. Previous investigations dealing with this issue, Valero-Garces, Navas, Machin, and de Estacion E (1997) and Navas, Valero-Garcés, Gaspar, and Machín (2009) identified increases in sediment yields and changes in erosion rates in sediment records accumulated during the last decades in the Pyrenean Barasona and Yesa reservoirs, in NE Spain. The subsequent reforestation that occurred in the 1970s and the 1980s has caused a strong reduction of run-off and sediment connectivity due to vegetation growth that protect soil from erosion (Buendia, Batalla, Sabater, Palau, & Marcé, 2016; Lizaga, Quijano, Palazón, Gaspar, & Navas, 2017).

Studies using the ^{137}Cs technique have confirmed its potential over the medium term (~50 years) for estimating soil redistribution rates (Alewell, Meusburger, Juretzko, Mabit, & Ketterer, 2014; Gaspar, Navas, Walling, Machín, & Gómez Arozamena, 2013; Mabit, Bernard, Makhlouf, & Laverdière, 2008; Navas & Walling, 1992; Sadiki, Faleh, Navas, & Bouhlassa, 2007) and for validating spatially distributed catchment erosion and sediment yield models (Collins, Walling, Sichingabula, & Leeks, 2001; Du & Walling, 2011; Mabit, Bernard, & Laverdiere, 2002; Mesrar et al., 2017; Quijano, Beguería, Gaspar, & Navas, 2016a).

Erosion rates need to be quantified to assess how relatively recent land use changes impacted on soil loss in Mediterranean agroecosystems. To date, there are only few studies using ^{137}Cs to quantify soil redistribution rates at catchment scale (Mabit & Bernard, 2007; Navas, López-Vicente, Gaspar, & Machín, 2013; Porto, Walling, Ferro, & di Stefano, 2003). Furthermore, fewer studies investigated the impact of recent land use changes on soil erosion (Evrard et al., 2010; Gaspar & Navas, 2013; Gharibreza et al., 2013; Navas, López-Vicente, Gaspar, Palazón, & Quijano, 2014). Accordingly, we quantify soil redistribution rates using fallout ^{137}Cs measurements and Geographic Information Systems to investigate changes in spatial variability of soil redistribution patterns resulting from land use change associated with vegetation cover in the recent decades. This research would contribute to a better understanding of soil redistribution dynamics in agricultural mountain landscapes and its effect on some of the main soil properties.

2 | MATERIALS AND METHODS

2.1 | The study catchment

The Barués study area (23 km^2) is an ephemeral stream catchment included in the Arba catchment located in the central part of the Ebro Basin (NE Spain; Figure 1). Rock outcrops in the catchment include two conformable Oligo–Miocene lithostratigraphic units of the Uncastillo Formation dominated by sandstones (Tirapu & Arenas, 1996). The geomorphological setting is clearly conditioned by the low angle dip of the bedding setting up the path of the streams following the strike of the beds. The climate is Continental–Mediterranean characterized by cold winters and hot and dry summers. Rainfall events mainly occur in spring (April and May) and autumn (September and October) and summer droughts occur between these two humid periods. The area is subject to very intense, though sometimes localized storms. The mean annual temperature is 13.4 °C and the mean annual rainfall is about 500 mm (recorded since 1929 in Yesa reservoir; Agencia Estatal de Meteorología). The most abundant soils in the catchment were classified by Machín (Estación Experimental de Aula Dei-Consejo Superior de Investigaciones Científicas) from field surveys (personal communication) as Calcisols and Cambisols (FAO, 2015). The soils developed on Quaternary deposits mainly composed by alluvial deposits that have basic pH, low soil organic carbon contents (1.5%), and secondary accumulation of carbonates.

The largest part of the Barués catchment was cultivated at the start of the 20th century. In the 1960s, 58% of the area was farmland. Of the total 13.5 km^2 that was cultivated, as much as 10.2 km^2 (75%) of the agricultural land had been abandoned for more than 50 years at the time of sampling. At present, only 16.5% of the catchment is still cultivated whereas afforestation and natural revegetation areas occupy the remaining 83.5% (Lizaga et al., 2017). The main land uses are agricultural (16%), pine afforestation (19%), natural forest, and scrubland (50%). The main crops are winter cereals (*Triticum aestivum* and *Hordeum vulgare* L.). The pine afforestation is mainly composed of *Pinus halepensis* Mill. with a mean tree cover density of 70% L. (Copernicus Land Monitoring Services). The natural forest and the scrubland are typical Mediterranean and are intermixed in many areas. They are mainly composed of *Quercux ilex* L.,

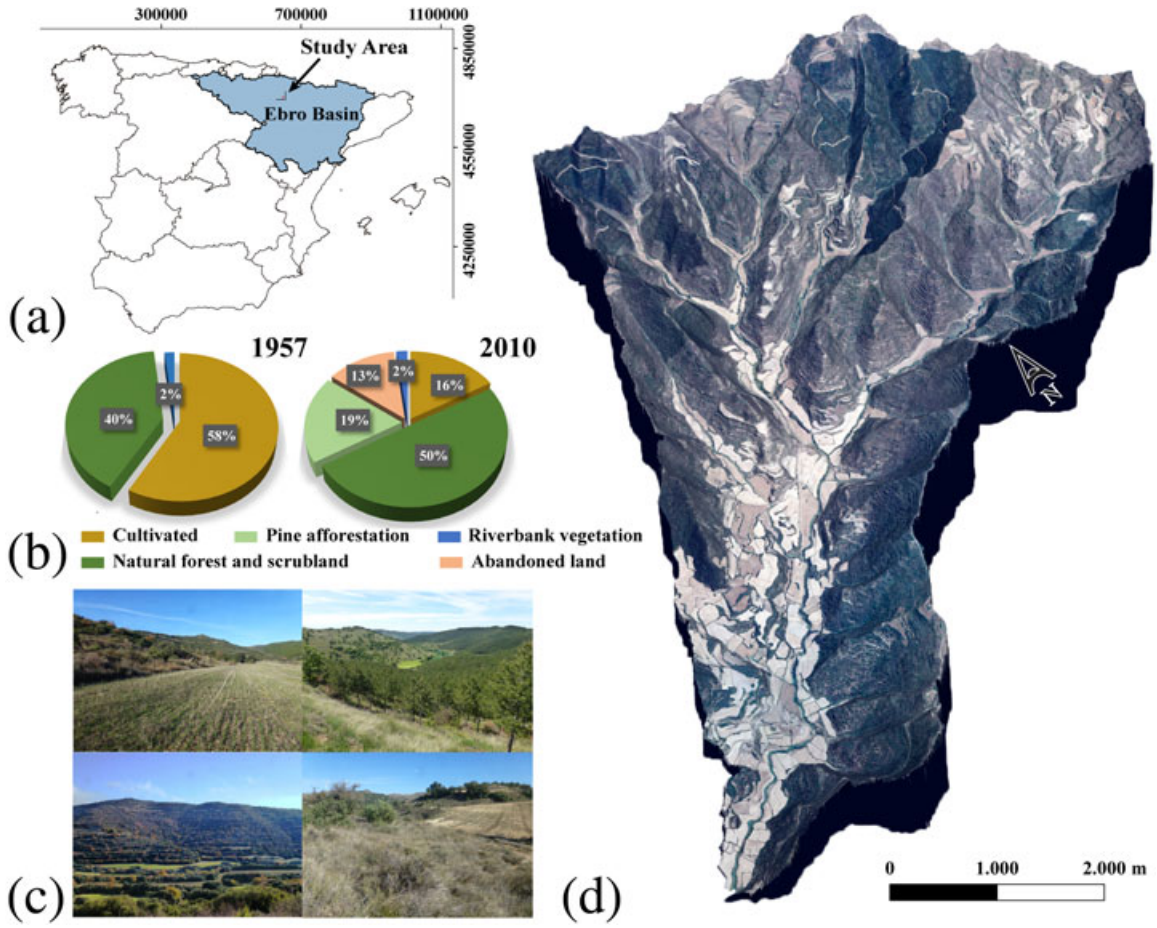

FIGURE 1 (a) Location of the study catchment in the central part of the Ebro Basin (NE Spain). (b) Percentage of the different land uses in 1957 and 2016. (c) Pictures of the main land uses in the study catchment. (d) 3D picture of Barués catchment created with a DEM and an orthophoto (National Plan of Aerial Orthophotography, Instituto Geográfico Nacional) [Colour figure can be viewed at wileyonlinelibrary.com]

Quercus coccifera L., *Rosmarinus officinalis* L., *Genista scorpium* (L.) DC. and *Juniperus communis* L. The scrubland is in the successional stages of natural revegetation and in the transition for becoming a Mediterranean forest.

Since 1957, a decrease in agricultural land and a transition to natural and revegetated cover have been documented (Figure 1). There has been a decrease in the number of individual cultivated fields but a trend for those fields to increase in size (Figure 2). The change in

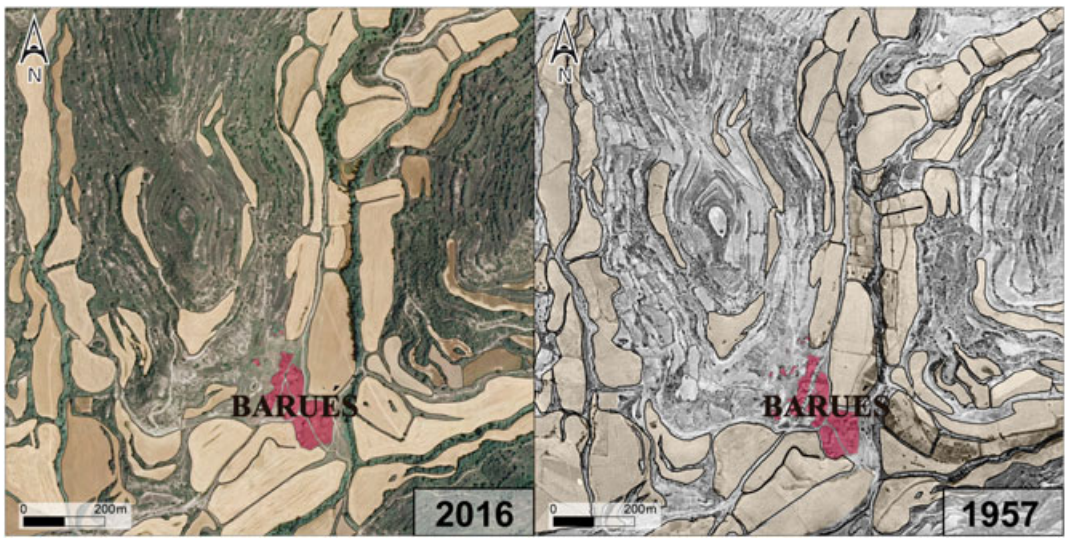

FIGURE 2 Comparison of the variations in size of the cultivated fields (delineated) between 2012 (left picture, Instituto Geográfico Nacional orthophoto) and 1957 (right picture, American aerial photograph) of an area located at the central part of the catchment [Colour figure can be viewed at wileyonlinelibrary.com]

size and number of fields may be a farmer's attempt to increase the efficiency of production through a decrease in the cost and the quantity of inputs utilized.

2.2 | Soil sampling

In 2013, 98 bulk core soil samples were collected. A motorized percussion corer equipped with a steel core-tube with 40.7-cm^2 surface area was used to collect two replicates of bulk soil samples at each sampling point from the surface until a depth varying from 20 to 54 cm depending on the local soil thickness.

The sampling points were distributed proportionally across the catchment surface using a previous 500 × 500 m grid created in Geographic Information Systems software to proportionally represent the percentage of surface occupied by the different land uses with a sampling density of 0.23 km^2 per sample. The grid location was preserved as much as possible although the cores were also taken in representative locations to characterize the condition and properties of the surrounding soil within that land use avoiding recently highly disturbed areas. For each sampling point data on land use, slope angle, altitude and solar radiation were recorded.

2.3 | Sample analysis and soil redistribution estimates

The two soil cores from each sampling site were mixed in the field and air-dried, grinded, homogenised, and sieved to ≤2 mm. The fraction >2 mm was weighed to account for the stone content. Particle size, soil organic matter (SOM), and ^{137}Cs were analysed in the ≤2-mm fraction for the 98 soil samples. The Beckman Coulter LS 13320 laser diffraction particle size analyser was used for grain size analysis. Prior to particle size measurements, the samples were mixed with H_2O_2 (10%) and heated (80 °C) to remove the organic fraction. Samples were then chemically dispersed with 2 ml of sodium hexametaphosphate (40%), stirred for 2 hr, and sonication was applied for a few minutes to facilitate dispersion.

SOM was estimated by multiplying SOC content by the Van Bemmelen conversion factor (1.724), assuming that organic matter contains 58% organic carbon. SOC was analysed by the dry combustion method using a LECO RC-612 multiphase carbon analyser. The methodology followed for ^{137}Cs analysis is widely described in the literature (Walling & Quine, 1991). The massic activity of ^{137}Cs was measured at the gamma lab of the Experimental Station of Aula-Dei (EEAD-CSIC, Spain) using a high resolution, low energy background, and coaxial high-purity germanium gamma-ray detector coupled to an amplifier and multichannel analyser. The detector had an efficiency of 50% and a 1.9-keV resolution at 1.33 MeV (^{60}Co; shielded to reduce background) and was calibrated using standard soil samples placed in containers of the same geometry as the measured samples. Gamma emission of ^{137}Cs was measured at the 661.6-keV photopeak and counted for 86,400 s. The analytical precision of the measurements was approximately ±3–5% at the 95% level of confidence, with a detection limit of 0.3 Bq kg^{-1}. The content of ^{137}Cs was expressed as a concentration or massic activity (Bq kg^{-1}) and as activity per unit area or inventory (Bq m^{-2}). The inventory was calculated using the mass of the fine fraction and the cross section of the core sampler (Navas, Machín, & Soto, 2005).

The values of ^{137}Cs inventory or areal activity density associated with the 98 individual sampling points were converted into estimates of soil redistribution rates (Mg ha^{-1} yr^{-1}) by using Soto and Navas (2004) and Soto and Navas (2008) conversion models for uncultivated and cultivated soils, respectively. The models compare the measured inventory with the local reference inventory and determine the erosion or deposition rate required to account for the depletion or increase of the measured inventory, relative to the reference inventory.

For uncultivated soils, the model is compartmental and divides the soil into horizontal layers of 1-cm thickness with homogeneous ^{137}Cs distribution in each compartment. A ^{137}Cs linear transference between each pair of successive compartments is supposed, whereby the isotope flux is proportional to the difference in concentration between the two compartments, the proportionality constant being a specific coefficient "k" extracted from reference profiles. In addition to the downward movement, the model also takes into account the ^{137}Cs deposition on the surface. The increases or decreases in concentration level due to ^{137}Cs fluxes are corrected by a factor accounting for the volume of the layers. This volume is taken as the working volume for ^{137}Cs adsorption, which is considered to be the same as that occupied by the soil fraction less than 2 mm.

For ploughed soils, the model has just one compartment that extends from the soil surface to a given cultivation depth (20–25 cm in the study area) and assumes a temporal evolution of the ^{137}Cs concentration in the compartment. The ^{137}Cs activity deposited is homogeneously distributed in the compartment within its effective volume.

In order to establish the local reference inventory for the study catchment, two areas were identified as reference sites in flat undisturbed locations under stable soil conditions, where neither erosion nor deposition was expected to have occurred. At these reference sites, 21 soil samples were collected with depths ranging from 25 cm up to 40 cm until the parent material was reached (sandstone strata). Sampling was done using a 40.7-cm^2 surface area automatic steel core driller, and five profiles were sectioned in 5-cm increments in order to study the vertical distribution of ^{137}Cs. These soil profiles have been reported in Quijano et al. (2016b). The reference sites were selected to cover both the upper and lower parts of the catchment in order to account for catchment-scale variability in the reference inventory (Navas et al., 2007; Porto, Walling, & Callegari, 2011).

The statistics of results were analysed using R. Pearson's correlation coefficients analyses were used to assess the relationships between SOM, grain size, ^{137}Cs activity and inventory, and topographic factors. A discriminant function analysis (DFA) was implemented with R software to identify the variables that better discriminate between the land use groups. A one-way analysis of variance was performed to assess if erosion and deposition rates were different in function of the land uses. An ordinary kriging with constant trend was selected to model the spatial distribution of the soil redistribution rates at the catchment scale and to spatially represent the erosion and deposition areas (Table 4). The kriging analysis was implemented for the two more homogenous land use distributions separately: the central area

(18.2%) with a predominant agricultural use (95%) and the rest of the catchment (81.8%) covered by scrubland and forests. To implement the kriging method, we removed eight points in an area located in the NE part of the catchment that had low variability (Table 4). This approach was justified by the different soil redistribution variances between both areas.

3 | RESULTS

3.1 | Soil and physiographic characteristics of the catchment

Most agricultural fields are located in the middle part of the catchment at the lowest altitudes. The scrubland and forest had similar slopes and altitudes although the pine afforestation areas occupy the highest altitudes with steep slopes.

Soils were alkaline, nonsaline, and calcareous. The coarse fraction content varied from 0% to 36% whereas the SOM contents were low ranging from 0.37 in agricultural land up to 5.93% in scrubland. Most soil samples (64%) had a silt-loam texture with proportions of silt varying between 47% and 60%. Twenty-one percent of the soil samples had a loam texture, 14% had a sandy-loam texture, and the remaining 1% with a 78% of sand had loamy sand texture. More than 75% of the ^{137}Cs massic activity values ranged between 1 and 7 Bq kg^{-1}, and 75% of the ^{137}Cs inventory data varied from 1,000 to 3,000 Bq m^{-2} (Table 1).

Only a small number of the investigated properties were significantly correlated (Table 2). ^{137}Cs was directly correlated with the coarse fraction ($p \leq .01$) and most strongly ($p \leq .001$) with the organic matter. The SOM was also significantly and directly correlated ($p \leq .05$) with the topographic properties, including altitude and slope although negative correlations were found with solar radiation ($p \leq .05$).

The mean values of altitude, slope, SOM, and ^{137}Cs activity in the agricultural land significantly differed from those under the other land uses ($p \leq .01$; Table 3). In croplands, the ^{137}Cs activity and SOM were lower and significantly different from those under the other land uses for both erosion and deposition points, with the largest differences in deposition points (Table 5). Forest and scrubland had mean altitude and slope significantly different ($p \leq .001$) from agricultural that occupied the gentle lowlands and pine afforestation located at higher altitudes with steeper slopes. Although no significant differences were found in the mean clay, silt, and sand contents among the different land uses, the agricultural soils were characterised by significantly different ($p \leq .05$) smaller means in the coarse fraction at erosion points.

At erosion sites, the means of ^{137}Cs massic activity under pine and scrubland were significantly lower ($p \leq .05$) than in natural forest. In scrubland and natural forest, the mean of SOM was significantly lower ($p \leq .05$) from that in deposition sites of pine afforestation.

The DFA including stoniness, clay, SOM, altitude, slope, and solar radiation as selected variables showed better results for erosion (62%) and deposition (83%) samples, when tested separately. In contrast, for

TABLE 1 Basic statistics of the different properties found in soils of Barués catchment

	Altitude (m)	Slope (°)	Solar radiation (WH m^{-2})	Stoniness (%)	Clay (%)	Silt (%)	Sand (%)	SOM (%)	^{137}Cs activity (Bq kg^{-1})	^{137}Cs inventory (Bq m^{-2})
Median	764.68	12.80	6,059.90	7.70	8.60	53.40	38.50	2.57	3.70	1,314.80
Mean	756.51	14.83	5,952.71	9.27	8.93	53.39	37.68	2.50	3.90	1,355.10
SD	98.57	9.03	3,41.17	8.49	2.42	9.69	11.51	1.25	2.40	722.7
Max	932.74	43.37	6,393.00	36.45	17.50	81.70	78.00	5.93	9.6	4,230.91
Min	554.90	1.27	4,724.50	0.00	3.80	18.20	5.90	0.37	0.00	0.00
CV	0.13	0.61	0.06	0.92	0.27	0.18	0.31	0.50	0.61	0.55

Note. CV =coefficient of variation; SD = standard deviation; SOM = soil organic matter.

TABLE 2 Pearson correlation coefficients between soil and physiographic properties at the sampling points

n = 98	Altitude (m)	Slope (°)	Solar radiation (WH m^{-2})	Stoniness (%)	Clay (%)	Silt (%)	Sand (%)	SOM (%)	^{137}Cs activity (Bq kg^{-1})
Altitude									
Slope	0.0442								
Solar radiation	**0.2642**	***−0.7449***							
Stoniness	***0.4484***	0.1297	0.0694						
Clay	−0.0042	**−0.2171**	0.1208	***−0.3686***					
Silt	−0.0462	−0.1	0.028	***−0.4539***	***0.6951***				
Sand	0.0396	0.1298	−0.049	***0.4598***	***−0.796***	***−0.9885***			
SOM	**0.252**	**0.241**	**−0.2095**	**0.2942**	−0.1061	−0.1527	0.1507		
^{137}Cs activity	**0.2434**	**0.2757**	**−0.2178**	**0.3248**	−0.1157	−0.1356	0.1385	***0.6068***	
^{137}Cs inventory	0.0424	0.0798	−0.0768	0.0712	−0.0053	−0.0468	0.0405	**0.2881**	**0.7825**

Bold numbers indicate statistical significance at $p \leq .05$ level. Bold and underlined numbers indicate statistical significance at $p \leq .01$. Bold, underlined, and italicized numbers indicate statistical significance at $p \leq .001$. SOM = soil organic matter.

TABLE 3 Basic statistics of the soil properties and physiographic characteristics of the sampling points under the different land uses in the study catchment

		n	Altitude (m)	Slope (°)	Solar radiation (WH/m^2)	Stoniness (%)	Clay (%)	Silt (%)	Sand (%)	SOM (%)	^{137}Cs activity (Bq kg^{-1})	^{137}Cs inventory (Bq m^{-2})
Agricultural	Median	20	671.84	5.85	6113.40	3.91	8.75	54.85	35.85	1.17	1.98	1427.47
	Mean		690.30	7.51	6129.94	5.32	9.12	53.38	37.51	1.37	2.20	1558.72
	SD		93.31	4.19	84.09	6.17	2.94	9.93	12.12	0.64	1.60	943.66
	Max		847.32	20.24	6333.60	23.03	17.50	65.50	78.00	3.62	7.98	4230.91
	Min		554.90	2.20	6015.20	0.00	3.80	18.20	23.00	0.66	0.00	0.00
	CV		0.14	0.56	0.01	1.16	0.32	0.19	0.32	0.47	0.73	0.61
Forest	Median	15	768.62	20.21	5901.90	9.28	9.20	52.30	39.40	2.98	5.68	1696.19
	Mean		750.65	17.75	5843.61	10.79	9.24	51.87	38.88	3.06	5.86	1718.91
	SD		93.21	7.07	228.11	7.41	2.06	8.42	9.38	0.83	2.03	591.30
	Max		863.36	25.67	6237.60	23.60	14.50	71.60	54.20	4.29	9.50	2970.45
	Min		557.04	2.65	5384.20	2.62	6.20	38.90	17.50	1.55	2.35	821.29
	CV		0.12	0.40	0.04	0.69	0.22	0.16	0.24	0.27	0.35	0.34
Pine	Median	15	826.64	19.43	6066.10	11.06	8.00	47.40	44.10	3.43	5.25	1446.03
	Mean		828.53	20.25	6012.70	12.45	7.93	50.23	41.84	3.15	4.33	1212.15
	SD		61.71	9.49	286.60	9.48	2.17	11.12	13.05	1.28	2.94	799.52
	Max		932.74	35.71	6350.40	35.84	13.30	71.80	65.30	4.90	9.55	2669.63
	Min		706.39	6.82	5419.70	1.65	3.90	30.80	14.90	0.67	0.00	0.00
	CV		0.07	0.47	0.05	0.76	0.27	0.22	0.31	0.41	0.68	0.66
Scrubland	Median	40	757.04	13.98	6049.65	7.86	8.65	53.65	37.90	2.73	3.94	1211.81
	Mean		763.41	15.27	5894.21	9.44	9.07	54.85	36.08	2.60	3.86	1172.96
	SD		96.07	9.19	419.03	8.93	2.36	9.49	11.34	1.26	2.12	592.39
	Max		926.37	43.37	6393.00	36.45	16.60	81.70	58.60	5.93	9.19	2545.57
	Min		583.05	1.27	4724.50	0.00	5.70	34.60	5.90	0.37	0.00	0.00
	CV		0.13	0.60	0.07	0.95	0.26	0.17	0.31	0.48	0.55	0.51

Note. CV =coefficient of variation; SD = standard deviation; SOM = soil organic matter.

TABLE 4 Mean values of soil properties and physiographic characteristics at erosion/deposition points under the different land uses

	n	Altitude (m)	Slope (°)	Solar radiation (WH m^{-2})	Stoniness (%)	Clay (%)	Silt (%)	Sand (%)	SOM (%)	^{137}Cs activity (Bq kg^{-1})	^{137}Cs inventory (Bq m^{-2})
Erosion											
Agricultural	11	689.37	5.38	6,110	4.21	8.75	52.46	38.80	1.19	1.42	986.54
Forest	7	734.60	16.39	5,781	11.40	9.57	51.07	39.36	3.21	4.35	1,223.49
Pine	8	847.13	15.76	5,982	13.16	8.10	51.31	40.59	2.74	2.78	717.27
Scrubland	36	759.71	17.06	5,828	9.30	9.14	54.81	36.05	2.53	3.00	936.22
Deposition											
Agricultural	9	691.45	6.53	6,154	5.68	9.58	54.50	35.92	1.58	3.15	2,258.04
Forest	8	764.70	12.67	5,897	10.26	8.95	52.58	38.46	2.92	7.18	2,152.40
Pine	6	800.63	12.60	6,044	11.38	7.68	48.60	43.72	3.76	6.67	1,954.47
Scrubland	12	774.52	15.99	6,090	9.85	8.85	54.98	36.17	2.82	6.44	2,070.29

Note. SOM = soil organic matter.

TABLE 5 Main kriging properties for both agricultural and scrubland and forest areas

	Range	Nugget	Partial sill	Area (km^2)	*n*
Agricultural	4,994	207	0	4.2	18
Scrubland and forests	8,464	0.5	0.04	18.9	72

the whole sample dataset, only 55% of the samples were correctly classified. When ^{137}Cs activity was included in the classification method, the percentages of correctly classified samples increased to 61% over the whole dataset, 72% for the eroding sites alone, and 91% for the deposition sites (Figure 3).

3.2 | Spatial patterns of soil redistribution

The ^{137}Cs reference inventory for the study area was 1,507 ± 92 Bq m^{-5} estimated based on 21 bulk and sectioned reference profiles (Quijano et al., 2016b). The allowable error was 6.1% at the 95% confidence level (Mabit et al., 2012). As much as 64% of the observations had ^{137}Cs inventories values ranging from 0 to 1,505 Bq m^{-2} that were lower than the local reference inventory. The remaining 36% observations were enriched in ^{137}Cs (range: 1,533 to 4,230 Bq m^{-2}).

The estimated mean soil redistribution rates for Barués catchment were 23.5 and 16.5 Mg ha^{-1} yr^{-1} for erosional and depositional sites, respectively. Figure 4 represents the magnitude and the spatial

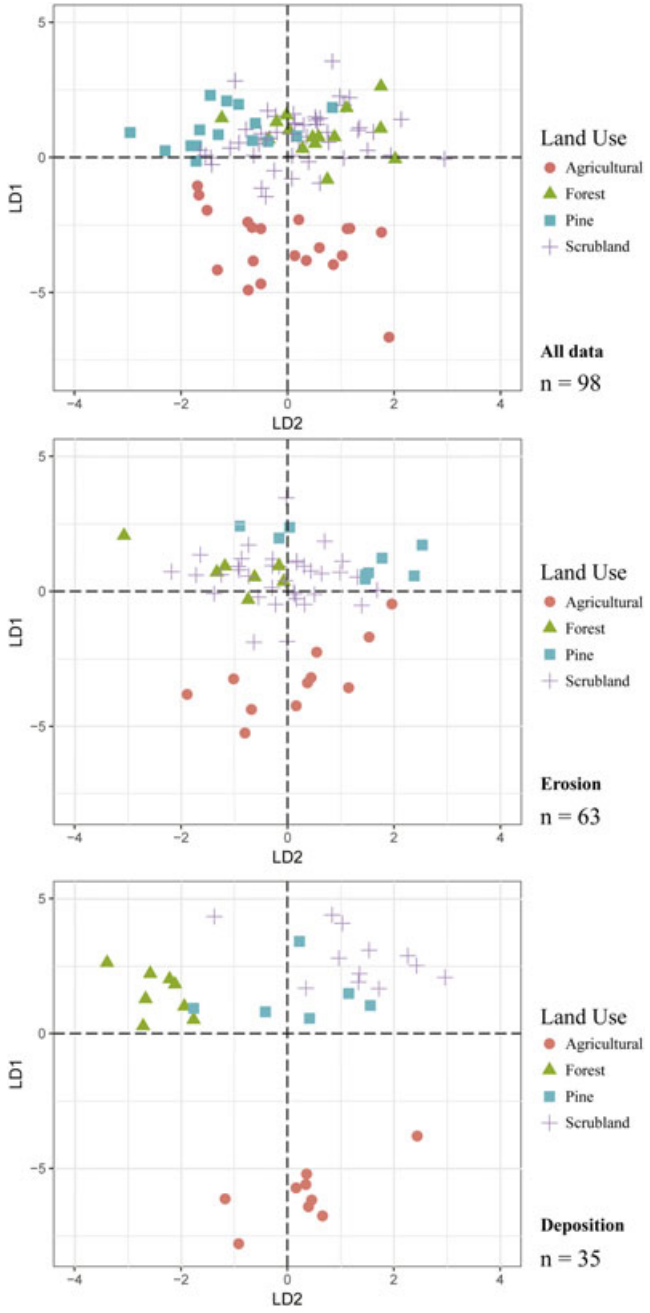

FIGURE 3 Discriminant function analysis for all study points and for erosion and deposition points in the catchment [Colour figure can be viewed at wileyonlinelibrary.com]

variability of the erosion and deposition rates estimated for the individual sampling points over the different land uses. Both erosion and deposition rates were higher in the central axis of the catchment and in the north at the headwaters whereas a lower soil redistribution rate was found in the eastern part of the catchment despite its steeper slopes.

The highest mean erosion and deposition rates were found in agricultural land whereas the lowest were estimated in natural forest. Soil redistribution ranged between 171.4 to 130.45 Mg ha^{-1} yr^{-1} in erosion and deposition agricultural sites. In forest, erosion and deposition rates ranged between 6.79 to 8.1 Mg ha^{-1} yr^{-1}, respectively.

An analysis of variance showed the occurrence of significant differences between the mean erosion/deposition rates ($p \leq .001$) under cropland versus the other land uses (Figure 5). A significant difference ($p \leq .05$) was also found between the naturally revegetated forest and the pine afforestation, although no significant differences were found between them and the scrubland in the deposition rates.

The kriging analysis identified that the catchment had up to 76% of its surface area affected by erosion whereas deposition occurred in the remaining 24% (Figure 6).

Estimates using the mean soil redistribution values over the isolevel areas extracted from the kriging for the whole catchment amounted to a net soil loss of 9,583 Mg yr^{-1} and specific sediment yield of 4.15 Mg ha^{-1} yr^{-1}. The central area with a predominant agricultural use had a net soil loss more than three-times higher than that under scrubland and forest areas (Table 6).

4 | DISCUSSION

4.1 | Soil and physiographic characteristics in the different land uses

The results have shown significant differences in all soil properties but not in grain size under cropland compared to the other land uses, indicating that this land use is one of the main factors contributing to soil erosion after five decades of land abandonment (Figure 1). The gentler slopes predominating in croplands correspond to a selection of flat terrains not only to facilitate tillage practices, sowing, and harvest but also to limit erosion as much as possible. For this reason, the values of altitude, slope, solar radiation, stoniness, SOM, and ^{137}Cs activity in the agricultural land differ from the other three land uses.

The absence of significant correlations between ^{137}Cs and the clay fraction is probably due to the limited range of clay contents (80% of the samples had clay content between 5% and 10%). This result is in agreement with those found in other Pre-Pyrenean catchments by Gaspar and Navas (2013) and by Quijano et al. (2016) in a 1.6-ha cultivated field located in this catchment.

The mobility of ^{137}Cs in soils is primarily controlled by highly selective sorption onto clay mineral surfaces that mostly occurs at the broken edges of the illitic-type clay minerals (Kim et al., 2006; Sawhney, 1970; Staunton, Dumat, & Zsolnay, 2002). However, SOM is also important in the adsorption of ^{137}Cs, which is supposed to produce a non-specific but a highly efficient mechanism for fixing the radionuclide (Rigol, Vidal, & Rauret, 2002). Moreover, the higher concentration of ^{137}Cs in the fine fraction of stony soils leads to good correlation between both, stoniness and the radionuclide concentration (Gaspar & Navas, 2013; Zhang, Long, Yu, & An, 2014). Higher stone volume and consequently lower clay volume results in a higher radionuclide concentration. Likewise, the distribution of the land uses across the catchment may also play a role in the high correlation between ^{137}Cs activity and stoniness. For example, agricultural lands occupy the lowest altitudes and have lower percentages of stoniness, SOM, and ^{137}Cs activity. This pattern is generally reported in different environments where zones with higher percentages of vegetation cover are related to high ^{137}Cs

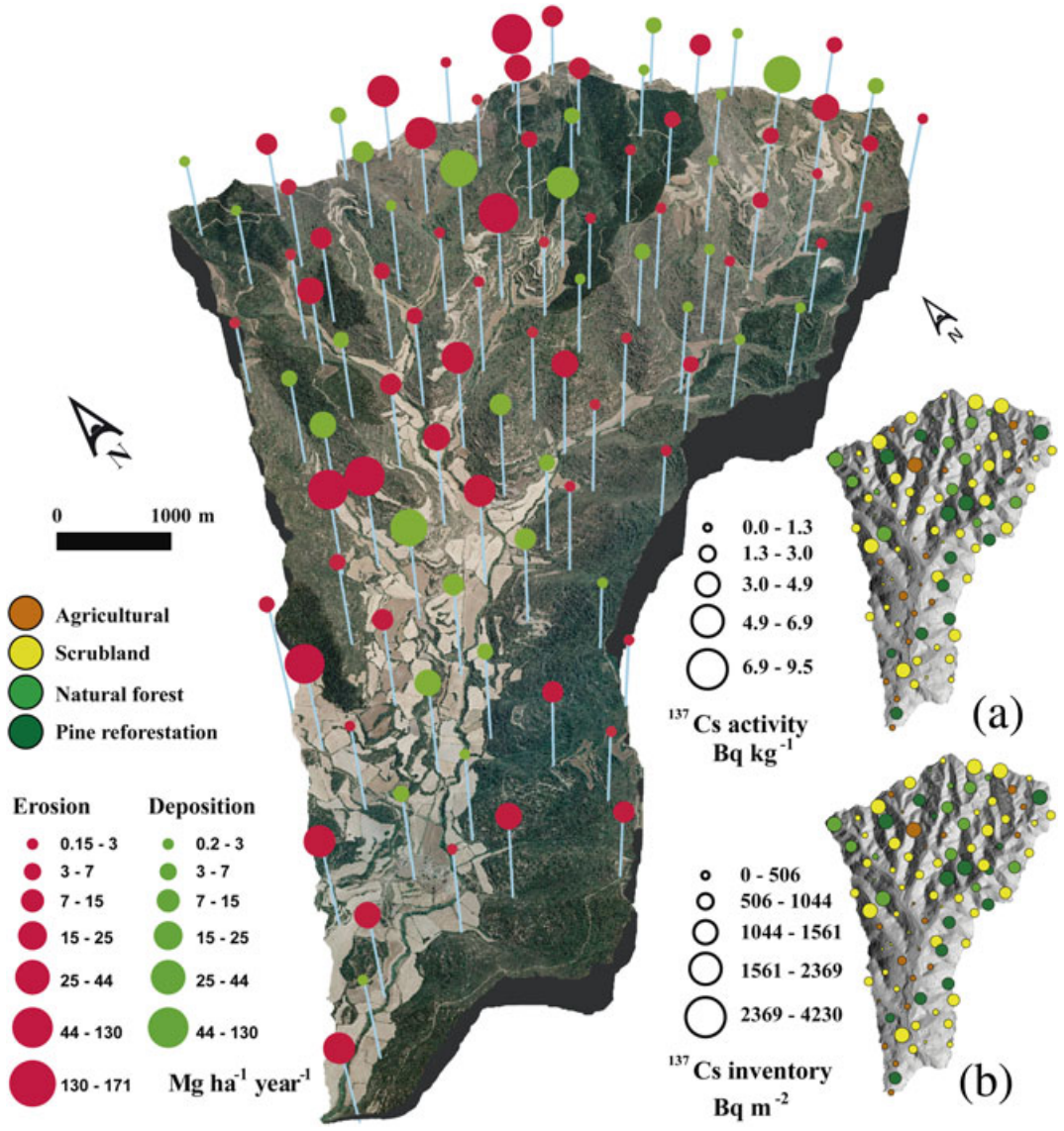

FIGURE 4 Soil redistribution rates at the sampling points of the Barués catchment under the different land uses. Rates are estimated from ^{137}Cs activities (a) and inventories (b) after applying conversion models [Colour figure can be viewed at wileyonlinelibrary.com]

activities (Fukuyama, Onda, Takenaka, & Walling, 2008; Navas, Gaspar, López-Vicente, & Machín, 2011; Schoorl, Boix Fayos, de Meijer, van der Graaf, & Veldkamp, 2004) and lower soil redistribution rates (Navas et al., 2014). In addition to the accumulation of fine particles at the bottom of hillslopes where most cultivated fields are located, tillage practices contribute to the breakdown of soil aggregates. Moreover, the manual clearing of stones to improve the conditions of the cultivated fields also contributes to the reduction of stoniness. Accordingly, higher stoniness is found at higher elevations where the natural and afforested areas dominate.

The higher SOM content in pine afforested and natural forest areas are due to the higher density of the vegetation cover and greater size of the trees resulting in larger aerial biomass. The lower SOM content in scrubland are likely because of the less mature plants. In general, scrub areas were abandoned more recently than natural forest areas, although poorer soil conditions at the time of abandonment cannot be totally excluded. Both ^{137}Cs and SOM were the lowest under cropland, which could both be related to the higher erosion rates that lead to the preferential export of fine particles enriched in ^{137}Cs and organic matter (Navas et al., 2014). Our spatial analysis indicated a similar distribution of ^{137}Cs and SOM suggesting both are influenced by similar redistribution processes. A similar result was found by Navas et al. (2011) and Quijano et al. (2016b) in similar environments.

The positive correlation of SOM with slope and altitude and the negative correlation with the solar radiation have also been observed by several authors in other mountainous areas (Dorji, Odeh, & Field, 2014; Ohtsuka et al., 2008). Altitude and slope correlate with SOM because of the past and present spatial distribution of the cultivated fields. The lands that were first abandoned were located in highest and steepest areas that are the farthest and the less accessible from the village. The early abandonment of these higher areas as cultivated fields and their subsequent revegetation likely contributed to their higher organic matter increment (Navas, Gaspar, Quijano, López-Vicente, Machín, 2012).

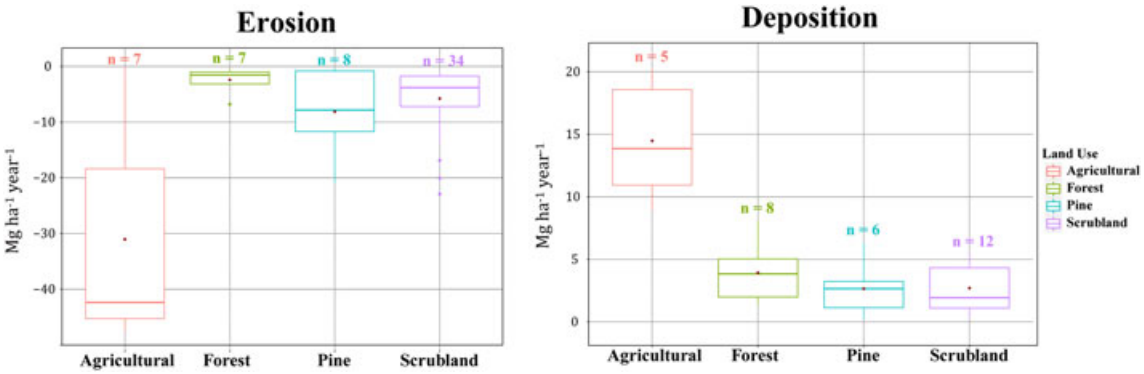

FIGURE 5 Boxplots of the soil redistribution rates under the different land uses over erosion and deposition areas in Barués catchment [Colour figure can be viewed at wileyonlinelibrary.com]

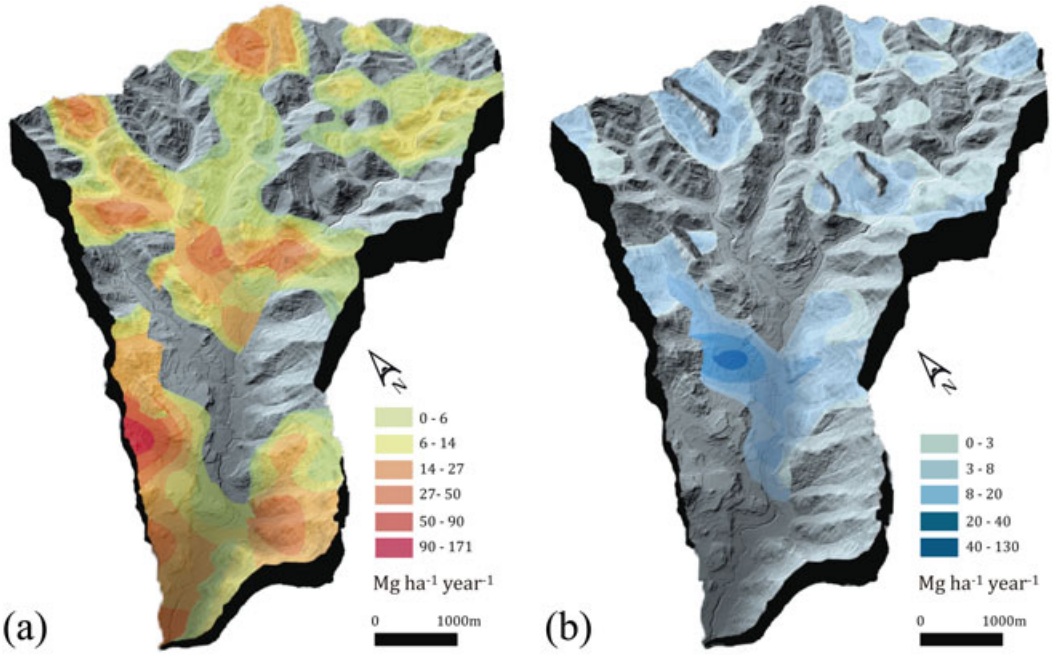

FIGURE 6 Spatial distribution of the erosion (a) and deposition (b) rates and the corresponding isocurves in the study catchment [Colour figure can be viewed at wileyonlinelibrary.com]

The inverse correlation of SOM with solar radiation is probably explained by the fact that in the less radiated areas, the temperature is lower and leads to higher levels of moisture and available water, and thus aids the increment of the aerial biomass (Lizaga et al., 2017). The correlation of stoniness with altitude and the inverse correlation of the slope with clay content were dependent on the land use distribution. However, higher erosion rates occurring on steeper slope areas also facilitate the movement of the fine grain particles.

The DFA analysis showed the usefulness of using ^{137}Cs to discriminate between different land uses. The lower discrimination percentage between forest and scrubland is probably explained by the fact that natural forest in many areas is intermixed with scrubland and its characteristics are not so different with woodlands in this intermediate successional status of the vegetation cover. Other tracers as compound-specific stable isotopes may offer potential to further discriminate among vegetation covers. This technique has been successfully tested in recent research to discriminate land uses as sediment sources (Alewell, Birkholz, Meusburger, Schindler Wildhaber, & Mabit, 2016; Blake, Ficken, Taylor, Russell, & Walling, 2012; Upadhayay et al., 2017) in different parts of the world.

4.2 | Soil redistribution rates

The principal factor affecting the soil redistribution rates is the change of land use that occurred in the last decades. This leads the significant differences in the means of soil redistribution ($p \leq .01$) between cropland and the other land uses found in both deposition and erosion areas (Table 3). In agreement with these findings, Navas et al. (2013) also found the highest rates of soil redistribution under cropland, whereas the lowest rates were found on forests and scrubland in nearby catchments. The key role of agriculture as the main driver of soil erosion is recognized in a variety of environments (Mabit et al., 2002; Navas et al., 2014; Navas & Walling, 1992; Quine, Navas, Walling, & Machin, 1994). In addition, the significant higher erosion

TABLE 6 Ranges of the isolevels curves of soil redistribution rates in erosion and deposition areas used to estimate the net soil loss and gain in the catchment

		Soil redistribution rates			Area	Areal value	
		Maximum	Minimum	Mean	ha	Mg yr^{-1}	Mg ha^{-1} yr^{-1}
Agricultural	Erosion areas	170.0	152.9	161.4	1.5	240.0	
		152.9	88.6	120.7	9.8	1,182.8	
		88.6	50.5	69.6	16.8	1,169.3	
		50.5	27.7	39.1	47.8	1,867.7	
		27.7	14.2	21.0	101.5	2,131.7	
		14.2	6.2	10.2	67.0	685.4	
		6.2	1.4	3.8	40.8	155.8	
	Total soil loss					7,192.7	25.4
	Deposition areas	−0.4	7.6	2.6	40.4	104.3	
		6.6	20.1	13.4	64.6	862.1	
		20.1	42.8	31.5	26.6	837.9	
		42.8	130.8	61.9	6.3	389.7	
	Total soil deposition					2,194.0	17.0
					Net soil loss	4,844.5	
				Specific sediment yield			8.3
Scrubland and forest	Erosion areas	22.9	11.2	17.0	89.1	1,516.6	
		11.2	5.8	8.5	240.2	2,032.5	
		5.8	3.3	4.5	270.1	1,224.8	
		3.3	2.2	2.7	232.7	635.8	
		2.2	1.6	1.9	111.6	212.7	
		1.6	1.4	1.5	73.5	112.3	
		1.4	0.9	1.1	134.1	153.9	
		0.9	0.0	0.4	282.4	90.9	
	Total soil loss					5,979.6	5.2
	Deposition areas	0.2	2.7	1.5	312.9	463.0	
		2.7	8.1	5.4	143.8	778.0	
	Total soil deposition					1,241.0	2.7
					Net soil loss	4,738.6	
				Specific sediment yield			2.5

rates of pine afforestation than in natural forest and scrubland suggest that these natural covers in some areas could better protect the slopes from erosion processes.

Although erosion rates in our catchment are not significant different ($p > .05$) between forest and scrubland, this is not the case in other more humid environments. In contrast with our findings, Navas et al. (2005) report in an abandoned Pyrenean catchment ^{137}Cs estimates that discriminate highly eroded scrubland in comparison with the naturally revegetated forest. Navas, Machín, Beguería, López-Vicente, and Gaspar (2008) concluded that this relationship was due to the much poorer soil conditions in the scrubland along with the steepest slopes and the higher solar radiation.

The introduction of additional tracers should be tested in future research to assess the possibility of discriminating differences in soil redistribution rates at different temporal scales. The $^{210}Pb_{ex}$ could offer such potential (Gaspar, Webster, & Navas, 2017; Mabit et al., 2014; Porto, Walling, Cogliandro, & Callegari, 2016) in correspondence with the time of the vegetation recovery in the succession status of the revegetation from scrubland to forest in relatively recently abandoned areas.

More mature vegetation is located at the upper parts of the catchment as the result of the early abandonment of the agricultural land. This fact is associated with lower soil erosion and deposition rates in this upper part compared to the central part of the catchment. The introduction of pine afforestation has also reduced soil redistribution rates.

The effect of soil redistribution processes on SOM dynamics is demonstrated by the differences between SOM contents found in the eroded and depositional sites as the higher the erosion rates the lower SOM contents. However, in the natural forest sites, this relation is not observed. This is probably due to high stability under forest as identified by the lower redistribution rates that only vary between −2.43 to 3.93 Mg ha^{-1} yr^{-1}; therefore, soil movement is not as high as to produce a marked contrast in SOM contents.

The results of the sediment budget for the study catchment evidence that higher soil redistribution rates are concentrated in the relatively small central agricultural area and do not occur over most of the catchment. The specific sediment yield in our catchment is comparable with values of 7.56 Mg ha^{-1} yr^{-1} obtained in nearby small endorheic catchment (Navas et al., 2014). A similar specific sediment yield of 4.7 Mg ha^{-1} yr^{-1} was computed in the Barasona reservoir catchment (Palazón & Navas, 2016). However, Porto, Walling, and Capra (2014) estimated higher mean annual soil loss of 26.39 Mg ha^{-1} yr^{-1} in a small-cultivated catchment (0.86 ha) in Sicily. The kriging approach divided the catchment in headwater areas mainly composed of woodlands and scrubland and the central part of the catchment composed of croplands and is presented as an alternative for the areal representation of soil redistribution rates over the different land uses. The study area has quite homogeneous lithology and landforms; however, a large variety of land uses may represent a constraint in the use of this methodology such as where the area has a complex land use mosaic. In our case, this approach has some benefits as it allows the differentiation between croplands that concentrate in the lower part of the catchment and scrubland and forests located at the highest altitudes.

5 | CONCLUSIONS

This study demonstrated the potential of ^{137}Cs measurements to quantify and spatialize information on soil redistribution rates in the context of the land use changes in the last decades. The application of the ^{137}Cs method to calculate soil redistribution enabled us to identify and discriminate the main erosion and deposition areas in the catchment under the different land uses. Some of the main factors triggering erosion are related to tillage or farming practices in general, whereas the reduction in erosion rates is related with the increase in the vegetated covers and its maturity.

The results from this study case demonstrate relationships between SOM and soil redistribution rates in cropland, scrubland, and pine afforestation areas. The absence of such relationships in forest is likely linked to greater stability and lower soil redistribution rates. The tillage practices and the fact that soil is left bare during part of the year of the predominant agricultural land use in the lowlands led to the higher soil redistribution rates. The lower rates of soil erosion were found under the land uses with more abundant vegetation on higher altitudes and slopes. Therefore, in this environment, land use was found to be the main controlling factor of soil redistribution rates.

Natural revegetation and reforestation in recent decades after land abandonment produced substantial changes that prevent the erosion and the soil loss. Natural Mediterranean open forests and pine afforestation occupying the highlands, intermixed with scrublands on high to moderate slopes efficiently protect the soil surface from erosion.

Although the ^{137}Cs method generates precise spatial distribution data, the extrapolation at catchment scale is complex but allows to gain a better understanding of the spatial extent, the severity of soil loss over a catchment, and the benefits of the natural revegetated areas.

The tentative sediment budget calculated for the Barués catchment could provide valuable information for implementing soil erosion control programmes in Mediterranean mountains agroecosystems. The present study improves the current knowledge on the relationships between the land use change and the spatial variability of soil redistribution, which may help to mitigate soil degradation, reservoir siltation and implement erosion control practices.

ACKNOWLEDGEMENTS

We would like to thank the three referees for their constructive reviews and insights that greatly enhanced the manuscript.

This research was financially supported by the project TRAZESCAR (CGL2014-52986-R) and the aid of a predoctoral contract (BES-2015-071780) funded by the Spanish Ministry of Economy and Competitiveness.

ORCID

Ivan Lizaga http://orcid.org/0000-0003-4372-5901
Laura Quijano http://orcid.org/0000-0002-2334-2818
Leticia Gaspar http://orcid.org/0000-0002-3473-7110
Ana Navas http://orcid.org/0000-0002-4724-7532

REFERENCES

Alewell, C., Birkholz, A., Meusburger, K., Schindler Wildhaber, Y., & Mabit, L. (2016). Quantitative sediment source attribution with compound-specific isotope analysis in a C3 plant-dominated catchment (central Switzerland). *Biogeosciences*, *13*, 1587–1596. https://doi.org/10.5194/bg-13-1587-2016

Alewell, C., Meusburger, K., Juretzko, G., Mabit, L., & Ketterer, M. E. (2014). Suitability of $^{239+240}$Pu and ^{137}Cs as tracers for soil erosion assessment in mountain grasslands. *Chemosphere*, *103*, 274–280. https://doi.org/10.1016/j.chemosphere.2013.12.016

Alonso-Sarría, F., Martínez-Hernández, C., Romero-Díaz, A., Cánovas-García, F., & Gomariz-Castillo, F. (2016). Main environmental features leading to recent land abandonment in Murcia region (Southeast Spain). *Land Degradation & Development*, *27*, 654–670. https://doi.org/10.1002/ldr.2447

Blake, W. H., Ficken, K. J., Taylor, P., Russell, M. A., & Walling, D. E. (2012). Tracing crop-specific sediment sources in agricultural catchments. *Geomorphology*, *139*, 322–329. https://doi.org/10.1016/j.geomorph.2011.10.036

Bruun, T. B., Elberling, B., de Neergaard, A., & Magid, J. (2015). Organic carbon dynamics in different soil types after conversion of forest to agriculture. *Land Degradation & Development*, *26*, 272–283. https://doi.org/10.1002/ldr.2205

Buendia, C., Batalla, R. J., Sabater, S., Palau, A., & Marcé, R. (2016). Run-off trends driven by climate and afforestation in a Pyrenean Basin. *Land Degradation & Development*, *27*, 823–838. https://doi.org/10.1002/ldr.2384

Chauchard, S., Carcaillet, C., & Guibal, F. (2007). Patterns of land-use abandonment control tree-recruitment and forest dynamics in Mediterranean mountains. *Ecosystems*, *10*, 936–948. https://doi.org/10.1007/s10021-007-9065-4

Colazo, J. C., & Buschiazzo, D. (2015). The impact of agriculture on soil texture due to wind erosion. *Land Degradation & Development*, *26*, 62–70. https://doi.org/10.1002/ldr.2297

Collins, A. L., Walling, D. E., Sichingabula, H. M., & Leeks, G. J. L. (2001). Using ^{137}Cs measurements to quantify soil erosion and redistribution rates for areas under different land use in the upper Kaleya River basin, southern Zambia. *Geoderma*, *104*, 299–323. https://doi.org/10.1016/S0016-7061(01)00087-8

Debussche, M., Lepart, J., & Dervieux, A. (1999). Mediterranean landscape changes: Evidence from old postcards. *Global Ecology and Biogeography*, *8*, 3–15. https://doi.org/10.1046/j.1365-2699.1999.00316.x

Dorji, T., Odeh, I. O. A., & Field, D. J. (2014). Vertical distribution of soil organic carbon density in relation to land use/cover, altitude and slope aspect in the eastern Himalayas. *Land*, *3*, 1232–1250. https://doi.org/10.3390/land3041232

Du, P., & Walling, D. E. (2011). Using ^{137}Cs measurements to investigate the influence of erosion and soil redistribution on soil properties. *Applied Radiation and Isotopes*, *69*, 717–726. https://doi.org/10.1016/j.apradiso.2011.01.022

Ellis, E. C., Kaplan, J. O., Fuller, D. Q., Vavrus, S., Klein Goldewijk, K., & Verburg, P. H. (2013). Used planet: A global history. *Proceedings of the National Academy of Sciences of the United States of America*, *110*, 7978–7985. https://doi.org/10.1073/pnas.1217241110

Ellis, E. C., Klein Goldewijk, K., Siebert, S., Lightman, D., & Ramankutty, N. (2010). Anthropogenic transformation of the biomes, 1700 to 2000. *Global Ecology and Biogeography*, *19*, 589–606. https://doi.org/10.1111/j.1466-8238.2010.00540.x

Evrard, O., Nord, G., Cerdan, O., Souchère, V., Le Bissonnais, Y., & Bonté, P. (2010). Modelling the impact of land use change and rainfall seasonality on sediment export from an agricultural catchment of the northwestern European loess belt. *Agriculture, Ecosystems & Environment*, *138*, 83–94. https://doi.org/10.1016/j.agee.2010.04.003

FAO. (2015). *World reference base for soil resources 2014*. Rome: FAO.

Foley, J. A., DeFries, R., Asner, G. P., Barford, C., Bonan, G., Carpenter, S. R., … Snyder, P. K. (2005). Global consequences of land use. *Science*, *309*, 570–574. https://doi.org/10.1126/science.1111772

Fukuyama, T., Onda, Y., Takenaka, C., & Walling, D. E. (2008). Investigating erosion rates within a Japanese cypress plantation using Cs-137 and Pb-210_{ex} measurements. *Journal of Geophysical Research: Earth Surface*, *113*, F02007. https://doi.org/10.1029/2006JF000657

Gaspar, L., & Navas, A. (2013). Vertical and lateral distributions of ^{137}Cs in cultivated and uncultivated soils on Mediterranean hillslopes. *Geoderma*, *207–208*, 131–143. https://doi.org/10.1016/j.geoderma.2013.04.034

Gaspar, L., Navas, A., Walling, D. E., Machín, J., & Gómez Arozamena, J. (2013). Using ^{137}Cs and ^{210}Pbex to assess soil redistribution on slopes at different temporal scales. *CATENA*, *102*, 46–54. https://doi.org/10.1016/j.catena.2011.01.004

Gaspar, L., Webster, R., & Navas, A. (2017). Fallout $^{210}Pb_{ex}$ and its relation with soil properties in soil profiles under forest and scrubland of the central Spanish Pre-Pyrenees. *European Journal of Soil Science*. https://doi.org/10.1111/ejss.12427

Gharibreza, M., Raj, J. K., Yusoff, I., Othman, Z., Tahir, W. Z. W. M., & Ashraf, M. A. (2013). Land use changes and soil redistribution estimation using ^{137}Cs in the tropical Bera Lake catchment, Malaysia. *Soil and Tillage Research*, *131*, 1–10. https://doi.org/10.1016/j.still.2013.02.010

Kim, Y., Cho, S., Kang, H.-D., Kim, W., Lee, H.-R., Doh, S.-H., … Jeong, G. Y. (2006). Radiocesium reaction with illite and organic matter in marine sediment. *Marine Pollution Bulletin*, *52*, 659–665. https://doi.org/10.1016/j.marpolbul.2005.10.017

Lasanta, T., Nadal-Romero, E., Errea, P., & Arnáez, J. (2016). The effect of landscape conservation measures in changing landscape patterns: A case study in Mediterranean mountains. *Land Degradation & Development*, *27*, 373–386. https://doi.org/10.1002/ldr.2359

Lizaga, I., Quijano, L., Palazón, L., Gaspar, L., & Navas, A. (2017). Enhancing connectivity index to assess the effects of land use changes in a Mediterranean catchment. *Land Degradation & Development*. https://doi.org/10.1002/ldr.2676

Mabit, L., Benmansour, M., Abril, J. M., Walling, D. E., Meusburger, K., Iurian, A. R., … Alewell, C. (2014). Fallout ^{210}Pb as a soil and sediment tracer in catchment sediment budget investigations: A review. *Earth-Science Reviews*, *138*, 335–351. https://doi.org/10.1016/j.earscirev.2014.06.007

Mabit, L., & Bernard, C. (2007). Assessment of spatial distribution of fallout radionuclides through geostatistics concept. *Journal of Environmental Radioactivity*, *97*, 206–219. https://doi.org/10.1016/j.jenvrad.2007.05.008

Mabit, L., Bernard, C., & Laverdiere, M. R. (2002). Quantification of soil redistribution and sediment budget in a Canadian watershed from fallout caesium-137 (^{137}Cs) data. *Canadian Journal of Soil Science*.

Mabit, L., Bernard, C., Makhlouf, M., & Laverdière, M. R. (2008). Spatial variability of erosion and soil organic matter content estimated from ^{137}Cs measurements and geostatistics. *Geoderma*, *145*, 245–251. https://doi.org/10.1016/j.geoderma.2008.03.013

Mabit, L., Chhem-Kieth, S., Toloza, A., Vanwalleghem, T., Bernard, C., Amate, J. I., … Gómez, J. A. (2012). Radioisotopics and physicochemical background indicators to assess soil degradation affecting olive orchards in southern Spain. *Agriculture, Ecosystems & Environment*, *159*, 70–80.

MacDonald, D., Crabtree, J. R., Wiesinger, G., Dax, T., Stamou, N., Fleury, P., … Gibon, A. (2000). Agricultural abandonment in mountain areas of Europe: Environmental consequences and policy response. *Journal of Environmental Management*, *59*, 47–69. https://doi.org/10.1006/jema.1999.0335

Mariani, L., & Parisi, S. G. (2014). Extreme rainfalls in the Mediterranean area. In N. Diodato, & G. Bellocchi (Eds.), *Storminess and environmental change* (pp. 17–37). Springer Netherlands.

Martinez-Casasnovas, J. A., Ramos, M. C., & Ribes-Dasi, M. (2002). Soil erosion caused by extreme rainfall events: Mapping and quantification in agricultural plots from very detailed digital elevation models. *Geoderma*, *105*, 125–140. https://doi.org/10.1016/S0016-7061(01)00096-9

Mesrar, H., Sadiki, A., Faleh, A., Quijano, L., Gaspar, L., & Navas, A. (2017). Vertical and lateral distribution of fallout ^{137}Cs and soil properties along representative toposequences of central Rif, Morocco. *Journal of Environmental Radioactivity*, *169–170*, 27–39. https://doi.org/10.1016/j.jenvrad.2016.12.012

Navas, A., Gaspar, L., López-Vicente, M., & Machín, J. (2011). Spatial distribution of natural and artificial radionuclides at the catchment scale (South Central Pyrenees). *Radiation Measurements*, *46*, 261–269. https://doi.org/10.1016/j.radmeas.2010.11.008

Navas, A., Gaspar, L., Quijano, L., López-Vicente, M., & Machín, J. (2012). Patterns of soil organic carbon and nitrogen in relation to soil movement under different land uses in mountain fields (South Central Pyrenees). *CATENA*, *94*, 43–52. https://doi.org/10.1016/j.catena.2011.05.012

Navas, A., López-Vicente, M., Gaspar, L., & Machín, J. (2013). Assessing soil redistribution in a complex karst catchment using fallout ^{137}Cs and GIS. *Geomorphology*, *196*, 231–241. https://doi.org/10.1016/j.geomorph.2012.03.018

Navas, A., López-Vicente, M., Gaspar, L., Palazón, L., & Quijano, L. (2014). Establishing a tracer-based sediment budget to preserve wetlands in Mediterranean mountain agroecosystems (NE Spain). *Science of the Total Environment*, *496*, 132–143. https://doi.org/10.1016/j.scitotenv.2014.07.026

Navas, A., Machín, J., Beguería, S., López-Vicente, M., & Gaspar, L. (2008). Soil properties and physiographic factors controlling the natural vegetation re-growth in a disturbed catchment of the Central Spanish Pyrenees. *Agroforestry Systems*, *72*, 173–185. https://doi.org/10.1007/s10457-007-9085-2

Navas, A., Machín, J., & Soto, J. (2005). Assessing soil erosion in a Pyrenean mountain catchment using GIS and fallout ^{137}Cs. *Agriculture, Ecosystems & Environment*, *105*, 493–506. https://doi.org/10.1016/j.agee.2004.07.005

Navas, A., Quine, T. A., Walling, D. E., Gaspar, L., Quijano, L., & Lizaga, I. (2017). Relating intensity of soil redistribution to land use changes in abandoned Pyrenean fields using fallout caesium-137. *Land Degradation & Development*, *28*, 2017–2029. https://doi.org/10.1002/ldr.2724

Navas, A., Valero-Garcés, B., Gaspar, L., & Machín, J. (2009). Reconstructing the history of sediment accumulation in the Yesa reservoir: An approach for management of mountain reservoirs. *Lake and Reservoir Management*, *25*, 15–27. https://doi.org/10.1080/07438140802714304

Navas, A., & Walling D. E. (1992). Using caesium-137 to assess sediment movement on slopes in a semiarid upland environment in Spain. *Erosion, debris flows and environment in mountain regions. Proc. international symposium, Chengdu, 1992* 129–138

Navas, A., Walling, D. E., Quine, T., Machín Gayarre, J., Soto, J., Domenech, S., … López-Vicente, M. (2007). Variability in ^{137}Cs inventories and potential climatic and lithological controls in the central Ebro valley, Spain. *Journal of Radioanalytical and Nuclear Chemistry*, *274*, 331. https://doi.org/10.1007/s10967-007-1119-8

Ohtsuka, T., Hirota, M., Zhang, X., Shimono, A., Senga, Y., Du, M., … Tang, Y. (2008). Soil organic carbon pools in alpine to nival zones along an altitudinal gradient (4400–5300 m) on the Tibetan Plateau. *Polar Science*, *2*, 277–285. https://doi.org/10.1016/j.polar.2008.08.003

Palazón, L., & Navas, A. (2016). Land use sediment production response under different climatic conditions in an alpine–prealpine catchment. *Catena*, *137*, 244–255. https://doi.org/10.1016/j.catena.2015.09.025

Porto, P., Walling, D. E., & Callegari, G. (2011). Using ^{137}Cs measurements to establish catchment sediment budgets and explore scale effects. *Hydrological Processes*, *25*, 886–900. https://doi.org/10.1002/hyp.7874

Porto, P., Walling, D. E., & Capra, A. (2014). Using ^{137}Cs and ^{210}Pbex measurements and conventional surveys to investigate the relative contributions of interrill/rill and gully erosion to soil loss from a small cultivated catchment in Sicily. *Soil and Tillage Research*, *135*, 18–27. https://doi.org/10.1016/j.still.2013.08.013

Porto, P., Walling, D. E., Cogliandro, V., & Callegari, G. (2016). Exploring the potential for using $^{210}Pb_{ex}$ measurements within a re-sampling approach to document recent changes in soil redistribution rates within a small catchment in southern Italy. *Journal of Environmental Radioactivity*, *164*, 158–168. https://doi.org/10.1016/j.jenvrad.2016.06.026

Porto, P., Walling, D. E., Ferro, V., & di Stefano, C. (2003). Validating erosion rate estimates provided by caesium-137 measurements for two small forested catchments in Calabria, southern Italy. *Land Degradation & Development*, *14*, 389–408. https://doi.org/10.1002/ldr.561

Quijano, L., Beguería, S., Gaspar, L., & Navas, A. (2016a). Estimating erosion rates using ^{137}Cs measurements and WATEM/SEDEM in a Mediterranean cultivated field. *Catena*, *138*, 38–51. https://doi.org/10.1016/j.catena.2015.11.009

Quijano, L., Gaspar, L., & Navas, A. (2016b). Spatial patterns of SOC, SON, ^{137}Cs and soil properties as affected by redistribution processes in a Mediterranean cultivated field (central Ebro Basin). *Soil and Tillage Research*, *155*, 318–328. https://doi.org/10.1016/j.still.2015.09.007

Quijano, L., Gaspar, L., & Navas, A. (2016). Lateral and depth patterns of soil organic carbon fractions in a mountain Mediterranean agrosystem. *The Journal of Agricultural Science*, *154*, 287–304. https://doi.org/10.1017/S002185961400135X

Quijano, L., Van Oost, K., Nadeu, E., Gaspar, L., & Navas, A. (2017). Modelling the Effect of Land Management Changes on Soil Organic Carbon Stocks in a Mediterranean Cultivated Field. *Land Degradation & Development*, *28*, 515–523. https://doi.org/10.1002/ldr.2637

Quine, T. A., Navas, A., Walling, D. E., & Machin, J. (1994). Soil erosion and redistribution on cultivated and uncultivated land near las bardenas in the central Ebro river basin, Spain. *Land Degradation & Development*, *5*, 41–55. https://doi.org/10.1002/ldr.3400050106

Rigol, A., Vidal, M., & Rauret, G. (2002). An overview of the effect of organic matter on soil–radiocaesium interaction: Implications in root uptake. *Journal of Environmental Radioactivity*, *58*, 191–216. https://doi.org/10.1016/S0265-931X(01)00066-2

Romanyà, J., & Rovira, P. (2011). An appraisal of soil organic C content in Mediterranean agricultural soils. *Soil Use and Management*, *27*, 321–332. https://doi.org/10.1111/j.1475-2743.2011.00346.x

Sadiki, A., Faleh, A., Navas, A., & Bouhlassa, S. (2007). Assessing soil erosion and control factors by the radiometric technique in the Boussouab catchment, Eastern Rif, Morocco. *Catena*, *71*, 13–20. https://doi.org/10.1016/j.catena.2006.10.003

Sawhney, B. L. (1970). Potassium and cesium ion selectivity in relation to clay mineral structure. *Clays and Clay Minerals*, *18*, 47–52.

Schoorl, J. M., Boix Fayos, C., de Meijer, R. J., van der Graaf, E. R., & Veldkamp, A. (2004). The ^{137}Cs technique applied to steep Mediterranean slopes (Part I): The effects of lithology, slope morphology and land use. *Catena*, *57*, 15–34. https://doi.org/10.1016/j.catena.2003.08.003

Soto, J., & Navas, A. (2004). A model of ^{137}Cs activity profile for soil erosion studies in uncultivated soils of Mediterranean environments. *Journal of Arid Environments*, *59*, 719–730. https://doi.org/10.1016/j.jaridenv.2004.02.003

Soto, J., & Navas, A. (2008). A simple model of Cs-137 profile to estimate soil redistribution in cultivated stony soils. *Radiation Measurements*, *43*, 1285–1293. https://doi.org/10.1016/j.radmeas.2008.02.024

Staunton, S., Dumat, C., & Zsolnay, A. (2002). Possible role of organic matter in radiocaesium adsorption in soils. *Journal of Environmental Radioactivity*, *58*, 163–173. https://doi.org/10.1016/S0265-931X(01)00064-9

Tirapu, G. P., & Arenas, C. (1996). Late Oligocene-Early Miocene syntectonic fluvial sedimentation in the Aragonese Pyrenean domain of the Ebro Basin: Facies models and structural controls. *Cuadernos de Geología Ibérica*, *21*, 277–296. https://doi.org/10.5209/rev_CGIB.1996.v21.2532

Upadhayay, H. R., Bodé, S., Griepentrog, M., Huygens, D., Bajracharya, R. M., Blake, W. H., … Boeckx, P. (2017). Methodological perspectives on the application of compound-specific stable isotope fingerprinting for sediment source apportionment. *Journal of Soils and Sediments*, *17*, 1537–1553. https://doi.org/10.1007/s11368-017-1706-4

Valero-Garces, B., Navas, A., Machin, J., & Estacion E, de A.D. (1997). Sediment deposition in the Barasona reservoir (central Pyrenees, Spain): Temporal and spatial variability of sediment yield and land use impacts.

Walling, D. E., & Quine, T. A. (1991). Use of ^{137}Cs measurements to investigate soil erosion on arable fields in the UK: Potential applications and limitations. *Journal of Soil Science*, *42*, 147–165. https://doi.org/10.1111/j.1365-2389.1991.tb00099.x

Zhang, Y., Long, Y., Yu, X., & An, J. (2014). A comparison of measured ^{137}Cs and excess ^{210}Pb levels in the cultivated brown and cinnamon soils of the Yimeng Mountain area. *Chinese Journal of Geochemistry*, *33*, 155–162. https://doi.org/10.1007/s11631-014-0671-5

How to cite this article: Lizaga I, Quijano L, Gaspar L, Navas A. Estimating soil redistribution patterns with ^{137}Cs measurements in a Mediterranean mountain catchment affected by land abandonment. *Land Degrad Develop*. 2017;1–13. https://doi.org/10.1002/ldr.2843

CHAPTER 5

Linking land use changes to variation in soil properties in a Mediterranean mountain agroecosystem

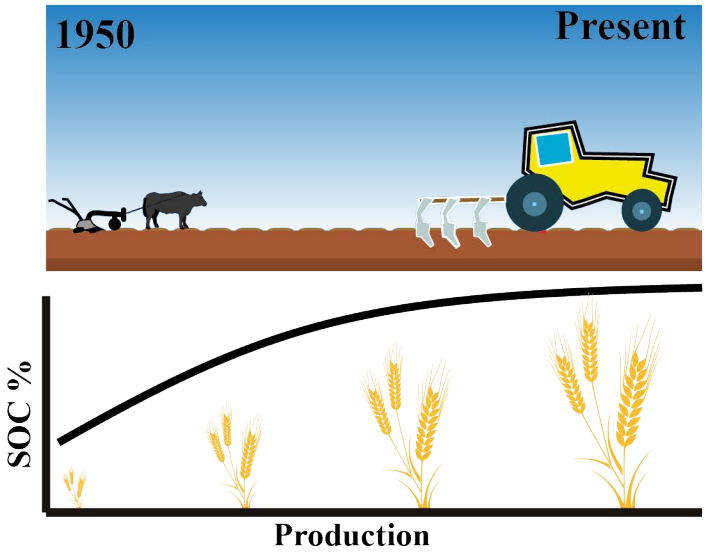

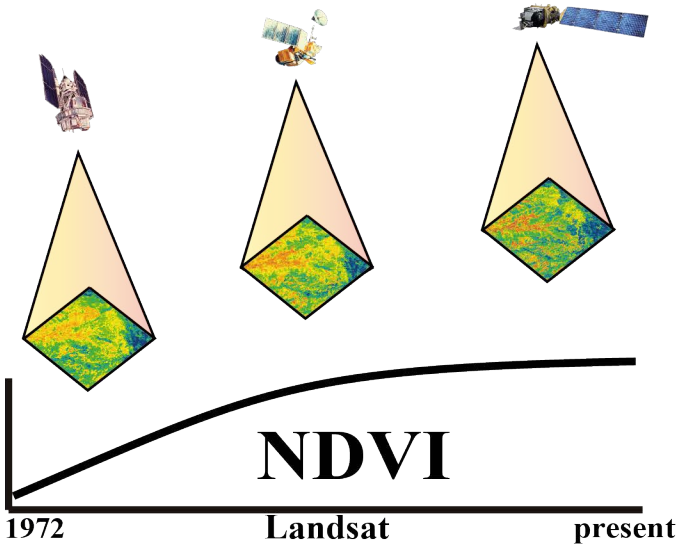

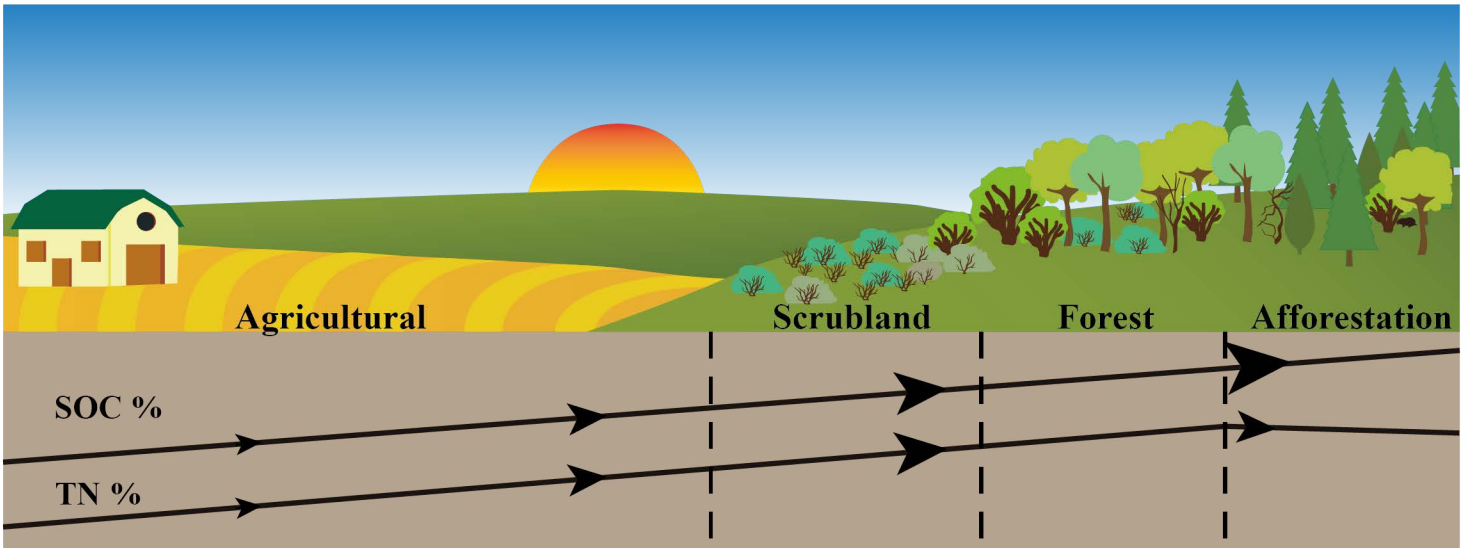

Catena 172 (2019) 516–527

Contents lists available at ScienceDirect

Catena

journal homepage: www.elsevier.com/locate/catena

Linking land use changes to variation in soil properties in a Mediterranean mountain agroecosystem

Ivan Lizaga[a,*], Laura Quijano[b], Leticia Gaspar[a], María Concepción Ramos[c], Ana Navas[a,*]

[a] Estación Experimental de Aula Dei, CSIC, Avenida Montañana, 1005, 50059 Zaragoza, Spain
[b] Université Catholique de Louvain, Georges Lemaître Centre for Earth and Climate Research - Earth and Life Institute, Belgium
[c] Departamento de Medio Ambiente y Ciencias del Suelo, Agrotecnio, Universidad de Lleida, Av. Rovira Roure 191, 25198 Lleida, Spain

ARTICLE INFO

Keywords:
Land use changes
Soil and physiographical properties
NDVI
SPEROS-C model
Catchment scale

ABSTRACT

Several decades of intensive rainfed farming in Mediterranean mountains and later land abandonment has led to rapid land use and land cover changes. During recent centuries, the conversion of rangelands into croplands has increased the surfaces prone to erosion. In the southern Pre-Pyrenees, the process was reversed during the middle of the twentieth century, allowing the recovery of vegetation and subsequent variation in land cover. This work aims to assess how land use changes after generalised land abandonment affect some major soil properties related to soil quality. For this purpose, 98 replicate bulk soil samples were collected in a 23 km^2 catchment that was mostly cultivated at the beginning of the last century. Soil samples were distributed over areas representing the main land uses (agricultural land, natural forest, pine afforestation and scrubland). Bulk density, stoniness, grain size, pH, carbonates, electrical conductivity, soil organic carbon (SOC), total nitrogen (TN), water retention capacity and magnetic properties (low frequency magnetic susceptibility (LF) and frequency dependence (FD)) were analysed in the samples from different land use areas. A past scenario was recreated using estimated data from the SPEROS-C model in order to evaluate changes in SOC over time. Furthermore, a multitemporal analysis of the Normalised Difference Vegetation Index of Landsat images was performed between 1972 and the present in order to assess the dynamics of revegetation. After land abandonment, 16.5% of the area remained as croplands, but afforestation and natural revegetation occupied 83.5% of the catchment. The highest mean value for SOC was found in the pine afforested area and the highest TN mean value was found in the natural forest. The lowest mean values for SOC and TN were recorded on the agricultural land. These results show the impact of soil changes produced by land use changes in fragile Mediterranean mountain agroecosystems.

1. Introduction

Changes in land use due to human activities are a widespread problem that often lead to land degradation, and are of considerable concern worldwide in the context of environmental degradation and global climate change (Celik, 2005). Over recent centuries, human activities have been the main drivers of ecosystem transformations through the conversion of natural landscapes into agricultural lands (Chauchard et al., 2007). The conversion of rangeland into cropland due to agricultural deforestation is a local and global environmental issue (Foley et al., 2005), resulting in changing soil properties and soil infiltration rates, and modifying soil physical characteristics that eventually increase soil erosion (Li et al., 2007). Poor soil management can rapidly deteriorate vast areas of land, and is becoming a major threat to rural subsistence in many countries (Chauchard et al., 2007).

The problems that these practices have created are particularly remarkable in mountainous areas and in regions with adverse environmental conditions (MacDonald et al., 2000), such as in Mediterranean mountains where the natural forest has been progressively cleared and replaced by croplands (Alonso-Sarría et al., 2016). These changes lead to losses of soil nutrients and reduced long-term soil productivity.

Mediterranean mountains are sensitive agroecosystems prone to land degradation, due to their climatic conditions characterised by irregular space-time distribution of high intensity rainfall events, followed by long dry periods (Mariani and Parisi, 2014). There has also been strong anthropogenic pressure during the past centuries (Romanyà and Rovira, 2011; Bruun et al., 2015). In the twentieth century, following socioeconomic changes, land abandonment notably increased

* Corresponding authors.
E-mail addresses: ilizaga@eead.csic.es (I. Lizaga), laura.quijano@uclouvain.be (L. Quijano), lgaspar@eead.csic.es (L. Gaspar), cramos@macs.udl.cat (M.C. Ramos), anavas@eead.csic.es (A. Navas).

https://doi.org/10.1016/j.catena.2018.09.019
Received 14 December 2017; Received in revised form 2 August 2018; Accepted 11 September 2018
Available online 15 September 2018
0341-8162/ © 2018 Elsevier B.V. All rights reserved.

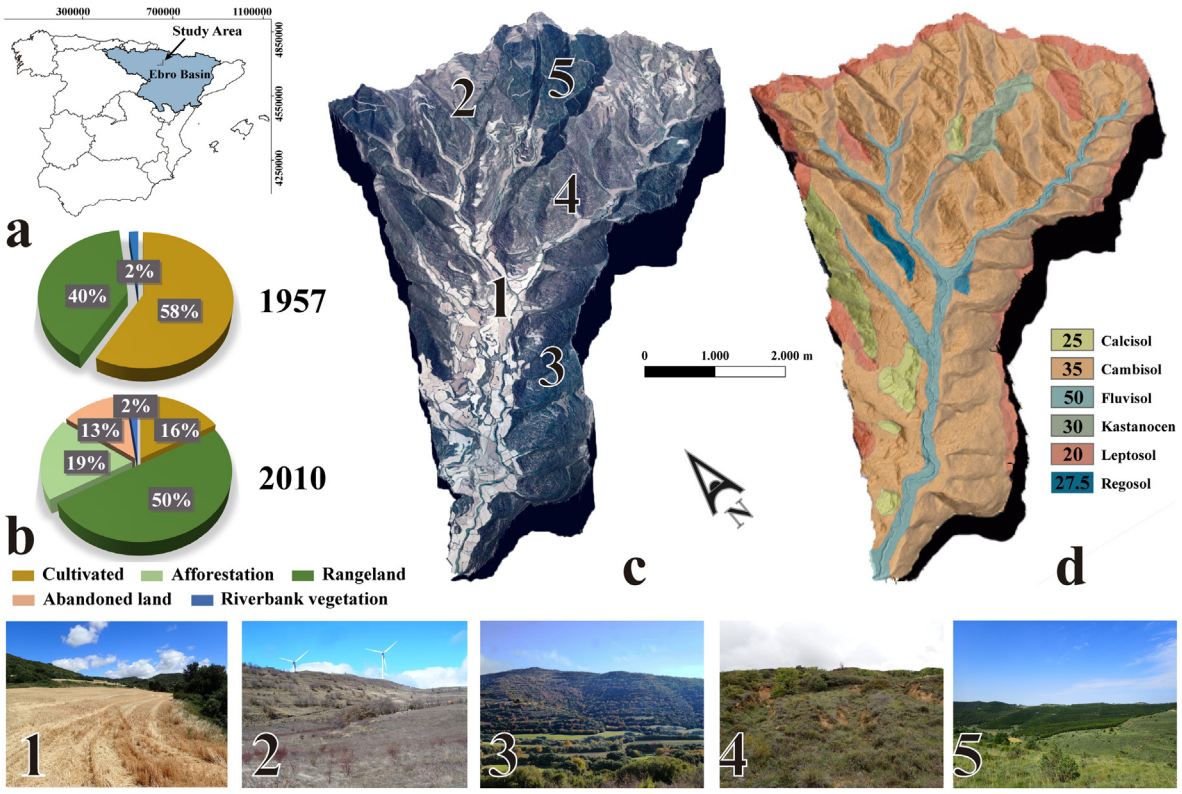

Fig. 1. Location of the study catchment in the central part of the Ebro Basin (NE Spain) (a). (b) Percentage of the different land uses in 1957 and 2016. (c) 3D picture of Barués catchment created with a DEM and an orthophoto (National Plan of Aerial Orthophotography, IGN). The numbers represent the pictures of the main land uses situated at the bottom of the figure. (d) 3D Map of soil types in the catchment (IUSS Working Group WRB, 2015). The number in the legend represents the average depth of each soil type.

from the mid-1950s onwards, leading to depopulation of rural areas and substantial landscape changes (Lasanta et al., 2016; Quijano et al., 2016a, 2016b; Navas et al., 2017).

Remote sensing enables the comparison of landscape evolution such as the recent land use changes on a multitemporal scale and has the potential to allow calculation of ecological indices. It has thus received increasing attention in the last decade for the purpose of deriving ecological measures that correlate with surface biophysical properties (Myneni et al., 1995). Such studies have confirmed the potential of remote sensing techniques for the estimation of different vegetation parameters that are directly related to plant vigour, density, and growth conditions and can be used to detect environmental conditions, human activities and modifications of the vegetation cover produced by land use changes (Melendez-Pastor et al., 2016). The most frequently used vegetation index is the Normalised Difference Vegetation Index (NDVI) as described by Rouse et al. (1974). It is also used as vegetation status data source in many environmental modelling approaches and ecological studies (Li et al., 2004; Pettorelli et al., 2005; Krishnaswamy et al., 2009). Several studies have tried to predict different soil properties and soil quality by combining remote sensing and soil sampling data (Ben-Dor and Banin, 1995; Vågen et al., 2013, 2016; Winowiecki et al., 2016). Most of these studies have included large agricultural areas, but few of them have considered mountain agroecosystems.

Tillage practices expose the less fertile subsoil, affecting the physical, biochemical and magnetic properties of the soil (Rahimi et al., 2013; Gao et al., 2017). Among the most important effects of continuous conventional tillage practices during recent centuries are changes in the soil organic carbon content (Bruce et al., 1999; Novara et al., 2015; Parras-Alcántara et al., 2015; Boix-Fayos et al., 2017). As a consequence of recent land use changes, estimates of SOC stocks and their variations over time are essential in order to understand carbon dynamics and identify the most efficient management practices that may contribute to increasing carbon in soils (Álvaro-Fuentes and Paustian, 2011). Due to a general lack of soil samples from past decades, SOC dynamic models have been developed to understand the short and long-term impact of land management on SOC stocks. This is the case for the SPEROS-C model (Van Oost et al., 2005) that combines the soil erosion SPEROS model (Van Oost et al., 2003) and the SOC dynamics Introductory Carbon Balance Model (Andrén and Kätterer, 1997), which was implemented in our study catchment by Quijano et al. (2017).

A major issue in Mediterranean agroecosystems is the effect of the abandonment of agricultural land in recent decades and its subsequent natural revegetation, as well as afforestation practices, on the variations of soil properties. There have been very few studies that asses these variations at the catchment scale (Navas et al., 2008; Nadal-Romero et al., 2016). One of the properties most sensitive to land use change is the soil organic carbon content that may increase or decrease depending on the previous land uses. We hypothesise that changes in agricultural management from conventional to conservation tillage practices, and increases in vegetation due to natural revegetation after abandonment of cultivated land lead to increases in SOC stocks. To date, only a few studies have focussed on this issue in Mediterranean agroecosystems (Francaviglia et al., 2012; Muñoz-Rojas et al., 2017).

The novelty of this study arises from two main aspects, combining NDVI from remote sensing data with soil nutrients as a tool for assessing temporal changes along with modelling and reconstructing the past SOC stocks at catchment scale. Furthermore, to our knowledge there are no published studies that use remote sensing data to discriminate and analyse different land uses and their changes over time, comparing satellite with soil sampling data.

With the aim of filling this gap we selected a representative Mediterranean mountain catchment that was mostly cultivated in the first half of the twentieth century and then abandoned in the mid-1950s. In this catchment we: i) estimate the variation in the percentage

vegetation cover during the successional changes of natural revegetation using the NDVI derived from remote sensed data; ii) identify the spatial patterns of major soil properties and the differences between land uses; iii) compare the NDVI with the distribution of soil nutrients to assess the impact of revegetation recovery in different land use areas; iv) test the previous hypotheses on the variations of SOC stocks due to land uses changes by applying a spatial distributed model, the SPEROS-C model (Van Oost et al., 2005). Therefore our multi-approach is aimed to determine how soil properties have changed in the last decades after land abandonment and subsequent natural revegetation and afforestation. The conditions of the study catchment represent a unique opportunity to track variations in soil properties associated with vegetation cover changes using satellite images from 1972 to present.

2. Materials and methods

2.1. The study catchment

The Barués area is an ephemeral stream catchment (23 km^2) of the Arba River located in the central part of the Ebro Basin (NE Spain) (Fig. 1). From a geological point of view, it lies in the distal part of the Pre-Pyrenean range with characteristically south – southwest low angle strata dipping between 5 and 8°. Rock outcrops in the catchment include two conformable Oligo - Miocene lithostratigraphic units of the Uncastillo Formation, mainly composed of sandstone (Tirapu and Arenas, 1996). The geomorphological setting is clearly conditioned by the low bedding strata, setting up the path of the streams following the strata direction. The climate is continental Mediterranean, characterised by cold winters and hot and dry summers. Rainfall events mainly occur in the spring (April and May) and autumn (September and October) and summer droughts occur between the two humid periods. The area is subject to very intense, though sometimes localised storms. The mean annual temperature is 13.4 °C and the mean annual rainfall is about 500 mm (recorded since 1929 at the Yesa reservoir; AEMET). The soil types in the catchment were classified and mapped in 2014 by Machín (EEAD-CSIC, personal communication) from field surveys, with Calcisols and Cambisols (IUSS Working Group WRB, 2015) being the most abundant soil types. The soils, developed on Quaternary deposits mainly formed by colluvial and alluvial deposits, are alkaline and have low soil organic carbon contents and secondary accumulation of carbonates.

Most of the Barués catchment was cultivated at the beginning of the 20th century. In the mid-1950s 58% of the area was farmland. Of the total 13.5 km^2 that was cultivated, as much as 10.2 km^2 had been abandoned for > 50 years at the time of sampling. At present only 16.5% of croplands remain, but pine afforestation and natural revegetation occupy 83.5% of the catchment (Lizaga et al., 2017). The main land uses in the catchment are agricultural land and rangeland (natural forest, pine afforestation and scrubland). The main crops are winter cereals (*Triticum aestivum* L. and *Hordeum vulgare* L.). The pine forest is mainly composed of *Pinus halepensis* Mill. with a mean tree cover density of 70%. The natural forest (*Quercux ilex* L., *Quercus coccifera* L., and *Juniperus communis* L.) and the scrubland (*Rosmarinus officinalis* L., *Thymus vulgaris* L., *Santolina chamaecyparissus* L., *Genista scorpium* (L.) DC., *Macrochloa tenacissima* (L.) Kunth/*Stipa tenacissima* L., and *Lygeum spartum* (L.) Kunth) are typically Mediterranean and in many areas are intermixed. The scrubland is the early phase of the successional stages of natural revegetation, in the transition to Mediterranean forest. Most agricultural fields are located in the middle part of the catchment at the lowest altitudes, on a Quaternary glacis with gentle slopes. The pine afforestation occupies the highest altitudes with steep slopes, and the natural forest and scrubland are located at intermediate altitudes.

Since the mid-1950s a decrease in agricultural land use and a transition to naturally revegetated cover and pine afforestation has been documented (Fig. 1). There has also been a decrease in the number of individual cultivated fields, along with an increase in their size, in an attempt by farmers to increase the efficiency of production and cost recovery.

Monthly rainfall and temperature data were extracted from the Castiliscar weather station, located 4 km downstream of the catchment. Due to the unavailability of data prior to 1980 and between 2010 and 2016, data from the Sádaba weather station (15 km downstream of the catchment) were also used.

2.2. Soil sampling and analysis

The sampling sites were distributed proportionally using a previously constructed 500 × 500 m grid created in GIS software that proportionally represents the percentages of the surface occupied by the different land uses in the catchment. The grid location was preserved as much as possible when collecting the samples in representative areas, in order to characterise the properties of the surrounding soil surface within that type of land, while avoiding recently highly disturbed areas. A motorised percussion corer equipped with a steel core tube with a surface area of 40.7 cm^2 was used to collect two replicate bulk soil samples at the 98 sampling sites. The soil was taken from the surface up to a depth that varied from 20 to 54 cm depending on the soil thickness.

The two soil cores from each sampling site were mixed, air dried, ground, homogenised and sieved to ≤ 2 mm. The > 2 mm fraction was weighed in order to account for the stone content. Particle size, soil organic carbon (SOC), TN, pH, $CaCO_3$, electrical conductivity (EC), wilting point, field capacity and magnetic properties (low frequency magnetic susceptibility (LF) and frequency dependence (FD)) were analysed in the ≤ 2 mm fraction for the 98 composite soil samples.

A Beckman Coulter LS 13320 laser diffraction particle size analyser was used for grain size analysis. Prior to particle size measurements, the organic fraction was removed by H_2O_2 (10%) heated to 80 °C. Samples were then chemically dispersed with 2 ml of sodium hexametaphosphate (40%), stirred for 2 h and sonicated for a few minutes to facilitate dispersion.

Soil salinity was measured in a conductivity cell (Orion 013605MD) and expressed as the electrical conductivity of a 1:5 soil:water extract (EC 1:5) at 25 °C in dS m^{-1}. Soil pH was measured in a 1:2.5 soil:water extract with a pH electrode (Orion 9157BNMD). Total carbonate content (%) was analysed using a calcimeter. SOC and TN were analysed by the dry combustion method using a LECO RC-612 multiphase carbon analyser and a LECO CN TruSpec carbon and nitrogen analyser, respectively. Mass specific magnetic susceptibility was measured in 10 ml topsoil and bulk soil samples at both low (0.47 kHz; χ_{lf}) and high (4.7 kHz; χ_{hf}) frequencies, using a Bartington Instruments dual-frequency MS2B sensor that operates with an alternating current and produces an alternating magnetic field at 80 A m^{-1} (Bartington Instruments Ltd., 2000). Mass specific magnetic susceptibility measurements at low and high frequency were expressed in units of 10^{-8} m^3 kg^{-1}. The results are the mean values of three measurements for each sample. Both allow to determine absolute mass specific dual frequency-dependent susceptibility (χfd), defined as the difference between the measure at low and high frequencies ($\chi fd = \chi lf - \chi hf$). Alternatively, this parameter is commonly expressed as a percentage, that is the percentage frequency-dependent susceptibility (χfd%) using the following equation:

$$\chi fd\% = [((\chi lf - \chi hf)/\chi lf) \times 100] \quad (1)$$

The results were statistically analysed using R. Pearson's correlation coefficients to assess the relationships between the soil properties over the different land uses. A non-parametric Kruskal–Wallis test was performed to assess whether soil properties differed as a function of the land use. An ordinary kriging with a constant trend was selected to improve the visualization of the spatial distribution of the main soil properties in the catchment. However, the kriging interpolation was not pursued for predicting the values of soil properties but to facilitate the visualization of their distribution patterns in the catchment. Thus, the

maximum exploratory trend surface analysis was selected, to use just a small subset of the data to generate a surface that keep much of the local variation in the data values.

2.3. Remote sensing

Satellite imagery data were analysed with digital image processing methods and spatial analysis techniques to detect spatial-temporal changes in vegetation and land use. A multitemporal Landsat satellite dataset formed the basis for the change detection procedure. A series of twelve Landsat images were acquired by the different multispectral sensors on board Landsat satellites. Image series were selected with temporal resolutions ranging from six to twelve years, beginning from the first Landsat image of the study area from 1972 and continuing up to 2017. All of the selected images were acquired between the end of July and the end of August, because these dates allow the detection of variability in forests and scrubland in the summer, as irradiance or temperature limit the photosynthetic capacity of plants (Valladares and Pearcy, 1997). The dates when images were available without cloud cover were 1972-08-20 (Landsat 1-MSS), 1975-07-09 (Landsat 2-MSS), 1984-07-10 (Landsat 5-MSS), 1984-08-20 (Landsat 5-TM), 1987-08-20 (Landsat 5-TM), 1990-07-27 (Landsat 5-TM), 2001-07-25 (Landsat 5-TM), 2003-07-31 (Landsat 5-TM), 2007-08-11 (Landsat 5-TM), 2010-07-18 (Landsat 5-TM), 2013-08-11 (Landsat 8-OLI), 2016-07-21 (Landsat 8-OLI) and 2017-08-22 (Landsat 8-OLI). The digital image processing procedure, which included pre-processing of satellite multispectral images to ensure temporal comparability between scenes, was carried out by the Earth Resources Observation and Science Center (EROS) (USGS) for the Landsat 8-OLI and Landsat 5-TM sensors. Furthermore, following the methodology proposed by Fan and Liu (2016) a total of 220 vegetation spectra were downloaded from the USGS spectral library (Kokaly et al., 2017). Comparing these spectra a linear interpolation was pursued to determine reflectance values at given wavelengths for both Landsat 5 TM and Landsat 8 OLI and quantify the spectral band adjustment factor (Fan and Liu, 2017). In addition, the Landsat 8 values were corrected to ensure temporal comparability between images from different sensors.

Due to the unavailability of MSS corrected images, atmospheric correction following the methodology proposed by Chavez, 1996 was used, followed by the calculation of a vegetation index to assess temporal changes in land cover. However, the NDVI calculated using images from different sensors may still not be comparable, due to differences in sensor bandwidths or illumination and sun-viewer geometries. Thus, to avoid large differences among datasets obtained from Landsat 8-OLI, Landsat 5-TM and the first Landsat MSS sensors, we split the image dataset by using two coincident Landsat images from July–August of 1984 that were recorded by both Landsat 5-TM and Landsat 5-MSS sensors. Thus, we use the 1984 Landsat 5-TM image for comparisons from 1984 to 2017 and the 1984 Landsat 5-MSS to compare time intervals between 1972 and 1984.

NDVI layers were created for the selected Landsat images. These transformations can provide information about the current state of the vegetation represented in a pixel, and can be used to determine if the study area changes from one date to another and to follow its evolution.

The NDVI (Rouse et al., 1974) is formulated as:

$$NDVI = \frac{(\rho NIR - \rho RED)}{(\rho NIR + \rho RED)} \quad (2)$$

where ρ*NIR* is the reflectance of the near infrared spectral band and ρ*RED* is the reflectance of the red spectral band. The NDVI images for each date were then compared with the previous temporal image to assess the evolution of the NDVI for each time interval.

To assess the recovery of natural vegetation, some former agricultural areas were selected where cultivation has ceased in the last six decades. The NDVI values for these areas were extracted and the percentage variation in the vegetation index was calculated to evaluate the evolution of the vegetation recovery. Furthermore, two afforested areas planted between 1984 and 1986 were selected to allow comparisons with the vegetation evolution in afforested areas. The selected areas were further classified as north and south facing areas in order to calculate difference in the NDVI and temporal evolution under different solar radiation conditions. The NDVI values from the 2013 image were correlated with the soil nutrient contents.

2.4. The SPEROS-C model

Due to the absence of SOC data prior to land abandonment we applied the results of the SPEROS-C model obtained by Quijano et al. (2017) on a 1.6 ha cultivated field located in the study catchment to approximate the SOC stocks that existed in the 1950s, prior to recent land use changes. This representative field has been cultivated with cereals since at least 1860 using three different management practices: traditional, conventional and conservation tillage. Traditional tillage practices were implemented until the 1960s using a chisel with animal traction. Conventional tillage was used from 1960 to 1995 using a mouldboard plough pulled by a tractor, and minimum-tillage conservation practices were carried out in recent decades (1995 to present) using a chisel with a tractor.

Analytical data obtained from 156 samples collected from a 10 × 10 m grid established in the 1.6 ha field were used as the input for the SPEROS-C model. The model represents the effect of land management on SOC stocks, SOC fluxes and changes in their spatial distribution. For this purpose, a correction factor between the present SOC (%) and the mid-1950s SOC (%) was extracted from the mean, maximum and minimum values of the SPEROS-C model results obtained from the 156 sampling sites by Quijano et al. (2017) in the 1.6 ha field.

At present in the Barués catchment, a total of 20 sampling sites remain as agricultural, land use at 41 sites has changed from being cultivated in the 1950s to natural forest, pine afforestation or scrubland, while another 37 sampling sites remain as forest, as they were in the 1950s. The correction factor extracted from the SPEROS-C model was therefore implemented on the data from the 20 agricultural sites where land use had not changed. To estimate the historical SOC stocks at the sites that had changed from cropland to rangeland or had been afforested, we applied the mean modelled value of the 20 agricultural sites in 1957, assuming that in the 1950s, the 41 revegetated sites had similar SOC as the other agricultural sampling sites. The 20 agricultural sites have low SOC values with a mean of 0.78% ± 0.37.

The present SOC inventory (kg m^2) was calculated for the 98 samples collected in the catchment using the following equation:

$$\text{SOC inventory} = \frac{\text{SOC}}{100} * \text{D} * soil\ depth \quad (3)$$

where SOC is the percentage of SOC in each sample, D is the bulk density (g cm^{-3}) for each sample measured in < 2 mm fraction and *soil depth* was estimated as the mean depth (cm) for each soil type extracted from the field surveys (Fig. 1).

To extrapolate the present data to the 1950s we extract the correction factor from the data obtained by Quijano et al. (2017) in a 1.6 ha cultivated field as follows:

$$\text{SPCF} = \frac{1957\ \text{SPEROS} - \text{C SOC (\%)}}{2010\ \text{SPEROS} - \text{C SOC (\%)}} \quad (4)$$

where 1957 SPEROS-C SOC (%) is the mean, median, min and max SOC (%) simulated for 1957 and 2010 SPEROS-C SOC (%) is the mean, median, min and max SOC (%) estimated by the model for 2010. Thus, as a result of the equation we obtain the differences in SOC percentage between 1957 and 2010. This correction factor (SPCF) is implemented in the next equation to calculate the SOC inventories in the agricultural land in the 1950s:

$$\text{SOC inventory in 1957} = \frac{\text{SOC}/100}{SPCF} * \text{D} * soil\ depth \quad (5)$$

where *SPCF* is the SPEROS-C model correction factor extracted from the values of the results obtained for the 156 sites from the SPEROS-C model by Quijano et al. (2017). Thus, the variation in the SOC inventory is calculated by using the mean, median, min and max values of the 20 unchanged agricultural sampling sites and extrapolating them to the present 41 revegetated sites.

3. Results

3.1. Soil characteristics

Soils were alkaline, with pH values ranging between 7.38 and 8.59, and had low salinity (with a mean value of 0.18 dS m^{-1}) and a high carbonate content (36%). > 64% of the soil samples had a silt loam texture, with the predominance of silt ranging between 47% and 60%. Twenty-one percent of the soil samples had loam texture, 14% sandy loam and the remaining 1% had loamy sand texture with a sand content higher than 78%. The soil content represented by the coarse fraction (> 2 mm) varied from 0% to 36%. The SOC and TN contents were low, ranging from 0.22% to 3.44% and from 0.02% to 0.74%, respectively. The mass magnetic susceptibility measured at low frequency (χ_{LF}) had a mean value of 34.25 10^{-8} m^3 kg^{-1}, and the mean value of the frequency dependent magnetic susceptibility (χ_{FD}) was 34. 5% (Table 1).

Only the saturation point, field capacity and permanent wilting point were significantly correlated with the grain size ($p \leq 0.05$), being positively correlated with clay and negatively with sand (Table 2). SOC and TN were significantly and directly correlated ($p \leq 0.05$) with stoniness, $CaCO_3$, EC and the magnetic properties.

The means of stoniness, SOC, $CaCO_3$, EC and pH in the agricultural soils significantly differed from those in other land use areas ($p \leq 0.01$) (Table 3). On agricultural land, the SOC content was lower and significantly different from the other land uses, with the highest values being found in the natural forest and in pine afforested areas. In addition, when tested separately, the SOC and TN contents had lower present day values at sampling sites that had changed from being agricultural land compared with those that had remained as forest since the 1960s (Table 4).

Although no significant differences were found in the mean values of clay, silt and sand contents among the different land uses, the agricultural soils were characterised by significantly smaller means ($p \leq 0.05$) in the coarse fraction (> 2 mm).

The means of TN in agricultural land and pine afforested land were lower than in the other land uses, but they were only significantly different ($p \leq 0.05$) in the agricultural land, which had the lowest TN content.

The spatial distribution maps produced by an ordinary kriging of all of the soil properties are shown in Fig. 2. There is a wide variation across the catchment; however, higher values for SOC, TN, magnetic properties (LF, FD) and EC were recorded in the northern half and the south-eastern part of the catchment, whereas lower values were measured in the central, northeast and southwest parts. In contrast to this pattern, the highest pH and $CaCO_3$ values were found in the southern half and the north-western part of the catchment. Relatively higher clay contents were recorded in the central and eastern parts of the catchment, while sand content showed no clear spatial distribution pattern. In addition, stoniness gradually increases from the southwest to the northeast. The field capacity and the wilting point do not show any clear distribution pattern in the catchment.

3.2. Variation in vegetation

An increase in the NDVI value from the 1970s to the present day is observed in most areas of the catchment (Figs. 3, 4). The highest increment occurred between 1987 and 2001 at the headwaters, where a second pine forest was planted between 1984 and 1988. A decrease in the NDVI values between 1984 and 1987 is observed in many parts of the catchment, except in the central part where the first afforestation was already planted. Between 1990 and 2001 a progressive increase in the NDVI values was observed all over the catchment. The same increase in aerial biomass remains at present, except in the northern part of the oldest pine afforestation where lower values of the NDVI were observed.

Natural revegetated and afforested areas showed an increasing trend in the study period, with higher values in north compared with south facing slopes (Fig. 4). Naturally revegetated areas show an increasing trend in NDVI values from the 1970s to the present day, with a stronger trend in the first decades. However, the highest increment in the NVDI in pine afforested areas was recorded between 1990 and 2001, six to sixteen years after planting. Both naturally revegetated and forested areas reported a more rapid increase in their first stages but the afforested areas quickly reached higher NDVI values. Since 1984, when the forest was planted, the north facing slopes showed larger increments in the NDVI until 2001 when a first peak was reached.

However, the total increase since the time of abandonment was greater in the naturally revegetated cover. A generalised increasing trend in the NDVI values was observed across the catchment. Nevertheless, there were some periods where the NDVI stabilised such as 1984–1987 and 2003–2007, and even some periods where it decreased, such as 2001–2003 and 2013–2016–2017 (Figs. 3, 4).

3.3. The SPEROS-C model

The modelled SOC showed an increase in SOC stocks at all study sites, with the highest increases in the areas where the land use changed from croplands to natural forest and pine afforestation. The mean present-day SOC inventory values for agricultural land was 3.94 kg m^{-2} which differed greatly from mean SOC inventory values of 6.21 kg m^{-2} in areas covered by forest and scrubs. The mean present-day agricultural SOC stocks value was 3.7 times higher at present than the modelled 1957 value (Table 5).

The lowest increases were found at sites that had remained under agricultural use since 1957. Scrubland sites showed higher mean SOC contents than agricultural land, but with high variability, scrubland sites exhibiting both the highest and lowest values for SOC content. The areas showing the highest increases were located at higher altitudes and on steeper slopes.

Table 1
Basic statistics of the different study properties in the Barués catchment.

n = 98	Stoniness	Clay	Sand	pH	EC	$CaCO_3$	Field capacity	Wilting point	SOC	χ_{LF}	χ_{FD}	TN	C:N
	%	%	%		dS m^{-1} 25 °C	%	% Vol	% Vol	%	10^{-8} m^3 kg^{-1}	%	%	
Mean	9.28	8.93	37.30	8.00	0.21	34.98	32.65	14.21	1.45	41.27	8.57	0.14	12.84
Median	7.70	8.60	38.50	8.03	0.18	36.29	33.12	13.72	1.49	34.45	9.05	0.13	12.15
SD	8.48	2.42	12.15	0.27	0.07	8.92	5.82	3.86	0.73	27.45	2.20	0.10	7.16
Min	0.00	3.80	0.00	7.38	0.10	3.53	18.17	5.35	0.22	7.50	2.98	0.02	0.98
Max	36.45	17.50	77.95	8.59	0.41	51.76	46.82	25.49	3.44	117.00	11.92	0.74	53.50

Table 2
Correlation coefficient of the different properties.

n = 98	Stoniness	Clay	Sand	pH	CE	$CaCO_3$	SOC	TN	χ_{LF}	χ_{FD}	Field capacity
Clay	***−0.3626***										
Sand	***0.4649***	***−0.7582***									
pH	**−0.2279**	0.0162	−0.1247								
CE	0.1541	−0.0131	0.1251	***−0.7885***							
$CaCO_3$	***−0.2846***	**−0.2307**	−0.0876	***0.3757***	***−0.5136***						
SOC	***0.2928***	−0.1014	0.1763	***−0.5233***	***0.5483***	***−0.4554***					
TN	**0.2459**	0.1011	0.0805	−0.1309	**0.2461**	***−0.4886***	***0.3736***				
χ_{LF}	***0.3637***	0.02	**0.251**	***−0.3427***	***0.4325***	***−0.6811***	***0.529***	***0.3916***			
χ_{FD}	0.0874	0.1146	0.0629	***−0.4305***	***0.4357***	***−0.4736***	***0.4276***	**0.2424**	***0.6405***		
Field capacity	***−0.3753***	***0.3367***	***−0.3748***	−0.1626	0.143	−0.1566	0.0702	−0.1335	0.062	0.0823	
Wilting point	**−0.2454**	***0.439***	**−0.304**	−0.1513	0.0767	0.086	0.0735	**−0.2304**	−0.0713	−0.0737	***0.7517***

Bold numbers indicate statistical significance at $p \leq 0.05$ level. Bold and italicized numbers indicate statistical significance at $p \leq 0.01$. Bold, italicized and underlined numbers, indicate statistical significance at $p \leq 0.001$.

The land used for agriculture in 1957 had a modelled mean SOC inventory value of 1.04 kg m^{-2} over a surface area of 13.42 km^2, while the present-day value over the agricultural area has a mean value of 3.94 kg m^{-2} over just 3.81 km^2. A total of 41% of the agricultural land in 1957 has become covered by vegetation, wherein the present-day SOC inventories are 7.66, 6.98 and 5.51 kg m^{-2} in natural forest, pine afforestation and scrubland, respectively.

4. Discussion

4.1. Variation in soil characteristics with different land uses

The results showed that there were significant differences in all soil properties except for grain size in croplands compared with the other land uses, indicating that land use is one of the main factors affecting the variation in soil properties after five decades of reversion of the generalised cultivation in the catchment (Fig. 1).

The non-significant difference in grain size among the different land uses could be explained by the homogeneity in texture across the catchment due to the limited range of clay content (80% of the samples had a clay content of 5–10%). These results are in agreement with results found in other Pre-Pyrenean environments (Gaspar and Navas, 2013) and by Quijano et al. (2016a, 2016b) in a cultivated field in the catchment studied here. However, the significant difference in stoniness in croplands is related to tillage practices that contribute to the breakdown of rock fragments and soil aggregates. Manual clearing of stones to improve the conditions of the cultivated fields also contributes to the reduced stoniness. Thus, higher stoniness is found where natural forests and revegetated land dominate. Likewise, the distribution of the land uses across the catchment may also play a role in the direct correlations between SOC, TN, EC and magnetic properties and the inverse correlations with pH and carbonates. In particular, the inverse correlation between carbonates and magnetic properties could be related to the content of calcite, which has diamagnetic properties, and results in negative values of magnetic susceptibility (Dearing, 1999). Thus, increased carbonate content ($CaCO_3$) may yield a decrease in magnetic susceptibility, as we observed in our study catchment and in agreement with Sarmast et al. (2017). In addition, the significant positive correlations between SOC content and the magnetic soil parameters measured in this study likely evidence the close relationship between magnetic properties and organic matter, as found by other authors (Jordanova, 2017), confirming the potential of using magnetic soil properties for tracking soil degradation in this environment (Quijano et al., 2014).

The scarce variation in pH is due to the homogeneous distribution of the lithology and the significant presence of carbonates in the underlying parent materials from which the different soil types are derived. The absence of a clear distribution pattern of the field capacity or

Table 3
Basic statistics of the soil properties and grain size of the sampling points under the different land uses in the study catchment.

		Stoniness	Clay	Sand	pH	CE	$CaCO_3$	Field capacity	Wilting point	SOC	χ_{LF}	χ_{FD}	TN	C:N
		%	%	%		dS m^{-1} 25 °C	%	% Vol	% Vol	%	10^{-8} m^3 kg^{-1}	%	%	
Agricultural	Mean	5.39a	9.10a	35.63a	8.20a	0.16a	38.82a	32.22a	14.17	0.79a	33.45a	8.01a	0.09a	11.21a
	Median	3.91	8.60	35.85	8.20	0.15	40.39	33.36	14.68	0.68	34.15	8.42	0.07	11.07
	SD	6.12	2.94	14.87	0.17	0.03	7.07	7.11	4.29	0.37	16.81	2.03	0.07	5.07
	Min	0.27	3.80	0.00	7.90	0.13	19.30	18.17	5.59	0.38	7.50	2.98	0.02	2.17
	Max	23.03	17.50	77.95	8.59	0.23	51.76	46.75	20.74	2.10	70.70	10.68	0.30	25.50
Forest	Mean	10.79b	9.24a	38.88a	7.91b	0.25b	28.79b	33.28a	13.82	1.77b	54.31b	9.32a	0.16b	12.61ab
	Median	9.28	9.20	39.40	7.88	0.24	27.48	32.18	13.07	1.73	53.70	9.36	0.16	12.75
	SD	7.41	2.06	9.38	0.24	0.09	10.68	3.92	2.96	0.48	27.29	1.29	0.09	4.43
	Min	2.62	6.20	17.50	7.45	0.14	9.61	27.17	9.49	0.90	17.40	7.18	0.05	3.79
	Max	23.60	14.50	54.20	8.36	0.41	42.20	40.89	20.17	2.49	117.00	11.62	0.43	24.33
Pine	Mean	12.45b	7.93a	41.84a	7.88b	0.24bc	35.15a	29.92a	12.24	1.83b	46.14b	9.21a	0.13b	15.69b
	Median	11.06	8.00	44.10	7.98	0.22	36.58	30.23	11.89	1.99	40.90	9.71	0.13	14.91
	SD	9.48	2.17	13.05	0.27	0.08	7.23	6.51	4.14	0.74	26.62	1.67	0.06	6.34
	Min	1.65	3.90	14.90	7.38	0.11	22.57	21.61	5.35	0.39	10.30	4.02	0.04	6.50
	Max	35.84	13.30	65.30	8.17	0.41	50.29	44.09	22.96	2.84	89.80	10.81	0.23	33.50
Scrubland	Mean	9.44b	9.07a	36.08a	7.97b	0.20c	35.27a	33.48a	14.96	1.51b	38.94ab	8.38a	0.16b	12.70ab
	Median	7.86	8.65	37.90	8.01	0.19	35.93	34.00	13.95	1.58	27.45	9.08	0.13	11.96
	SD	8.93	2.36	11.34	0.26	0.06	8.71	5.37	3.69	0.73	30.25	2.56	0.13	8.58
	Min	0.00	5.70	5.90	7.43	0.10	3.53	20.57	7.94	0.22	7.90	3.18	0.02	0.98
	Max	36.45	16.60	58.60	8.58	0.36	50.03	46.82	25.49	3.44	111.40	11.92	0.74	53.50

Letters a, b and c in the means column represents the groups that are significantly different from the others.

Table 4
SOC percentage and inventory in 1957 calculated with the SPCF and the data from the 98 core samples collected.

		n	SOC %				SOC stock (kg m^{-2})			
			Mean	Median	Max	Min	Mean	Median	Max	Min
1957	Agricultural	20	0.21	0.21	0.23	0.19	1.04	1.02	2.15	0.50
2013	Agricultural	20	0.79a	0.68	2.10	0.38	3.94a	3.85	8.12	1.89
	Forest	15	1.42b	1.43	2.04	0.90	7.66b	6.98	13.71	4.23
	Pine	15	1.91c	1.99	2.79	0.89	6.98b	8.13	11.94	0.88
	Scrubland	48	1.36b	1.37	2.82	0.38	5.51b	5.21	13.68	0.85

Letters a, b and c in the means column represents the groups that are significantly different from the others.

wilting point is probably related to the generally homogenous texture in the soils of the catchment. The coincident distribution of LF and FD values with nutrients results from magnetic values being generally positively correlated with SOC values (Quijano et al., 2014). The contrasting distribution of pH and $CaCO_3$ compared with SOC and TN could be related to the land use distribution in the catchment. Thus, the highest values of pH and carbonates are found in agricultural land, along with the lowest values of SOC and TN.

The spatial distribution of the soil properties shows good agreement with the distribution of the different land uses. The agricultural lands that occupy the lowest altitudes correspond to the selection of flat terrains to facilitate tillage, sowing and harvest practices, affecting the different soil properties. The lands that were abandoned first are located in the highest and steepest areas that were more difficult to access and were farther from the village, as found in other Pyrenean valleys (Navas et al., 2017). The earlier abandonment of the areas with more difficult access and their subsequent revegetation likely contributed to their greater increases in organic matter, as found by Navas et al. (2012).

The higher SOC contents in pine afforested areas and natural forest are due to the higher density of the vegetation cover and the greater size of the trees, resulting in larger aerial biomass, in agreement with results found in other Mediterranean environments by Navas et al. (2008) and Nadal-Romero et al. (2016). In comparison, the lower SOC content in scrubland is because the less mature plants in general scrub are younger in these abandoned lands than in natural forest, although poorer soil conditions at the time of abandonment cannot be totally excluded. Both TN and SOC were lower in the croplands, which could be also related to the higher erosion rates that lead to losses of fine soil components including organic matter, as found by Navas et al. (2014) in nearby mountain agroecosystems. The higher percentage of SOC and TN in rangelands is commonly reported in different environments where higher percentages of vegetation cover are related to higher contents of SOC and TN (Navas et al., 2011; Nadal-Romero et al., 2016; Korkanç, 2014). The lower SOC and TN values found at sites that have changed from agricultural land to rangeland or afforestation in the recent decades could be related to poorer soil conditions at the time of the abandonment compared with the areas that have remained as rangeland since the 1960s. The similar values of SOC in pine afforested areas that previously were croplands or rangeland suggest a higher capacity to sequester carbon in the pine afforestation. However, in natural rangelands SOC and TN values increase gradually from the time of land abandonment because of the slower growth rate of the mixed vegetation. On the other hand, the significantly higher contents of TN in the natural forest and the higher values in scrubland compared with pine afforestation suggest that rangeland has a greater capacity to fix nitrogen. Thus, the vegetation succession in response to land abandonment positively influences soil quality, since SOC and TN are higher in the abandoned areas, as also found by Van Hall et al. (2017) in a humid Mediterranean landscape.

The SOC stocks have increased from the 1960s to the present day mainly induced by the land use changes. Furthermore, the significant differences between the cropland and the naturally revegetated or afforested areas suggest that non-agricultural land uses such as open forest, pine afforestation and scrubland produce more fertile soils. Accordingly, the higher SOC and TN values found in the areas located in the northern half and the south-eastern part of the catchment coincide with greater abundance of rangeland and afforested areas. The increased SOC stocks since the 1950s simulated with the SPEROS-C model are likely produced by changes in agricultural practices. The change from traditional tillage with animal traction to conventional tillage after the introduction of the machinery increased crop productivity. Conservation practices were introduced after 1995, reducing losses of soil organic carbon. Increased SOC due to a change from conventional tillage to conservation tillage has been reported by several authors in the last decade (Balota et al., 2004; Jacobs et al., 2009; Busari et al., 2015). However, the main SOC stock increase in this study was due to land abandonment and the transition from agricultural land to natural and afforested areas, as also reported by Celik (2005), Liu et al. (2015), Selassie et al. (2015), and Lasanta et al. (2016) in different environments. On the other hand, the vegetation expansion reduces erosion rates at the catchment scale as found by Lizaga et al. (2018) in this study catchment. This increase is also supported by the positive correlation between the NDVI and SOC contents (Fig. 5). Relationships between SOC and TN data and the NDVI suggest that natural cover produces increases of nitrogen in the soil (Lizaga et al., 2019). However, the higher SOC values in the afforested areas are likely produced due to the more rapid ascent in the NDVI. In addition, the lowest correlation between NDVI and SOC/TN in scrubland is likely due to high vegetation heterogeneity together with the largest variation of SOC and TN in this land use. On the contrary, we observe high correlation between NDVI and SOC/TN in pine afforestation was linked to the uniform vegetation cover.

4.2. Temporal analysis of the evolution of the vegetation cover

From the images used to calculate the NDVI, the overall increase in the value of the index from the 1970s to the present day indicates an increase in vegetation cover and density. For most of the catchment this was produced by the gradual abandonment of the agricultural land and its progressive transition to natural revegetated cover, in parallel with afforestation. The decrease in the NDVI values in the northern part of the catchment to 1984 was produced by the clearance and regularisation of the slopes by terracing that was done prior to the introduction of the pine afforestation, planted after 1984. The greatest rise in the NDVI values was in the 1970s, caused by large increases in vegetation on recently abandoned croplands and an increase in the aerial biomass of the oldest reforested areas. Furthermore, in 2001 images, a second peak in the NDVI values occurs because of the growth of pine trees planted in the previous afforestation works and a progressive increase in vegetation cover on most of the abandoned croplands, along with higher rainfall in the nineties (Fig. 4). Thus, it is likely that as the forest matures, the forest volume initially starts to grow at a slower rate until the forest reaches a steady state. Then, the volume begins to grow rapidly and reaches a maximum, beyond which the rate of volume growth begins to decline (Ryan et al., 2015). A third peak was detected in 2013

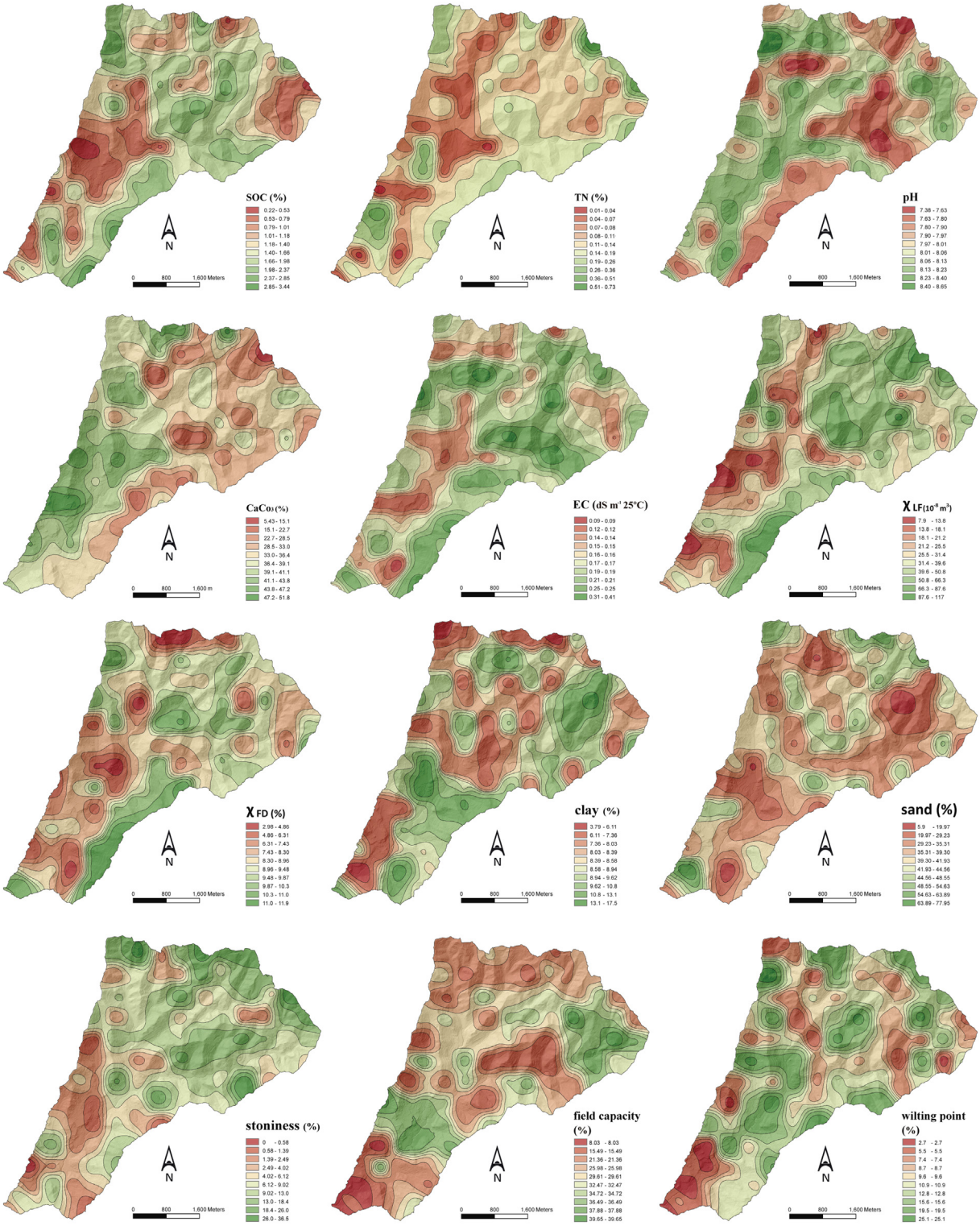

Fig. 2. Spatial distribution of the assayed physical and chemical properties produced by an ordinary kriging and the corresponding isocurves in the study catchment.

due to an increase in all vegetation cover and a rising trend of vegetation growth after grazing in the catchment ceased. However, after these three peaks, there are changes in the NDVI due to the onset of dry periods with higher temperatures that inverted the increasing trend. In addition, these dry periods in the summers from 1984 to 1987 and 2003 to 2005 led not only to a generalised decrease in the NDVI for these periods but also to a stabilisation or reduction in the increasing trend in the following periods (Fig. 4). Furthermore, after the dry periods, north facing slopes showed a greater decrease in NDVI values, likely due to the greater increase produced in the wet periods.

The inversion of the trend at present has clearly been triggered by the dry period reported since 2016, with no precipitation experienced in the summer. Moreover, maintenance works involving thinning that removed part of the trees have also prompted a significant decrease in the oldest pine afforestation.

The greater vegetation cover on north compared with south facing

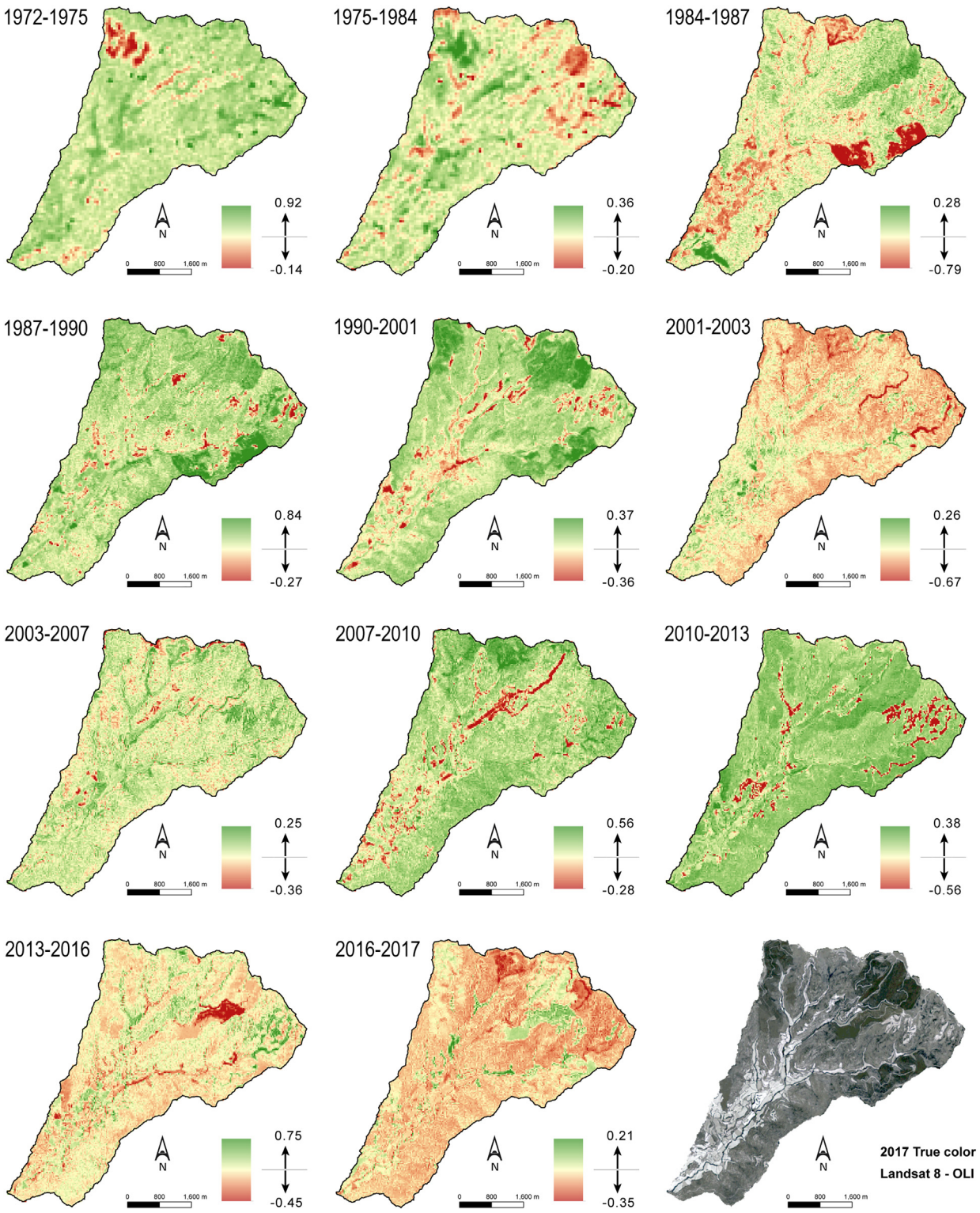

Fig. 3. Image comparison of the variations of the NDVI index between 1972 and 2017 in the Barués catchment. Stretch type method: Standard Deviation.

areas was also reported by Lizaga et al. (2017) in the Barués catchment, expressed in total aerial biomass (TAB) inside the pine afforestation. Furthermore, variation between areas with different solar radiation showed different temporal evolution for natural cover and pine afforested areas. The afforested areas showed no difference in NDVI at the time when they were planted (1984); nevertheless, in 1987 they started to differentiate, reaching a maximum NDVI in 2001 due to higher precipitation in the nineties. However, natural cover already showed a clear difference in 1972 between areas with higher and lower solar radiation values. This indicates that in < 15 years after land abandonment, natural vegetation had already covered the abandoned agricultural areas.

5. Conclusions

After land abandonment, the soil physico-chemical properties vary

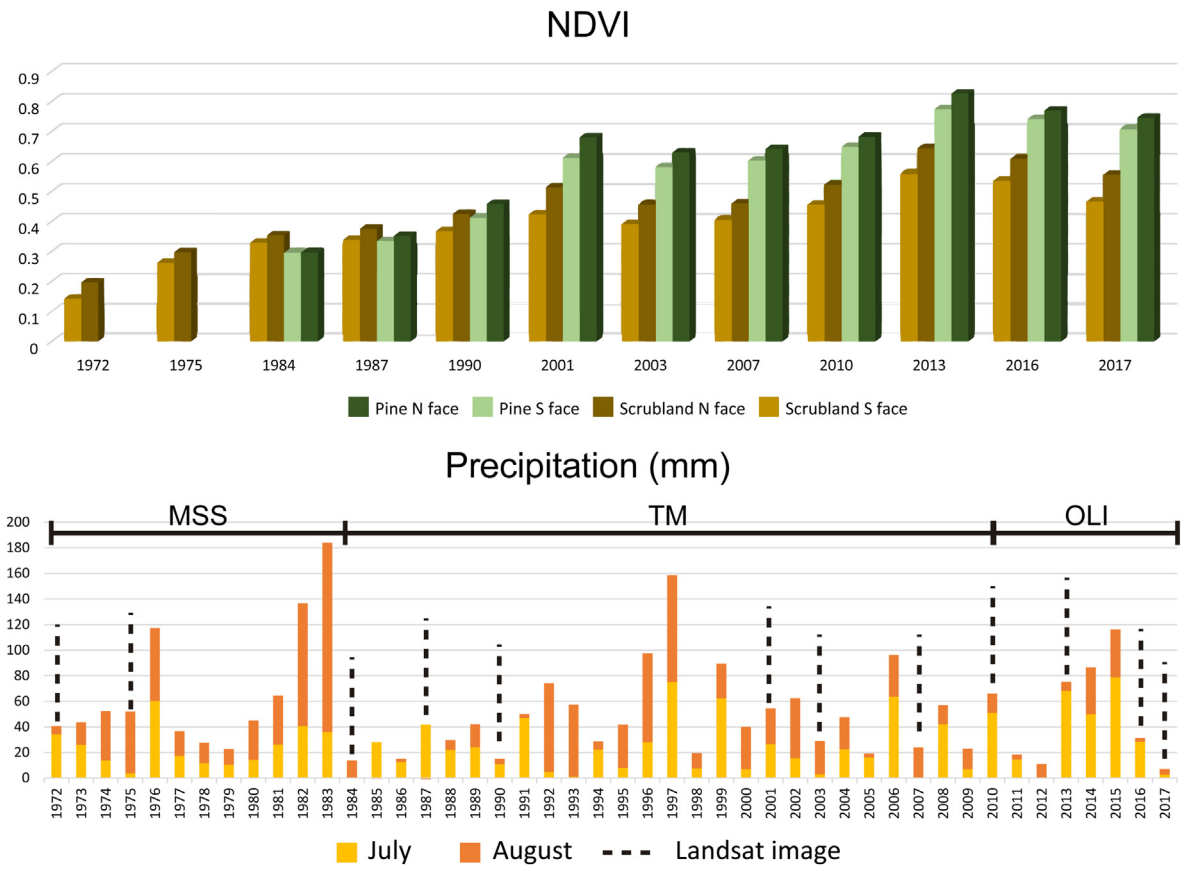

Fig. 4. Comparison between the natural revegetated and the afforested areas and their north and south faces since 1972. a) Bar plot of the NDVI evolution in the natural and afforested areas. b) Mean monthly precipitation plot since 1972 for July and August when the satellite images where recorded.

Table 5
SOC and TN percentages in rangeland (forest and scrubland) and pine afforestation points in areas that were rangeland in sixties and areas that have change from agricultural land.

	Rangeland in 1957			Agricultural in 1957		
	n	SOC (%)	TN (%)	n	SOC (%)	TN (%)
Forest	9	2.00	0.19	6	1.42	0.13
Pine	5	1.96	0.15	10	1.91	0.12
Scrubland	21	1.68	0.16	27	1.36	0.14

significantly among different land uses in this mountain agroecosystem. The SOC, TN, pH and $CaCO_3$ values indicate that agricultural land has less fertile soils. Due to afforestation and natural revegetation, soil organic carbon stocks and total nitrogen have significantly increased, supporting the key role of management of agricultural lands in soil organic carbon and nitrogen dynamics.

Multitemporal satellite imagery is a fundamental tool for the quantification of spatial and temporal vegetation changes and the effects of human intervention, which could not be attempted through conventional mapping.

The results extracted from remote sensing analysis and soil nutrient quantification suggest that in the short term, afforestation produces a faster increase in SOC than natural cover, although an increase is not observed in TN. After > 50 years since land abandonment, the soil quality was similar under naturally revegetated and afforested cover. Furthermore, the abandoned land became naturally revegetated with native species 15 years after abandonment. The use of mixtures of native and fast-growing species such as pine promotes increases in SOC

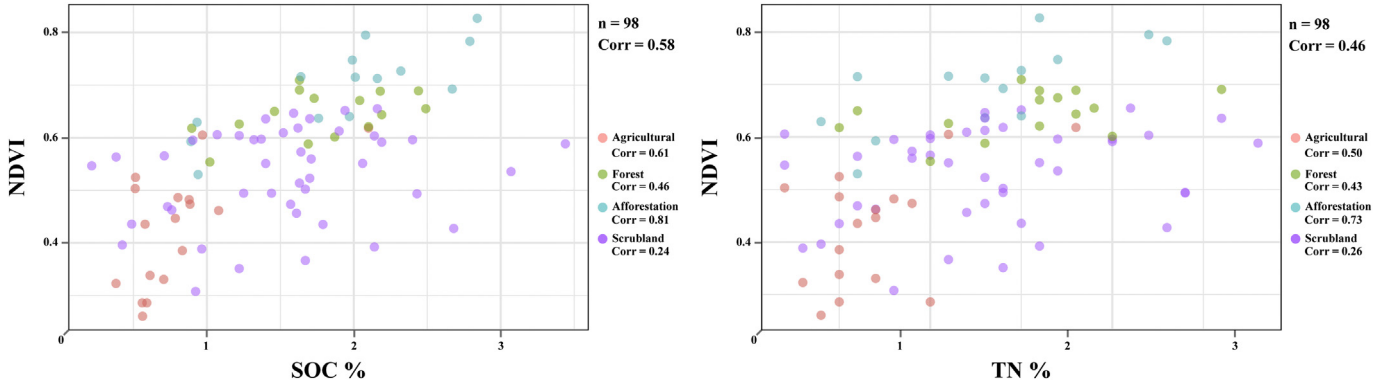

Fig. 5. Correlation between the NDVI and the SOC % and TN % values of the 98 sampling points in the different land uses in the Barués catchment.

and TN, and good soil recovery. It could therefore be a suitable alternative to cost intensive afforestation with pine monoculture.

The implementation of the SPEROS-C model and its extrapolation at catchment scale can be used as an approximation to assess variations in SOC stocks due to land use changes. It also underlines the importance of preserving natural forests. The effects of recent land use changes on soil properties should be considered in the design of future afforestations. The results of this research could be useful to environmental planners in decisions about best practices after land abandonment and future afforestation programmes.

Acknowledgments

This research was financially supported by the project TRAZESCAR (CGL2014-52986-R) with the aid of a predoctoral contract (BES-2015-071780) funded by the Spanish Ministry of Science, Innovation and Universities.

References

Alonso-Sarría, F., Martínez-Hernández, C., Romero-Díaz, A., Cánovas-García, F., Gomariz-Castillo, F., 2016. Main environmental features leading to recent land abandonment in Murcia region (Southeast Spain). Land Degrad. Dev. 27, 654–670. https://doi.org/10.1002/ldr.2447.

Álvaro-Fuentes, J., Paustian, K., 2011. Potential soil carbon sequestration in a semiarid Mediterranean agroecosystem under climate change: quantifying management and climate effects. Plant Soil 338, 261–272. https://doi.org/10.1007/s11104-010-0304-7.

Andrén, O., Kätterer, T., 1997. Icbm: the introductory carbon balance model for exploration of soil carbon balances. Ecol. Appl. 7, 1226–1236. https://doi.org/10.1890/1051-0761(1997)007[1226:ITICBM]2.0.CO;2.

Balota, E.L., Colozzi Filho, A., Andrade, D.S., Dick, R.P., 2004. Long-term tillage and crop rotation effects on microbial biomass and C and N mineralization in a Brazilian Oxisol. Soil Tillage Res. 77, 137–145. https://doi.org/10.1016/j.still.2003.12.003.

Bartington Instruments Ltd., 2000. Operation manual for MS2 Magnetic Susceptibility System. Bartington Instruments Ltdpg., pp. 72.

Ben-Dor, E., Banin, A., 1995. Near-infrared analysis as a rapid method to simultaneously evaluate several soil properties. Soil Sci. Soc. Am. J. 59, 364–372. https://doi.org/10.2136/sssaj1995.03615995005900020014x.

Boix-Fayos, C., Martínez-Mena, M., Cutillas, P.P., de Vente, J., Barberá, G.G., Mosch, W., Navarro Cano, J.A., Gaspar, L., Navas, A., 2017. Carbon redistribution by erosion processes in an intensively disturbed catchment. Catena 149, 799–809. https://doi.org/10.1016/j.catena.2016.08.003.

Bruce, J.P., Frome, M., Haites, E., Janzen, H., Lal, R., Paustian, K., 1999. Carbon sequestration in soils. J. Soil Water Conserv. 54, 382–389.

Bruun, T.B., Elberling, B., de Neergaard, A., Magid, J., 2015. Organic carbon dynamics in different soil types after conversion of forest to agriculture. Land Degrad. Dev. 26, 272–283. https://doi.org/10.1002/ldr.2205.

Busari, M.A., Kukal, S.S., Kaur, A., Bhatt, R., Dulazi, A.A., 2015. Conservation tillage impacts on soil, crop and the environment. Int. Soil Water Conserv. Res. 3, 119–129. https://doi.org/10.1016/j.iswcr.2015.05.002.

Celik, I., 2005. Land-use effects on organic matter and physical properties of soil in a southern Mediterranean highland of Turkey. Soil Tillage Res. 83, 270–277. https://doi.org/10.1016/j.still.2004.08.001.

Chauchard, S., Carcaillet, C., Guibal, F., 2007. Patterns of land-use abandonment control tree-recruitment and forest dynamics in Mediterranean mountains. Ecosystems 10, 936–948. https://doi.org/10.1007/s10021-007-9065-4.

Chavez, J., 1996. Image-based atmospheric corrections - revisited and improved. Photogramm. Eng. Remote. Sens. 62, 1025–1036.

Dearing, J., 1999. Environmental magnetic susceptibility: using the bartington MS2 system. Chi Publishing, Keniloworth.

Fan, X., Liu, Y., 2016. A global study of NDVI difference among moderate-resolution satellite sensors. ISPRS J. Photogramm. Remote Sens. 121, 177–191. https://doi.org/10.1016/j.isprsjprs.2016.09.008.

Fan, X., Liu, Y., 2017. A generalized model for intersensor NDVI calibration and its comparison with regression approaches. IEEE Trans. Geosci. Remote Sens. 55, 1842–1852. https://doi.org/10.1109/TGRS.2016.2635802.

Foley, J.A., DeFries, R., Asner, G.P., Barford, C., Bonan, G., Carpenter, S.R., Chapin, F.S., Coe, M.T., Daily, G.C., Gibbs, H.K., Helkowski, J.H., Holloway, T., Howard, E.A., Kucharik, C.J., Monfreda, C., Patz, J.A., Prentice, I.C., Ramankutty, N., Snyder, P.K., 2005. Global consequences of land use. Science 309, 570–574. https://doi.org/10.1126/science.1111772.

Francaviglia, R., Coleman, K., Whitmore, A.P., Doro, L., Urracci, G., Rubino, M., Ledda, L., 2012. Changes in soil organic carbon and climate change – application of the RothC model in agro-silvo-pastoral Mediterranean systems. Agric. Syst. 112, 48–54. https://doi.org/10.1016/j.agsy.2012.07.001.

Gao, L., Becker, E., Liang, G., Houssou, A.A., Wu, H., Wu, X., Cai, D., Degré, A., 2017. Effect of different tillage systems on aggregate structure and inner distribution of organic carbon. Geoderma 288, 97–104. https://doi.org/10.1016/j.geoderma.2016.11.005.

Gaspar, L., Navas, A., 2013. Vertical and lateral distributions of 137Cs in cultivated and uncultivated soils on Mediterranean hillslopes. Geoderma 207–208, 131–143. https://doi.org/10.1016/j.geoderma.2013.04.034.

IUSS Working Group WRB, 2015. World Reference Base for Soil Resources 2014. In: International soil classification system for naming soils and creating legends for soil maps. World Soil Resources Reports No. 106. FAO, Rome. (update 2015).

Jacobs, A., Rauber, R., Ludwig, B., 2009. Impact of reduced tillage on carbon and nitrogen storage of two Haplic Luvisols after 40 years. Soil Tillage Res. 102, 158–164. https://doi.org/10.1016/j.still.2008.08.012.

Jordanova, N., 2017. Chapter 10 - Applications of soil magnetism. In: Jordanova, N. (Ed.), Soil Magnetism. Academic Press, pp. 395–436. https://doi.org/10.1016/B978-0-12-809239-2.00010-3.

Kokaly, R.F., Clark, R.N., Swayze, G.A., Livo, K.E., Hoefen, T.M., Pearson, N.C., Wise, R.A., Benzel, W.M., Lowers, H.A., Driscoll, R.L., Klein, A.J., 2017. USGS Spectral Library Version 7 (USGS Numbered Series No. 1035), Data Series. U.S. Geological Survey, Reston, VA.

Korkanç, S.Y., 2014. Effects of afforestation on soil organic carbon and other soil properties. Catena 123, 62–69. https://doi.org/10.1016/j.catena.2014.07.009.

Krishnaswamy, J., Bawa, K.S., Ganeshaiah, K.N., Kiran, M.C., 2009. Quantifying and mapping biodiversity and ecosystem services: utility of a multi-season NDVI based Mahalanobis distance surrogate. Remote Sens. Environ. 113, 857–867. https://doi.org/10.1016/j.rse.2008.12.011.

Lasanta, T., Nadal-Romero, E., Errea, P., Arnáez, J., 2016. The effect of landscape conservation measures in changing landscape patterns: a case study in Mediterranean mountains. Land Degrad. Dev. 27, 373–386. https://doi.org/10.1002/ldr.2359.

Li, J., Lewis, J., Rowland, J., Tappan, G., Tieszen, L.L., 2004. Evaluation of land performance in Senegal using multi-temporal NDVI and rainfall series. J. Arid Environ. 59, 463–480. https://doi.org/10.1016/j.jaridenv.2004.03.019.

Li, X.-G., Li, F.-M., Zed, R., Zhan, Z.-Y., Bhupinderpal-Singh, 2007. Soil physical properties and their relations to organic carbon pools as affected by land use in an alpine pastureland. Geoderma 139, 98–105. https://doi.org/10.1016/j.geoderma.2007.01.006.

Liu, S., An, N., Yang, J., Dong, Y., Wang, C., 2015. Effects of different land-use types on soil organic carbon and its prediction in the mountainous areas in the middle reaches of Lancang River. Ying Yong Sheng Tai Xue Bao 26, 981–988.

Lizaga, I., Quijano, L., Palazón, L., Gaspar, L., Navas, A., 2017. Enhancing connectivity index to assess the effects of land use changes in a Mediterranean catchment. Land Degrad. Dev. https://doi.org/10.1002/ldr.2676. (07/07/2017).

Lizaga, I., Quijano, L., Gaspar, L., Navas, A., 2018. Estimating soil redistribution patterns with 137Cs measurements in a Mediterranean mountain catchment affected by land abandonment. Land Degrad. Dev. 29, 105–117. https://doi.org/10.1002/ldr.2843.

Lizaga, I., Gaspar, L., Quijano, L., Dercon, G., Navas, A., 2019. NDVI, 137Cs and nutrients for tracking soil and vegetation development on glacial landforms in the Lake Parón Catchment (Cordillera Blanca, Peru). Sci. Total Environ. https://doi.org/10.1016/j.scitotenv.2018.09.075.

MacDonald, D., Crabtree, J.R., Wiesinger, G., Dax, T., Stamou, N., Fleury, P., Gutierrez Lazpita, J., Gibon, A., 2000. Agricultural abandonment in mountain areas of Europe: environmental consequences and policy response. J. Environ. Manag. 59, 47–69. https://doi.org/10.1006/jema.1999.0335.

Mariani, L., Parisi, S.G., 2014. Extreme rainfalls in the Mediterranean area. In: Diodato, N., Bellocchi, G. (Eds.), Storminess and Environmental Change, Advances in Natural and Technological Hazards Research. Springer Netherlands, pp. 17–37. https://doi.org/10.1007/978-94-007-7948-8_2.

Melendez-Pastor, I., Hernández, E.I., Navarro-Pedreño, J., Gómez, I., Koch, M., 2016. Multitemporal Analysis in Mediterranean Forestland With Remote Sensing. https://doi.org/10.5772/63721.

Muñoz-Rojas, M., Abd-Elmabod, S.K., Zavala, L.M., De la Rosa, D., Jordán, A., 2017. Climate change impacts on soil organic carbon stocks of Mediterranean agricultural areas: a case study in Northern Egypt. Agric. Ecosyst. Environ. 238, 142–152. https://doi.org/10.1016/j.agee.2016.09.001.

Myneni, R.B., Hall, F.G., Sellers, P.J., Marshak, A.L., 1995. Interpretation of spectral vegetation indexes. IEEE Trans. Geosci. Remote Sens. 33, 481–486. https://doi.org/10.1109/36.377948.

Nadal-Romero, E., Cammeraat, E., Pérez-Cardiel, E., Lasanta, T., 2016. Effects of secondary succession and afforestation practices on soil properties after cropland abandonment in humid Mediterranean mountain areas. Agric. Ecosyst. Environ. 228, 91–100. https://doi.org/10.1016/j.agee.2016.05.003.

Navas, A., Gaspar Ferrer, L., Quijano Gaudes, L., López-Vicente, M., Machín Gayarre, J., 2012. Patterns of Soil Organic Carbon and Nitrogen in Relation to Soil Movement Under Different Land Uses in Mountain Fields (South Central Pyrenees). https://doi.org/10.1016/j.catena.2011.05.012.

Navas, A., Machín, J., Beguería, S., López-Vicente, M., Gaspar, L., 2008. Soil properties and physiographic factors controlling the natural vegetation re-growth in a disturbed catchment of the Central Spanish Pyrenees. Agrofor. Syst. 72, 173–185. https://doi.org/10.1007/s10457-007-9085-2.

Navas, A., Gaspar, L., López-Vicente, M., Machín, J., 2011. Spatial distribution of natural and artificial radionuclides at the catchment scale (South Central Pyrenees). Radiat. Meas. 46, 261–269. https://doi.org/10.1016/j.radmeas.2010.11.008.

Navas, A., López-Vicente, M., Gaspar, L., Palazón, L., Quijano, L., 2014. Establishing a tracer-based sediment budget to preserve wetlands in Mediterranean mountain agroecosystems (NE Spain). Sci. Total Environ. 496, 132–143. https://doi.org/10.1016/j.scitotenv.2014.07.026.

Navas, A., Quine, T.A., Walling, D.E., Gaspar, L., Quijano, L., Lizaga, I., 2017. Relating intensity of soil redistribution to land use changes in abandoned Pyrenean fields using fallout caesium-137. Land Degrad. Dev. https://doi.org/10.1002/ldr.2724.

Novara, A., Artemi, C., Carmelo, D., Giuseppe, L.P., Antonino, S., Luciano, G., 2015.

Effectiveness of carbon isotopic signature for estimating soil erosion and deposition rates in Sicilian vineyards. Soil Tillage Res. 152, 1–7. https://doi.org/10.1016/j.still.2015.03.010.
Parras-Alcántara, L., Lozano-García, B., Brevik, E.C., Cerdá, A., 2015. Soil organic carbon stocks assessment in Mediterranean natural areas: a comparison of entire soil profiles and soil control sections. J. Environ. Manag. 155, 219–228. https://doi.org/10.1016/j.jenvman.2015.03.039.
Pettorelli, N., Vik, J.O., Mysterud, A., Gaillard, J.-M., Tucker, C.J., Stenseth, N.C., 2005. Using the satellite-derived NDVI to assess ecological responses to environmental change. Trends Ecol. Evol. 20, 503–510. https://doi.org/10.1016/j.tree.2005.05.011.
Quijano, L., Chaparro, M.A.E., Marié, D.C., Gaspar, L., Navas, A., 2014. Relevant magnetic and soil parameters as potential indicators of soil conservation status of Mediterranean agroecosystems. Geophys. J. Int. 198, 1805–1817. https://doi.org/10.1093/gji/ggu239.
Quijano, L., Gaspar, L., Navas, A., 2016a. Lateral and depth patterns of soil organic carbon fractions in a mountain Mediterranean agrosystem. J. Agric. Sci. 154, 287–304. https://doi.org/10.1017/S002185961400135X.
Quijano, Laura, Gaspar, L., Navas, A., 2016b. Spatial patterns of SOC, SON, 137Cs and soil properties as affected by redistribution processes in a Mediterranean cultivated field (Central Ebro Basin). Soil Tillage Res. 155, 318–328. https://doi.org/10.1016/j.still.2015.09.007.
Quijano, L., Van Oost, K., Nadeu, E., Gaspar, L., Navas, A., 2017. Modelling the effect of land management changes on soil organic carbon stocks in a Mediterranean cultivated field. Land Degrad. Dev. 28, 515–523. https://doi.org/10.1002/ldr.2637.
Rahimi, M.R., Ayoubi, S., Abdi, M.R., 2013. Magnetic susceptibility and Cs-137 inventory variability as influenced by land use change and slope positions in a hilly, semiarid region of west-central Iran. J. Appl. Geophys. 89, 68–75. https://doi.org/10.1016/j.jappgeo.2012.11.009.
Romanyà, J., Rovira, P., 2011. An appraisal of soil organic C content in Mediterranean agricultural soils. Soil Use Manag. 27, 321–332. https://doi.org/10.1111/j.1475-2743.2011.00346.x.
Rouse Jr., J.W., Haas, R.H., Schell, J.A., Deering, D.W., 1974. Monitoring Vegetation Systems in the Great Plains with Erts. 351. NASA Special Publication, pp. 309.
Ryan, M., O'Donoghue, C., Phillips, H., 2015. Modelling financially optimal afforestation and forest management scenarios using a bio-economic model. Open J. For. 06, 19. https://doi.org/10.4236/ojf.2016.61003.
Sarmast, M., Farpoor, M.H., Esfandiarpour Boroujeni, I., 2017. Magnetic susceptibility of soils along a lithotoposequence in southeast Iran. Catena 156, 252–262. https://doi.org/10.1016/j.catena.2017.04.019.
Selassie, Y.G., Anemut, F., Addisu, S., 2015. The effects of land use types, management practices and slope classes on selected soil physico-chemical properties in Zikre watershed, North-Western Ethiopia. Environ. Syst. Res. 4 (3). https://doi.org/10.1186/s40068-015-0027-0.
Tirapu, G.P., Arenas, C., 1996. Late Oligocene - Early Miocene syntectonic fluvial sedimentation in the Aragonese Pyrenean domain of the Ebro Basin: facies models and structural controls. Cuad. Geol. Iber. 21, 277–296. https://doi.org/10.5209/rev_CGIB.1996.v21.2532.
Vågen, T.-G., Winowiecki, L.A., Abegaz, A., Hadgu, K.M., 2013. Landsat-based approaches for mapping of land degradation prevalence and soil functional properties in Ethiopia. Remote Sens. Environ. 134, 266–275. https://doi.org/10.1016/j.rse.2013.03.006.
Vågen, T.-G., Winowiecki, L.A., Tondoh, J.E., Desta, L.T., Gumbricht, T., 2016. Mapping of soil properties and land degradation risk in Africa using MODIS reflectance. Geoderma 263, 216–225. https://doi.org/10.1016/j.geoderma.2015.06.023.
Valladares, F., Pearcy, R.W., 1997. Interactions between water stress, sun-shade acclimation, heat tolerance and photoinhibition in the sclerophyll Heteromeles arbutifolia. Plant Cell Environ. 20, 25–36. https://doi.org/10.1046/j.1365-3040.1997.d01-8.x.
Van Hall, R.L., Cammeraat, L.H., Keesstra, S.D., Zorn, M., 2017. Impact of secondary vegetation succession on soil quality in a humid Mediterranean landscape. Catena 149, 836–843. https://doi.org/10.1016/j.catena.2016.05.021.
Van Oost, K., Govers, G., Van Muysen, W., 2003. A process-based conversion model for caesium-137 derived erosion rates on agricultural land: an integrated spatial approach. Earth Surf. Process. Landf. 28, 187–207. https://doi.org/10.1002/esp.446.
Van Oost, K., Govers, G., Quine, T.A., Heckrath, G., Olesen, J.E., De Gryze, S., Merckx, R., 2005. Landscape-scale modeling of carbon cycling under the impact of soil redistribution: the role of tillage erosion. Glob. Biogeochem. Cycles 19, GB4014. https://doi.org/10.1029/2005GB002471.
Winowiecki, L., Vågen, T.-G., Huising, J., 2016. Effects of land cover on ecosystem services in Tanzania: a spatial assessment of soil organic carbon. Geoderma 263, 274–283. https://doi.org/10.1016/j.geoderma.2015.03.010.

CHAPTER 6

FingerPro model: A step by step procedure to quantify soil particles provenance from different land uses

FingerPro

unmixing model

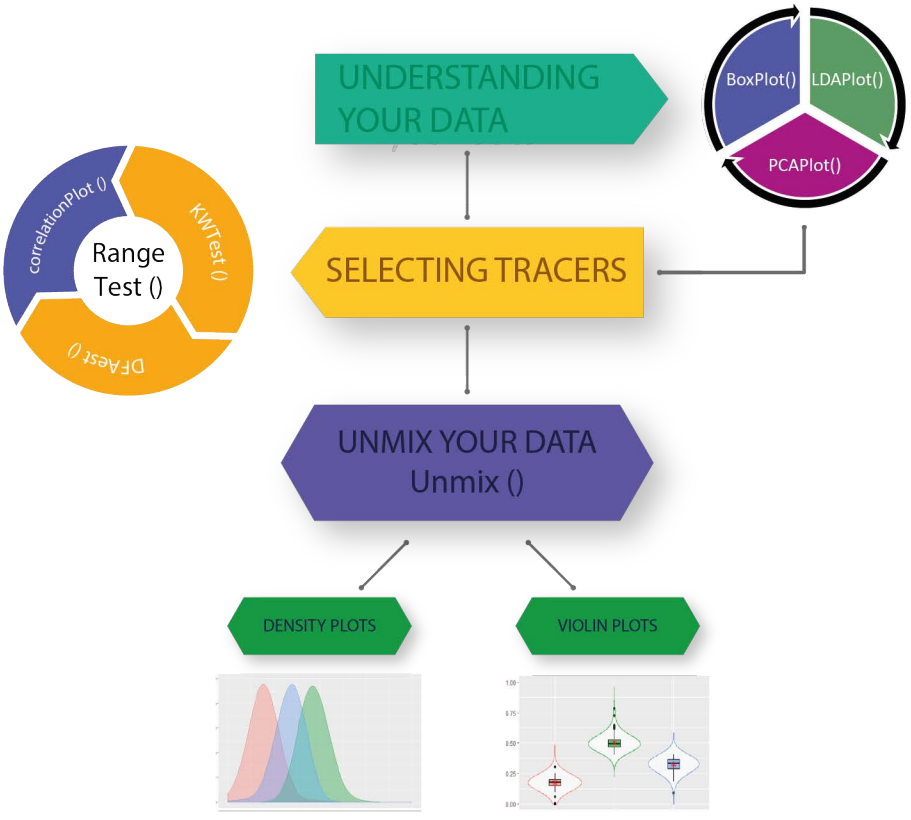

FingerPro model: A step by step procedure to quantify soil particles provenance from different land uses

Ivan Lizaga *, Borja Latorre, Leticia Gaspar, Ana Navas *

Experimental station of Aula Dei (EEAD-CSIC), Avenida Montañana, 1005, 50059 Zaragoza (Spain).

ABSTRACT

Soil loss by erosion processes is one of the largest challenges for food production and reservoir siltation around the world. Information on sediment, nutrients and pollutants is required for designing effective control strategies. The estimation of sediment sources are difficult to get using conventional techniques, but sediment fingerprinting is a potentially valuable tool. This procedure intends to develop methods that enable to identify the apportionment of sediment sources from sediment mixtures.

We developed a new tool to quantify the provenance of sediments in an agroforest catchment. For the first time, the procedure for selection of the best combination of sediment tracers was included in the tool package. An unmixing model algorithm is applied to the sediment samples in order to estimate the contribution of each possible source. The operations are compiled in an R package named FingerPro, which unmix sediment samples after selecting the optimum set of tracers and providing the percentage contribution of each sediment source. An example from a well-studied Mediterranean catchment is included in the package to test the model. The sediment source apportionments are compared with results from a previous study of soil redistribution where ^{137}Cs derived rates validate the unmixing results thus highlighting the potential of sediment fingerprinting for quantifying the main sediment provenance. Fingerprinting techniques will allow us to better comprehend catchment sediment transport to water ecosystems and reservoirs and its detrimental effect on the quality of the water and aquatic habitats.

Keywords:

FingerPro

Unmixing model

Sediment source

fingerprinting

Source variability

R package

1. Introduction

Reliable information on sediment loads transported by a river or stream is crucial to evaluate the severity of reservoir siltation and river pollution. However, determining sediment provenance or sediment budgets in catchments using conventional monitoring techniques is often challenging. However, in most situations, it can be provided by applying tracing techniques. Fingerprinting techniques can be used to recognise sediment sources and to determine their relative contribution, thereby allowing the identification of areas or land uses prone to erosion processes (Schuller et al., 2013). Thus, soil erosion and the subsequent sediment transport are related to the loss of nutrients and their distribution in the catchment (Lizaga et al., 2019). To assess this issue, several software and indices have been developed to quantify the effects of different erosion mechanisms, such as connectivity (Lizaga et al., 2018; Shore et al., 2013), river bank (Ben et al., 2018), sheet and rill (Molnár and Julien, 1998), wind erosion (Schmidt et al.. 2017; Liu et al., 2019) and the subsequent effects on water quality (Quesada et al., 2014). However, sediment source fingerprinting has been developed in recent decades for catchment sediment and pollutants investigation as the most powerful tool to assess this problem. The procedure identifies sediment provenance and estimates the relative contribution of each potential source, using the selected tracer properties.

The first fingerprinting approach dates back to the seventies, based on mineralogical and grain size characterization (Klages and Hsieh, 1975). The earliest fingerprinting researches were fundamentally qualitative in their result, but the introduction of quantitative mixing models was a methodological advance which enabled researchers to obtain quantitative results of the relative contribution from different sediment sources (Collins et al., 1997; Walling, 2005). Since these early works, sediment source fingerprinting applications have been greatly expanding with the development of new techniques (Owens et al., 2016).

The traditional approach for applying source-tracing methods is to define the relevant tracer properties that provide a particular signature between all source samples and unequivocally discriminate the different sources (Collins and Walling, 2002). Due to the inherent complexity of catchment characteristics, with large variations in climate, geology, land

use, vegetation, soil, and management practices, commonly, no unique tracer can discriminate between multiple sediment sources. Consequently, different tracer properties need to be analysed, such as radionuclides (Wallbrink et al., 1998; Evrard et al., 2016), geochemistry (Martínez-Carreras et al., 2010; Smith and Blake, 2014; Meusburger et al., 2016; Zupančič et al., 2018) and CSSI (Reiffarth et al., 2016).

The fundamental theory that supports this technique is that the tracer properties of the sediment mixtures are directly comparable to the sediment of the sources. A common procedure, the so-called "range test", checks if sediment tracers are conservative excluding the tracers of the mixture/s outside the minimum and maximum values in the potential sediment sources. This procedure prevents the inclusion in the optimum tracers of the fingerprint properties exhibiting non-conservative behaviour. However, the exclusion of a great number of fingerprint properties likely suggests that not all sources have been correctly identified or characterised. Thus, methodologies for tracer selection is an open question that is being discussed at present by several authors since different tracer selection methods could lead models to different results (Pulley et al., 2015; Owens et al., 2016; Gaspar et al., 2019). Following this assumption, the two-stage statistical procedure previously proposed by Collins and Walling, 2002, is commonly used to assess this conservativeness. Thus, the Kruskal Wallis H test (KW) and discriminant function analysis (DFA) test the ability of individual tracers to discern between sediment sources and select the best combination of tracers. This procedure was used to select the smallest combination of tracers that provided the maximum discrimination of the identified source categories and it is implemented by several authors as a common procedure when using frequentist (Collins et al., 2002; Evrard et al., 2013; Palazón et al., 2015; Lin et al., 2015) and Bayesian (Koiter et al., 2013; Barthod et al., 2015) unmixing models. Subsequently, the relative contribution of each identified source is estimated using a linear multivariate unmixing model. Due to the growing use of fingerprinting methods, other unmixing models, such as SIFT (Pulley and Collins, 2018), MixSIR (Moore and Semmens, 2008) and IsoSource (Phillips and Gregg, 2003), appeared in the last years for pollution and ecological purposes.

However, due to operational complexity and the need to use different statistical software not included in the packages the use of unmixing models is generally restricted to academics with a good knowledge of the procedure. Our new R approach combines for the first time the tools needed to unmix sediment samples and the previous statistical tests to select optimum tracers. This paper presents the FingerPro package, a user-friendly application and freely available software for users with limited or nor expertise in statistics. Thus, any user could implement the fingerprinting procedure with limited previous experience in the technique and with no need of another software for statistical analyses. Furthermore, unlike previous models, this new tool to identify sediment provenance has been successfully tested with artificial samples (Gaspar et al., 2019). Through an example, this paper exposes the utility of FingerPro for applying tools for pre-processing input data or combine sources without significant differences before or after running the unmixing model. Furthermore, a study catchment has been selected as representative of mountain headwaters (South Pyrenean region) that supply water to reservoirs as siltation and pollution is one of the main environmental issues worldwide (Valero-Garcés et al., 1999). Therefore, it is necessary to identify the sediment sources to establish management strategies for ensuring water supply to the lowlands while preserving water quality. Refinement of the sediment source fingerprinting techniques requires open source models such as FingerPro that help the user in tracer selection decision and optimize this time-consuming process for non-expert and academics with low programming and statistical skills by including the essential statistical functions and plots. Thus, the aim of this work is to provide an easy and straightforward way to apply the sediment fingerprinting technique aimed to beginners or non R users. The analyses described in this research are based on the reproducible "small" catchment example included in the package. To further describe the capability of the package, an example of an ongoing research in a medium size catchment is also described.

2. Methods

Sediment fingerprinting requires a preliminary analysis to select a subset of conservative tracers that discriminate the potential sources. Then, the relative contribution of each source is estimated using a linear multivariate unmixing model. This procedure is iterated considering the variability of the sediment sources to obtain the statistical distribution of the source contribution.

2.1 Statistical analysis for the selection of tracer properties

Several statistical tests can be used to confirm source discrimination and select the optimal subset of conservative tracer properties, such as the procedure suggested by Collins and Walling (2002). However, the use of many tests could remove a considerable number of tracers and therefore restrict the discrimination between sediment sources.

Consequently, none of the functions included in the FingerPro package are mandatory and the tracer exclusions can be based on 'expert judgement' after visualising boxplots and results from the statistical tests included. The tracer selection methods implemented in the package are

i) Range test: the minimum and maximum values of the tracer properties in the sediment sources are compared to

those of the mixtures. The tracers falling out of the range of the selected sources are removed from subsequent analyses. These properties may not be conservative or their exclusion supports the existence of an additional hidden source.

ii) Kruskal-Wallis H test: this is a rank-based nonparametric test used to determine if there are significant differences between the medians of selected groups or sources. This procedure removes tracers which do not show significant differences between at least two of the sediment sources.

iii) Discriminant Function Analysis: identifies the optimum set of tracers that maximises the discrimination between the sediment sources whilst minimising the number of tracers. This function executes a stepwise forward variable selection for classification using the Wilk's Lambda criterion. The function selects the tracers on the basis of how much they decrease Wilks' lambda. At each step, the function includes the variable that minimises the overall Wilks' lambda.

Fig. 1. Location of the study area. 3D picture of the catchment created with a DEM and land cover map.

2.2 Mixing model

The relative contribution of each potential sediment source is determined using a standard linear multivariate mixing model:

$$\sum_{j=1}^{m} a_{i,j} \cdot \omega_j = b_i$$

which satisfies:

$$\sum_{j=1}^{m} \omega_j = 1$$

$$0 \leq \omega_j \leq 1$$

where b_i is the tracer property i (i =1 to n) of the sediment mixture, $a_{i,j}$ represents the tracer property i in the source type j (j =1 to m), ω_j is the unknown relative contribution of the source type j, m represents the number of potential sediment sources and n is the number of tracer properties selected.

This system of equations is mathematically determined if the number of tracers is greater than or equal to the number of potential sources minus one ($n \geq m - 1$). The procedure tries to find the source proportions that conserve the mass balance for all tracers. All possible combinations of each source contribution (0-100%) are examined in small increments, using Latin hypercube sampling (LHS) (McKay et al., 1979). The quality of each candidate is measured using the following function or goodness of fit (GOF), based on the sum of squares of the relative error:

$$GOF = 1 - \frac{1}{n} \times \left(\sum_{i=1}^{n} \frac{\left| b_i - \sum_{j=1}^{m} \omega_j a_{i,j} \right|}{\Delta_i} \right)$$

where Δ_i is the range of the tracer property i, used as a normalisation factor. The combinations that reproduce the observed sediment mixture with the maximum GOF is selected as the solution.

2.3 Variability analysis of the sources

In small to large size catchments, the heterogeneity of sediment tracers, defined by different land uses, geomorphic processes, soil types or human activity, is always present. For this reason, fingerprinting studies should correctly characterise source variability by means of collecting several samples of each source. Thus, evaluation of the variability in tracer data used to characterise sediment sources is important to correctly interpret the source apportionment results.

Variability analysis is assessed following classical frequentist inference by means of a Monte-Carlo method (Helton, 1994). A succession of deterministic calculations are executed, each with different input values sampled from their respective distributions, to obtain probability distributions of the targeted outcomes.

The heterogeneity of each source is considered as a t-distribution for each property. The fingerprinting analysis of each sediment mixture is repeated by randomly sampling the source probability distributions. For the first iteration, the central value of the source distributions is used as a reference result. The corresponding output values are gathered to infer the probability distribution of the potential source contributions. Several samples must be collected for characterising each source in order to compute the mean and the SD of the analysed tracer properties.

3. The FingerPro package

Application of the functions in the package allows the user to i) characterise the different tracer properties and select the relevant variables; ii) unmix the sediment samples and quantify the different source apportionment; iii) assess the effect of the source variability; and iv) visualise and export the results. Thus, FingerPro package proposes a step by step procedure divided into three main sections in order to help users in their decisions.

3.1 The example dataset

The package includes a soil dataset from a small Mediterranean catchment (4 km^2) that contains high-quality radionuclides and geochemistry data to test the operation of the functions and help the user to understand the model (Fig.1). This study area was selected due to its heterogeneous land uses/land covers which are likely to exhibit large differences in sediment tracer contents. Furthermore, the study area is located in a well-studied catchment where several studies of soil redistribution ^{137}Cs derived rates were pursued (Quijano et al., 2016; Lizaga et al., 2018). Thus, soil redistribution rates were used to evaluate FingerPro model as a suitable tool in the Prepyrenean region. The results obtained by Lizaga et al. (2018) found that net soil loss values were 4 times higher in agricultural lands than in pine forest highlighting the importance of the vegetation cover and land management to prevent erosion processes and subsequent land degradation.

The study area dataset is composed of 21 source sediment samples from 4 different sources and 1 mixture sample. The sources are divided in agricultural (AG), old pine forest (PI), recent pine forest (PI1) and degraded soil named subsoil (SS) which occupies 9%, 32%, 58% and 1% of the catchment area, respectively. The agricultural land use is mainly composed by winter cereals crops and the pine afforestation forest is predominantly *Pinus halepensis* Mill. The average temperature range from 5 °C to 18 °C and the mean annual rainfall is about 520mm (AEMET).

3.2 Input data

The input variables need to be stored as an R table object. The dataset must satisfy the following requirements: i) the first column represents the sample *id*; ii) the second column is the source classification, containing target samples in the last place.

3.3 Characterising the sediment samples

One of the advantages of the FingerPro package is that it allows the user to analyse and visually compare different tracer properties, using the state of the art of R packages:

The boxPlot() function displays a boxplot of each tracer property to help the user in the decision by visualising the different concentration of each tracer versus the mixture sample. A parameter (tracers) with the number of tracer properties in the boxplots is provided. The number of columns (columns) refers to the number of plots per row in the display (Fig. 2). The boxPlot () function could be used for tracer selection by helping the user to visualise and select the tracers based on the boxplots and its expert knowledge. Thus, the user visualizes in the example dataset that most of the $^{210}Pb_{ex}$ in the mixture sample likely comes from PI and PI1 sources and that ^{40}K is almost out of range (Fig. 3). Furthermore, by repeating this function after implementing each test for tracer selection, users can envisage how representative the remaining tracers are.

The correlationPlot()function displays a correlation matrix of each tracer, divided by the different sources to help the user by testing the conservatism of tracers by visualising the relationships between the different tracers and sediment mixtures following the methodology proposed by Pulley et al. (2015). A parameter (n) with the number of tracer properties in the correlation matrix is provided, along with the possibility to include the sediment mixture (mixtures = T) in the matrix or to exclude it (by default). In addition, in the correlation plot, once the users have selected the optimum set of tracers, it is possible to visualise if the mixture samples fit inside the source distributions. If a mixture sample is outside the sources distribution, then no solution exists or the mixing model assumptions are not met.

The PCAPlot() function performs a principal components analysis on the given data matrix and displays a biplot of the results, divided by the different sources, to help the user in the decision. A parameter (components) with the number of principal components to display is included.

The LDAPlot() function performs a linear discriminant analysis and visualises the data in the relevant dimensions. A parameter (P3D) allows the user to display a 3D LDA graph (Fig. 4).

This set of functions allows the user to visualise the principal components plot and the linear discriminant plot after the statistical selection procedure. Thus, the plots help the user to visually identify whether the excluded variables increase or decrease the discrimination capacity between sources. Furthermore, the LDAPlot function was used in the catchment example to visualize the number of sources that shows good discrimination with this set of tracers (Figure 3). The function shows a large overlap between PI and PI1 that would suggest merging both sources. Thus, after grouping PI and PI1 the discriminant plot shows better discrimination between selected sources (Fig. 4).

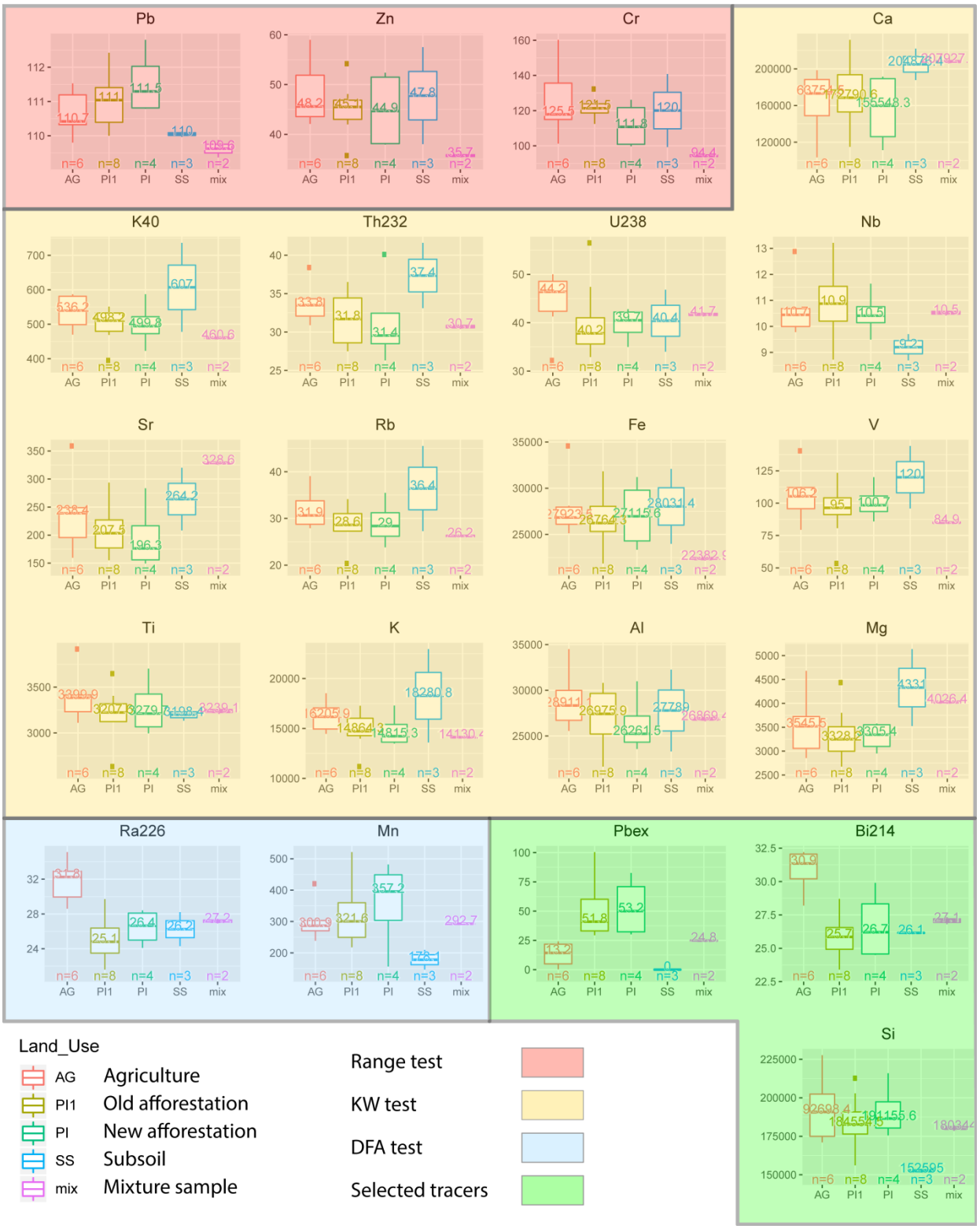

Fig. 2. Boxplot of the tracer properties included in the data example (catchment). In different colours, the tracers removed by each statistical test.

3.4 Statistical test for selecting the optimal set of tracers

Selection of the optimal tracers is usually based on the two-step procedure proposed by Collins and Walling (2002), which includes some previous statistical procedures such as the "range test", the KW and the DFA test. Thus, FingerPro has included these functions to support user decision. However, this procedure might remove too many tracers or include some inadequate properties and could, therefore, restrict the discrimination between sediment sources. Hence, the procedure is included as an individual and informative function to only use the steps needed and to prevent a reduction in the source discriminations. For this reason, the

tracer selection procedure cannot be only based on statistical tests but also in the expert knowledge of the geomorphological and hydrological processes of the catchment (Blake et al., 2018). Thus, boxplot chart, LDA plots and correlation plot included in the FingerPro package were implemented to help the users in the decision.

The rangeTest()function excludes the tracer properties of the mixture/s outside the lowest and highest values in the sediment sources.

The KW()function excludes tracers from the original dataset which do not show a significant difference between sources. This function performs a Kruskal-Wallis rank sum test using the kruskal.test () function from the R package stats. A parameter to select the p-value (pvalue) is provided.

The DFA() function executes a stepwise forward variable selection, using the Wilk's Lambda criterion, which maximises the discrimination between the sources whilst minimising the number of tracers. This function performs a stepwise forward variable selection using the greedy.wilks () function from the R package klaR. A parameter to select the niveau (niveau) for an approximate F-test decision is provided with a default value of 0.1. This value could be reduced to be more restrictive in the tracer selection procedure. However, by reducing the value below 0.05 the statistical test could remove the majority of the tracers with the subsequent decrease in the discrimination of the different sources. These three tracer selection methods were applied in the example dataset. In Fig.3 the tracers removed by each method can be seen and, based on the boxplot graph, to decide if it is suitable to use all of them or if the selected tracers represent a good approximation of the dataset. After the implementation of the range test function, we can see in the boxplot graph that effectively Pb, Zn and Cr have been removed. However, there are other tracers such as ^{40}K, Sr, Fe, and V that remain in the dataset though they should not be considered as tracer inside the sources range. Furthermore, by using the LDA and PCA plots we can decide if the use of other tracer selection methods decreases the discrimination or if by using them we could remove a tracer with specific information. The flow chart presented in Fig. 1 shows the preferential order to follow in the fingerprinting procedure. As shown in Fig.5, by removing ^{226}Ra and Mn from the dataset by using the DFA after KW test the LDA plot shows similar results. In addition, the arrows of the removed tracers in the PCA plot were parallel to those that remain in the dataset. Thus, in this example, the plot information suggests that including or removing ^{226}Ra and Mn should not produce important variations in the discrimination of sources or in the model results as it is evident in Fig. 5.

3.5 Sediment unmixing

The unmix() function assesses the relative contribution of the selected sediment sources for each mixture in the dataset.

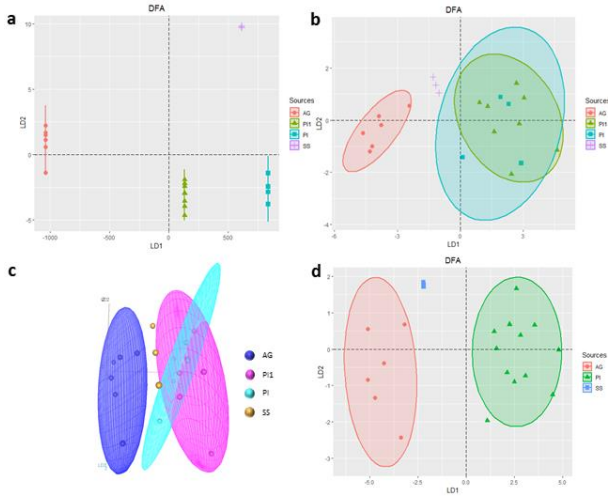

Fig. 3. LDA plot of the data example (catchment). a) Before running the statistical test, the dataset shows collinearity. b & c) 2D and 3D LDA display of the dataset after running the statistical selection. d) LDA display after merging both pines sources PI and PI1.

A parameter (samples) with the number of samples of the LHS is provided. The number of iterations (iter) in the source variability analysis is also configurable. However, if the number of iterations is set as 1, results are produced in a single analysis considering the sources mean value. The result of this function displays a plot with the density distribution of the model solutions and a table with the mean value and the standard deviation of the model solutions (Fig. 5). Besides, users can display the results in violin plots instead of density plots by adding the word True to the violin option.

After the tracer selection procedure, FingerPro results reveal that 18% of the mean sediment supply comes from agricultural land use and 34% and 47% from bare soil and pine forest, respectively. The small standard deviation of the three sources together with the high GOF value shows a good fit of the model to efficiently discriminate the selected sources (Fig. 5). However, users should be cautious about using GOF as an assessment of model reliability. Recent research has shown models with a high GOF can still deliver inaccurate results (Palazón et al., 2015; Gaspar et al., 2019), but also has shown that all models with low GOF always deliver wrong results.

The results of the example dataset are supported by soil erosion rates estimated with ^{137}Cs by Lizaga et al. (2018) in a Mediterranean catchment comprising the one studied here. Thus, 18% of the sediment contribution is supplied from 9% of the area under agricultural management and 47% of the contribution comes from pine forest that occupies 90% of the study catchment. Relatively the subsoil was the main source with 34% of the contribution for just only 1% of the area taken by the bare soil in the study catchment. Our results highlight the hazards that subsoils on supplying important amounts of sediments to the water systems.

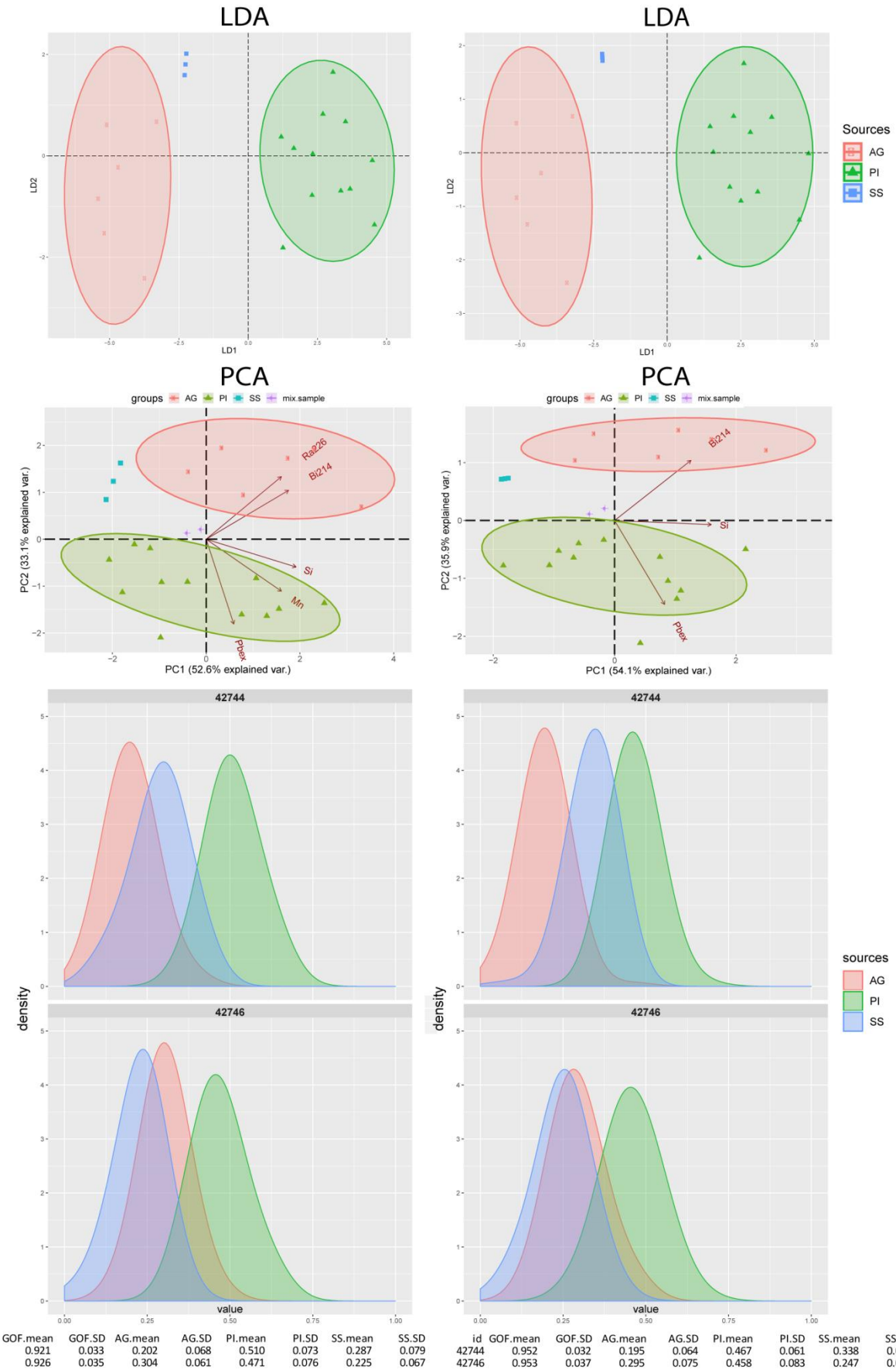

id	GOF.mean	GOF.SD	AG.mean	AG.SD	PI.mean	PI.SD	SS.mean	SS.SD
42744	0.921	0.033	0.202	0.068	0.510	0.073	0.287	0.079
42746	0.926	0.035	0.304	0.061	0.471	0.076	0.225	0.067

id	GOF.mean	GOF.SD	AG.mean	AG.SD	PI.mean	PI.SD	SS.mean	SS.SD
42744	0.952	0.032	0.195	0.064	0.467	0.061	0.338	0.062
42746	0.953	0.037	0.295	0.075	0.458	0.083	0.247	0.077

Fig. 4. LDA, PCA and the density plot of the unmixing process before and after the use of the DFA test.

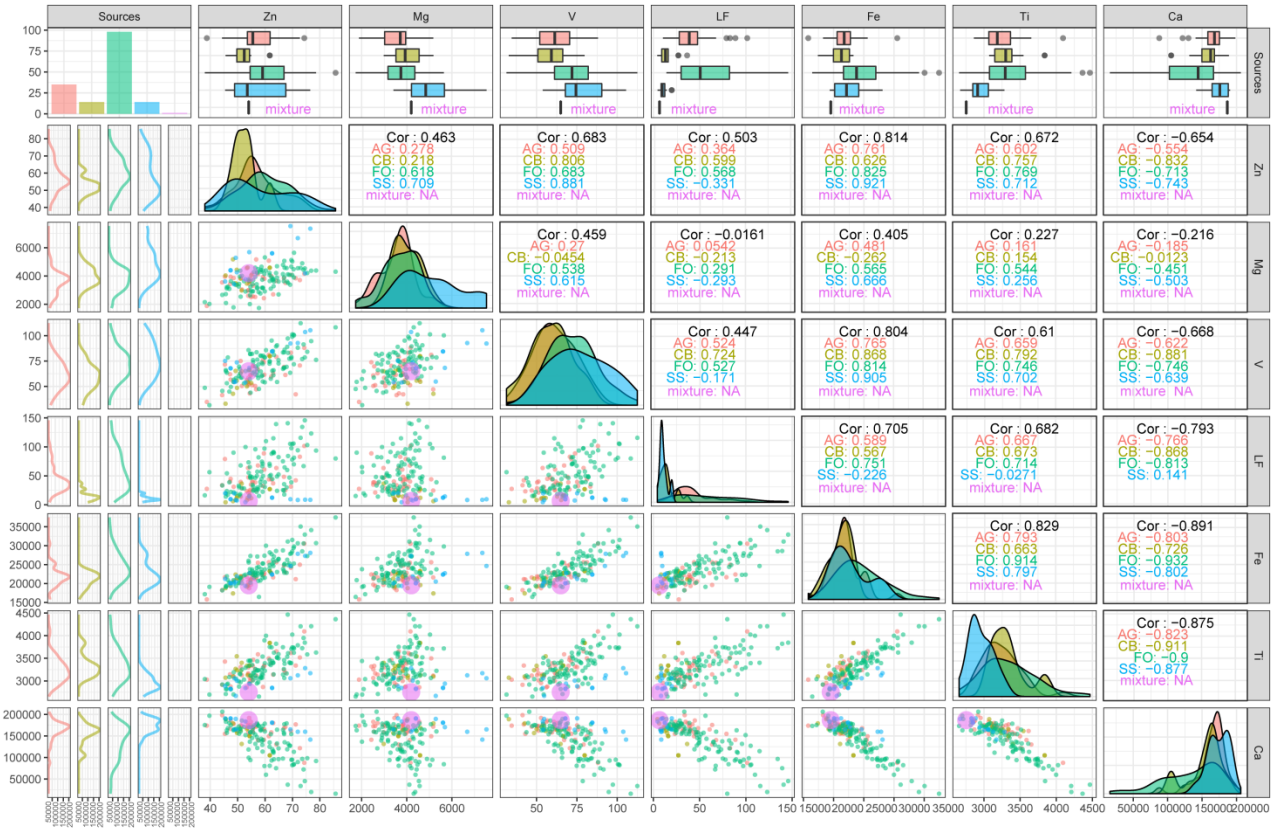

Fig. 5. Correlation plot of seven of the tracer properties of the medium size catchment example.

3.6 Application in a Medium-Size catchment

In this section, as way of example results of applying the FingerPro package in a medium size catchment (Lizaga et al., 2019) are described. Its larger surface area and higher number of sources result in a more complex unmixing. For this reason, all the tools added in the FingerPro package to help the users and characterise the unmixing dataset are essential to reach robust results. Here, we highlight the most important decisions made during the fingerprinting procedure and how the different tools included in the package help the authors to unmix their data. In order to avoid repetition in this manuscript, only one mixture sample collected at the outlet of the catchment is used to describe the FingerPro utilities.

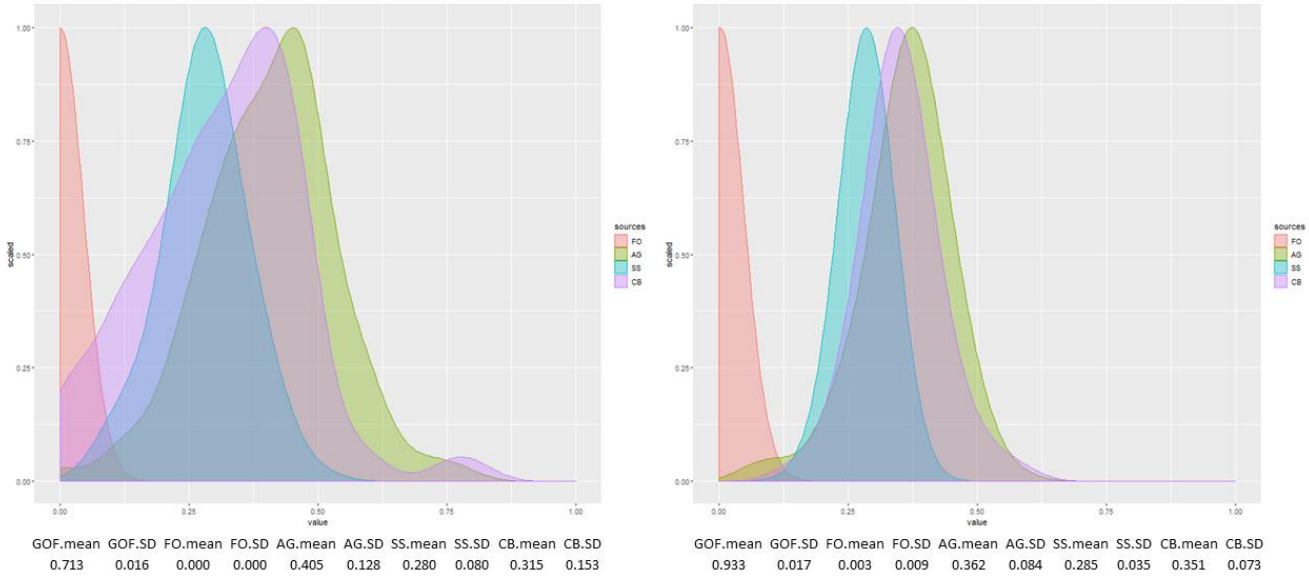

Fig. 6. Density plot and results of the unmixing process after the two different tracer selection approaches

.

Following the application of the range test and Kruskal Wallis test, the final selection was made based on expert judgment using the boxplots and correlation plots to finally identify the tracers that were conservative. Fig. 6 illustrates how some tracers pass the selection tests, such as RT, KW and DFA, but show non-conservative behaviour, i.e. LF, Fe, Ti and Ca. In addition, if we analyse the correlation plot of the tracers that shows non- conservative behaviour, the mixture sample is located almost out of the point cloud. On the other hand, the sample mixture is located inside the point cloud of the conservative tracers. Thus, based on this information it was decided to select the tracers after passing the KW test using expert knowledge, thus obtaining more defined results and higher GOF (Fig. 7). Hence, all the tools added in the FingerPro package to remove the tracers that violate the principles of conservativeness are needed in fingerprinting studies. This methodology suggests that including tracers with discordant information into fingerprinting models does not add valuable information and could lead the model to unpredictable results.

4. Conclusions

The application of mixing models it is necessary to understand source-tracer relationships what is generally performed by applying different software's to select the best combination of sediment tracers. With FingerPro, diverse test and mechanisms have been incorporated for tracer selection in a single software. Furthermore, the inclusion of several plot functions such as boxPlot, correlationPlot, LDAPlot and PCAPlot allows the user to check if the selected tracers are suitable for the unmixing process. This package for sediment source fingerprinting in hydrological systems offers a wider and easier application in catchments affected by natural and human-induced changes.

Due to the increasing attention in tracing sediment methods and the need to select the best tracer combination, an open source tool that includes all the steps for sediment unmixing is a key tool to the unmixing process. The example dataset included in FingerPro provides evidence of the large sediment supply and severe soil loss caused by land degradation and bare soil. In addition, the agreement between the unmixing results obtained from the example dataset with the ^{137}Cs derived rates supports the capability of the model for sediment fingerprinting task. These results reflect the high importance of creating a low time-consuming and open source mixing model that combines the necessary tools to solve environmental issues such as reservoir siltation or soil loss and trace the sediment provenance.

FingerPro provides the users with tools to i) characterise the different sediment sources, establish correlations between the tracers and assist the selection of the optimal tracers; ii) graph the results, using the state of the art of R packages; iii) unmix sediment samples to estimate the apportionment of the sediment sources. iiii) test the model using data from a Mediterranean study catchment included in the package.

In addition, the example dataset and the results of a medium size catchment explained introduce the users on to the functioning and potential of the tools included in the FingerPro package also showing the advantages of the fingerprinting technique to improve the understanding of sediment supply processes.

Acknowledgements

This work was performed within the framework of a Spanish national project called TRAZESCAR and was sponsored by the Spanish Ministry of Science, Innovation and Universities.

COMPUTER CODE AVAILABILITY

The R package source files are available via:
GitHub platform: https://github.com/eead-csic-eesa/fingerPro
Name of code: fingerPro
Name of the manual: fingerPro_manual 1.2.pdf
Developer and contact address:
Ivan Lizaga Villuendas (ilizaga@eead.csic.es)
Borja Latorre (borja.latorre@csic.es)
Year first available: 2018
Software required: R Program language: R

References

Barthod LRM, Liu K, Lobb DA, et al (2015) Selecting Color-based Tracers and Classifying Sediment Sources in the Assessment of Sediment Dynamics Using Sediment Source Fingerprinting. Journal of Environmental Quality 44:1605–1616. https://doi.org/10.2134/jeq2015.01.0043

Ben Slimane, A., Raclot, D., Rebai, H., Le Bissonnais, Y., Planchon, O., Bouksila, F., (2018). Combining field monitoring and aerial imagery to evaluate the role of gully erosion in a Mediterranean catchment (Tunisia). CATENA 170, 73–83. https://doi.org/10.1016/j.catena.2018.05.044

Blake, W. H., Boeckx, P., Stock, B. C., Smith, H. G., Bodé, S., Upadhayay, H. R., Gaspar, L., Goddard, R., Lennard, A. T., Lizaga, I., Lobb, D. A., Owens, P. N., Petticrew, E. L., Kuzyk, Z. Z. A., Gari, b. d., Munishi, L., Mtei, k., Nebiyu, A., Mabit, L., Navas, A., Semmens, B.X. (2018). A deconvolutional Bayesian mixing model approach for

river basin sediment source apportionment. Scientific Reports, 8: 13073. https://doi.org/10.1038/s41598-018-30905-9.

Collins AL, Walling DE (2002) Selecting fingerprint properties for discriminating potential suspended sediment sources in river basins. Journal of Hydrology 261:218–244. https://doi.org/10.1016/S0022-1694(02)00011-2

Collins AL, Walling DE, Leeks GJL (1997) Fingerprinting the Origin of Fluvial Suspended Sediment in Larger River Basins: Combining Assessment of Spatial Provenance and Source Type. Geografiska Annaler: Series A, Physical Geography 79:239–254. https://doi.org/10.1111/j.0435-3676.1997.00020.x

Evrard O, Laceby JP, Huon S, et al (2016) Combining multiple fallout radionuclides (137Cs, 7Be, 210Pbxs) to investigate temporal sediment source dynamics in tropical, ephemeral riverine systems. J Soils Sediments 16:1130–1144. https://doi.org/10.1007/s11368-015-1316-y

Evrard O, Poulenard J, Némery J, et al (2013) Tracing sediment sources in a tropical highland catchment of central Mexico by using conventional and alternative fingerprinting methods. Hydrol Process 27:911–922. https://doi.org/10.1002/hyp.9421

Gaspar, L., Blake, W.H., Smith, H.G., Lizaga, I., Navas, A., 2019. Testing the sensitivity of a multivariate mixing model using geochemical fingerprints with artificial mixtures. Geoderma 337, 498–510. https://doi.org/10.1016/j.geoderma.2018.10.005

Helton JC (1994) Treatment of Uncertainty in Performance Assessments for Complex Systems. Risk Analysis 14:483–511. https://doi.org/10.1111/j.1539-6924.1994.tb00266.x

Klages MG, Hsieh YP (1975) Suspended Solids Carried by the Gallatin River of Southwestern Montana: II. Using Mineralogy for Inferring Sources. Journal of Environmental Quality 4:68–73. https://doi.org/10.2134/jeq1975.00472425000400010016x

Koiter AJ, Lobb DA, Owens PN, et al (2013) Investigating the role of connectivity and scale in assessing the sources of sediment in an agricultural watershed in the Canadian prairies using sediment source fingerprinting. J Soils Sediments 13:1676–1691. https://doi.org/10.1007/s11368-013-0762-7

Lin, J., Huang, Y., Wang, M., Jiang, F., Zhang, X., Ge, H., (2015). Assessing the sources of sediment transported in gully systems using a fingerprinting approach: An example from South-east China. CATENA 129, 9–17. https://doi.org/10.1016/j.catena.2015.02.012

Liu, B., Qu, J., Ning, D., Han, Q., Yin, D., Du, P., (2019). WECON: A model to estimate wind erosion from disturbed surfaces. CATENA 172, 266–273. https://doi.org/10.1016/j.catena.2018.08.037

Lizaga I, Quijano L, Palazón L, Gaspar L, Navas A (2017) Enhancing Connectivity Index to Assess the Effects of Land Use Changes in a Mediterranean Catchment. Land Degrad Develop n/a-n/a. https://doi.org/10.1002/ldr.2676

Lizaga I, Quijano L, Gaspar L, Navas A (2018) Estimating soil redistribution patterns with 137Cs measurements in a Mediterranean mountain catchment affected by land abandonment. Land Degrad Dev 29:105–117. https://doi.org/10.1002/ldr.2843

Lizaga, I., Quijano, L., Gaspar, L., Ramos, M.C., Navas, A., (2019a). Linking land use changes to variation in soil properties in a Mediterranean mountain agroecosystem. CATENA 172, 516–527. https://doi.org/10.1016/j.catena.2018.09.019

Lizaga, I., Gaspar, L., Blake, W., Latorre, B., Navas, A (2019b). Fingerprinting changes of source apportionments from mixed land uses in stream sediments before and after an exceptional rainstorm event. Geomorphology. https://doi.org/10.1016/j.geomorph.2019.05.015

Martínez-Carreras, N., Krein, A., Udelhoven, T., Gallart, F., Iffly, J.F., Hoffmann, L., Pfister, L., Walling, D.E., (2010). A rapid spectral-reflectance-based fingerprinting approach for documenting suspended sediment sources during storm runoff events. J Soils Sediments 10, 400–413. https://doi.org/10.1007/s11368-009-0162-1

McKay MD, Beckman RJ, Conover WJ (1979) A Comparison of Three Methods for Selecting Values of Input Variables in the Analysis of Output from a Computer Code. Technometrics 21:239–245. https://doi.org/10.2307/1268522

Meusburger K, Mabit L, Ketterer M, et al (2016) A multi-radionuclide approach to evaluate the suitability of 239 + 240Pu as soil erosion tracer. Science of The Total Environment 566–567:1489–1499. https://doi.org/10.1016/j.scitotenv.2016.06.035

Molnár, D.K., Julien, P.Y., (1998). Estimation of upland erosion using GIS. Computers & Geosciences 24, 183–192. https://doi.org/10.1016/S0098-3004(97)00100-3

Moore JW, Semmens BX (2008) Incorporating uncertainty and prior information into stable isotope mixing models. Ecology Letters 11:470–480. https://doi.org/10.1111/j.1461-0248.2008.01163.x

Owens, P.N., Blake, W.H., Gaspar, L., Gateuille, D., Koiter, A.J., Lobb, D.A., Petticrew, E.L., Reiffarth, D.G., Smith, H.G., Woodward, J.C., 2016. Fingerprinting and tracing the sources of soils and sediments: Earth and ocean science, geoarchaeological, forensic, and human health applications. Earth-Science Reviews 162, 1–23. https://doi.org/10.1016/j.earscirev.2016.08.012

Palazón L, Latorre B, Gaspar L, et al (2015) Comparing catchment sediment fingerprinting procedures using an auto-evaluation approach with virtual sample mixtures. Science of The Total Environment 532:456–466. https://doi.org/10.1016/j.scitotenv.2015.05.003

Phillips DL, Gregg JW (2003) Source partitioning using stable isotopes: coping with too many sources. Oecologia 136:261–269. https://doi.org/10.1007/s00442-003-1218-3

Pulley, S., Foster, I., Antunes, P., 2015. The uncertainties associated with sediment fingerprinting suspended and recently deposited fluvial sediment in the Nene river basin. Geomorphology 228, 303–319. https://doi.org/10.1016/j.geomorph.2014.09.016

Quesada, S., Tena, A., Guillén, D., Ginebreda, A., Vericat, D., Martínez, E., Navarro-Ortega, A., Batalla, R.J.,

Barceló, D., 2014. Dynamics of suspended sediment borne persistent organic pollutants in a large regulated Mediterranean river (Ebro, NE Spain). Science of The Total Environment 473–474, 381–390. doi:10.1016/j.scitotenv.2013.11.040

Quijano L, Gaspar L, Navas A (2016) Spatial patterns of SOC, SON, 137Cs and soil properties as affected by redistribution processes in a Mediterranean cultivated field (Central Ebro Basin). Soil and Tillage Research 155:318–328. https://doi.org/10.1016/j.still.2015.09.007

Reiffarth DG, Petticrew EL, Owens PN, Lobb DA (2016) Sources of variability in fatty acid (FA) biomarkers in the application of compound-specific stable isotopes (CSSIs) to soil and sediment fingerprinting and tracing: A review. Science of The Total Environment 565:8–27. https://doi.org/10.1016/j.scitotenv.2016.04.137

Schmidt S, Meusburger K, de Figueiredo T, Alewell C (2017) Modelling Hot Spots of Soil Loss by Wind Erosion (SoLoWind) in Western Saxony, Germany. Land Degrad Develop 28:1100–1112. https://doi.org/10.1002/ldr.2652

Schuller P, Walling DE, Iroumé A, et al (2013) Using 137Cs and 210Pbex and other sediment source fingerprints to document suspended sediment sources in small forested catchments in south-central Chile. Journal of Environmental Radioactivity 124:147–159. https://doi.org/10.1016/j.jenvrad.2013.05.002

Shore M, Murphy PNC, Jordan P, et al (2013) Evaluation of a surface hydrological connectivity index in agricultural catchments. Environmental Modelling & Software 47:7–15. https://doi.org/10.1016/j.envsoft.2013.04.003

Smith HG, Blake WH (2014) Sediment fingerprinting in agricultural catchments: A critical re-examination of source discrimination and data corrections. Geomorphology 204:177–191. https://doi.org/10.1016/j.geomorph.2013.08.003

Valero-Garcés BL, Navas A, Machín J, Walling D (1999) Sediment sources and siltation in mountain reservoirs: a case study from the Central Spanish Pyrenees. Geomorphology 28:23–41. https://doi.org/10.1016/S0169-555X(98)00096-8

Wallbrink PJ, Murray AS, Olley JM, Olive LJ (1998) Determining sources and transit times of suspended sediment in the Murrumbidgee River, New South Wales, Australia, using fallout 137Cs and 210Pb. Water Resour Res 34:879–887. https://doi.org/10.1029/97WR03471

Walling DE (2005) Tracing suspended sediment sources in catchments and river systems. Science of The Total Environment 344:159–184. https://doi.org/10.1016/j.scitotenv.2005.02.011

Zhang XC (John), Liu BL (2016) Using multiple composite fingerprints to quantify fine sediment source contributions: A new direction. Geoderma 268:108–118. https://doi.org/10.1016/j.geoderma.2016.01.031

Zupančič, N., Turniški, R., Miler, M., Grčman, H., 2018. Geochemical fingerprint of insoluble material in soil on different limestone formations. CATENA, 170, 10–24. https://doi.org/10.1016/j.catena.2018.05.040

CHAPTER 7

Fingerprinting changes of source apportionments from mixed land uses in stream sediments before and after an exceptional rainstorm event

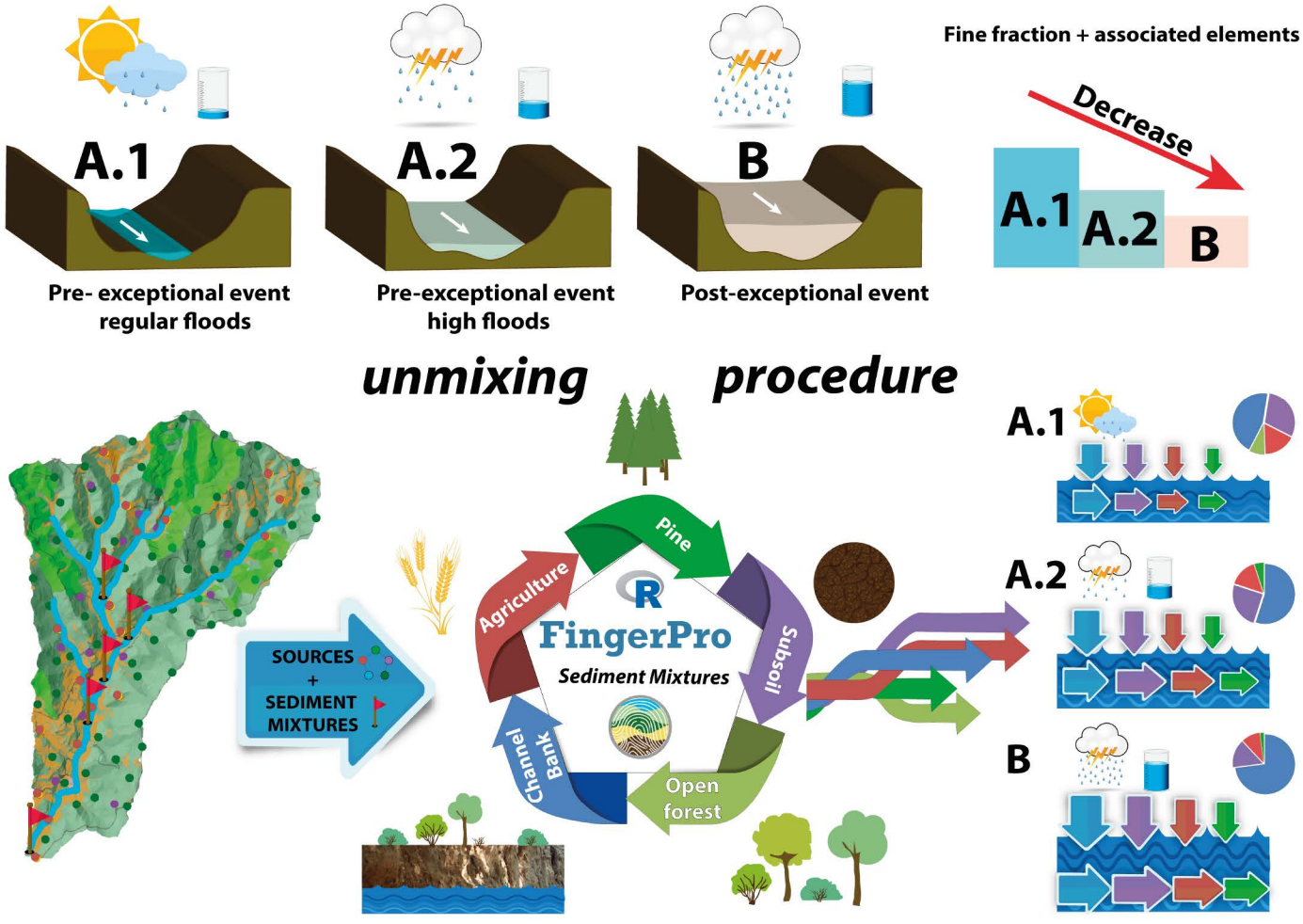

Geomorphology 341 (2019) 216–229

Contents lists available at ScienceDirect

Geomorphology

journal homepage: www.elsevier.com/locate/geomorph

Fingerprinting changes of source apportionments from mixed land uses in stream sediments before and after an exceptional rainstorm event

Ivan Lizaga [a,*], Leticia Gaspar [a], William H. Blake [b], Borja Latorre [a], Ana Navas [a,*]

[a] Department of Soil and Water, Estación Experimental de Aula-Dei, Spanish National Research Council (EEAD-CSIC), Avenida Montañana, 1005, 50059 Zaragoza, Spain
[b] School of Geography, Earth and Environmental Sciences, University of Plymouth, UK

ARTICLE INFO

Article history:
Received 4 January 2019
Received in revised form 22 May 2019
Accepted 23 May 2019
Available online 28 May 2019

Keywords:
Radionuclides
Geochemistry
FingerPro unmixing model
Virtual mixtures

ABSTRACT

The loss of fertile topsoil is one of the principal soil degradation problems in mountain agroecosystems worldwide. Soil erosion rates reach their maximum during exceptional storm events that remove soil particles, especially from unprotected topsoil. In Mediterranean mountainous environments, several centuries of non-irrigated agriculture and the subsequent removal of natural vegetation for developing agriculture has increased the surface area prone to erosion. In addition, the irregularity in exceptional precipitation events results in a great loss of fertile soil, the subsequent siltation of reservoirs and a decrease in water quality. To analyse the soil response to exceptional events, 161 source samples were collected in a 23 km^2 catchment that was mostly cultivated at the beginning of the last century. Source samples were distributed over the five main land use/land covers such as agricultural land, pine afforestation, open forest, bare soil and channel bank areas. Furthermore, 20 channel bed sediment samples were collected along the main streams before and after the exceptional storm event to document changes in the sediments. In addition, floodplain sediments were collected to provide a close replication of sediments deposited during regular storm events. Source apportionments were calculated using the FingerPro unmixing model in the pre-event, regular events and post-event scenarios.
The unmixing outputs displayed a large variation of source apportionments from the upper part to the lower part of the catchment and from pre- to post-event sediments. After the event, a decrease of >70% of the clay fraction and its associated elements such as Fe, Al, K, Ba, Sr, Rb, Pb, Zn, V, ^{137}Cs, ^{40}K, ^{232}Th and SOC along with a rise in contents of elements associated with the coarse fraction (Si, Nb, Zr, Ti, P and ^{226}Ra) was recorded in the channel bed sediments. At the catchment outlet, the pre-event sediment showed substantial contributions from bare soil (29%) and from agriculture and channel banks, which both reached 35%, while the channel bank was the main source along the catchment ranging between 44 and 71%. The low contribution from soil under natural covers with a mean value <4% underlines the benefits of vegetation to prevent soil loss. In the post-event sediment, the channel bank contribution increased up to 63% at the catchment outlet. Our findings highlight the hazards of exceptional storm events on modifying sediment source contribution and exporting fine sediment.
© 2019 Elsevier B.V. All rights reserved.

1. Introduction

The impact of soil erosion on mountain agroecosystems has received increasing attention due to the vulnerability of shallow soil to erosion processes, which are the main cause of soil loss and subsequent land degradation. Very intense rainstorms after dry periods are relatively frequent in the Mediterranean region (Serrano-Notivoli et al., 2017). Mediterranean agroecosystems are susceptible to degradation due to irregular space-time distribution of high-intensity rainfall and storm events, followed by long dry periods (Mariani and Parisi, 2014). The importance of these exceptional rainstorms has been highlighted, and they have been found to be responsible for major geomorphological changes including piping, gully formation, landslides and subsequent soil loss (Grodek et al., 2012; Nadal-Romero et al., 2013). Thus, fragile soils with low nutrient contents existing in Mediterranean mountain agroecosystems, along with an absence of dense vegetation cover due to deforestation in the past century, have created areas prone to erosion (Navas et al., 2017). Soils without vegetation cover are easily erodible during exceptional storm events such as the three-day long exceptional rainstorm event that occurred in 2012 in northeastern Spain (Serrano-Muela et al., 2015).

Exceptional rainfall events accelerate soil and bedrock erosion on hillslopes, which commonly results in higher sediment mobilisation and variations in sediment sources released into the streams. Exported fine sediment produces an important indirect impact such as rapid siltation of downstream water bodies that reached a maximum in the Mediterranean mountains due to land abandonment in the mid-1950s

* Corresponding authors.
E-mail addresses: ilizaga@eead.csic.es (I. Lizaga), anavas@eead.csic.es (A. Navas).

https://doi.org/10.1016/j.geomorph.2019.05.015
0169-555X/© 2019 Elsevier B.V. All rights reserved.

(Navas et al., 2009). Since the 1950s, Mediterranean mountain agroecosystems were commercialised through technological progress and the EU Common Agricultural Policy (CAP), which favoured the expansion of certain management systems focused on more fertile and accessible land. These practices produced a decline in traditional farming methods and converted mountain agriculture into marginal agricultural land leading to the abandonment of the countryside (Lasanta et al., 2016; Quijano et al., 2016a; Borrelli et al., 2017). Subsequent natural vegetation regrowth (Navas et al., 2008) and afforestation during the 1960s and 1980s produced a large effect on reducing slope-channel coupling and runoff due to an increase in plant cover (Cavalli et al., 2013; Heckmann et al., 2018; Llena et al., 2019). Thus, Mediterranean agricultural soils suffered significant modifications due to land use/land cover changes (Romanyà and Rovira, 2011). As a consequence of such changes, cultivated Mediterranean fields show large variability in soil losses with average soil redistribution rates between −30 to 15 Mg ha^{-1} yr^{-1}, while in other land uses that offer protection to the soil surface (such as open forest), rates are much more moderate, varying from −3 to 5 Mg ha^{-1} yr^{-1} (Navas et al., 2014; Lizaga et al., 2018a).

Currently, soil erosion is an estimated 10–40 times greater than soil formation rates (Pimentel, 2006; Verheijen et al., 2009). Various approaches have been suggested for sediment yield monitoring and quantification of soil redistribution rates (Favis-Mortlock, 2008; Walling and Collins, 2008; Dutta, 2016; Wynants et al., 2018). However, erosion processes are mostly influenced by a variety of driving forces such as slope, land management, altitude, vegetation cover, land use, soil type and changing weather patterns and extremes under current climate (Renard et al., 2011; Lana-Renault et al., 2013; Lecce, 2013; Buendia et al., 2016; Nadal-Romero et al., 2019; Shang et al., 2019). Thus, to control soil erosion, it is important to recognise the most susceptible areas, soils or land uses exposed to erosion processes as these processes lead to the loss of soil nutrients.

Concerns about the nutrient loss associated with fine particles due to soil erosion have led to analysis methods for quantifying and predicting erosion rates of fine grain sediment. To this purpose geochemistry, magnetic properties, radiotracers and modelling approaches offer considerable potential for studying erosion processes and calculating soil redistribution rates (Navas et al., 2005; Gaspar et al., 2013; Quijano et al., 2016b; Masselink et al., 2017). In areas where rill erosion is dominant, studies at the slope scale have proven effective (Li et al., 2009). However, few studies quantify soil redistribution rates at catchment or river scale (Mabit et al., 2002; Porto et al., 2003; Navas et al., 2013; Lizaga et al., 2018a; Chen et al., 2019).

Large-scale erosion after exceptional rainstorm events has occurred irregularly in the northeastern part of the Spanish Peninsula (Gutiérrez et al., 1998; White et al., 1997; García-Ruiz et al., 2002). Exceptional storm events and the subsequent overflow of river banks typically increase sediment transfer and suspended sediment loads in river catchments triggering variations in sediment solute concentrations (Winston and Criss, 2002).

The large increase in fine grain sediment mobilised during exceptional storm events has been demonstrated to be one of the most widespread contaminants in aquatic ecosystems, compromising water quality and causing reservoir siltation (Navas et al., 2004). For these reasons, defining the sources of eroded fine-grained sediment is a fundamental requirement for catchment management as well as for understanding the evolution of landscapes and delineating the most sensitive areas to soil loss.

Determining sediment provenance in catchments using conventional monitoring techniques is often challenging, but in most environments it can be undertaken by applying sediment source fingerprinting methods. Due to the growing use of fingerprinting methods, several unmixing models such as IsoSource (Phillips and Gregg, 2003), MixSIR (Moore and Semmens, 2008), SIFT (Pulley and Collins, 2018) and FingerPro (Palazón et al., 2015a; Lizaga et al., 2018b) have appeared over the last years for pollution and ecological purposes. To date, there are several studies on identifying source apportions by fingerprinting techniques (Klages and Hsieh, 1975; Walling et al., 1979; Yu and Oldfield, 1989; Collins et al., 1996; Evrard et al., 2013; Schuller et al., 2013; Palazón et al., 2015b; Meusburger et al., 2018; Upadhayay et al., 2018), but only a few have quantified the sediment provenance after an exceptional rainstorm event (Martínez-Carreras et al., 2010; Zhang et al., 2017), and none of these studies have compared whether there were changes in the provenance of sediment before and after an exceptional storm event.

To evaluate the unstudied effect of this unstudied phenomenon, its source apportions were calculated using the new R package FingerPro unmixing model (Lizaga et al., 2018b) that was tested with artificial samples by Gaspar et al. (2019a). For this purpose, we implemented the unmixing model in two different datasets, before and after a three-day exceptional rainstorm event in a representative catchment of the Prepyrenean region. The 2012 event corresponded to a return period of 142 yr calculated at the outlet of the Yesa reservoir located 30 km north from the catchment (Serrano-Muela et al., 2015). Our objectives are (i) to analyse whether sediment properties vary along the main streams before and after the exceptional storm event, (ii) to quantify and trace the sediment provenance before the 2012 exceptional rainstorm event in different parts of the study catchment and (iii) to examine whether sediment source apportionments after the exceptional storm event differed from the ones during normal discharge.

Therefore, our multi-approach combining spatiotemporal analysis of soil properties and fingerprinting modelling is aimed to determine how an exceptional storm event modifies the sediment properties of the streambed sediments and how contributions from sediment sources might change. To this aim, our work represents a unique opportunity to track the changes in sediment contribution associated with exceptional storm events due to the availability of pre-event sediment and floodplain mixtures that were resampled after the storm event. This paper sheds new light on the effect of heavy storms in agriculture catchments and points out the most sensitive areas to these highly erosive processes.

2. Material and methods

2.1. The study area

The study catchment (23 km^2) is drained by an ephemeral stream tributary of the Arba River located in Barués in the middle part of the Ebro Basin (Fig. 1). From the geomorphological perspective, the catchment structure is dominated by the low angle dip of the bedding and the presence of a Quaternary glacis located at the lower eastern part of the catchment. The climate is characterised by cold winters and hot and dry summers. The rainfall periods are concentrated in the spring and autumn seasons while the droughts take place between these two humid periods. The area is subjected to very intense though sometimes localised storms. The maximum and minimum annual temperatures are 30 °C and −6 °C, respectively. The mean annual rainfall is about 500 mm.

At the start of the twentieth century, most of the catchment was agricultural land. In the 1960s, nearly 60% of the catchment was croplands. However, during the next 10 yr, 75% of the agricultural land was abandoned. Currently, ~16% of the catchment is still cultivated while open forest and pine occupy the remaining 83.5% (Lizaga et al., 2017). The main land use/land covers are agricultural, open forest and pine afforestation, occupying 16%, 50% and 19% of the catchment area, respectively. In addition, most of the agricultural land is located on a Quaternary glacis and on fluvial terraces with gentle slopes occupying the valley floors. The upper part of the Quaternary glacis is dissected by the La Reina tributary stream, an ephemeral stream with documented exceptional discharges under heavy rainfalls. Rangelands occupy the highest altitudes and the revegetated abandoned crops are mostly located at intermediate altitudes where most of the abandoned crops were located in the

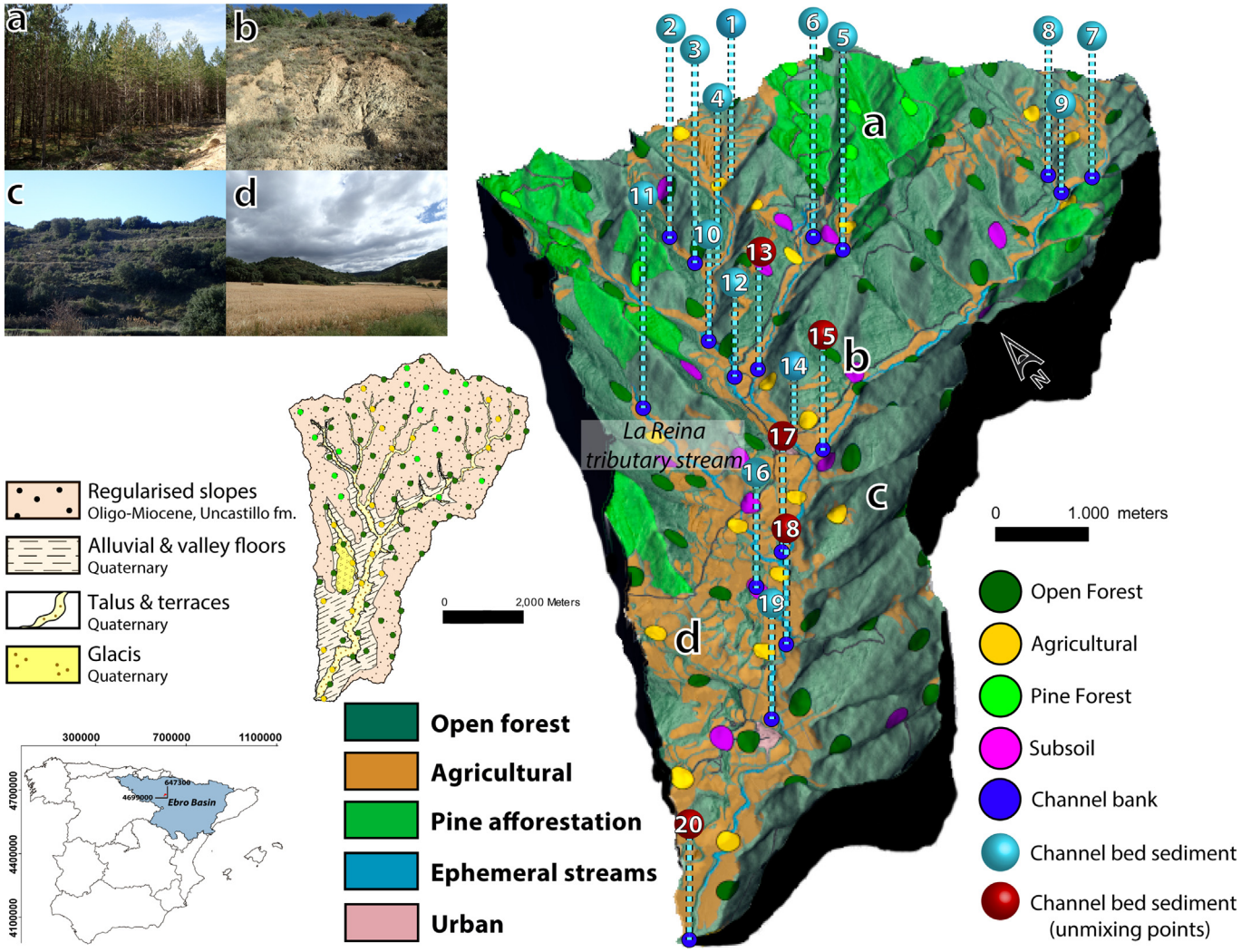

Fig. 1. Location of the study catchment in the central part of the Ebro Basin (NE Spain). 3D map of the different land uses in the catchment with the sources and mixture sampling point distribution through the catchment. (a) Pine afforestation, (b) subsoil, (c) open forest and (d) agricultural.

past. Interspersed patches of highly disturbed areas, including bare soil (subsoil), are dispersed all over the catchment, although it is more abundant on the middle part on south-facing slopes. Valley floors are infilled by eroded sediment from the slopes and are deeply incised by streams, especially from the middle part of the catchment. The stream channel banks composed of loess type material have steep talus that remains uncovered by vegetation. Thus, channel banks of these upland agroecosystem catchments are characterised by deep straight walls due to flow incision by high water energy released during heavy rainfalls.

2.2. Soil sampling and analysis

Potential sediment sources and sediment sampling locations were manually identified during fieldwork campaigns in a design sampling scheme. Special attention was paid to the connectivity index (Lizaga et al., 2017) and soil properties such as $CaCO_3$, pH, EC, SOC, grain size, land use, soil classification (Lizaga et al., 2019) and soil redistribution rates (Lizaga et al., 2018a).

A total of 161 source sediment samples were taken with a cylindrical core 5 cm long and 6 cm in diameter, with four replicates at each sampling point combined in the field to create a representative composite sample following the accepted methodology proposed in fingerprinting studies (Owens et al., 2016; Collins et al., 2017). Fingerprinting studies collect sediment source samples of variable depths, though 2 cm depth is frequently used. However, heavy rainfall events in upland Mediterranean agroecosystems produce deep rilling and can remove >2 cm of surface soil. Thus, a 5 cm sample depth was selected in this study for the appropriate characterisation of sediment eroded by exceptional rainfall events.

Samples were collected from cropland (AG), open forest (OF), pine afforestation (PI), eroded subsoil (SS) and channel bank (CB). Source samples were distributed over the land uses (AG, OF and PI) across the catchment using a 500 × 500 m grid to represent the areal percentage of each land use. The sample points retained their grid location as much as possible avoiding recent highly disturbed areas that could not be representative of the sampling source. Furthermore, 14 subsoil samples were collected on eroded bare soil distributed over the catchment, and another 18 samples were collected along the main streams on the channel banks near the mixture samples (Fig. 1).

Two different types of sediment mixture samples were collected in the channel bed along the main streams from the headwaters to the outlet of the catchment, before and after the secondary tributary streams. Mixture sediment samples are: (i) 20 channel bed samples collected before and after the 2012 storm event (identified as SMP 1–20), and (ii) 8 floodplain sediment mixture collected at sampling points 2, 3, 6, 12, 14, 15, 17 and 20. Channel bed and floodplain sediment lie on top of sandstone outcrops and these surface sediments can be easily

Table 1
Main statistics of the analysed properties for the potential sediment sources.

Properties	AG					CB					OF					PI					SS				
	m	sd	md	min	max	m	sd	md	min	max	m	sd	md	min	max	m	sd	md	min	max	m	sd	md	min	max
Clay (%)	15.9	3.1	16.5	7.9	20.4	13.0	2.4	13.3	8.0	17.4	15.8	2.3	16.0	11.0	21.4	16.2	3.2	16.1	11.0	21.8	12.9	3.8	12.3	7.8	20.0
Silt (%)	77.9	2.9	78.0	70.6	81.6	72.6	3.5	71.7	65.7	78.2	75.7	4.0	76.3	65.7	83.9	75.2	3.0	75.1	70.3	79.0	73.9	6.1	74.0	60.7	82.8
Sand (%)	6.3	4.6	5.4	1.0	21.5	14.4	4.8	15.2	4.4	22.1	8.5	3.7	8.4	1.3	18.4	8.6	3.3	8.9	2.9	13.5	13.8	8.0	14.3	0.0	30.8
ACF (%)	0.9	0.3	0.8	0.5	1.7	0.7	0.3	0.7	0.1	1.0	1.9	0.9	1.7	0.5	4.9	2.1	1.5	1.8	0.8	5.9	0.2	0.2	0.2	0.0	0.4
SCF (%)	0.5	0.1	0.5	0.3	0.9	0.4	0.1	0.4	0.2	0.6	0.8	0.3	0.8	0.2	1.4	0.8	0.3	0.9	0.3	1.4	0.1	0.1	0.1	0.0	0.3
^{137}Cs (Bq kg^{-1})	3.7	2.2	3.3	0.0	10.0	0.4	0.9	0.0	0.0	2.8	12.8	6.3	12.5	1.3	30.7	9.6	7.5	8.0	1.4	28.0	0.2	0.5	0.0	0.0	1.3
^{40}K (Bq kg^{-1})	482.5	58.6	466.5	390.0	587.0	477.8	61.0	484.0	359.0	569.0	526.6	57.3	527.5	332.0	647.0	512.1	63.5	526.0	395.0	646.0	540.3	120.1	520.0	338.0	736.0
^{226}Ra (Bq kg^{-1})	29.9	2.6	29.8	24.8	35.1	28.7	3.4	28.1	22.8	36.5	29.6	4.2	28.9	21.1	41.6	27.1	4.4	26.1	21.6	38.8	28.4	2.4	28.0	24.3	32.7
^{232}Th (Bq kg^{-1})	31.9	3.1	32.1	26.0	38.6	33.0	2.5	32.7	28.4	38.7	34.8	4.3	33.6	25.6	45.5	33.5	4.4	33.9	26.3	42.3	32.9	4.5	32.5	27.0	41.6
^{238}U (Bq kg^{-1})	39.8	9.4	39.6	0.0	53.1	40.4	9.1	39.9	23.4	60.4	42.7	9.8	41.2	22.4	74.8	43.0	10.3	39.0	32.9	75.4	41.4	8.1	41.8	30.5	56.6
χLF (10^{-8} m^3 kg^{-1})	42.6	20.9	38.7	10.4	101.5	17.1	10.0	14.5	4.3	36.5	59.6	34.8	49.8	14.1	145.8	60.8	28.7	65.2	17.5	105.2	12.3	4.5	9.7	8.2	19.9
Ba (mg/kg)	294.4	43.3	288.4	221.0	389.4	332.8	29.5	323.3	296.1	387.1	280.3	37.6	282.7	190.0	385.2	281.4	31.4	293.2	225.4	327.5	360.3	47.9	348.7	301.8	477.4
Nb (mg/kg)	10.9	1.1	10.7	9.1	14.5	10.8	0.9	10.9	8.8	12.5	11.3	1.5	11.0	8.6	15.7	11.1	1.7	10.9	8.5	14.5	10.4	0.7	10.5	9.1	11.4
Zr (mg/kg)	198.4	42.0	192.1	138.5	374.3	232.5	46.6	230.4	177.5	335.7	219.0	51.8	208.4	119.8	373.5	212.7	50.3	212.1	141.9	302.1	156.3	50.1	143.9	88.2	243.6
Sr (mg/kg)	420.6	73.0	429.8	237.3	549.3	484.9	108.3	471.2	268.5	657.5	338.4	149.4	337.4	109.4	1128.4	301.5	70.3	278.9	225.1	466.1	579.9	162.9	547.7	309.8	872.8
Rb (mg/kg)	73.7	10.0	74.1	48.7	99.1	69.3	8.0	70.4	54.2	82.8	79.6	10.8	81.2	49.7	105.5	77.0	11.2	75.3	52.4	95.1	83.1	19.4	79.4	52.8	120.2
Pb (mg/kg)	15.1	2.4	14.6	11.9	21.6	14.2	2.0	14.0	10.8	17.8	18.2	5.0	16.8	10.0	32.8	16.5	4.0	16.7	9.9	23.6	13.6	2.7	12.7	10.6	19.7
Zn (mg/kg)	56.7	8.2	55.4	38.8	74.3	51.9	3.8	51.3	45.6	61.7	60.7	9.0	59.5	38.0	85.7	58.0	7.6	59.0	39.7	69.2	56.7	11.9	52.3	39.7	76.5
Fe (mg/kg)	21878	2624	21716	15806	30550	20741	1606	21125	17397	23292	24697	4226	24084	16473	37476	24115	2843	23391	19122	28765	22559	3395	22153	16653	28108
Mn (mg/kg)	303.1	62.2	306.8	207.0	429.0	298.3	71.0	297.8	181.9	470.2	341.0	100.9	315.2	162.6	659.2	321.8	83.4	299.9	188.2	466.4	260.9	49.1	246.0	186.9	337.1
Cr (mg/kg)	71.8	11.9	71.2	41.0	93.9	55.2	13.1	53.4	32.2	77.0	77.5	12.6	77.0	51.6	119.8	81.8	12.2	84.2	55.3	105.2	67.3	11.9	67.8	46.4	87.2
Ti (mg/kg)	3230	269	3176	2816	4093	3305	194	3273	3072	3839	3375	396	3353	2656	4465	3263	293	3263	2699	3745	2948	182	2919	2652	3283
Ca (mg/kg)	164624	20691	169621	87781	198379	158867	19105	161540	105090	189001	132000	44600	142179	16106	206335	140607	30511	136722	93134	197015	173801	15373	173568	141657	194264
K (mg/kg)	14507	1565	14732	10161	17474	13700	1444	13861	10943	15702	15201	1622	15306	9901	18986	14692	1822	14502	10568	17402	15971	3358	15476	10799	21994
Al (mg/kg)	39129	4034	39539	28588	47629	38337	2841	38643	33481	43034	40660	4453	41204	26529	49442	39640	5225	40497	30074	49020	42353	6422	41524	31497	53130
P (mg/kg)	1110	99	1105	841	1315	1076	99	1051	932	1321	1027	228	997	647	1582	950	151	979	678	1245	758	67	783	640	861
Si (mg/kg)	172707	12610	169531	155240	212081	180590	12504	177640	167459	216673	185527	24898	179790	142369	252520	180855	17199	175710	153479	213395	164428	6813	160999	156789	178267
Mg (mg/kg)	3560	722	3679	1882	5169	3870	627	3774	2906	5176	3792	770	3885	1733	5639	3361	718	3380	2013	4418	5007	1448	4840	3003	7528
V (mg/kg)	61.0	12.8	61.0	34.6	88.0	57.7	12.0	55.1	32.8	79.8	73.5	15.1	73.1	43.7	112.4	68.0	14.3	65.9	31.4	95.2	76.6	18.5	74.4	53.9	105.4

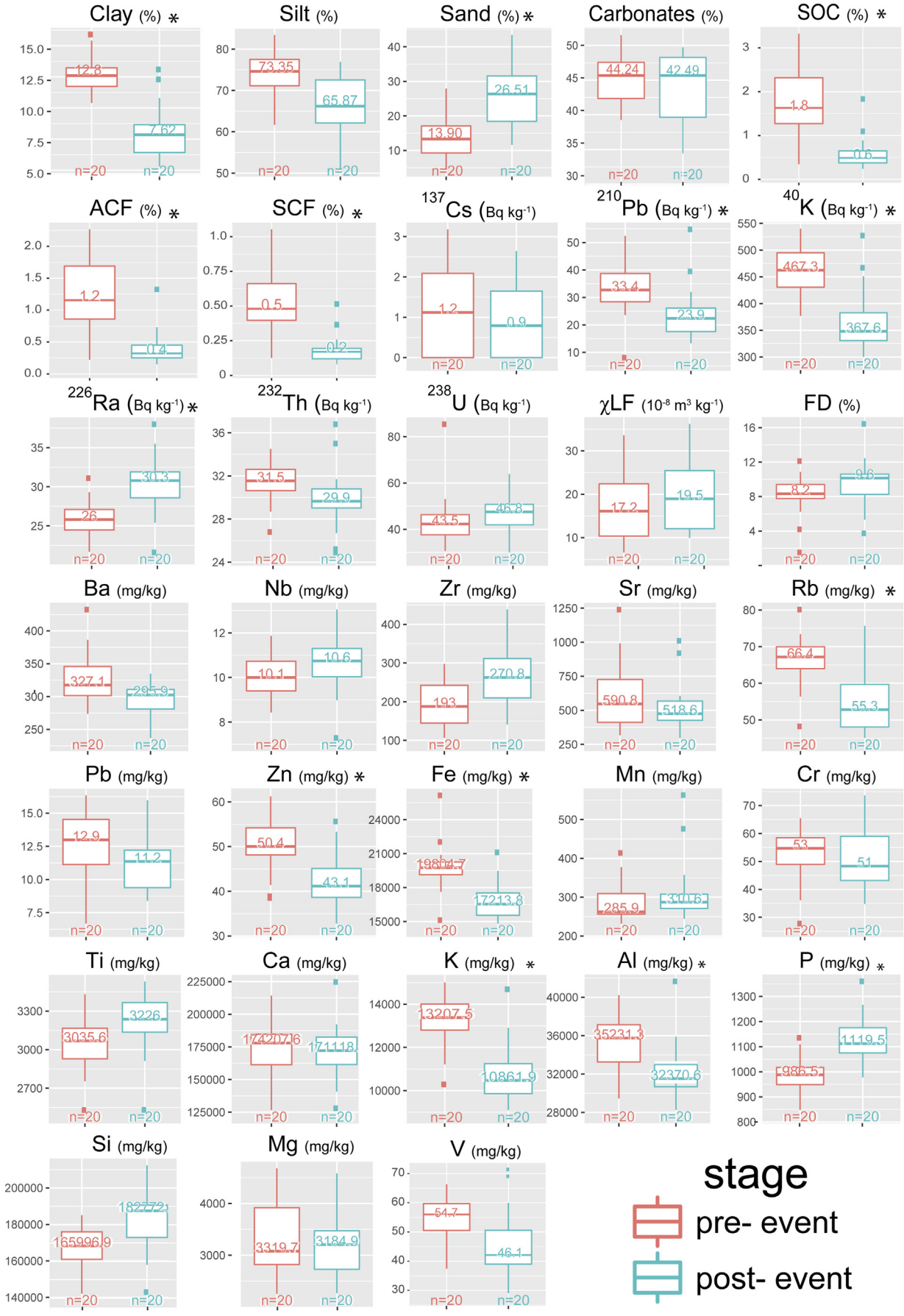

Fig. 2. Boxplots of pre- and post-storm sediment properties. Asterisks represent the elements that are significantly different between stages.

washed away during heavy autumn rainfall events. Thus, the aim of these different sampling methods was to provide a close replication of sediments deposited before and after the exceptional discharge event and the sediment in floodplains that corresponds to regular high discharge events (named as SFMP). Channel bed sediments were taken with a cylindrical core 5 cm long and 6 cm in diameter with three replicates at each sampling point. The same methodology was used for collecting the sediment in floodplains.

The samples were air-dried, grinded, homogenised and sieved to ≤0.063 mm following the most widespread methodology (Owens et al., 2016; Collins et al., 2017). In addition, the selection of the ≤0.063 mm particle size for sources and mixtures was related to the predominant silt texture of soils in the catchment (Table 1) and also because the content of sand, silt and clay fractions were similar between source and mixture samples (Table 1 and Fig. 2). Furthermore, the relationships between tracers and the size fractions support that ≤0.063 mm fraction compiles the existing range of variation for most of the study tracers. Particle size, stable elements, magnetic susceptibility and radionuclides were analysed in the ≤0.063 mm fraction for all 161 sediment samples.

Grain size and magnetic susceptibility were analysed following the same methodology as in Lizaga et al. (2019). The analyses of the stable elements were performed at the Consolidated Radio-isotope Facility (CORIF, University of Plymouth) by X-Ray Fluorescence (XRF) using a Niton XL3T 950 He GOLDD+ XRF Analyser. Samples were analysed for major and minor elements (Ba, Nb, Zr, Sr, Rb, Pb, Zn, Fe, Mn, Cr, V, Ti, Ca, K, Al, Si, and Mg). Concentrations, obtained after three measurements per element, are expressed in mg/kg.

Gamma emissions of ^{137}Cs, ^{226}Ra, ^{238}U, ^{232}Th and ^{40}K were analysed at the gamma lab of the Experimental station of Aula-Dei (EEAD-CSIC) following the methodology used in Lizaga et al. (2017) and Navas et al. (2018). The radionuclide activities are expressed as massic activity in Bq kg^{-1} dry soil and counted for 43,200 s.

2.3. Statistical analysis and sources selection

The laboratory results were statistically analysed using R. A non-parametric Kruskal Wallis test was used to evaluate whether sediment mixture properties varied between the pre- and post-storm event (Fig. 2). Correlation plots (Fig. 3) were used to evaluate the relationships and the differences between pre- and post-event soil properties. Furthermore, to identify the relationships of the different sources in the selected sediment mixtures, a Euclidian distance matrix with the normalised values and a cluster analysis using the ward.D2 method was used with all the study properties (Fig. 4). As each mixture point

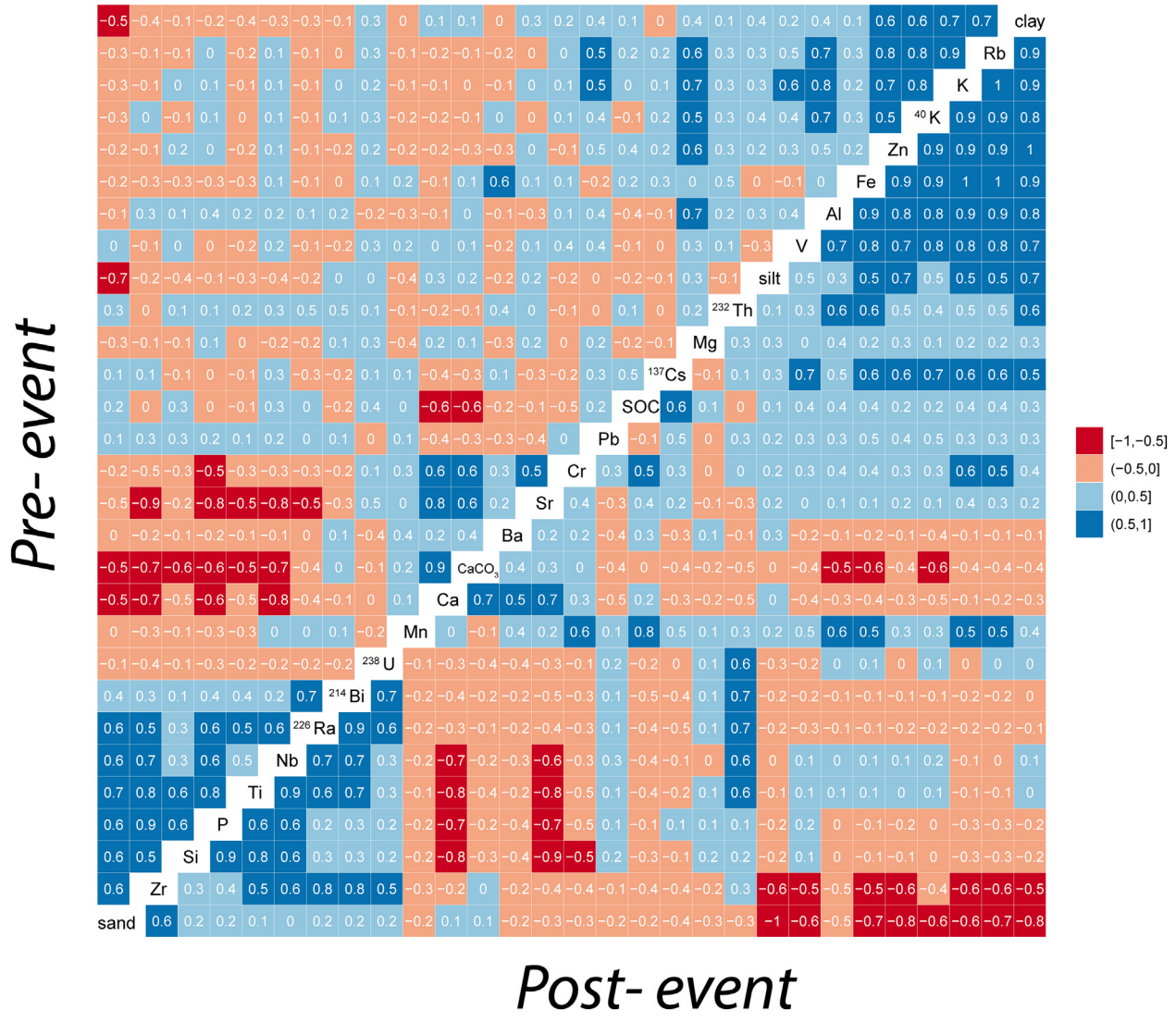

Fig. 3. Correlation coefficients of the different sediment properties before and after the exceptional storm event.

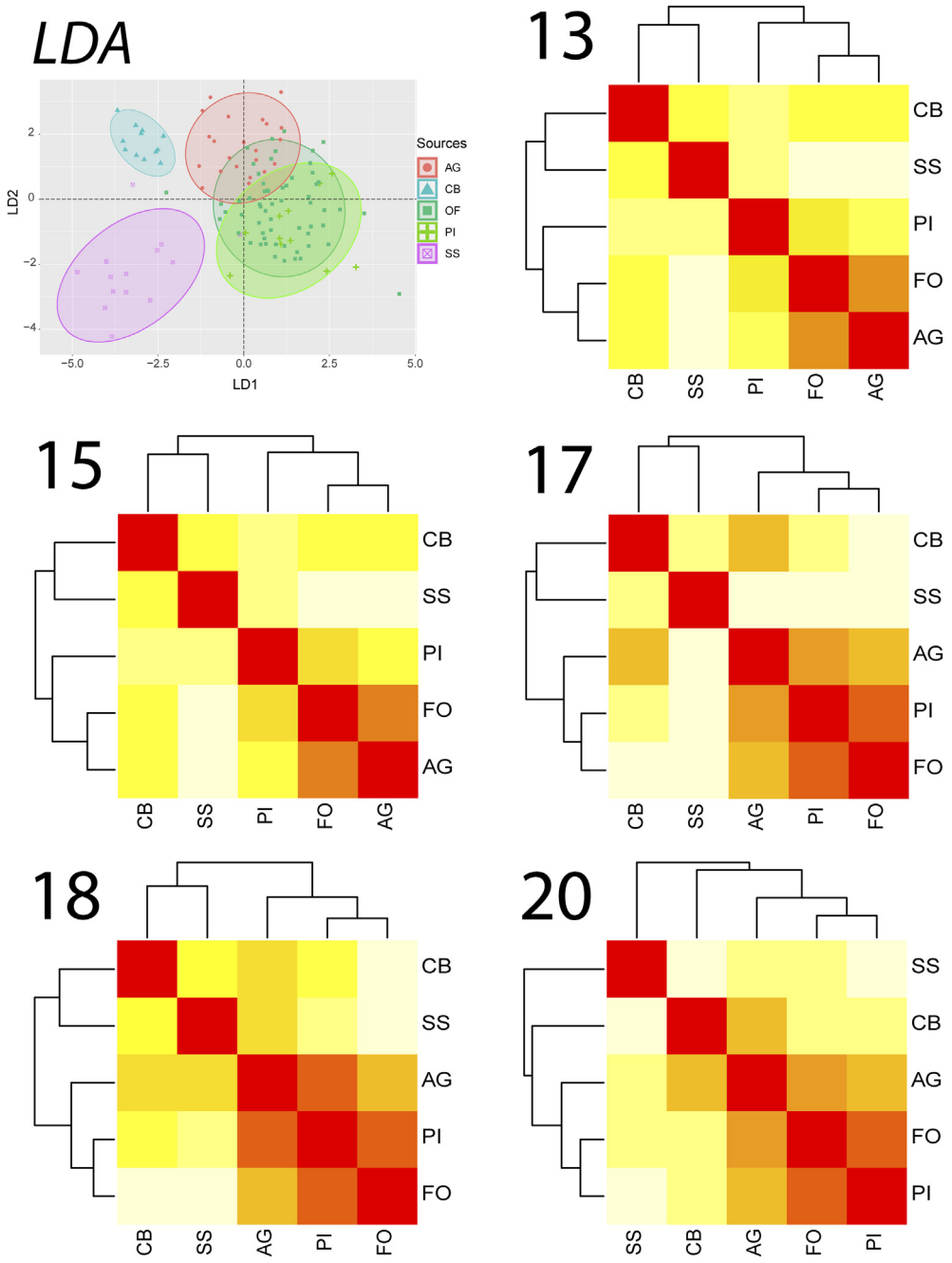

Fig. 4. Linear discrimination analysis (LDA) plot of the different sources in the Barués catchment. (13–20) Cluster analysis of the different sources presented in the mixture points. The darker colours show a stronger correlation while the brighter colours show a lower correlation.

has different source samples, the subsequent clusters may vary from one point to another and from headwater to lowlands.

2.4. FingerPro unmixing model and tracer selection

The estimation of the relative contribution of each potential sediment source to the pre- and post-event sediment mixtures and the statistical tests were done with the FingerPro unmixing model and package.

Source apportionment solutions were defined by the mean and standard deviation (SD) calculated from the results selected by the model. The SD of the selected solutions and the density graph of the model help to compare and evaluate the solution scattering as large values indicate poor source contribution ascription.

A crucial requirement in fingerprint assessment is the implementation of previous statistical tests to identify individual fingerprint properties, which discriminate between potential sources to select the optimum set of fingerprint properties (Yu and Oldfield, 1989; Walling and Woodward, 1995; Collins et al., 1996; Collins et al., 1997; Palazón et al., 2015a; Collins et al., 2017). Several studies following the methodology implemented by Collins and Walling (2002) compare the range in the sources to the range in the sediment mixture or target for each fingerprint property (Smith and Blake, 2014; Koiter et al., 2018). The two-step statistical procedure proposed by Collins et al. (1997) and Walling (2005) is included as an optional step in the FingerPro R package and was used in this study. In addition, because of the type of sediment mixtures and its temporal storage in the channel bed, P, SOC and grain size properties were considered non-conservative, and they were excluded from the analysis following Koiter et al. (2013).

As the first step in tracer selection, the range test cannot definitively identify all tracers that are behaving non-conservatively but it removes the tracers with the largest differences with the mixture sample that could also reveal the existence of a non-sampled source. As an intermediate step we used biplot charts as proposed by Pulley et al. (2015) using the correlationPlot () function included in the FingerPro package to further check the conservative behaviour of each pair of tracers. The second step suggested using the KW test to remove those tracers that do not show significant differences between the selected sources. The tracer selection should not be only based on statistical tests but also in expert knowledge of the hydrological and geomorphological processes in the study area. However, the use of many tests could remove a considerable number of tracers that might restrict the discrimination between sediment sources (Blake et al., 2018). For this reason, boxplot charts, LDA (Linear Discriminant Analysis) plots and correlation plots are included in the FingerPro package to help in the decision. Three-step tracer selection was implemented in this study: the range test and Kruskal-Wallis followed by the inclusion or exclusion of some tracers based on 'expert judgement' informed by visualising the tools included in the FingerPro package. None of the functions included in the package are mandatory, and the tracer exclusions can be based on the charts and results from the statistical tests.

To check the quality of FingerPro model, a set of virtual mixtures based on the unmixing results and using the selected tracers at each sediment mixture point were created. By unmixing the virtual mixtures versus the mean values of the sources for the selected tracers it is possible to obtain for each mixture the RMSE values of the model. Thus, by using virtual mixtures the results allow us to validate the model performance.

3. Results

3.1. Temporal variation of soil properties along the streams

The measured properties of the sediment mixtures collected in the pre- and post-event campaigns are shown in Fig. 2. Mean clay content decreased from 12.7% to 7.6% for pre- and post-event sediments, respectively. In pre-event sediment, SOC contents were significantly higher (range: 0.46–3.31%) than in post-event sediment (range: 0.24–1.8%). Mean radionuclide activities decreased from pre- to post-event sediments for ^{137}Cs (1.1–0.9 Bq kg^{-1}), ^{40}K (467.3–367.6 Bq kg^{-1}) and ^{232}Th (31.5–29.9 Bq kg^{-1}) but increased for ^{226}Ra (26.0–30.3 Bq kg^{-1}), and ^{238}U (43.5–46.8 Bq kg^{-1}). Major element contents varied in pre- and post-event sediment. Mean values were: Si (165,996–182,772 mg/kg), Al (35,231–32,370 mg/kg), Ca (174,207–171,118 mg/kg), Mg (3320–3185 mg/kg), K (13,208–10,862 mg/kg), Ti (3036–3226 mg/kg), Fe (19,805–17,214 mg/kg), Mn (286–311 mg/kg) and P (987–1120 mg/kg).

A decrease of about 38% in fine fraction content in the post-event sediment was coincidental with a decrease of stable elements and properties that were positively correlated with clay fraction such as SOC, ^{137}Cs, ^{40}K, ^{232}Th, Ba, Sr, Rb, Pb, Zn, Fe, K, Al and V (Figs. 2 and 3). On the contrary, the study properties with negative correlation with clay but positively correlated with the coarse fraction, such as the magnetic properties ^{226}Ra, Nb, Zr, Ti, P and Si, were enriched in the sediment after the storm event. ^{238}U, Mn, Ca and carbonates were not correlated with any grain size fraction and did not show any clear trend between pre- and post-event sediment. In general, there was an increase in the intercorrelation between the study elements and properties that were correlated with grain size fractions in post-event sediment (Fig. 3).

There were important variations when comparing the pre- and post-event study properties between at the headwaters, the middle and lower part of the catchment. A higher decrease in clay content (70%) was recorded in the middle part than in the headwaters and lower part of the catchment, but the opposite was observed for sand, which reached higher contents (59%) in the middle part of the catchment. Thus, most properties positively correlated with clay showed similar decreasing trends in the headwaters, middle and lower parts of the catchment.

The floodplain sediment as an intermediate stage between pre- and post- event sediments showed a transitional variation in elements and properties. Thus, the clay fraction in pre-event sediment decreased significantly ($p < 0.05$) in floodplains (17%), but the decrease reached as much as 42% in post-event sediment accompanied by a subsequent increase in sand fraction of 10% and 100% in floodplain and post-event sediment, respectively. Most of the properties such as ^{137}Cs, ^{40}K, ^{226}Ra, ^{232}Th, Nb, Sr, Zr, Rb, Zn, Fe, K, Al, Ti, P, Si and V differed significantly between these stages and showed similar increasing or decreasing trends (Fig. 5). Furthermore, Ba, Cr, Ca, SOC and SOC fractions had similar values in pre-event and floodplain sediment with a sharp decrease in post-event sediment. However, ^{238}U, χLF, Pb, Mn and Ca did not show a clear trend between stages (Table 3).

3.2. Sources and tracers selection

The statistics of grain size, SOC and trace element properties for the potential sediment sources are presented in Table 1. The SOC contents were low, with a mean value of 2% and the SOC fractions ACF and SCF ranged from 0.3% to 5.9% and from 0.036% to 1.38%, respectively. The low frequency (χLF) and frequency dependent (χFD) mass magnetic susceptibility had a mean value of 46.64 10^{8}m^{3} kg^{-1} and 7.31%, respectively. In AG, CB and SS sources, SOC contents were lower and significantly different from the other sources, with the highest values found in OF and PI. Furthermore, the means of ^{137}Cs, Ba, Sr and P in AG were significantly lower than those in the other land uses (OF, PI) ($p \leq 0.05$). Most properties in CB and SS significantly differed from the other sources except for radionuclides. Major elements such as Si, Al,

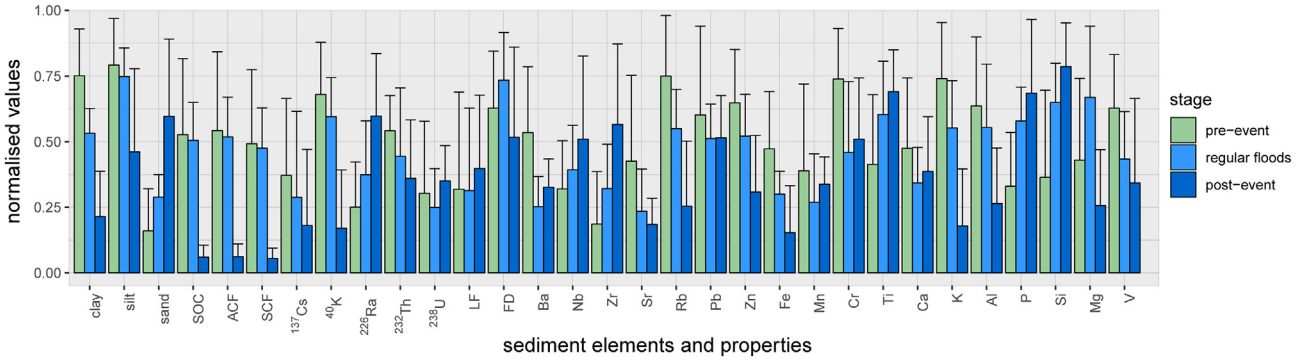

Fig. 5. Bar plot of sediment properties for the three different flood stages: pre-event, regular flood and post-event.

Table 2
Optimum set of tracers selected for each sampling point along the streams pre- and post- event.

20		18		17		15		13		20	17	15
pre-	post-	pre-	post-	pre-	post-	pre-	post-	pre-	post-	floodplains		
^{137}Cs	^{137}Cs	^{137}Cs	^{137}Cs	^{137}Cs	^{137}Cs	^{137}Cs	^{137}Cs	^{137}Cs	^{137}Cs	^{137}Cs	^{137}Cs	^{137}Cs
^{40}K	χLF	χLF	χLF	^{40}K	χLF	^{238}U	χLF	χLF	χLF	Ba	χLF	^{238}U
Zr	Sr	Ba	Ba	χLF	Sr	χLF	Pb	Ba	Ba	Pb	Ba	χLF
Zn	Zn	Zr	Zr	Rb	Mn	Ba	Ti	Zr	Zr	Zn	Cr	Ba
Cr	Fe	Cr	Sr	Pb	Cr	Mn	Cr	Sr	Sr	Mn	Ti	Zr
Mg	Mn	Si	Mn	Cr	Si	Cr		Mn	Mn	Cr	Si	Ti
V	Cr	V	Ti	Mg	Ti			Si	Si	Si	Mg	
			Ca					V	V	χLF	V	

Ca, Mg, K, Ti, Fe, Mn and P only had significant differences in SS compared to the other sources except for Fe and K, which had the lowest mean values in CB.

The LDA plot created with all the source samples showed overlapping between land use sources and illustrated low discrimination capacity for AG, OF and PI (Fig. 4). The discrimination of sources that are not well characterised might reduce discrimination or lead to erroneous model results. Thus, land uses were grouped in two different combinations based on their spatial distribution in the catchment along with results from a cluster analysis pursued with tracer data. In the lower part of the catchment, cluster analysis showed the highest similarities between land uses with arboreal vegetation (OF and PI) (Fig. 4). Furthermore, AG predominated in the lower part of the catchment and had different mean values of ^{137}Cs, χLF, Ba, Zr, Fe, Mn, Ca, P and Sr than in OF and PI. Thus, it was decided to merge both arboreal land uses in one source (OF+PI). On the other hand, at the headwaters where PI dominates, AG and OF showed the highest similarities in the analysed tracers (Fig. 4). In addition, the tracers selected by the statistical test in each mixture point before and after grouping sources mostly coincide, supporting the adopted merging. This methodology was implemented to homogenise the results and to avoid including non-contributing or very low-contributing sources into our unmixing model.

Following this approach and the different source points selected for each sediment mixture, it was decided to create a set of optimum tracers for each mixture point. Table 2 shows the optimum set of tracers selected for unmixing sediment mixtures along the stream for the pre- and post- event sediment mixtures and floodplain sediment. In addition, the low RMSE values calculated when comparing the unmixing results for the virtual mixtures with that of the channel bed and floodplain sediment mixtures validate the results and the performance of the FingerPro model (Table 3).

3.3. Sediment source contributions pre- and post- 2012 rainstorm event

The average mean relative contributions of each potential source to the sediment mixtures indicates that overall, CB was the predominant source both before and after the event ranging between 35 ± 7 to 87 ± 13%, followed by SS with a mean contribution of 24 ± 9%. On the other hand, AG contributed around 21 ± 9% at the lower part of the catchment but much less in the headwaters. In contrast, PI contributed around 10 ± 9% at the headwaters, but it was almost insignificant at the lower part of the catchment. The sediment contribution supplied by OF+PI was only noticeable in the middle part of the catchment at point 17 with a mean apportionment of 16 ± 6% in the pre-event sediment.

Large variations in source contributions were recorded for each sediment mixture, especially between sediment mixtures located at the headwaters and in the middle and lower parts of the catchment (Fig. 1). Furthermore, sediment mixtures varied greatly between the pre- and post- exceptional event.

In the headwaters, SS and CB were the main contributing sources. However, following the cluster group and the significant apportionment (16% and 17%) of the forests (OF+PI), it was decided to merge AG and OF (AG+OF) and separate the PI source. The results for sediment mixture points (SMP) 13 and 15 showed a mean sediment supply of 16% and 10% from the pine afforestation. The contribution from forests (OF+PI) was not observed downstream from SMP 17. For the downstream sediment mixture points, there were also significant differences between SMP 17 located in the central part of the catchment and both SMP 18 and SMP 20 located downstream from the La Reina tributary stream. The agricultural source contribution reached a maximum close to the outlet of the catchment (SMP 18 and SMP 20) and decreased marginally in upstream sediment. On the contrary, at SMP 17 the

Table 3
Mean percentages of GOF calculated following Palazón et al. (2015b), source contributions (standard deviations in parentheses) and relative source contributions (RSC; apportion (%) divided area (%)) from the FingerPro model for open forest (OF), agricultural (AG), pine afforestation (PI), subsoil (SS), channel bank(CB) to the mixture samples. RMSE was calculated by comparing the unmixing results for the virtual mixtures with the channel bed sediment mixtures.

	ID	RMSE	GOF	OF		PI		AG		SS		CB	
		%	%	%	RSC	%	RSC	%	RSC	%	RSC	%	RSC
Pre-event	13	0.1	83.5 (4.5)	0.4 (1.9)	1.2	16.3 (10.7)	29.17			12 (8.9)	1200	71.3 (14.7)	4519.5
	15	2.7	86.4 (6.2)	0.4 (1.5)	0.5	10.3 (5.2)	66.60			29.7 (6.4)	990	59.5 (7.1)	4370.1
	17	3.9	85.0 (3.2)	14.9 (4.5)	24.2	–	–	0.2 (1.6)	1.2	18.5 (7.1)	925	66.2 (6.8)	3890.0
	18	1.2	83.1 (3.7)	1.5 (3.2)	2.6	–	–	21.0 (9.5)	134.8	31.3 (7.8)	1565	46.1 (10.5)	2708.9
	20	2	90.0 (3.1)	0.9 (3.1)	1.5	–	–	36.7 (7.7)	188.8	28.9 (6.1)	1445	33.5 (6.5)	2162.6
Floodplain	15	1.6	80.2 (5.1)	4.0 (6.4)	5.7	26.5 (13)	171.36	–		46 (14.2)	1533.33	23.5 (15.6)	1726.0
	17	2.60	73.9 (3.6)	0.0 (0.1)	0.0	–	–	29.8 (11.5)	191.41	9.9 (7.3)	495.00	60.2 (12.7)	3537.5
	20	3.3	82.2(2.7)	0.48 (2.1)	0.8	–	–	39.8 (9.2)	214.17	10.3 (7.8)	515.00	49.4	3043.7
Post-event	13	3.6	82 (4.4)	4.6 (7.5)	14.6	6.0 (9)	10.74	–	–	2.5 (4.8)	25	86.8 (13.3)	5451.0
	15	1.7	87.9 (5.5)	1.4 (3.3)	2.0	0.8 (2.1)	5.17	–	–	57.6 (19.5)	1900	40.2 (19)	2938.0
	17	3.1	89.4 (4)	1.1 (2.1)	1.9	–	–	3.7 (4.9)	23.77	27.8 (9.1)	1390	67.2 (9.8)	3948.8
	18	1.0	87.5 (2.6)	0.8 (2.6)	1.3	–	–	39.4 (9.3)	253.07	21.8 (6.9)	1090	37.9 (10.2)	2227.1
	20	1.9	92.9 (2.1)	4.8 (5.8)	8.3	–	–	29.0(12.7)	156.1	0.6 (1.8)	30	65.41 (8.3)	4030.2

contribution of AG was negligible. However, the presence of sediment from forests was detected with a mean contribution of up to 14%, being <2% in SMP located downstream of SMP 17.

In the headwaters (SMP 13 and SMP 15) PI sediment was mostly washed out from the streams in post-event sediment mixtures. SMP 13 showed a similar decrease in SS, thus increasing CB contribution up to 80%. However, SS in SMP15 increased slightly with the subsequent decrease in CB proportion. The middle part of the catchment also experienced a sharp decrease in contributions from the different land uses. Moreover, the SS apportionment in the middle part increased from 18% in the pre-event sediment to up to 27% in the post-event sediment. A different history occurs downstream the La Reina tributary stream at SMP 18 where agricultural apportionments increased largely while SS and CB decreased. At the catchment outlet, a large increment in CB apportionment was recorded along with a sharp decrease in SS and a small decrease of AG in the post-event sediment. Furthermore, a slight increase from the forest source (OF+PI) was recorded. The SS decrease recorded at the outlet of the catchment was supported by the results extracted from the SFMP where 90% of the sediment contribution was supplied by CB and AG. In addition, the unmixing results of the SFMP indicated an increase of PI and SS sediment in regular high discharge events but the disappearance of PI sediment during exceptional events. SFMP 17 revealed an increase in AG and a slight decrease in SS sediment in the floodplain while it showed a sharp increase in SS with a total wash out of AG sediment during the exceptional event. Besides that, at the catchment outlet SFMP 20 showed a decrease in AG and SS sediment but a progressive CB increase as seen in Table 3.

4. Discussion

4.1. Variation in soil properties due to the exceptional event

Compared with the other sources, the significant differences in most properties found in SS (except for the radionuclides) are because SS is composed of very degraded soils that expose the substrate. In addition, SS is mostly located in areas with high hydrological connectivity, likely increasing its delivery to streams during storm events. In the talus of the streams, CB sediment consisting of loess type materials infilling the valley floor is the nearest available source to be deposited in the channel. As such, SS and CB are the most distinctive sources from the others. However, Fig. 4 shows some similarities between CB and AG sources likely because the agricultural land is mostly located on the valley floor on alluvial materials infilling the valleys that comprise the CB source.

The significant differences in mean contents of SOC, ^{137}Cs, Ba, Sr and P in agricultural land compared with PI and OF suggest that land use is one of the principal factors affecting the variation in soil properties after five decades of land abandonment as found by Lizaga et al. (2019). In addition, the scarce vegetation cover and the presence of more degraded soils with specific locations in the catchment point to AG, CB and SS sources as the most erodible areas. Thus, due to soil redistribution processes, these sources show significant differences in the study properties. However, in the headwaters the croplands recently abandoned due to more difficult access, which support less intensive farming, show more similarities with OF. Furthermore, the higher connectivity between OF that surrounds the AG areas in the headwaters further contributes to similarities found in their soil properties. All these factors operating together in the headwaters likely increase similarities between AG and OF as seen in the results of the cluster analysis.

Exceptional rainfall events produce increases in connectivity and suspended sediment loads and modify the channel bed sediments by decreasing or increasing the concentration of different size particles during floods. The significant differences for most study properties between pre- and post-event sediment point to exceptional storm events as the main factors in causing sediment mobilisation from different sources, resulting in subsequent variation of geochemistry and sediment properties as was also reported by Martins et al. (1995). The sharp decrease experienced by the fine fraction and the increase in the coarse fraction suggests that exceptional storm events export high quantities of sediment composed mostly of fine sediment as was also found by Bortoluzzi et al. (2013) in a Brazilian catchment. This hypothesis is supported by the decrease in most sediment properties positively correlated with the clay fraction. However, the non-significant differences in ^{137}Cs and magnetic properties could be explained by the large variability of these properties across the catchment.

During heavy storm events, the sediment begins to be exported and reach a maximum, beyond which the sediment exported begins to decline leading to an ordered sedimentation and the increase of the mobilised element correlation (Quesada et al., 2014; Gaspar et al., 2019b) (Fig. 3). In our catchment, high sediment mobilisation is supported by the increase in overall intercorrelation of the study elements that are correlated with the grain size.

4.2. Temporal and spatial variation of sediment mixture properties

The variation of sediment properties in the stream channel before and after the exceptional event as well as in the floodplains at an intermediate stage of sediment deposited by regular high floods is related to the export of the fine grain size fractions. Thus, the loss of fine material produces the subsequent enrichment in the content of coarse fractions after rainfall events as was also found by Smith and Olyphant (1994) resulting in the highest sand content in channel bed sediment after the exceptional rainfall event.

The elements positively correlated with argillaceous materials such as ^{137}Cs, Rb, Sr, Fe, Zn, Al, Cr, Pb, contained in the fine fraction, show a clear decreasing trend from pre-event, floodplain and post-event sediment due to the reduction of fine materials that are exported during high floods. Mitchell et al. (1997) and Quiquerez et al. (2008) also reported high export rates of fine sediment material and associated nutrients. Thus, vanadium, which is finely incorporated into clay minerals during weathering, is also exported. There are some elements such as Ba and Mn that have limited mobility because they are easily precipitated as sulphates and carbonates. Furthermore, Ba and Mn can also be strongly absorbed by clay minerals, which also explains the slight decrease of Ba and Mn in floodplain and post-event sediment and supports the hypothesis of high fine sediment export during storm events. On the other hand, Si is directly correlated with the coarse fraction due to the high content of silicon grains in the sandstone strata. Many Ti-containing minerals are resistant to weathering (also Zr) and increase with the coarse fraction. Additionally, Nb exhibits a strong affinity with Ti and Zr. All these mineral-element associations lead to increases of Ti, Zr, Nb and Si after the storm event in parallel with the increase in the coarse fraction. Therefore, the chemical changes observed are due to the mixing of soil sediment mobilised during the exceptional event with pre-existing soil sediments mobilised during regular rainfalls.

4.3. Sediment source contributions variation

The contribution of channel bed changes before and after the event (but also from headwaters to the lower part of the catchment) is due to the great modification power of these exceptional storm events. In SMP 13 located in the headwaters, 30% of apportions come from PI and SS sources, but during floods most of these sediments are exported, and thus CB becomes the predominant source. Our results suggest that during the exceptional event, most of the channel bed sediment is efficiently exported. PI sediment was also exported in SMP 15 during the storm event; however, due to the proximity of steep slopes (19 to

Fig. 6. Results of the unmixing procedure before and after the exceptional storm event in each mixture point. An ANOVA test was performed to assess whether source contribution differed between pre- and post-event mixtures. Different letters indicate significant differences at the 95% level.

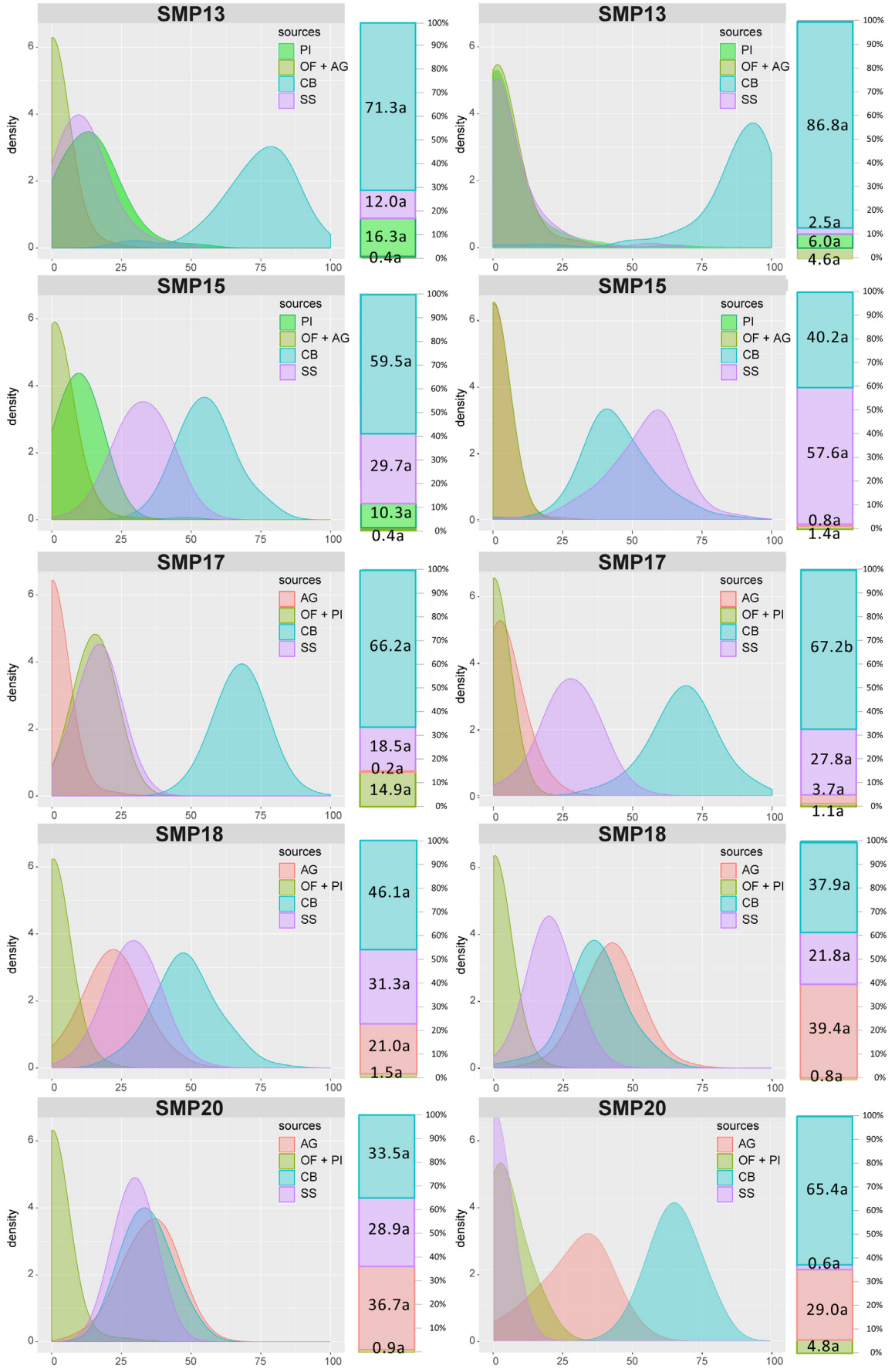
SMP13
sources
PI
OF + AG
CB
SS
density
71.3a
12.0a
16.3a
0.4a
SMP13
86.8a
2.5a
6.0a
4.6a
SMP15
59.5a
29.7a
10.3a
0.4a
SMP15
40.2a
57.6a
0.8a
1.4a
SMP17
AG
OF + PI
66.2a
18.5a
0.2a
14.9a
SMP17
67.2b
27.8a
3.7a
1.1a
SMP18
46.1a
31.3a
21.0a
1.5a
SMP18
37.9a
21.8a
39.4a
0.8a
SMP20
33.5a
28.9a
36.7a
0.9a
SMP20
65.4a
0.6a
29.0a
4.8a
Pre- event
Post- event

25°) with highly disturbed areas and the predominance of bare soils in the contributing area, SS appears as the dominant source after the storm event.

Results obtained from both the floodplain sediment and the channel bed sediment mixtures at SMP 15 where subsoil apportions are predominant suggest that during storm events, sediment from surrounding slopes with highly degraded soils directly reaches the stream. This interpretation is also supported by results at SMP 17 located in the middle part of the catchment downstream from SMP 15 with a similarly high subsoil contribution. The subsoil contribution then gradually decreases in the lower part of the catchment (SMP 18 and 20) after the storm event. Such exceptional rainfalls produce large variations on the sediment mobilised from different sources thus changing sediment source contributions to the streams as can be seen in Fig. 6.

A different behaviour is observed in sediment mixtures located upstream from the La Reina ephemeral stream and those located in the lower part of the catchment at SMP 18 and 20. At these points, the fingerprinting analysis shows a high increase of AG provenance that is likely related to the incision of the main stream over the agricultural land located on the glacis and the sediment apportion from the La Reina ephemeral stream.

The deep incision of the streams and the almost vertical slopes of the channel banks along with the nature of non-cohesive infilling material are the reason that CB is the source that produces the highest sediment supply. The incision of the streams is highly variable across the catchment, but overall, it increases downstream from the La Reina ephemeral stream where the glacis starts. In addition, during heavy storms, geomorphological processes such as piping, topples and landslides are likely to increase apportionment from CB sources (Gaspar et al., 2019b).

During heavy rainfalls, sediment resuspension due to energy expenditure in the channel is higher in the headwaters and the middle part of the catchment (i.e., SMP 13, SMP 15 and SMP 17) than in the lower part of the catchment. Sediment resuspension could produce deposition downstream due to the loss of energy thus increasing the sediment storage in the lower part of the catchment. This is similar, though on a different scale, to what has been observed in the lower part of the Ebro River by Quesada et al. (2014). The cluster analysis results also support the different functioning of the headwaters and the lower part of the catchment. Furthermore, the results of the relative source contribution (RSC) (Table 3) highlight the high sediment export from subsoil and emphasise the low apportions from natural covers such as OF. These results are in good agreement with studies by López-Tarazón et al. (2009) and Palazón et al. (2016) and further support the idea of bare soil as one of the main environmental problems for river ecosystems.

5. Conclusions

Large changes in the characteristics of sediment were produced by an exceptional storm event, modifying element concentrations and sediment provenance. The significant differences between pre- and post-storm sediment mixtures highlight the great impact of such storm events on channel bed sediment. Bearing in mind the observed spatial variations in sediment properties and grain-size distributions, one may conclude that the sediment mobilisation and transfer produced in the catchment was highly dynamic.

Placing the channel bed sediment apportionments in a geomorphological context, our model results indicate an important input from SS despite its spatial coverage in the catchment in amounts <2%. Therefore, the subsoil is suggested to be an important environmental problem with hot spots that are worth controlling. In contrast, the insignificant sediment apportionment from forests underlines the benefits of natural covers to prevent soil loss.

Composite fingerprints provide the opportunity to efficiently trace sediment sources before and after exceptional rainstorm events. Overall, our results provide evidence of the severe erosion produced by this exceptional rainstorm event and reveal important variations in sediment source patterns. Stream bank failure induced by natural tunnelling or piping and landslides significantly contributed to sediment delivery. The magnitude of agricultural and bare soil mobilisation during the course of this exceptional rainstorm was much greater than under normal discharge regimes. Similar conclusions are derived from the analysis of variations in sediment properties between pre-event SMP, SMFP and post-event SMP. The geomorphological analysis, the fingerprinting procedure, and the low RMSE obtained with virtual mixtures support the good performance of the new FingerPro unmixing model to quantify the different sediment source apportionments.

Acknowledgements

This work has been supported by project CGL2014-52986-R funded by the Spanish Ministry of Science, Innovation and Universities and the aid of a predoctoral contract (BES-2015-071780).

Appendix A. Supplementary data

Supplementary data to this article can be found online at https://doi.org/10.1016/j.geomorph.2019.05.015.

References

Blake, W.H., Boeckx, P., Stock, B.C., Smith, H.G., Bodé, S., Upadhayay, H.R., Gaspar, L., Goddard, R., Lennard, A.T., Lizaga, I., Lobb, D.A., Owens, P.N., Petticrew, E.L., Kuzyk, Z.Z.A., Gari, B.D., Munishi, L., Mtei, K., Nebiyu, A., Mabit, L., Navas, A., Semmens, B.X., 2018. A deconvolutional Bayesian mixing model approach for river basin sediment source apportionment. Sci. Rep. 8, 13073. https://doi.org/10.1038/s41598-018-30905-9.

Borrelli, P., Robinson, D.A., Fleischer, L.R., Lugato, E., Ballabio, C., Alewell, C., Meusburger, K., Modugno, S., Schütt, B., Ferro, V., Bagarello, V., Oost, K.V., Montanarella, L., Panagos, P., 2017. An assessment of the global impact of 21st century land use change on soil erosion. Nat. Commun. 8, 2013. https://doi.org/10.1038/s41467-017-02142-7.

Bortoluzzi, E.C., dos Santos, D.R., Santanna, M.A., Caner, L., 2013. Mineralogy and nutrient desorption of suspended sediments during a storm event. J. Soils Sediments 13, 1093–1105. https://doi.org/10.1007/s11368-013-0692-4.

Buendia, C., Batalla, R.J., Sabater, S., Palau, A., Marcé, R., 2016. Runoff Trends Driven by climate and Afforestation in a Pyrenean Basin. Land Degrad. Develop. 27, 823–838. https://doi.org/10.1002/ldr.2384.

Cavalli, M., Trevisani, S., Comiti, F., Marchi, L., 2013. Geomorphometric assessment of spatial sediment connectivity in small Alpine catchments. Geomorphology, Sediment sources, source-to-sink fluxes and sedimentary budgets 188, 31–41. https://doi.org/10.1016/j.geomorph.2012.05.007.

Chen, J., Shi, Z., Wen, A., Yan, D., Chen, T., 2019. ^{137}Cs-based variation of soil erosion in vertical zones of a small catchment in Southwestern China. Int. J. Environ. Res. Public Health 16, 1371. https://doi.org/10.3390/ijerph16081371.

Collins, A.L., Walling, D.E., 2002. Selecting fingerprint properties for discriminating potential suspended sediment sources in river basins. J. Hydrol. 261, 218–244. https://doi.org/10.1016/S0022-1694(02)00011-2.

Collins, A., Walling, D., Leeks, G.J.L., 1996. Composite fingerprinting of the spatial source of fluvial suspended sediment: a case study of the Exe and Severn river basins, United Kingdom. Géomorphologie: relief, processus, environnement 2, 41–53. https://doi.org/10.3406/morfo.1996.877.

Collins, A.L., Walling, D.E., Leeks, G.J.L., 1997. Source type ascription for fluvial suspended sediment based on a quantitative composite fingerprinting technique. CATENA 29, 1–27. https://doi.org/10.1016/S0341-8162(96)00064-1.

Collins, A.L., Pulley, S., Foster, I.D.L., Gellis, A., Porto, P., Horowitz, A.J., 2017. Sediment source fingerprinting as an aid to catchment management: a review of the current state of knowledge and a methodological decision-tree for end-users. Journal of Environmental Management, Sediment source fingerprinting for informing catchment management: methodological approaches, problems and uncertainty 194, 86–108. https://doi.org/10.1016/j.jenvman.2016.09.075.

Dutta, S., 2016. Soil erosion, sediment yield and sedimentation of reservoir: a review. Model. Earth Syst. Environ. 2, 123. https://doi.org/10.1007/s40808-016-0182-y.

Evrard, O., Poulenard, J., Némery, J., Ayrault, S., Gratiot, N., Duvert, C., Prat, C., Lefèvre, I., Bonté, P., Esteves, M., 2013. Tracing sediment sources in a tropical highland catchment of Central Mexico by using conventional and alternative fingerprinting methods. Hydrol. Process. 27, 911–922. https://doi.org/10.1002/hyp.9421.

Favis-Mortlock, D., 2008. Soil erosion and sediment redistribution in river catchments: measurement, modelling and management, edited by P. N. Owens and A. J. Collins. CABI, Wallingford, UK, 2006. ISBN 978 0 85199 050 7, xiv+328 pp. Land Degrad. Dev. 19, 694. https://doi.org/10.1002/ldr.872.

García-Ruiz, J.M., Martí-Bono, C., Lorente, A., Beguería, S., 2002. Geomorphological consequences of fraquent and infrequent rainfall and hydrological events in Pyrennez Mountains of Spain. Mitig. Adapt. Strateg. Glob. Chang. 7, 303–320. https://doi.org/10.1023/A:1024479630433.

Gaspar, L., Navas, A., Walling, D.E., Machín, J., Gómez Arozamena, J., 2013. Using ^{137}Cs and ^{210}Pb$_{ex}$ to assess soil redistribution on slopes at different temporal scales. Catena, Scales in Soil Erosion 102, 46–54. https://doi.org/10.1016/j.catena.2011.01.004.

Gaspar, L., Blake, W.H., Smith, H.G., Lizaga, I., Navas, A., 2019a. Testing the sensitivity of a multivariate mixing model using geochemical fingerprints with artificial mixtures. Geoderma 337, 498–510. https://doi.org/10.1016/j.geoderma.2018.10.005.

Gaspar, L., Lizaga, I., Blake, W.H., Latorre, B., Quijano, L., Navas, A., 2019b. Fingerprinting changes in source contribution for evaluating soil response during an exceptional rainfall in Spanish Pre-Pyrenees. J. Environ. Manag. 240, 136–148. https://doi.org/10.1016/j.jenvman.2019.03.109.

Grodek, T., Jacoby, Y., Morin, E., Katz, O., 2012. Effectiveness of exceptional rainstorms on a small Mediterranean basin. Geomorphology 159–160, 156–168. https://doi.org/10.1016/j.geomorph.2012.03.016.

Gutiérrez, F., Gutiérrez, M., Sancho, C., 1998. Geomorphological and sedimentological analysis of a catastrophic flash flood in the Arás drainage basin (Central Pyrenees, Spain). Geomorphology 22, 265–283. https://doi.org/10.1016/S0169-555X(97)00087-1.

Heckmann, T., Cavalli, M., Cerdan, O., Foerster, S., Javaux, M., Lode, E., Smetanová, A., Vericat, D., Brardinoni, F., 2018. Indices of sediment connectivity: opportunities, challenges and limitations. Earth Sci. Rev. 187, 77–108. https://doi.org/10.1016/j.earscirev.2018.08.004.

Klages, M.G., Hsieh, Y.P., 1975. Suspended solids carried by the Gallatin River of Southwestern Montana: II. Using Mineralogy for Inferring Sources. Journal of Environmental Quality 4, 68–73. https://doi.org/10.2134/jeq1975.00472425000400010016x.

Koiter, A.J., Owens, P.N., Petticrew, E.L., Lobb, D.A., 2013. The behavioural characteristics of sediment properties and their implications for sediment fingerprinting as an approach for identifying sediment sources in river basins. Earth Sci. Rev. 125, 24–42. https://doi.org/10.1016/j.earscirev.2013.05.009.

Koiter, A.J., Owens, P.N., Petticrew, E.L., Lobb, D.A., 2018. Assessment of particle size and organic matter correction factors in sediment source fingerprinting investigations: an example of two contrasting watersheds in Canada. Geoderma 325, 195–207. https://doi.org/10.1016/j.geoderma.2018.02.044.

Lana-Renault, N., Nadal-Romero, E., Serrano-Muela, M.P., Alvera, B., Sánchez-Navarrete, P., Sanjuan, Y., García-Ruiz, J.M., 2013. Comparative analysis of the response of various land covers to an exceptional rainfall event in the central Spanish Pyrenees, October 2012. Earth Surf. Process. Landf. 39, 581–592. https://doi.org/10.1002/esp.3465.

Lasanta, T., Nadal-Romero, E., Errea, P., Arnáez, J., 2016. The effect of landscape conservation measures in changing landscape patterns: a case study in Mediterranean Mountains. Land Degrad. Develop. 27, 373–386. https://doi.org/10.1002/ldr.2359.

Lecce, S.A., 2013. Stream power, channel change, and channel geometry in the Blue River, Wisconsin. Phys. Geogr. 34, 293–314. https://doi.org/10.1080/02723646.2013.847311.

Li, M., Yao, W., Ding, W., Yang, J., Chen, J., 2009. Effect of grass coverage on sediment yield in the hillslope-gully side erosion system. J. Geogr. Sci. 19, 321–330. https://doi.org/10.1007/s11442-009-0321-8.

Lizaga, I., Quijano, L., Palazón, L., Gaspar, L., Navas, A., 2017. Enhancing connectivity index to assess the effects of land Use changes in a Mediterranean catchment. Land Degrad. Develop., 663–675 https://doi.org/10.1002/ldr.2676.

Lizaga, I., Quijano, L., Gaspar, L., Navas, A., 2018a. Estimating soil redistribution patterns with ^{137}Cs Measurements in a Mediterranean mountain catchment affected by land abandonment. Land Degrad Develop 105–117. https://doi.org/10.1002/ldr.2843.

Lizaga, I., Latorre, B., Gaspar, L., Navas, A., 2018b. FingerPro: an R Package for Sediment Source Tracing. https://CRAN.R-project.org/package=fingerPro https://doi.org/10.5281/zenodo.1402029.

Lizaga, I., Quijano, L., Gaspar, L., Ramos, M.C., Navas, A., 2019. Linking land use changes to variation in soil properties in a Mediterranean mountain agroecosystem. Catena 172, 516–527. https://doi.org/10.1016/j.catena.2018.09.019.

Llena, M., Vericat, D., Cavalli, M., Crema, S., Smith, M.W., 2019. The effects of land use and topographic changes on sediment connectivity in mountain catchments. Sci. Total Environ. 660, 899–912. https://doi.org/10.1016/j.scitotenv.2018.12.479.

López-Tarazón, J.A., Batalla, R.J., Vericat, D., Francke, T., 2009. Suspended sediment transport in a highly erodible catchment: the River Isábena (Southern Pyrenees). Geomorphology 109, 210–221. https://doi.org/10.1016/j.geomorph.2009.03.003.

Mabit, L., Bernard, C., Laverdiere, M.R., 2002. Quantification of Soil Redistribution and Sediment Budget in a Canadian Watershed from Fallout Caesium-137 (^{137}Cs) Data (Canadian journal of soil science).

Mariani, L., Parisi, S.G., 2014. Exceptional Rainfalls in the Mediterranean Area, in: Storminess and Environmental Change. Advances in Natural and Technological Hazards Research. Springer, Dordrecht, pp. 17–37 https://doi.org/10.1007/978-94-007-7948-8_2.

Martínez-Carreras, N., Krein, A., Udelhoven, T., Gallart, F., Iffly, J.F., Hoffmann, L., Pfister, L., Walling, D.E., 2010. A rapid spectral-reflectance-based fingerprinting approach for documenting suspended sediment sources during storm runoff events. J. Soils Sediments 10, 400–413. https://doi.org/10.1007/s11368-009-0162-1.

Martins, A.A.A., Madeira, M.V., Refega, A.A.G., 1995. Influence of rainfall on properties of soils developed on granite in Portugal. Arid Soil Res. Rehabil. 9, 353–366. https://doi.org/10.1080/15324989509385904.

Masselink, R.H., Temme, A.J. a. M., Giménez Díaz, R., Casalí Sarasíbar, J., Keesstra, S.D., 2017. Assessing hillslope-channel connectivity in an agricultural catchment using rare-earth oxide tracers and random forests models. 10.18172/cig.3169

Meusburger, K., Porto, P., Mabit, L., La Spada, C., Arata, L., Alewell, C., 2018. Excess lead-210 and plutonium-239+240: two suitable radiogenic soil erosion tracers for mountain grassland sites. Environ. Res. 160, 195–202. https://doi.org/10.1016/j.envres.2017.09.020.

Mitchell, A.W., Bramley, R.G.V., Johnson, A.K.L., 1997. Export of nutrients and suspended sediment during a cyclone-mediated flood event in the Herbert River catchment. Australia. Mar. Freshwater Res. 48, 79–88. https://doi.org/10.1071/mf96021.

Moore, J.W., Semmens, B.X., 2008. Incorporating uncertainty and prior information into stable isotope mixing models. Ecol. Lett. 11, 470–480. https://doi.org/10.1111/j.1461-0248.2008.01163.x.

Nadal-Romero, E., Martínez, T.L., González-Hidalgo, J.C., de Luis, M., García-Ruiz, J.M., 2013. The effect of intense rainstorm events on the suspended sediment response under various land uses: the Aísa Valley experimental station. Cuadernos de Investigación Geográfica 38, 27–47. https://doi.org/10.18172/cig.1274.

Nadal-Romero, E., Khorchani, M., Lasanta, T., García-Ruiz, J.M., 2019. Runoff and solute outputs under different land uses: long-term results from a Mediterranean mountain experimental station. Water 11, 976. https://doi.org/10.3390/w11050976.

Navas, A., Valero-Garcés, B.L., Machín, J., 2004. An approach to integrated assessement of reservoir siltation: the Joaquín Costa reservoir as case study. Hydrol. Earth Syst. Sci. 8 (6), 1193–1199. https://doi.org/10.5194/hess-8-1193-2004.

Navas, A., Machín, J., Soto, J., 2005. Assessing soil erosion in a Pyrenean mountain catchment using GIS and fallout ^{137}Cs. Agric. Ecosyst. Environ. 105, 493–506 https://doi.org/10.1016/j.agee.2004.07.005.

Navas, A., Machín, J., Beguería, S., López-Vicente, M., Gaspar, L., 2008. Soil properties and physiographic factors controlling the natural vegetation re-growth in a disturbed catchment of the Central Spanish Pyrenees. Agrofor. Syst. 72 (3), 173–185. https://doi.org/10.1007/s10457-007-9085-2.

Navas, A., Valero-Garcés, B.L., Gaspar, L., Machín, J., 2009. Reconstructing the history of sediment accumulation in the Yesa reservoir: an approach for management of mountain reservoirs. Lake and Reservoir Management 25 (1), 15–27 https://doi.org/10.1080/07438140802714304.

Navas, A., López-Vicente, M., Gaspar, L., Machín, J., 2013. Assessing soil redistribution in a complex karst catchment using fallout ^{137}Cs and GIS. Geomorphologys. 196, 231–241. https://doi.org/10.1016/j.geomorph.2012.03.018.

Navas, A., López-Vicente, M., Gaspar, L., Palazón, L., Quijano, L., 2014. Establishing a tracer-based sediment budget to preserve wetlands in Mediterranean mountain agroecosystems (NE Spain). Sci. Total Environ. 496, 132–143. https://doi.org/10.1016/j.scitotenv.2014.07.026.

Navas, A., Quine, T.A., Walling, D.E., Gaspar, L., Quijano, L., Lizaga, I., 2017. Relating intensity of soil redistribution to land use changes in abandoned Pyrenean fields using fallout caesium-137. Land Degrad. Develop. 28, 2017–2029. https://doi.org/10.1002/ldr.2724.

Navas, A., Serrano, E., López-Martínez, J., Gaspar, L., Lizaga, I., 2018. Interpreting environmental changes from radionuclides and soil characteristics in different landform contexts of Elephant Island (Maritime Antarctica). Land Degrad. Dev. 29, 3141–3158. https://doi.org/10.1002/ldr.2987.

Owens, P.N., Blake, W.H., Gaspar, L., Gateuille, D., Koiter, A.J., Lobb, D.A., Petticrew, E.L., Reiffarth, D.G., Smith, H.G., Woodward, J.C., 2016. Fingerprinting and tracing the sources of soils and sediments: Earth and ocean science, geoarchaeological, forensic, and human health applications. Earth Sci. Rev. 162, 1–23. https://doi.org/10.1016/j.earscirev.2016.08.012.

Palazón, L., Gaspar, L., Latorre, B., Blake, W.H., Navas, A., 2015a. Identifying sediment sources by applying a fingerprinting mixing model in a Pyrenean drainage catchment. J. Soils Sediments 15, 2067–2085. https://doi.org/10.1007/s11368-015-1175-6.

Palazón, L., Latorre, B., Gaspar, L., Blake, W.H., Smith, H.G., Navas, A., 2015b. Comparing catchment sediment fingerprinting procedures using an auto-evaluation approach with virtual sample mixtures. Sci. Total Environ. 532, 456–466. https://doi.org/10.1016/j.scitotenv.2015.05.003.

Palazón, L., Latorre, B., Leticia Gaspar, G., Blake, W.H., Smith, H.G., Navas, A., 2016. Combining catchment modelling and sediment fingerprinting to assess sediment dynamics in a Spanish Pyrenean river system. Sci. Total Environ. 569–570, 1136–1148. https://doi.org/10.1016/j.scitotenv.2016.06.189.

Phillips, D.L., Gregg, J.W., 2003. Source partitioning using stable isotopes: coping with too many sources. Oecologia 136, 261–269. https://doi.org/10.1007/s00442-003-1218-3.

Pimentel, D., 2006. Soil erosion: a food and environmental threat. Environ. Dev. Sustain. 8, 119–137. https://doi.org/10.1007/s10668-005-1262-8.

Porto, P., Walling, D.E., Ferro, V., di Stefano, C., 2003. Validating erosion rate estimates provided by caesium-137 measurements for two small forested catchments in Calabria, southern Italy. Land Degrad. Dev. 14, 389–408. https://doi.org/10.1002/ldr.561.

Pulley, S., Collins, A.L., 2018. Tracing catchment fine sediment sources using the new SIFT (SedIment Fingerprinting Tool) open source software. Sci. Total Environ. 635, 838–858. https://doi.org/10.1016/j.scitotenv.2018.04.126.

Pulley, S., Foster, I., Antunes, P., 2015. The uncertainties associated with sediment fingerprinting suspended and recently deposited fluvial sediment in the Nene river basin. Geomorphology 228, 303–319.

Quesada, S., Tena, A., Guillén, D., Ginebreda, A., Vericat, D., Martínez, E., Navarro-Ortega, A., Batalla, R.J., Barceló, D., 2014. Dynamics of suspended sediment borne persistent organic pollutants in a large regulated Mediterranean river (Ebro, NE Spain). Sci. Total Environ. 473–474, 381–390. https://doi.org/10.1016/j.scitotenv.2013.11.040.

Quijano, L., Gaspar, L., Navas, A., 2016a. Spatial patterns of SOC, SON, ^{137}Cs and soil properties as affected by redistribution processes in a Mediterranean cultivated field (Central Ebro Basin). Soil Tillage Res. 155, 318–328. https://doi.org/10.1016/j.still.2015.09.007.

Quijano, L., Beguería, S., Gaspar, L., Navas, A., 2016b. Estimating erosion rates using ^{137}Cs measurements and WATEM/SEDEM in a Mediterranean cultivated field. CATENA 138, 38–51. https://doi.org/10.1016/j.catena.2015.11.009.

Quiquerez, A., Brenot, J., Garcia, J.-P., Petit, C., 2008. Soil degradation caused by a high-intensity rainfall event: Implications for medium-term soil sustainability in Burgundian vineyards. CATENA 73, 89–97. https://doi.org/10.1016/j.catena.2007.09.007.

Renard, K.G., Yoder, D.C., Lightle, D.T., Dabney, S.M., 2011. Universal soil loss equation and revised universal soil loss equation, in: Handbook of Erosion Modelling. Wiley-Blackwell, pp. 135–167. doi:https://doi.org/10.1002/9781444328455.ch8.

Romanyà, J., Rovira, P., 2011. An appraisal of soil organic C content in Mediterranean agricultural soils. Soil Use Manag. 27, 321–332. https://doi.org/10.1111/j.1475-2743.2011.00346.x.

Schuller, P., Walling, D.E., Iroumé, A., Quilodrán, C., Castillo, A., Navas, A., 2013. Using ^{137}Cs and ^{210}Pb$_{ex}$ and other sediment source fingerprints to document suspended sediment sources in small forested catchments in south-Central Chile. Journal of Environmental Radiactivity 124, 147–159. https://doi.org/10.1016/j.jenvrad.2013.05.002.

Serrano-Muela, M.P., Nadal-Romero, E., Lana-Renault, N., González-Hidalgo, J.C., López-Moreno, J.I., Beguería, S., Sanjuan, Y., García-Ruiz, J.M., 2015. An exceptional rainfall event in the central western Pyrenees: spatial patterns in discharge and impact. Land Degrad. Dev. 26, 249–262.

Serrano-Notivoli, R., Mora, D., Ollero, A., Sánchez-Fabre, M., Sanz, P., Saz, M.Á., 2017. Floodplain occupation and flooding in the Central Pyrenees. Cuadernos de Investigación Geográfica 43, 309–328. https://doi.org/10.18172/cig.3057.

Shang, Z.H., Cao, J.J., Degen, A.A., Zhang, D.W., Long, R.J., 2019. A four year study in a desert land area on the effect of irrigated, cultivated land and abandoned cropland on soil biological, chemical and physical properties. CATENA 175, 1–8. https://doi.org/10.1016/j.catena.2018.12.002.

Smith, H.G., Blake, W.H., 2014. Sediment fingerprinting in agricultural catchments: A critical re-examination of source discrimination and data corrections. Geomorphology 204, 177–191. https://doi.org/10.1016/j.geomorph.2013.08.003.

Smith, L.C., Olyphant, G.A., 1994. Within-storm variations in runoff and sediment export from a rapidly eroding coal-refuse deposit. Earth Surf. Process. Landf. 19, 369–375. https://doi.org/10.1002/esp.3290190407.

Upadhayay, H.R., Smith, H.G., Griepentrog, M., Bodé, S., Bajracharya, R.M., Blake, W., Cornelis, W., Boeckx, P., 2018. Community managed forests dominate the catchment sediment cascade in the mid-hills of Nepal: A compound-specific stable isotope analysis. Sci. Total Environ. 637–638, 306–317. https://doi.org/10.1016/j.scitotenv.2018.04.394.

Verheijen, F.G.A., Jones, R.J.A., Rickson, R.J., Smith, C.J., 2009. Tolerable versus actual soil erosion rates in Europe. Earth Sci. Rev. 94, 23–38. https://doi.org/10.1016/j.earscirev.2009.02.003.

Walling, D.E., 2005. Tracing suspended sediment sources in catchments and river systems. Sci. Total Environ. 344, 159–184. https://doi.org/10.1016/j.scitotenv.2005.02.011.

Walling, D.E., Collins, A.L., 2008. The catchment sediment budget as a management tool. Environmental Science & Policy, Monitoring and modelling diffuse pollution from agriculture for policy support: UK and European experience. 11, 136–143. https://doi.org/10.1016/j.envsci.2007.10.004.

Walling, D.E., Woodward, J.C., 1995. Tracing sources of suspended sediment in river basins: a case study of the River Culm, Devon, UK. Mar. Freshw. Res. 46, 327–336.

Walling, D.E., Peart, M.R., Oldfield, F., Thompson, R., 1979. Suspended sediment sources identified by magnetic measurements. Nature 281, 281110a0. doi:https://doi.org/10.1038/281110a0.

White, S., García-Ruiz, J.M., Martí, C., Valero, B., Errea, M.P., Gómez-Villar, A., 1997. The 1996 Biescas campsite disaster in the Central Spanish Pyrenees, and its temporal and spatial context. Hydrol. Process. 11, 1797–1812. https://doi.org/10.1002/(SICI)1099-1085(199711)11:14<1797::AID-HYP605>3.0.CO;2-7.

Winston, W.E., Criss, R.E., 2002. Geochemical variations during flash flooding, Meramec River basin, May 2000. J. Hydrol. 265, 149–163. https://doi.org/10.1016/S0022-1694(02)00105-1.

Wynants, M., Solomon, H., Ndakidemi, P., Blake, W.H., 2018. Pinpointing areas of increased soil erosion risk following land cover change in the Lake Manyara catchment, Tanzania. Int. J. Appl. Earth Obs. Geoinf. 71, 1–8. https://doi.org/10.1016/j.jag.2018.05.008.

Yu, L., Oldfield, F., 1989. A multivariate mixing model for identifying sediment source from magnetic measurements. Quat. Res. 32, 168–181. https://doi.org/10.1016/0033-5894(89)90073-2.

Zhang, J., Yang, M., Zhang, F., Zhang, W., Zhao, T., Li, Y., 2017. Fingerprinting sediment sources after an exceptional rainstorm event in a small catchment on the Loess Plateau, PR China. Land Degrad. Dev. 28, 2527–2539. https://doi.org/10.1002/ldr.2803.

CHAPTER 8

Consensus ranking as a method to identify non-conservative and dissenting tracers in fingerprinting studies

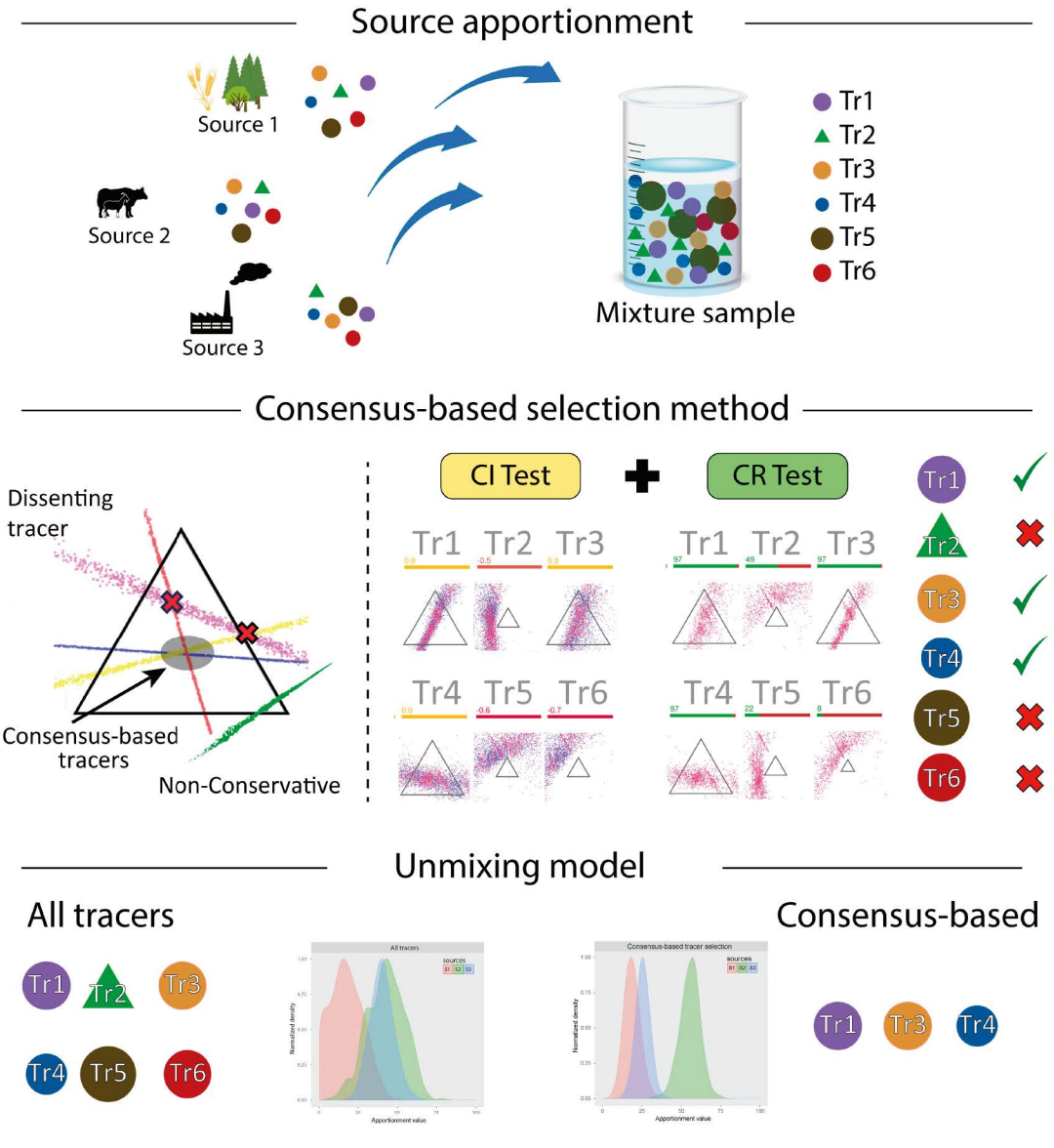

Science of the Total Environment 720 (2020) 137537

Contents lists available at ScienceDirect

Science of the Total Environment

journal homepage: www.elsevier.com/locate/scitotenv

Consensus ranking as a method to identify non-conservative and dissenting tracers in fingerprinting studies

Ivan Lizaga *, Borja Latorre, Leticia Gaspar, Ana Navas *

Estación Experimental de Aula-Dei (EEAD-CSIC), Spanish National Research Council, Avenida Montañana, 1005, 50059 Zaragoza, Spain

HIGHLIGHTS

- A novel method is proposed for identifying non-conservative tracers.
- Predictions of each tracer are quantified by using the mixture information.
- A clustering method discriminates groups of similar tracers.
- A consensus ranking identifies non-conservative and dissenting tracers.
- Inclusion of tracers with dissenting information produces inconsistent results.

GRAPHICAL ABSTRACT

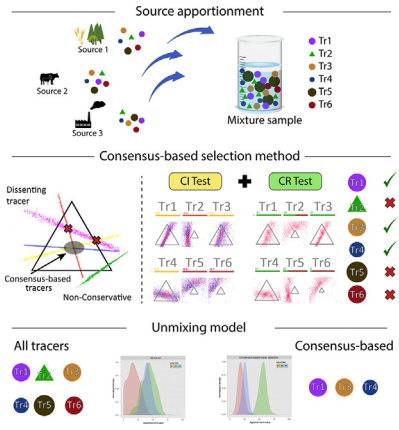

ARTICLE INFO

Article history:
Received 12 November 2019
Received in revised form 21 February 2020
Accepted 23 February 2020
Available online 24 February 2020

Editor: Christian Herrera

Keywords:
Sediment fingerprinting
Tracer selection
Consensus ranking
Artificial mixture
Conservativeness index

ABSTRACT

Soil erosion and fine particle transport are two of the major challenges in food security and water quality for the growing global population. Information of the areas prone to erosion is needed to prevent the release of pollutants and the loss of nutrients. Sediment fingerprinting is becoming a widely used tool to tackle this problem, allowing to identify the sources of sediments in a catchment. Methods in fingerprinting techniques are still under discussion with tracer selection at the centre of the debate.

We propose a novel method, termed as consensus ranking (CR), that combines the predictions of single-tracer models to identify non-conservative tracers. In this context, a numerical procedure to quantify the predictions of individual tracers is first delivered. The scoring function to rank the tracers is based on several random debates between tracers in which the tracer that prevents consensus is discarded. Based on these results, a conservativeness index (CI) is presented along with a clustering method to identify groups of similar tracers.

To illustrate the CI and CR procedures, an artificial mixture created with real soil to independently test the method is analysed. The results demonstrate the capability of our method to identify non-conservative tracers beyond the capability of currently used selection methods. Further, a real sediment sample from a Mediterranean mountain catchment is evaluated to emphasise its utility in complex natural environments. To test the utility of our method, it was decided to include the conservative and consensus-enforcing tracers extracted by this new approach with two different unmixing models. Furthermore, CR and CI procedures are displayed together with

* Corresponding authors.
E-mail addresses: ilizaga@eead.csic.es, lizaga.ivan10@gmail.com (I. Lizaga), anavas@eead.csic.es (A. Navas).

https://doi.org/10.1016/j.scitotenv.2020.137537
0048-9697/© 2020 Elsevier B.V. All rights reserved.

the most widespread statistical tests and the within-a-polygon approach used for tracer selection in fingerprinting studies. The new proposed method will enable the research community to homogenise results for replicability as well as allowing comparisons among study areas.

© 2020 Elsevier B.V. All rights reserved.

1. Introduction

Soil erosion increases fine sediment and pollutant transport into river ecosystems (Owens et al., 2005). Tracking the sources of sediment and its associated contaminants is a vital step towards mitigation (Walling and Collins, 2008; Quesada et al., 2014). It is necessary to identify the areas most vulnerable to soil erosion in order to preserve soil nutrients and land as vital resources (Quijano et al., 2016; Lloyd et al., 2019). Reliable information on sediment provenance is needed to preserve water quality and to safeguard water resources to the lowlands (Navas et al., 2009).

To evaluate this problem, several tools have been developed to quantify the effects of different erosion mechanisms, such as connectivity (Lizaga et al., 2018a; Llena et al., 2019), spatiotemporal dynamics (Rovira et al., 2012; Wynants et al., 2020) and wind erosion (Schmidt et al., 2017; Zhang et al., 2018). However, the determination of sediment provenance in catchments using traditional monitoring techniques is frequently expensive. Thus, some preliminary work was carried out in the early 1980s showed fingerprinting techniques as key to addressing this problem (Klages and Hsieh, 1975). The procedure identifies sediment provenance and estimates the relative contribution of each potential source, using a variety of selected tracer properties.

Initial fingerprinting studies were performed based on a single tracer (Walling et al., 1979). However, the inclusion of quantitative mixing models enabled researchers to discriminate more than two sources with the subsequent increase in the number of tracers (Walling et al., 1993; Zhang and Liu, 2016). The contribution of each source is estimated using a linear multivariate mixing model. Nowadays, numerous studies use fingerprinting techniques to examine specific catchment management problems (Palazón et al., 2015; Schuller et al., 2013), to evaluate processes (Laceby et al., 2019) and contamination in the river and coastal waters (McCarthy et al., 2017; Evrard et al., 2019). In recent years, there has been a growing interest in this technique, and for this reason, different approaches have appeared. The differences of these proposals are mainly on three features: (a) different fingerprinting models (e.g. SourceTracker, MixSIAR, FingerPro); (b) the use of correction factors (Koiter et al., 2018); and (c) tracer selection methodologies, as can be seen in different reviews (Collins et al., 2017; Owens et al., 2016; Smith and Blake, 2014). The concern about tracer selection methodologies, including different statistical methods, has been discussed by several authors (Pulley et al., 2015; Palazón et al., 2015).

Tracer selection methods rely on the information of the sources to determine the tracer's ability to differentiate sediment sources. The most widespread methodology consisted of an initial mass conservation test, usually termed as range test (RT), followed by the two-step statistical procedure proposed by Collins and Walling (2002) that uses the Kruskal–Wallis (KW) and discriminant function analysis (DFA) tests. This procedure tests the ability of individual tracers to differentiate between sources and identifies the best combination of tracers that provides the maximum discrimination of the source classes. The main limitation of this widely used two-step statistical procedure is that it does not incorporate the information of the sediment mixtures in the analysis. Phillips and Gregg (2003) established that in a linear mixing model, the mixture sample must be within a polygon bounding the signatures of the sources as a requirement of conservativeness. More recently, following this hypothesis, Smith et al. (2013) created an R code to assess the geometry of the mixing space and to ensure that the mixture samples fit inside the sources. If a mixture sample is outside this polygon, then no physical solution exists for that mixture as one or more tracers are non-conservative. In this context, some researchers have implemented the biplot test that displays the mixture samples versus two tracers as a more restrictive condition than the traditional range test (Lizaga et al., 2019; Pulley et al., 2015).

Despite the interest of tracer selection in fingerprinting studies, to the best of our knowledge no one has studied the information provided by individual tracers in an unmixing context. Within this framework, we propose a new methodology to identify non-conservative tracers and select those with conservative and coherent information. Thus, we developed, in R code, a tool that shows the individual nature of each tracer, taking into account the information of the mixture. This study aims to independently validate the methodology using an artificial mixture created with real soils and mixed in the laboratory. These types of samples were specifically chosen to test the method and to avoid non-geochemical sense data which increases its validity compared to virtual samples or virtually altered samples. In this research, we aim to validate the new tool by using an artificial sample and show its utility in a real study case.

In order to investigate and select the best tracers for each fingerprinting study, we propose a novel ensemble technique, termed as consensus method, which combines the predictions of single-tracer models to identify non-conservative and dissenting tracers. Based on these results, a conservativeness index (CI) is presented along with a clustering method to identify groups of tracers with similar information and to analyse their correlations. Besides, a scoring function based on several random debates between tracers, in which the tracer that prevents consensus is discarded, was implemented as a decision support ranking (CR). This novel method highlights the importance of selecting the right tracers for each individual mixture and avoids the inclusion of tracers out of consensus or with non-conservative behaviour by using both the CR and CI procedures.

2. Methods

To illustrate the procedure of detecting non-conservative and dissenting tracers, two different datasets were selected. One dataset is composed of an artificial mixture created in the lab with real soils from three sources that included the following elements: Ba, Nb, Zr, Sr, Rb, Pb, Zn, Fe, Mn, Cr, V, Ti, Ca, K, Al, Si, and Mg. This dataset was extracted from Gaspar et al. (2019). The second dataset is a real example from a study case in a Mediterranean catchment that was chosen to emphasise the potential of our method for application in complex natural environments. The study case is composed of three sources. In addition, to the mentioned stable elements, gamma-emitting radionuclides, ^{137}Cs, ^{226}Ra, ^{238}U, ^{232}Th and ^{40}K and low frequency magnetic susceptibility (χLF) were also included as additional tracers. The results obtained were used to validate the method and visualise its utility.

2.1. Single-tracer model

In fingerprinting studies, measured tracer values of the sediment mixtures are usually compared to those of the sources in order to identify robust tracers that can discriminate the potential sediment sources. However, only a few of these tracers exist, requiring the inclusion of additional tracers in a composite fingerprint of poor discriminators (Pulley et al., 2017). Under this scenario, it is essential to quantify the specific information of each tracer in order to understand its contribution to the final prediction and to assist the selection of relevant tracers.

Standard linear mixing models require n tracers to determine the contributions of $n + 1$ sources to the mixture (Phillips and Gregg, 2003). For example, with three potential sources and two tracers, the following system of mass balance equations can be solved to obtain the contribution of each source to the mixture:

$$AX = B$$
$$A = (a_{11}\, a_{12} a_{13} a_{21} a_{22} a_{23} 111), X = (x_1\, x_2 x_3), B = (b_1\, b_2 1)\, B \quad (1)$$
$$X = A^{-1}$$

where A contains the tracer values of each source, X represents the unknown source contributions, and B contains tracer values of the sediment mixture. The last equation of this system constrains the contributions to sum to one, requiring only two tracers to solve three potential sources.

In order to quantify the predictions of each individual tracer, we propose to use the determined mass balance equations and fabricate the remaining required tracers using two different procedures. The first method consists in designing random virtual tracers (RVT). For each tracer, a random number in the range (0,1) is assigned to each source. Then, another random number is assigned to the mixture between the minimum and the maximum values obtained in the previous step. Considering the example of three potential sources and two tracers, only one additional tracer must be fabricated:

$$\begin{cases} a_{21} = random(0,1)\ a_{22} = random(0,1)\ a_{23} = random(0,1) \\ b_2 = random(\ \min(a_{21}, a_{22}, a_{23}),\ \max(a_{21}, a_{22}, a_{23})) \end{cases} \quad (2)$$

The virtual tracer is then incorporated in Eq. (1) to solve the system of equations and obtain the contribution of each source. This procedure is repeated several times, resulting in a set of solutions or density distribution that contains all the possible predictions of the considered individual tracer.

In the second method, the required tracers are randomly chosen (RCT) from the remaining ones. This technique is indicated when a high number of tracers are measured. The set of solutions obtained in this case is a subset of that obtained with random virtual tracers, resulting in all the possible predictions of each tracer in the context defined by the experimental dataset. The propagation of errors in this framework is assessed using a simple Monte Carlo iterative technique (Sherriff et al., 2015) to quantify the effect of the dispersion of the sources and the mixture on the predictions of each individual tracer.

The results from the single-tracer model can be used to define a conservativeness index (CI). The set of possible predictions from each tracer is sorted according to the Euclidian distance to the perfectly balanced mix where all contributions are equal:

$$d_i = \sqrt{\sum_{j=1}^{3} \left(w_{i,j} - \frac{1}{3}\right)^2} \quad (3)$$

A percentile of the sorted solutions is chosen to compute the CI as the root mean square error (RMSE) of the non-conservative part (nc) of the apportionments from the selected solution:

$$CI = -\sqrt{\sum_{j=1}^{3} (nc(w_{i,j}))^2}, nc(x) = \begin{cases} -x, \text{if } x<0 \\ 0, \text{if } 0\le x\le 1 \\ x-1, \text{if } x>1 \end{cases} \quad (4)$$

2.2. Tracer clustering

The classification of tracers into groups requires a method for computing the dissimilarity between each pair of tracers. The results obtained by the single-tracer models are used for this purpose. This technique provides a set of solutions derived from the experimental tracer data and a series of random numbers, which are used to fabricate virtual tracers or to randomly select from the remaining tracers in the experimental database. If the same random series is used in the different models, similar tracers will show similar predictions while distant tracers will present inconsistent responses.

Correlation-based distance considers two tracers to be similar if their predictions are highly correlated, even though the values may be far apart. For this reason, the dissimilarity between each pair of tracers was computed by the Euclidean distance between the two series of predictions. The results of each pair of tracers are gathered in a distance matrix that is square, nonnegative and symmetric. We use a widely used hierarchical clustering method T based on the Ward algorithm (Murtagh and Legendre, 2014) to group the tracers.

2.3. Consensus ranking

Feature ranking is a flexible selection process commonly used in machine learning for classification problems when a large number of attributes are present in the dataset (Hong et al., 2008). This technique orders the features by the value of some scoring function to identify uninformative or redundant features which can be removed to increase the accuracy of the model. Supervised models perform this task using a curated training dataset while unsupervised models try to discover patterns in the data without guidance using self-organisation (Solorio-Fernández et al., 2019).

Several approaches can be proposed to calculate the relevance of the tracers. In this study, we focus on consensus or agreement as a criterion to identify non-conservative tracers. Consensus models have been used in Group Decision Making (GDM) to select from different opinions of a group of people, frequently referred to as experts (Herrera-Viedma et al., 2014). Consensus reaching processes proceed in a convergent multistage way, where experts present their opinions and they discuss and negotiate to bring positions closer by modifying their initial opinions (Pérez et al., 2018). Exclusion of dissenting experts, focusing the attention where agreement is most likely, is also contemplated.

Consensus ranking (CR) is implemented combining the predictions of single-tracer models in several random debates. Debate is a technique used in Group Decision Making methods to obtain a better knowledge about experts' preferences. Experts debate and share their ideas in order to reach a common conclusion. The consensus represents a quantitative measurement of the expert agreement on the final decision (Morente-Molinera et al., 2019). In each debate, a random subset of the tracers is selected. Its number corresponds to the minimum number of equations to overdetermine the system plus one. For example, with three potential sources four random tracers are needed. In each debate, several rounds are held excluding one tracer at a time. The consensus of each round is measured through the mathematical compatibility of the resulting system of equations. The tracer whose exclusion produces a higher consensus is marked as dissenting. Repeating this process through several debates, each tracer obtains a number of participations and a number of lost debates. The consensus is simply defined as the ratio of these two numbers with possible outcomes between 0 and 100. A low consensus indicates that a tracer is often in conflict with the opinion of other groups while a high consensus represents a frequent agreement with the group.

$$consensus = 100\left(1 - \frac{lost\ debates}{total\ debates}\right) \quad (5)$$

Each debate results in an overdetermined system similar to Eq. (1) but with an additional equation.

$$AX = B + \epsilon$$

$$A = (a_{11}\, a_{12} a_{13} a_{21} a_{22} a_{23} a_{31} a_{32} a_{33} 111), X = (x_1\, x_2 x_3), B = (b_1\, b_2 b_3 1), \epsilon = (\varepsilon_1\, \varepsilon_2 \varepsilon_3 \varepsilon_4) \quad (6)$$

Its solution is approximated using a least squares method that minimises the sum of the squared errors (Sherriff et al., 2015), represented as ϵ in the previous equation. The consensus of each debate is measured using the RMSE of the mass balance equations.

$$RMSE = \sqrt{\sum_{i=1}^{3} \left(\sum_{j=1}^{3} a_{ij} x_j - b_i \right)^2} \quad (7)$$

3. Results

3.1. Single-tracer model

To quantify the predictions from individual tracers, our method incorporates the mixture information in the analysis. This knowledge may be used to predict the role of each tracer in the unmixing model and to understand how different tracers are grouped. The single-tracer model was applied to the two above described datasets.

To illustrate the results, ternary diagrams were created representing all the possible predictions from each tracer for the selected mixture. The results of the artificial mixture and the real sample are presented in Figs. 1 and 2, respectively. The contribution of a source is 100% in the corresponding triangle vertex and 0% at the opposite side. Thus, each side of the triangle corresponds to a binary composition of the mixture. Moreover, a line parallel to a side of the triangle represents mixtures with constant composition in the source situated in the opposite vertex (see legend in Fig. 2). The results of the single-tracer model with random virtual tracers (RVT) are represented with blue points, and the solutions of randomly chosen tracers (RCT) are superimposed using red points. The point clouds presented in Figs. 1 and 2 confirm that RCT solutions are a subset of the RVT results. Visual inspection of Fig. 1 indicates that among others Sr or Cr discriminate Source 1, while Ba or K discern Source 2 and Zn or Mg differentiate Source 3. Other tracers, such as V, Al or Si, are not parallel to a side of the triangle and require a more complex interpretation. Most of the tracers of Fig. 1 present line patterns and some of them are narrow (Sr, K) while others are wider (Ba or Cr). The single-tracer model quantifies the effect of (a) the dispersion of the corresponding tracer in the sources; (b) the distance of the average value of the sources, and (c) the relative position of the tracer in the mixture. The results of the real sample present higher dispersion than those of the artificial mixture but linear patterns are also visible, like for instance Cr discriminates Source 1, P differentiates Source 2, and ^{137}Cs discriminates Source 3 (Fig. 2).

The conservativeness of a tracer can also be reported from the ternary diagrams, counting how many solutions fall within the triangle or, otherwise, how distant are these solutions from its centre. This property has been quantified using the proposed conservativeness index (CI) and visually assigned using a colour scale, red and black representing the less conservative tracers and yellow representing the most conservative ones. A percentile of 25% has been selected in this study so a negative CI means that at least the 75% of the solutions from the single-tracer model present non-conservative apportionments. All tracers corresponding to the artificial mixture are conservative (yellow bars) and are presented in no particular order (Fig. 1). However, tracers corresponding to the real sample exhibit a different behaviour (Fig. 2). Some of them are conservative (yellow bars) while others perform within the limit (orange bars) and the rest remain clearly non-conservative (red and black bars).

Fingerprinting studies usually mention the minimum number of tracers needed to apply an unmixing model (Eq. (1)). This argument is based on the mathematical nature of the model, requiring a minimum number of independent equations to be solved. Ternary diagrams provide a visual reference of the consistency of the tracers. The intersection of their point clouds represents the solution of the corresponding system of equations. In the case of three sources, two independent tracers are needed with non-parallel lines in the ternary diagrams. This argument promotes the use of tracers with a small intersection area regardless of their individual ability to discriminate one of the sources. For instance, Rb and S from Fig. 1, could be perfectly used to unmix the artificial sample, even though its line patterns are not parallel to a side of the triangle.

The theoretical contributions of the artificial mixture are represented in Fig. 1 using a black circle. Some tracers cross this point while others remain distant. This fact illustrates that the information transmitted by some tracers, as Al or Si, may be erroneous. The causes of this deviation could be an insufficient description of the sources or the heterogeneity of the samples.

The existence of conservative tracers that could provide unreliable information, as can be seen in Fig. 1, is the evidence which motivates the consensus ranking as a necessary additional criterion. A common solution to overcome this problem is to include all available tracers in the model, expecting that errors are independent and will be cancelled. However, our approach consists in identifying and excluding the

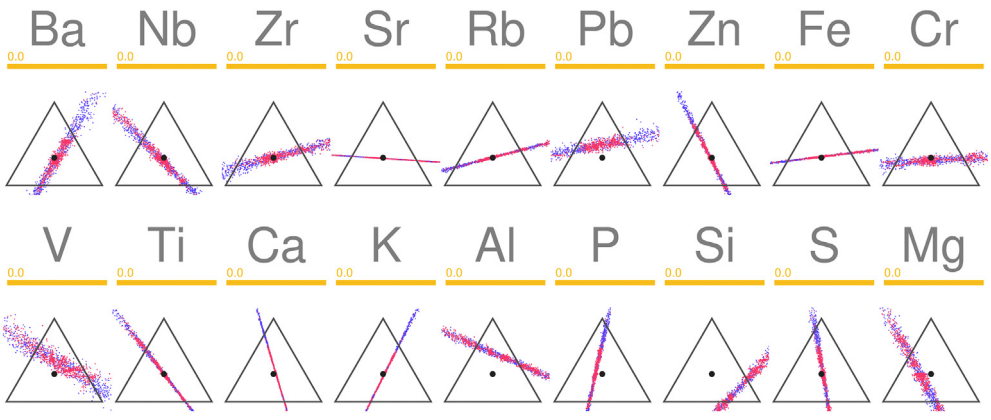

Fig. 1. Ternary diagrams of all the possible predictions from each tracer for the artificial mixture. Blue and red points represent the results of the single-tracer model with random virtual tracers (RVT) and with randomly chosen tracers (RCT), respectively. The black circle located in the centre of the triangle represents the theoretical contributions of the artificial mixture with equal contribution for each of the three sources. CI values of each tracer are also represented. (For interpretation of the references to colour in this figure legend, the reader is referred to the web version of this article.)

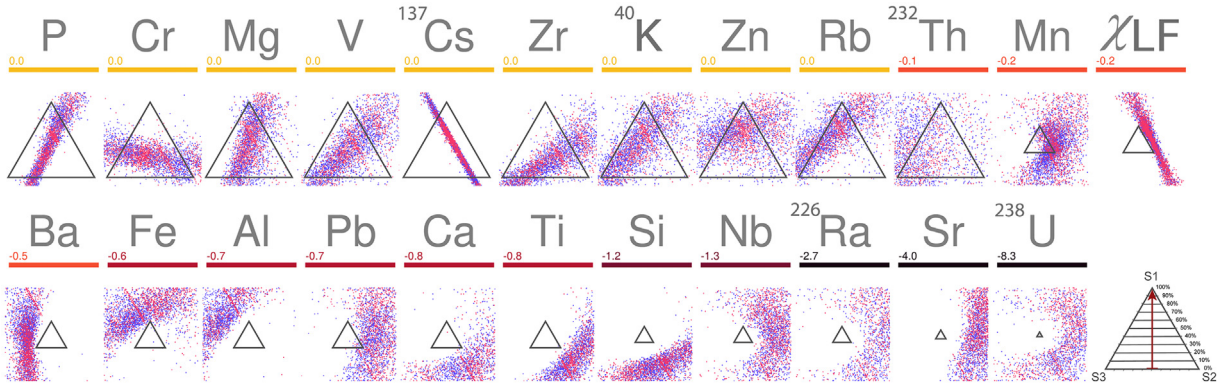

Fig. 2. Ternary diagrams of all the possible predictions from each tracer for the real mixture. Blue and red points represent the results of the single-tracer model with random virtual tracers (RVT) and with randomly chosen tracers (RCT), respectively. The tracers were ordered according to the CI values, represented numerically and by a colour scale. (For interpretation of the references to colour in this figure legend, the reader is referred to the web version of this article.)

erroneous tracers in order to include in the unmixing model only those that present a conservative and consistent behaviour.

3.2. Tracer clustering

The information provided from the single-tracer model can be used to identify groups of similar tracers. These relations can be observed in the ternary diagrams where, for instance, in Fig. 1, Sr and Fe or Zn and Ti are pairs of tracers that exhibit similar patterns.

The methodology presented in Section 2.2 was applied to the two described datasets, computing first a correlation-based distance using the RVT results and then implementing a classical hierarchical clustering method. Tracers have been ordered in Figs. 3 and 4 according to the cluster tree or dendrogram, also displayed in the figures under the ternary diagrams, in which the vertical axis represents the distance or dissimilarity between tracers.

The tracers from the artificial mixture (Fig. 3) are grouped in clusters mainly according to the source they discriminate. The blue branch of the dendrogram corresponds to tracers that differentiate Source 1, while the orange and yellow branches discriminate Source 2 and Source 3, respectively. The rest of the tracers are grouped in the green branch except Si that turns out to be isolated by its singular behaviour. Similar groups are found in the tracers from the real sample where only the conservative tracers have been represented (Fig. 4).

Tracer clustering is also related to the concept of mathematical consistency. Selecting tracers from the same branch will typically produce elongated intersections of the point clouds and high dispersion in the corresponding unmixing model.

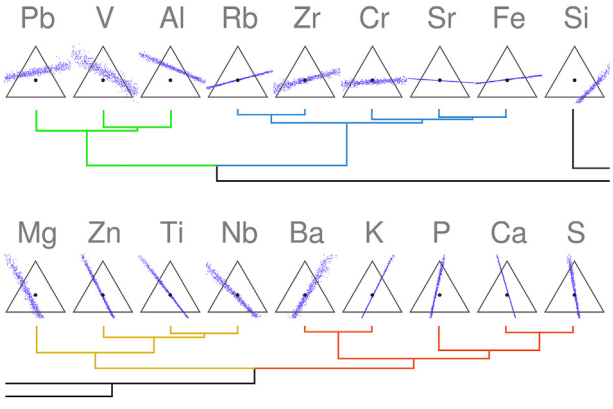

Fig. 3. Dendrogram plots of the ternary diagrams of the artificial sample grouped according to the source they discriminate.

3.3. Consensus ranking

The results presented in Section 3.1 indicate the existence of conservative tracers which transmit erroneous information. This statement is supported by the known theoretical contributions of the artificial mixture. Therefore, it is necessary to generalise this concept in order to study real samples where the contribution of the sources is unknown.

The notion of consensus can be illustrated with the following example. A ternary graph with the results of four tracers from the artificial mixture is presented in Fig. 5. All the tracers present line patterns and apparent conservative behaviour. However, only three of them (Sr, Rb and Ca) intersect on a small area while the fourth tracer, Al, has different intersections with each of the remaining tracers. In the case of three sources, only two tracers are needed to unmix the sample. Choosing the minimum number of required tracers from the first group of tracers will produce similar solutions while the inclusion of the fourth tracer will introduce inconsistent contribution values. The first group of tracers is compatible in the mathematical sense, or presents a general consensus on the possible solutions, while the fourth tracer is mathematically incompatible with the rest, or its specific information is out of consensus.

This example illustrates one of the random debates implemented in the consensus ranking computation in which the tracer whose exclusion produces a higher consensus is marked as dissenting. This suggests that including tracers with dissenting information does not add valuable information to the model and can lead to unpredictable results. Repeating these debates in random iterations assigns problematic tracers a low consensus rank in order to be identified as problematic and to avoid its inclusion in the unmixing model.

Consensus was calculated considering 5000 random debates per tracer for the two described datasets. Tracers are ordered in Figs. 6 and 7 according to the resulting scoring, and consensus values are also presented with horizontal bar graphs. Accompanying ternary graphs correspond to the single-tracer models using RCT, as this is the information that comes into play in the random debates.

Tracers from the artificial mixture (Fig. 6) present a high correlation between the rank and the accuracy of the line patterns. The proposed ranking is able to identify problematic tracers, that remain distant from the theoretical solution, and also to quantify differences in the variability and discrimination, visible in the thickness of the line patterns. It is important to note that these results can be considered a blind test, as the theoretical contribution of the artificial mixture is not provided during the calculus of the consensus.

When this methodology is applied to the real sample (Fig. 7), non-conservative tracers (from LF to Sr) and also tracers with high variability (^{232}Th, Mn) are assigned the lowest positions in the rank. Tracers with high consensus (^{137}Cs, Mg and P) present conservative behaviour,

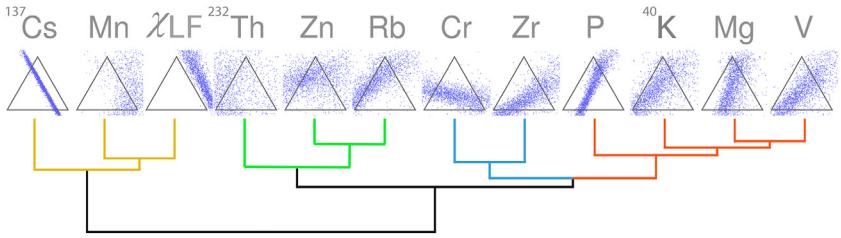

Fig. 4. Dendrogram plots of the ternary diagrams of the real sample grouped according to the source they discriminate.

lower variability and higher discrimination. In comparison with the results of the artificial mixtures (Fig. 6), conservative tracers of the real sample (Fig. 7) present higher consensus values in the horizontal bar graphs. As expected, the dissenting and non-conservative tracers that are not present in the artificial sample influence these results. This highlights the importance of the resulting ranking over the specific consensus values obtained in each dataset.

The consensus calculus for the real sample was repeated discarding non-conservative tracers (from LF to Sr) from the database, obtaining the exact same rank positions for the remaining tracers. This result indicates that the proposed CR is robust and can be applied to all available tracers with no prior filtering or screening.

With the completion of the previous steps and all the information extracted, we can select the tracers that follow the general consensus. To test the utility of the new method, it was decided to include the relevant tracers (from ^{137}Cs to Rb) of the real sample in two different unmixing models: FingerPro (Lizaga et al., 2018b) and MixSIAR (Stock and Semmens, 2016). Thus, the models were tested, including all the tracers that pass the range test that excludes the tracers of the sediment mixture outside the minimum and maximum values in the sediment sources. Then, RT model results are compared with those obtained for tracers selected with the CR method. As shown in Fig. 8, the unmixing results obtained after application of the CR method show more defined and accurate contributions. Furthermore, both FingerPro and MixSIAR models showed comparable results after the application of the CR method.

3.4. An improved tool for detecting non-conservative tracers

CI and CR represent an alternative to the conservativeness tests frequently used, such as the range test (RT) or the within-a-polygon (W-a-P) approach. The RT pursued in this study removes the tracers outside the minimum and maximum values in the potential sediment sources.

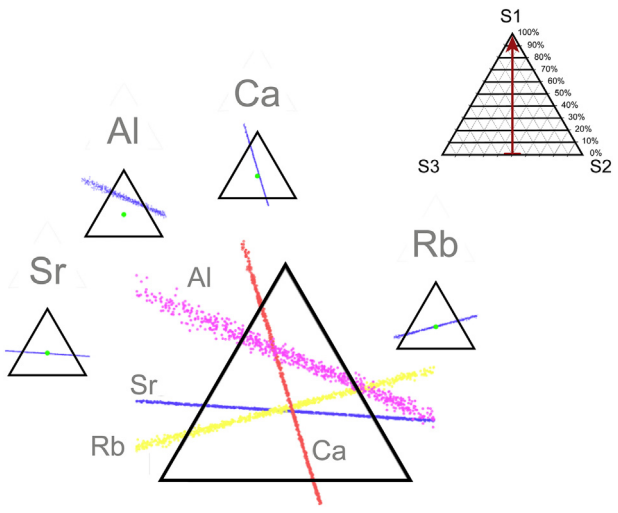

Fig. 5. Ternary diagram with the results of four tracers from the artificial dataset. The schematic diagram above and to the right shows how to interpret the ternary diagrams.

On the other hand, the second approach requires that the mixture samples must be within a polygon bounding the source signatures. Furthermore, this second approach needs to be done for each pair of tracers, increasing the complexity of the analysis, and is dependent on a relationship between at least two tracer properties. In addition, two selection methods, the Kruskal–Wallis H Test with a p-value of 0.05 and the DFA Test with a niveau of 0.05 were displayed together with the CI and CR procedures.

The proposed method creates a ranking of tracers suitable to select tracers based on its conservativeness and consensus rank. Furthermore, it is possible to detect those tracers with non-coherent information that could not be detected by other statistical tests. The CR methodology was implemented in the real sample dataset to show its usefulness (Fig. 9). Furthermore, these results were compared with different statistical tests and the within-a-polygon approach.

As shown in Fig. 9, different statistical tests have selected different tracers as convenient for the fingerprinting study. The selection produced by the within-a-polygon approach and the RT correlates favourably with those of the CR and CI methods. Furthermore, the tracers excluded by these two methods coincide with the lowest CR and CI values.

However, both the KW and the KW + DFA tests select as more convenient some tracers with low CR and CI values and their subsequent high dispersion and likely non-conservative behaviour. The KW test includes LF, Pb, Ba and Ti while the DFA includes Ba as selected tracers for their high discrimination of the different sources. Both methods, KW and DFA, do not use the mixture information to select the optimum set of tracers. Thus, the solutions could end up outside the physical solution space due to the relative position of the tracer in the mixture.

However, this will decrease the CI and CR values of the tracer, and the tracer would be excluded. Thus, the CR and CI approaches can effectively remove non-conservative and dissenting tracers that pass the most widespread tests used in fingerprinting studies. These findings further support our methodology that represents a groundbreaking alternative for tracer selection methods.

4. Discussion

4.1. The new information of individual tracers

This work reveals for the first time the individual information or the signal that each tracer contributes to the unmixing models. This information helps to better understand the outcomes of unmixing models and to select the correct set of tracers without including tracers with non-coherent information that could lead models to erroneous and unpredicted results. Furthermore, as seen in Fig. 3, the tracers with the lowest consensus value are also classified into independent groups and present the highest error from the known solution.

This new method also aids to classify and discriminate the different groups of tracers, which is of interest to track the tracer's origin or the process to which tracers are subjected and their possible relationships. Furthermore, as a novelty, a conservativeness index is presented with a continuous numerical value, in contrast to the previous methodologies that only discriminates between conservative and non-conservative tracers.

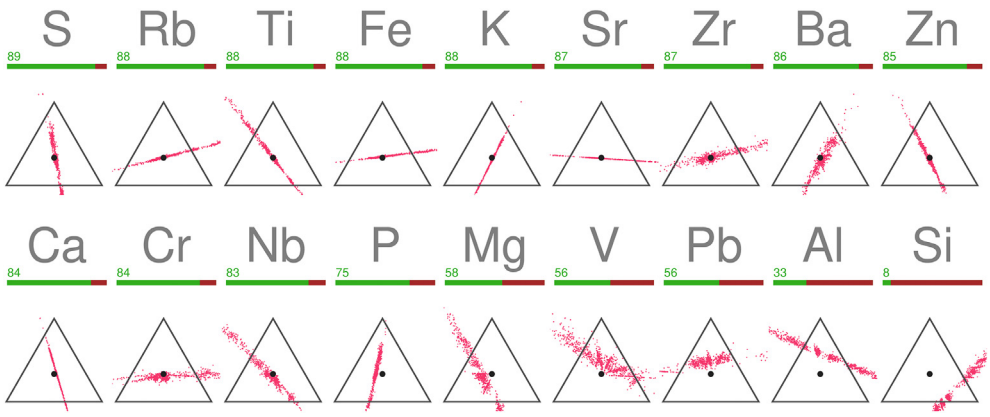

Fig. 6. Ternary diagrams of the results of the single-tracer model from each tracer for the artificial dataset with randomly chosen tracers (RCT) ordered according to the CR values. The black circle located in the centre of the triangle represents the theoretical contributions of the artificial mixture with equal contribution for each of the three sources.

Most of the previous studies assumed that all tracers with conservative behaviour or those selected after using the most widespread methodologies can be directly included in fingerprinting models (Collins et al., 2017; Owens et al., 2016; Smith and Blake, 2014). Our results do not confirm this hypothesis; in fact, they prove that tracers with apparent conservative behaviour but with non-coherent information in the mixture can introduce errors in the unmixing models.

4.2. The novel CR and future perspectives

In most studies identifying sediment provenance by using the fingerprinting technique, the first requirement that a tracer should fulfil to be selected for unmixing is being conservative. In this regard, Smith et al. (2018) proposed a tracer selection method to identify and remove tracers that exhibit non-conservative behaviour during transport between catchment sources and sediment sampling locations. Our results support the idea that tracer selection methodologies are needed in order to exclude non-conservative tracers but also those with non-coherent information in the mixture. This new method shows the existence of tracers with erroneous or non-conservative information that could be selected when using the previously established tracer selection methods.

We provide a new method to identify non-conservative and non-coherent or dissenting tracers. As can be seen in Fig. 6, those tracers with lower consensus present higher errors from the known solution in the artificial mixture, thus supporting the method's capability. In addition, in the case of the real sample example, the tracers with the lowest consensus value show the least coherent information and most of their possible solutions fall outside the triangle that represents the space of the physical solution. Our findings appear to be well substantiated by the results of the two different unmixing models tested and corroborate that the tracer selection is not a model-dependent issue.

Recent research has suggested the mixing polygon approach proposed by Phillips and Gregg (2003) as the alternative to the previously established methods for tracer selection methods. However, our findings suggest that the Phillips and Greg's method likely includes as fully conservative low-conservative or even non-conservative tracers. Furthermore, in this study, we prove the existence of tracers with dissenting information that are selected as suitable tracers by the other methods that can introduce erroneous information to the models. For this reason, the CR shows how each tracer behaves in relation to the other tracers included in the dataset and which information each tracer delivers to the model. Thus, this new method composed by the CI and the CR represents a groundbreaking alternative for tracer selection.

The CR and CI procedures represent a novel attempt that fills the gap created by the previous methodologies that are user-dependent and do not use the mixture information after the mass conservation test. Thus, without this new information, final tracer selections could incorporate dissenting and non-conservative tracers leading models to erroneous results.

5. Conclusions

The application of unmixing models is necessary to understand source-tracer relationships, which is generally performed by applying different software to select the best combination of sediment tracers. However, evidences from this study suggest that tracer selection methods are crucial in fingerprinting studies, as the use of one or another tracer could substantially modify the output of the

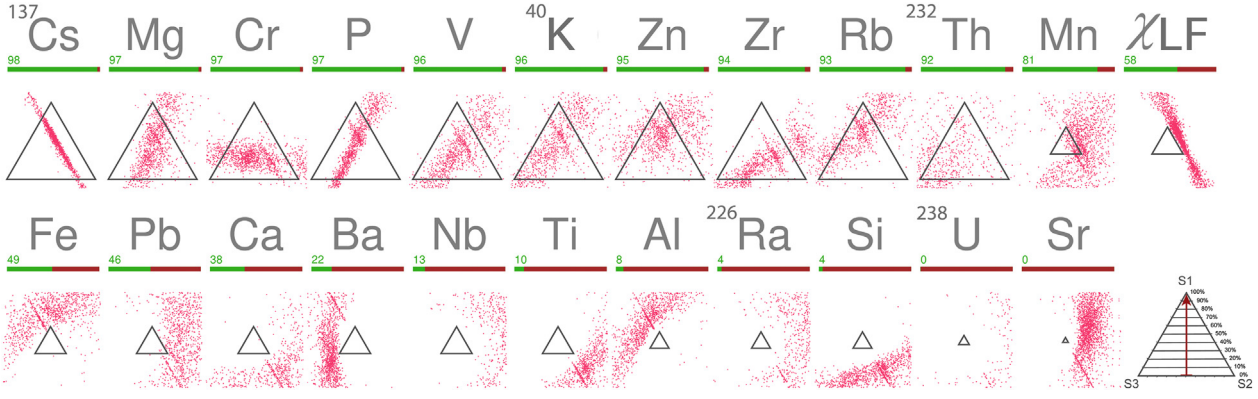

Fig. 7. Ternary diagrams of the results of the single-tracer model from each tracer for the real dataset with randomly chosen tracers (RCT) ordered according to the CR values.

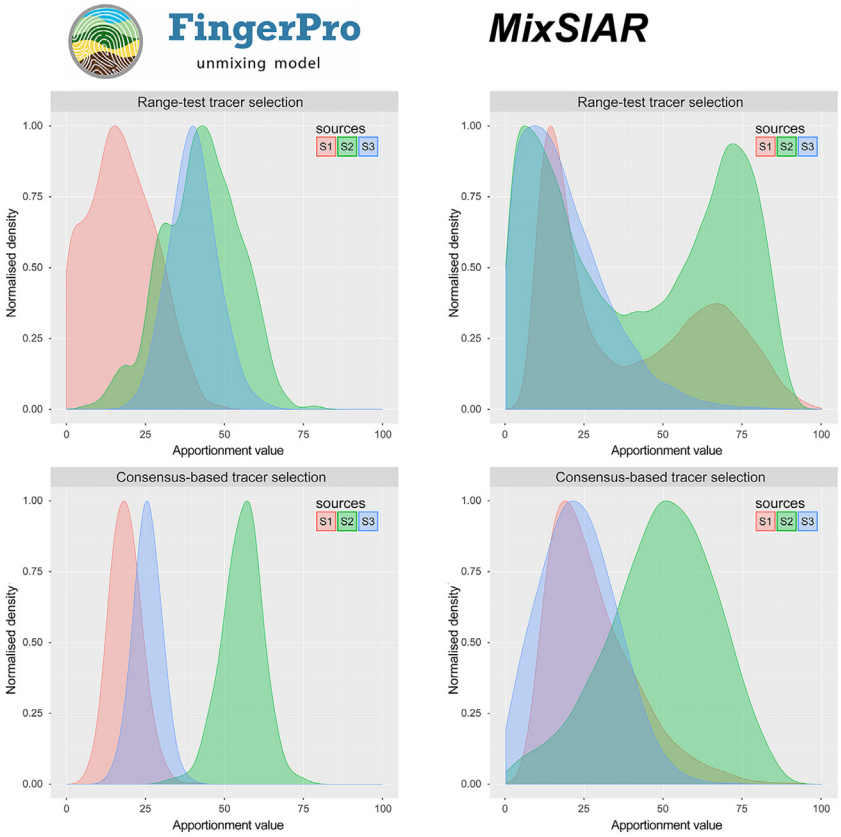

Fig. 8. Results of the unmixing procedure before and after implementing the CR and CI methods in the real mixture.

models. Our results prove that including tracers with dissenting information produces inconsistent results. In addition, some conservative tracers could provide unreliable information and may be erroneous.

Unmixing models cannot estimate reliable contributions of sediment sources if the tracer selection procedure applied does not account for tracers with non-coherent information. Thus, in this research, we have devised an innovative methodology to identify non-conservative and dissenting tracers that enables to understand datasets and, likewise, the effect of each tracer.

The currently used methods without CI and CR information may lead to selecting dissenting and non-conservative tracers. Our study provides the framework for a new way to obtain individual tracer information to prevent the inclusion of erroneous information into fingerprinting studies.

CRediT authorship contribution statement

Ivan Lizaga: Conceptualization, Writing - original draft, Software, Data curation, Methodology, Formal analysis, Investigation, Resources. **Borja Latorre:**Conceptualization, Writing - review & editing, Software, Supervision, Methodology, Formal analysis, Investigation, Resources.**Leticia Gaspar:**Conceptualization, Validation, Data curation, Investigation, Resources, Writing - review & editing.**Ana Navas:**Conceptualization,

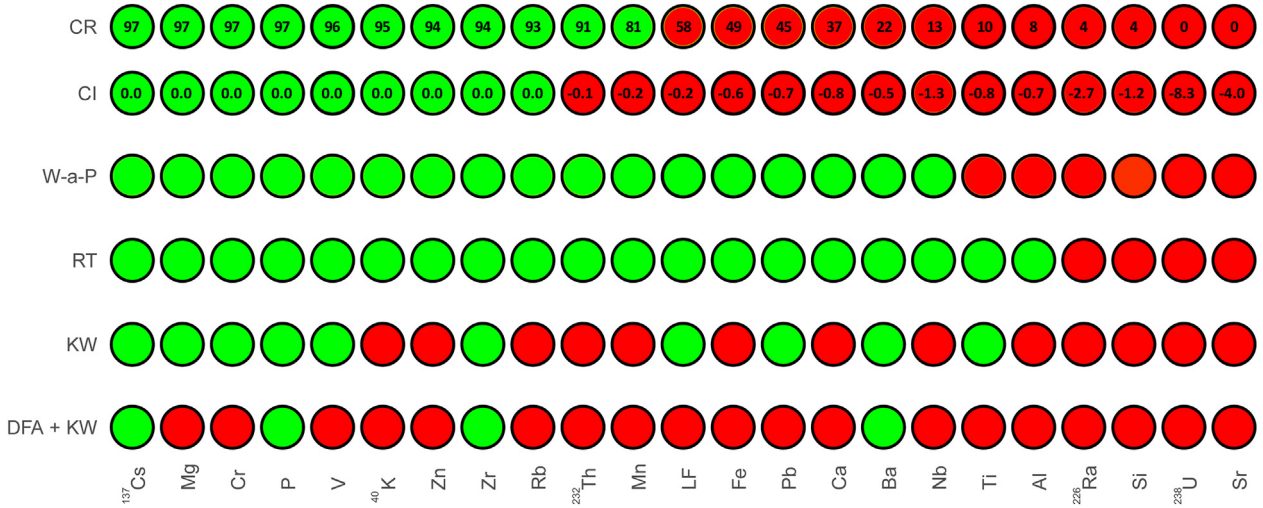

Fig. 9. Tracer selections produced by the most widespread tracer selection methods implemented in fingerprinting studies.

Methodology, Investigation, Writing - review & editing, Supervision, Project administration, Funding acquisition.

Declaration of competing interest

The authors declare that they have no known competing financial interests or personal relationships that could have appeared to influence the work reported in this paper.

Acknowledgements

This research was financially supported by the project TRAZESCAR (CGL2014-52986-R) and the aid of a predoctoral contract (BES-2015-071780), funded by the Spanish Ministry of Science and Innovation.

References

Collins, A.L., Walling, D.E., 2002. Selecting fingerprint properties for discriminating potential suspended sediment sources in river basins. J. Hydrol. 261, 218–244. https://doi.org/10.1016/S0022-1694(02)00011-2.

Collins, A.L., Pulley, S., Foster, I.D.L., Gellis, A., Porto, P., Horowitz, A.J., 2017. Sediment source fingerprinting as an aid to catchment management: a review of the current state of knowledge and a methodological decision-tree for end-users. J. Environ. Manag. 194, 86–108. https://doi.org/10.1016/j.jenvman.2016.09.075 Sediment source fingerprinting for informing catchment management: methodological approaches, problems and uncertainty.

Evrard, O., Laceby, J.P., Ficetola, G.F., Gielly, L., Huon, S., Lefèvre, I., Onda, Y., Poulenard, J., 2019. Environmental DNA provides information on sediment sources: A study in catchments affected by Fukushima radioactive fallout. Sci. Total Environ. 665, 873–881. https://doi.org/10.1016/j.scitotenv.2019.02.191.

Gaspar, L., Blake, W.H., Smith, H.G., Lizaga, I., Navas, A., 2019. Testing the sensitivity of a multivariate mixing model using geochemical fingerprints with artificial mixtures. Geoderma 337, 498–510. https://doi.org/10.1016/j.geoderma.2018.10.005.

Herrera-Viedma, E., Cabrerizo, F.J., Kacprzyk, J., Pedrycz, W., 2014. A review of soft consensus models in a fuzzy environment. Information Fusion, Special Issue: Information Fusion in Consensus and Decision Making vol. 17, pp. 4–13. https://doi.org/10.1016/j.inffus.2013.04.002.

Hong, Y., Kwong, S., Chang, Y., Ren, Q., 2008. Consensus unsupervised feature ranking from multiple views. Pattern Recogn. Lett. 29, 595–602. https://doi.org/10.1016/j.patrec.2007.11.012.

Klages, M.G., Hsieh, Y.P., 1975. Suspended solids carried by the Gallatin River of southwestern Montana: II. Using mineralogy for inferring sources. J. Environ. Qual. 4, 68–73. https://doi.org/10.2134/jeq1975.00472425000400010016x.

Koiter, A.J., Owens, P.N., Petticrew, E.L., Lobb, D.A., 2018. Assessment of particle size and organic matter correction factors in sediment source fingerprinting investigations: an example of two contrasting watersheds in Canada. Geoderma 325, 195–207. https://doi.org/10.1016/j.geoderma.2018.02.044.

Laceby, J.P., Gellis, A.C., Koiter, A.J., Blake, W.H., Evrard, O., 2019. Preface—evaluating the response of critical zone processes to human impacts with sediment source fingerprinting. J. Soil. Sediment. 19, 3245–3254. https://doi.org/10.1007/s11368-019-02409-0.

Lizaga, I., Gaspar, L., Blake, W., Latorre, B., Navas, A., 2019. Fingerprinting changes of source apportionments from mixed land uses in stream sediments before and after an exceptional rainstorm event. Geomorphology https://doi.org/10.1016/j.geomorph.2019.05.015.

Lizaga, I., Quijano, L., Palazón, L., Gaspar, L., Navas, A., 2018a. Enhancing connectivity index to assess the effects of land use changes in a Mediterranean catchment. Land Degrad. Dev. 29, 663–675. https://doi.org/10.1002/ldr.2676.

Lizaga, I., Latorre, B., Gaspar, L., Navas, A., 2018b. fingerPro: An R Package for SedimentSource Tracing. CRAN https://doi.org/10.5281/zenodo.1402029.

Llena, M., Vericat, D., Cavalli, M., Crema, S., Smith, M.W., 2019. The effects of land use and topographic changes on sediment connectivity in mountain catchments. Sci. Total Environ. 660, 899–912. https://doi.org/10.1016/j.scitotenv.2018.12.479.

Lloyd, C.E.M., Johnes, P.J., Freer, J.E., Carswell, A.M., Jones, J.I., Stirling, M.W., Hodgkinson, R.A., Richmond, C., Collins, A.L., 2019. Determining the sources of nutrient flux to water in headwater catchments: examining the speciation balance to inform the targeting of mitigation measures. Sci. Total Environ. 648, 1179–1200. https://doi.org/10.1016/j.scitotenv.2018.08.190.

McCarthy, D.T., Jovanovic, D., Lintern, A., Teakle, I., Barnes, M., Deletic, A., Coleman, R., Rooney, G., Prosser, T., Coutts, S., Hipsey, M.R., Bruce, L.C., Henry, R., 2017. Source tracking using microbial community fingerprints: method comparison with hydrodynamic modelling. Water Res. 109, 253–265. https://doi.org/10.1016/j.watres.2016.11.043.

Morente-Molinera, J.A., Kou, G., Samuylov, K., Ureña, R., Herrera-Viedma, E., 2019. Carrying out consensual Group Decision Making processes under social networks using sentiment analysis over comparative expressions. Knowl.-Based Syst. 165, 335–345. https://doi.org/10.1016/j.knosys.2018.12.006.

Murtagh, F., Legendre, P., 2014. Ward's hierarchical agglomerative clustering method: which algorithms implement Ward's criterion? J. Classif. 31, 274–295. https://doi.org/10.1007/s00357-014-9161-z.

Navas, A., Valero-Garcés, B., Gaspar, L., Machín, J., 2009. Reconstructing the history of sediment accumulation in the Yesa reservoir: an approach for management of mountain reservoirs. Lake Reservoir Manage. 25, 15–27. https://doi.org/10.1080/07438140802714304.

Owens, P.N., Batalla, R.J., Collins, A.J., Gomez, B., Hicks, D.M., Horowitz, A.J., Kondolf, G.M., Marden, M., Page, M.J., Peacock, D.H., Petticrew, E.L., Salomons, W., Trustrum, N.A., 2005. Fine-grained sediment in river systems: environmental significance and management issues. River Res. Appl. 21, 693–717. https://doi.org/10.1002/rra.878.

Owens, P.N., Blake, W.H., Gaspar, L., Gateuille, D., Koiter, A.J., Lobb, D.A., Petticrew, E.L., Reiffarth, D.G., Smith, H.G., Woodward, J.C., 2016. Fingerprinting and tracing the sources of soils and sediments: earth and ocean science, geoarchaeological, forensic, and human health applications. Earth Sci. Rev. 162, 1–23. https://doi.org/10.1016/j.earscirev.2016.08.012.

Palazón, L., Gaspar, L., Latorre, B., Blake, W.H., Navas, A., 2015. Identifying sediment sources by applying a fingerprinting mixing model in a Pyrenean drainage catchment. J. Soils Sediments 15, 2067–2085. https://doi.org/10.1007/s11368-015-1175-6.

Pérez, I.J., Cabrerizo, F.J., Alonso, S., Dong, Y.C., Chiclana, F., Herrera-Viedma, E., 2018. On dynamic consensus processes in group decision making problems. Inf. Sci. 459, 20–35. https://doi.org/10.1016/j.ins.2018.05.017.

Phillips, D.L., Gregg, J.W., 2003. Source partitioning using stable isotopes: coping with too many sources. Oecologia 136, 261–269. https://doi.org/10.1007/s00442-003-1218-3.

Pulley, S., Foster, I., Antunes, P., 2015. The uncertainties associated with sediment fingerprinting suspended and recently deposited fluvial sediment in the Nene river basin. Geomorphology 228, 303–319. https://doi.org/10.1016/j.geomorph.2014.09.016.

Pulley, S., Foster, I., Collins, A.L., 2017. The impact of catchment source group classification on the accuracy of sediment fingerprinting outputs. J. Environ. Manag. 194, 16–26. https://doi.org/10.1016/j.jenvman.2016.04.048 Sediment source fingerprinting for informing catchment management: methodological approaches, problems and uncertainty.

Quesada, S., Tena, A., Guillén, D., Ginebreda, A., Vericat, D., Martínez, E., Navarro-Ortega, A., Batalla, R.J., Barceló, D., 2014. Dynamics of suspended sediment borne persistent organic pollutants in a large regulated Mediterranean river (Ebro, NE Spain). Sci. Total Environ. 473–474, 381–390. https://doi.org/10.1016/j.scitotenv.2013.11.040.

Quijano, L., Gaspar, L., Navas, A., 2016. Spatial patterns of SOC, SON, 137Cs and soil properties as affected by redistribution processes in a Mediterranean cultivated field (Central Ebro Basin). Soil Tillage Res. 155, 318–328. https://doi.org/10.1016/j.still.2015.09.007.

Rovira, A., Alcaraz, C., Ibáñez, C., 2012. Spatial and temporal dynamics of suspended load at-a-cross-section: the lowermost Ebro River (Catalonia, Spain). Water Res. 46, 3671–3681. https://doi.org/10.1016/j.watres.2012.04.014.

Schmidt, S., Meusburger, K., Figueiredo, T. de, Alewell, C., 2017. Modelling hot spots of soil loss by wind erosion (SoLoWind) in Western Saxony, Germany. Land Degrad. Dev. 28, 1100–1112. https://doi.org/10.1002/ldr.2652.

Schuller, P., Walling, D.E., Iroumé, A., Quilodrán, C., Castillo, A., Navas, A., 2013. Using 137Cs and 210Pbex and other sediment source fingerprints to document suspended sediment sources in small forested catchments in south-central Chile. J. Environ. Radioact. 124, 147–159. https://doi.org/10.1016/j.jenvrad.2013.05.002.

Sherriff, S.C., Franks, S.W., Rowan, J.S., Fenton, O., Ó'hUallacháin, D., 2015. Uncertainty-based assessment of tracer selection, tracer non-conservativeness and multiple solutions in sediment fingerprinting using synthetic and field data. J. Soils Sediments 15, 2101–2116. https://doi.org/10.1007/s11368-015-1123-5.

Smith, H.G., Blake, W.H., 2014. Sediment fingerprinting in agricultural catchments: a critical re-examination of source discrimination and data corrections. Geomorphology 204, 177–191. https://doi.org/10.1016/j.geomorph.2013.08.003.

Smith, J.A., Mazumder, D., Suthers, I.M., Taylor, M.D., 2013. To fit or not to fit: evaluating stable isotope mixing models using simulated mixing polygons. Methods Ecol. Evol. 4, 612–618. https://doi.org/10.1111/2041-210X.12048.

Smith, H.G., Karam, D.S., Lennard, A.T., 2018. Evaluating tracer selection for catchment sediment fingerprinting. J. Soils Sediments 18, 3005–3019. https://doi.org/10.1007/s11368-018-1990-7.

Solorio-Fernández, S., Carrasco-Ochoa, J.A., Martínez-Trinidad, J.F., 2019. A review of unsupervised feature selection methods. Artif. Intell. Rev. https://doi.org/10.1007/s10462-019-09682-y.

Stock, B.C., Semmens, B.X., 2016. Unifying error structures in commonly used biotracer mixing models. Ecology 97, 2562–2569. https://doi.org/10.1002/ecy.1517.

Walling, D.E., Collins, A.L., 2008. The catchment sediment budget as a management tool. Environmental Science & Policy, Monitoring and Modelling Diffuse Pollution From Agriculture for Policy Support: UK and European Experience. 11, pp. 136–143. https://doi.org/10.1016/j.envsci.2007.10.004.

Walling, D.E., Peart, M.R., Oldfield, F., Thompson, R., 1979. Suspended sediment sources identified by magnetic measurements. Nature 281, 281110a0. https://doi.org/10.1038/281110a0.

Walling, D.W., Woodward, J.C., Nicholas, A.P., 1993. A multi-parameter approach to fingerprinting suspended-sediment sources. Tracers in Hydrology. Proc. International Symposium, Yokohama. 1993, pp. 329–338.

Wynants, M., Millward, G., Patrick, A., Taylor, A., Munishi, L., Mtei, K., Brendonck, L., Gilvear, D., Boeckx, P., Ndakidemi, P., Blake, W.H., 2020. Determining tributary sources of increased sedimentation in East-African Rift Lakes. Sci. Total Environ. 717, 137266. https://doi.org/10.1016/j.scitotenv.2020.137266.

Zhang, X.C. (John), Liu, B.L., 2016. Using multiple composite fingerprints to quantify fine sediment source contributions: a new direction. Geoderma 268, 108–118. https://doi.org/10.1016/j.geoderma.2016.01.031.

Zhang, H., Fan, J., Cao, W., Harris, W., Li, Y., Chi, W., Wang, S., 2018. Response of wind erosion dynamics to climate change and human activity in Inner Mongolia, China during 1990 to 2015. Sci. Total Environ. 639, 1038–1050. https://doi.org/10.1016/j.scitotenv.2018.05.082.

CHAPTER 9

Variations in transport of fine sediment and associated elements induced by rainfall and agricultural cycle in a Mediterranean agroforestry catchment

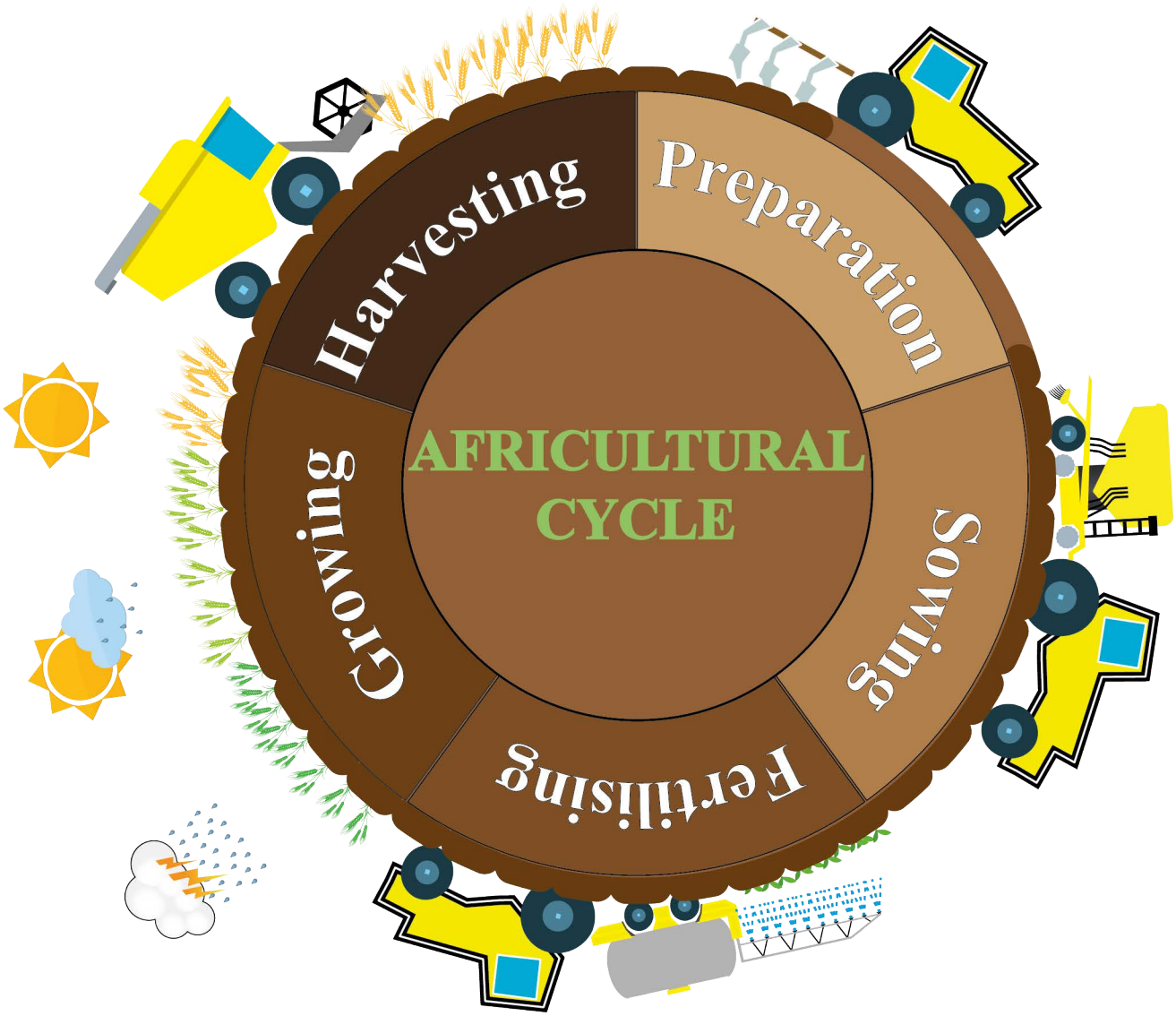

Variations in transport of fine sediment and associated elements induced by rainfall and agricultural cycle in a Mediterranean agroforestry catchment

Ivan Lizaga *, Borja Latorre, Leticia Gaspar, Ana Navas *
Experimental station of Aula Dei (EEAD-CSIC), Avenida Montañana, 1005, 50059 Zaragoza (Spain).

ABSTRACT

Soil erosion and fine particles exports are two of the major concerns of soil nutrients loss and water quality decrease nowadays. In Mediterranean mountainous environments, developing agriculture has increased the surface area prone to erosion in the last century. In addition, agricultural practices during different cropland stages likely increase sediment supplies. The present stability in agricultural productions is wholly dependent on chemicals in the form of pesticides, together with fertilisers needed to supply plants the adequate content of nutrients. Thus, the surface runoff and percolation water of the drainage system export fertilisers and pesticides out into the drainage system that finally reach rivers and accumulate in water bodies. In this study, we attempt to evaluate the soil response to different agricultural practices implemented during the agricultural cycle by applying the sediment fingerprinting technique together with the newly consensus-based tracer selection method in a medium-sized agroforestry catchment. To this purpose 128 source samples were distributed over the four main land use/land covers and geomorphic elements existing in the study area: cropland, rangeland, subsoil (exposed bare soil) and channel bank. To analyse the variability of source contributions from the headwaters to the outlet of the catchment during two hydrological years, three sampling stations were established for collecting suspended sediments mixtures. To further analyse the temporal variation of the exported suspended sediment, 21 mixture samples were collected during seven seasonal campaigns, and the bare soil cropland area monitored through the use of remote sensing. At the catchment outlet, the sediment sample weights were three to four times higher than at headwaters, being significantly and positively correlated with the cropland area. Certain elements such as As, Co, Li, Mn, Zn and 238U were above source ranges in the sediment mixtures. The enriched elements showed higher concentration in the sediment mixtures during sowing an after harvest periods. Besides, an enrichment of phosphorous during both agricultural practices periods points out to agricultural activities as the main cause of sediment and pollutants export to streams. The consensus method was used to shows the individual messages of each tracer revealing non-conservative and dissenting tracers, followed by a DFA to select the best set of tracers for each mixture. Overall, the unmixing model outputs displayed channel bank and agriculture as the main contributing sources for all the seasonal campaigns. Nevertheless, the agricultural contribution was higher during the periods when the soil surface in croplands had no plant cover protection. Thus, in the subcatchment with less bare soil cropland area, the agriculture source contributed with the lowest percentages. Our results support the protection of croplands, especially in periods of vegetation cover absence to prevent the loss of fertile soil and the export of pollutants to downstream water bodies.

Keywords:
Agricultural practices
Pollutants export
FingerPro unmixing model
Temporal scale fingerprinting
Consensus-based Method

1. Introduction

A goal of present and future agriculture is to meet the food need for the growing global population. However, the current agricultural production is wholly dependent on chemicals in the form of pesticides to the efficient control of pathogens and pests, together with fertilisers to supply the plants with the adequate content of nutrients (Prashar and Shah, 2016; Sharma and Singhvi, 2017). These chemicals associated with modern agriculture are usually sprayed in the fields and can be transported to the surrounding land and water supplies. One of the major pathways of these chemicals to reach water systems is in dissolved or particulate forms (National Research Council, 1993).

On the other hand, recent findings regarding new detection techniques have led researchers to gain knowledge on new ways of sediment mobilisation and the chemicals and nutrients associated with its transport (Quesada et al., 2014; Casado et al., 2019; Lizaga et al., 2019a). The significant increase in fine sediment transported to water bodies has been demonstrated to be one of the most widespread contaminants in aquatic ecosystems, compromising water quality and its deleterious effect on water storage capacity caused by reservoir siltation (Navas et al., 2004). As a first step, it is

essential to understand where the sediments and associated pollutants came from, and thus, analyse the role played by soil and sediment sources. Preliminary studies tracking the source of sediments were firstly pursued by Klages and Hsieh. (1975) and Walling et al. (1979) and the technique was termed as fingerprinting.

In agricultural landscapes, the agricultural cycle and the different crop stages from sowing, growth, ripening and harvesting modify the soil cover, from fully covered by vegetation to merely bare soil surface. As it is widely known, the vegetation cover of croplands is one of the major factors protecting soil from erosion and preventing the mobilisation of nutrients (Gómez et al., 2009; Gaspar et al., 2019c). More recently, the concerns about soil loss and the subsequent nutrient loss have led to developing methods for quantifying and predicting erosion rates of fine-grain sediment.

Thus, to control soil erosion, it is crucial to identify the most vulnerable areas exposed to erosion as main driver of soil loss and the subsequent mobilisation of nutrients and chemicals (Estrany et al., 2010; Smith and Blake, 2014; Owens et al., 2016). To this purpose, research has been conducted to involve different sets of tracers such as geochemistry, magnetic properties and radiotracers as fingerprints to identify the primary source of sediments by applying unmixing models (Martínez-Carreras et al., 2010; Evrard et al., 2013; Palazón et al., 2015b; Pulley et al., 2015; Meusburger et al., 2018; Gaspar et al., 2019a). Besides, as an aid tool technology such as remote sensing enables monitoring large areas within a short period of time. Satellite images providing information about soil properties, crop management, human activities and modifications of the vegetation cover are of value to relate the variations in sediment export rates with the susceptibility of specific areas to be eroded (Schillaci et al., 2017; Lizaga et al., 2019b, 2019c; Useya and Chen, 2019; Wang et al., 2019).

Evaluation on main drivers, natural or anthropogenic, that lead to the supply of fine sediments can be fostered by combining fingerprinting techniques with information derived from satellite images. To this aim our research re-examines the usefulness of the fingerprinting technique not only to identify the sediment provenance but also as a pollutant control technique to track the changes in sediment contribution associated with rainfall and agricultural activities. During two hydrological years (2014-2016) the sediment provenance is assessed in an agroforestry south Pyrenean catchment to understand the main factors leading to transport sediment and associated pollutants. To this purpose we develop an innovative multi-approach combining the spatiotemporal analysis of the sediment properties, remote sensing techniques and fingerprinting modelling to i) determine which is the primary source of the sediment and related pollutants, ii) analyse the links of sediment export with the agricultural cycle and iii) evaluate the effects of enriched tracers due to agricultural activities in the fingerprinting procedure.

2. Materials and methods

2.1 Study Area

The study area (23 km^2) is drained by an ephemeral stream tributary of the Arba River located in the middle part of the Pre-Pyrenean range (Fig. 1). The Barués catchment structure is dominated by the low angle dip of the Uncastillo Miocene formation bedding and the presence of a Quaternary glacis located at the Middle Eastern part occupied by most croplands. The climate is characterised by cold winters and hot and dry summers. The rainfall periods are variable along the year being mainly concentrated in the spring and autumn-winter seasons while the droughts take place in summer. However, the area is subjected to intense and localised storms during the second half of the summer period. The mean annual rainfall is nearly 500 mm and the maximum, and minimum annual temperatures are between 30°C and -6°C, respectively.

At the start of the twentieth century, most of the catchment was cultivated, remaining as croplands nearly 60% of the area during the 1960s. However, as much as 75% of the agricultural land was abandoned during the following decade. Currently, ~16% of the catchment is still cultivated while the rangeland occupies the remaining 83.5 % (Lizaga et al., 2018a). The main land use/land covers are cropland (AG) and rangeland (RG) which is composed by Mediterranean open forest and pine afforestation. Besides, most croplands are located on a Quaternary glacis and on fluvial terraces with gentle slopes covering the valley floors. Rangeland occupies the upper part of the catchment and the highest altitudes. Interspersed patches of highly disturbed areas such as bare soil (subsoil) are dispersed across the catchment. The valley floor is infilled by eroded sediment from the surrounding slopes which is deeply incised, especially in the middle part of the catchment where its thickness reaches its maximum up to 4 m. The stream channel banks are mainly composed by loess type sediment characterised by steep talus without vegetation cover.

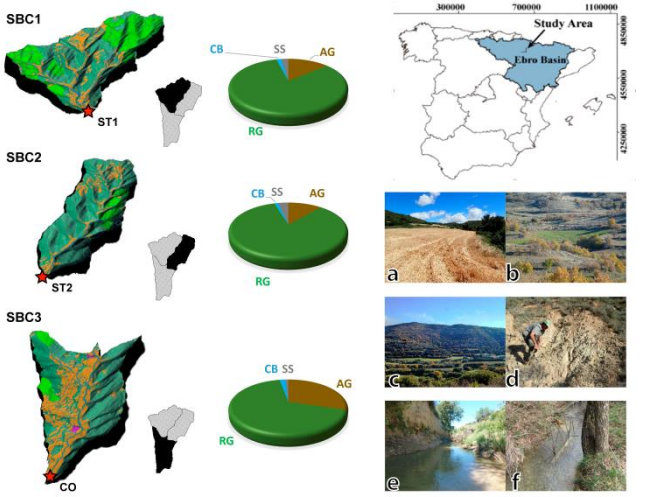

Fig. 1. Location of the study catchment in the central part of the Ebro Basin (NE Spain). 3D map of the land uses in the three subcatchments. (a) cropland, (b) gully erosion produced in a crop surrounded by rangeland, (c) open forest and terraced crops, (d) eroded subsoil area, (e) channel bank, and (f) sampling station (ST).

The Barués catchment is constituted by three subcatchments with different percentages of land use/ land cover (LU/LC). Thus, the AG land use predominates in the lower part of the catchment while RG spread over the catchment occupying the East part and the headwaters. During the previous decades, the abandonment of croplands

was substantially larger at headwaters due to the shallow soils and more steep slopes that hinder the use of machinery (Navas et al., 2017).

2.2. Soil sampling and analysis

The potential sediment sources and sediment sampling locations established in this study were identified during reconnaissance surveys following previous research conducted in this catchment about connectivity (Lizaga et al., 2018a), changes in soil properties after land abandonment (Lizaga et al., 2019a) and estimates of spatial soil redistribution rates (Lizaga et al., 2018b).

A total of 128 source sediment samples were taken with a 2 cm cylindrical sampler with a total surface area of 127 cm^2. Sediment source samples of variable depths are commonly collected for fingerprinting, though 2 cm depth is frequently used for average time study periods. Four replicates were collected at each sampling point and later combined in the field to create a representative composite sample following Owens et al. (2016).

Source samples were collected from cropland (AG), rangeland (RG), eroded subsoil (SS) and channel bank (CB) following the methodology proposed in Lizaga et al. (2019b). Thus, fourteen subsoil samples were collected over the catchment, and another sixteen samples were collected along the main streams on the channel banks. Suspended sediment mixtures (SSM) samples were collected following the methodology proposed by Phillips et al. (2000) in the middle part of the channel bed along the main streams from the headwaters to the outlet of the catchment in three sampling stations (ST). The locations were carefully selected in order to assemble the variability between the three main subcatchments.

SSM samples were collected during a two hydrological years period, from October 2014 to June 2016. In this project, it was decided to collect them each three months in order to analyse the seasonal variability. However, due to technical problems it was not possible to retrieve the SSM samples corresponding to the 2^{nd} seasonal campaign that had an extended time lapse. The objective of the sampling schedule was to provide a close replication of sediments transported during each season for evaluating both seasonality and the effect of the different crop practices such as sowing, fertilising and harvesting.

The samples were air-dried, ground, homogenised and sieved to ≤63µm following the most widespread methodology (Palazón et al., 2015a; Owens et al., 2016; Collins et al., 2017). Besides, the selection of the ≤63µm particle size for sources and mixtures was related to the predominant silt texture of soils in the catchment (Table 1). The relationships between tracers and the size fractions support that ≤63µm fraction compiles the existing range of variation for most of the study tracers. Particle size, stable elements, magnetic susceptibility and radionuclides were analysed in the ≤0.063mm fraction for all the 128 source sediment and 21 sediment mixtures samples.

Grain size and magnetic susceptibility were analysed following the same methodology as in Lizaga et al. (2019b). Total elemental composition was analysed by ICP-AES after total acid digestion pursued in two cycles with HF (48 %), HNO_3 and H_2O_2 and a second cycle with HNO_3, HCL, and Milli-Q water in a microwave oven (Navas and Machín, 2002). Samples were analysed for the following 28 elements: Al, As, Be, Bi, B, Ca, Cd, Co, Cr, Cu, Fe, K, Li, Mg, Mn, Na, Ni, Pb, P, Rb, Sb, Se, S, Sr, Ti, Tl, V, Zn. The resulting concentration was expressed in milligrams per kilogram (mg kg^{-1}). Gamma emissions of ^{137}Cs, ^{226}Ra, ^{238}U, ^{232}Th and ^{40}K were analysed at the gamma lab of the Experimental station of Aula-Dei (EEAD-CSIC) following the methodology used in Navas et al. (2014). The radionuclide activities were counted for 86400 seconds and expressed as massic activity in Bq kg^{-1} dry soil.

2.3. Cropland rotation and vegetation variation monitoring

Satellite imagery data was analysed with digital image processing methods and spatial analysis techniques to detect spatial and temporal changes in vegetation and cropland rotation. A multitemporal Landsat and Sentinel 2 satellite dataset formed the basis for monitoring the land use change and the variation of the cropland area during the study seasons. A series of one Landsat 8 image and seven Sentinel 2 images were acquired by the different multispectral sensors onboard Landsat and Sentinel satellites. Image series were selected with the nearest sensing period to the sample collection campaigns. The dates when images were available without cloud cover were 2014-10-17 (Landsat 8-OLI), 2015-04-11 (Sentinel 2A), 2015-07-06 (Sentinel 2A), 2015-09-24 (Sentinel 2A), 2015-12-03 (Sentinel 2A), 2016-03-12 (Sentinel 2A), 2016-05-01 (Sentinel 2A), 2016-06-23 (Sentinel 2A). The procedure for pre-processing satellite multispectral images to ensure temporal comparability between scenes was carried out by the Earth Resources Observation and Science Center (EROS) (USGS) for the Landsat 8-OLI and by using the sen2cor.exe for the Sentinel 2 satellites. This correction was done to ensure the data comparability between scenes. However, the different scenes were only used to visually compare and delineate the area that remains as bare croplands through the analysed time-lapse. The bare soil of cropland areas for each date was then compared with the previous temporal image to assess the evolution of the crop rotation and the different plant growth stages for each time interval.

2.4. Tracer selection and unmixing modelling

In order to select the best set of tracers, the results extracted from the analytical determinations were statistically analysed using R. Correlation plots created with the CorrPlot () function included in the FingerPro R package (Lizaga et al., 2018) were used to evaluate the relationships between the different element and soil properties analysed in the SSM. Besides, a Euclidian distance matrix with the normalised values and cluster analysis using the ward.D2 method was applied to group the tracers with similar behaviour through the study periods and investigate their relationships. A state-of-the-art unmixing model implemented as an R package-FingerPro (Lizaga et al., 2018) was applied for estimating sediment source contributions of each potential sediment source for the different SSM samples. Source apportionment solutions were expressed by the mean and standard deviation calculated from the model results (Table 4).

Table 1. Main statistics of the analysed properties for the potential sediment sources.

			AG					CB					RG					SS				
			m	sd	md	min	max	m	sd	md	min	max	m	sd	md	min	max	m	sd	md	min	max
Clay	%	13.2	2.9	13.3	8.0	20.5	12.9	2.7	13.4	8.0	17.4	14.5	5.1	12.8	5.8	31.0	13.4	3.9	12.9	7.8	20.0
Silt	%	71.3	3.0	71.3	66.3	76.4	72.4	3.8	71.4	65.7	78.2	69.0	5.1	68.7	55.6	81.3	74.9	5.1	74.0	66.8	82.8
Sand	%	15.5	3.1	14.8	9.1	21.8	14.7	5.5	16.3	4.4	22.1	16.7	4.6	15.9	4.1	26.9	12.4	6.9	14.3	0.0	23.0
^{137}Cs	Bq Kg^{-1}	4.1	5.7	2.8	0.0	27.4	0.0	0.0	0.0	0.0	0.0	11.3	7.7	9.9	0.8	32.7	0.0	0.0	0.0	0.0	0.0
^{40}K	Bq Kg^{-1}	427	59	426	320	579	469	63	480	359	563	451	64	444	338	645	555	114	520	411	736
^{226}Ra	Bq Kg^{-1}	28.8	2.6	28.9	24.8	33.7	29.6	3.2	29.3	25.9	36.5	29.2	4.9	28.3	22.4	52.7	28.7	2.4	28.2	24.3	32.7
^{232}Th	Bq Kg^{-1}	29.8	3.2	29.6	24.9	36.3	32.9	2.8	32.7	28.4	38.7	32.2	4.7	31.2	23.7	48.6	33.3	4.6	32.5	27.0	41.6
^{238}U	Bq Kg^{-1}	43.1	9.1	44.9	23.4	53.9	40.1	10.6	39.0	23.4	60.4	41.8	10.4	43.7	12.8	60.2	42.8	7.9	42.9	32.4	56.6
*X*LF	10^{-8}m^3 kg^{-1}	34.6	18.4	31.7	9.1	76.0	14.2	9.1	11.9	4.3	36.5	45.7	33.6	36.7	6.8	187.9	11.0	4.8	9.2	4.5	19.9
Al	mg/kg	14082	8273	13255	4024	24250	23520	1961	23570	20180	26590	18992	10455	21830	3859	42600	24923	3023	24320	21150	30700
As	mg/kg	2.2	1.3	2.2	0.0	5.3	0.8	1.0	0.5	0.0	3.1	1.7	1.1	1.6	0.0	4.5	0.8	0.6	0.8	0.0	1.8
Be	mg/kg	1.0	0.2	1.0	0.7	1.7	1.0	0.1	1.0	0.7	1.2	1.1	0.3	1.0	0.6	1.8	1.1	0.3	1.1	0.8	1.7
Bi	mg/kg	14.7	2.1	14.9	11.5	18.1	17.4	1.8	17.0	14.6	20.7	15.9	2.6	15.9	8.8	21.8	20.6	3.1	20.2	16.1	27.9
B	mg/kg	3036	851	2994	1356	4400	3953	620	4133	2540	4668	3204	664	3212	1494	4521	5193	1191	5602	3375	7529
Ca	mg/kg	90669	22726	90605	50790	129400	93107	15422	93350	63390	123400	81321	23726	83915	11100	126100	105724	9968	106650	82070	118400
Cd	mg/kg	0.4	0.5	0.5	0.0	2.1	0.3	0.3	0.5	0.0	0.7	0.5	0.3	0.6	0.0	1.1	0.5	0.3	0.6	0.0	0.8
Cr	mg/kg	50.6	6.8	52.0	34.2	59.6	52.3	7.3	53.2	39.4	63.3	60.7	16.5	57.4	32.6	130.1	64.7	14.7	62.4	42.0	85.0
Cu	mg/kg	12.7	1.8	12.8	9.5	16.9	12.1	0.7	12.2	10.7	12.9	12.5	3.2	11.6	6.4	24.1	11.8	1.5	11.9	9.6	14.7
Fe	mg/kg	15978	2354	16120	11730	19370	16985	2209	16890	13350	20530	18132	3842	17600	10640	31220	19815	4413	19030	13740	27410
K	mg/kg	10638	1862	10700	7265	15900	11037	1021	10930	9203	12460	10909	2065	10905	5962	16750	13160	2771	12445	9552	17490
Li	mg/kg	32.7	5.4	33.2	22.4	41.7	37.2	3.7	37.8	30.1	43.6	36.0	7.3	35.6	20.7	58.4	43.5	7.3	42.7	35.2	57.2
Mg	mg/kg	3209	806	3156	1953	4672	3438	727	3190	2342	4571	3401	857	3262	2000	5963	4286	609	4167	3129	5327
Mn	mg/kg	330	44	332	263	402	337	46	330	270	444	344	69	329	178	553	320	35	317	276	379
Mo	mg/kg	0.2	0.3	0.0	0.0	0.6	0.7	0.1	0.7	0.6	0.8	0.9	1.4	0.6	0.0	6.9	1.3	0.5	1.4	0.6	2.2
Na	mg/kg	4210	617	4107	3325	5221	4692	416	4644	3961	5477	4448	755	4310	2679	6644	5233	631	5199	4310	6527
Ni	mg/kg	28.3	4.1	28.2	22.5	37.6	31.5	2.3	31.8	26.8	35.2	31.6	8.6	29.5	17.8	64.9	40.8	5.7	40.9	30.0	49.3
Pb	mg/kg	20.1	3.0	19.9	15.1	25.4	22.8	1.2	22.6	20.9	24.4	23.1	5.1	22.8	13.0	38.8	25.0	3.1	24.0	20.1	30.6
P	mg/kg	409.9	88.0	410.7	201.2	562.8	279.7	23.4	278.4	246.6	324.8	283.8	96.7	271.3	166.8	1026.0	276.3	22.8	272.3	231.5	310.1
Rb	mg/kg	38.8	9.9	39.9	18.0	61.8	45.4	9.1	43.5	33.4	63.2	42.2	17.3	40.3	10.7	101.7	41.2	5.8	38.9	33.6	53.8
Sb	mg/kg	0.3	0.3	0.3	0.0	0.9	0.4	0.4	0.5	0.0	0.9	0.4	0.4	0.5	0.0	1.4	0.3	0.4	0.3	0.0	0.9
Se	mg/kg	5.4	0.9	5.5	3.9	7.5	5.7	0.7	5.9	4.7	6.8	6.3	2.0	5.9	3.6	14.6	7.1	1.5	7.2	4.4	8.8
S	mg/kg	689	116	690	453	856	860	415	734	493	2011	682	139	695	237	1180	983	369	807	671	1904
Sr	mg/kg	299.1	48.4	302.7	212.3	397.5	334.3	86.5	315.2	237.1	515.1	271.0	111.8	249.3	63.9	1002.0	434.9	147.9	416.4	194.3	673.4
Ti	mg/kg	3006	452	2988	2313	4603	3402	326	3294	3145	4328	3123	561	3041	1805	5085	3187	205	3144	2877	3580
Tl	mg/kg	126	24	128	84	169	140	23	134	101	176	131	26	126	83	203	165	22	162	130	203
V	mg/kg	58.3	10.8	59.8	40.1	93.0	61.1	6.3	60.4	50.4	69.7	60.2	11.1	60.4	33.2	88.9	70.0	15.4	66.2	50.1	94.4
Zn	mg/kg	41.6	7.0	42.0	30.1	64.3	40.2	4.0	39.5	33.7	47.6	44.6	8.3	43.3	25.1	64.1	44.9	7.1	42.8	35.1	57.7

An essential step in fingerprinting studies is the implementation of previous statistical tests in order to identify the set of tracers which better discriminate between potential sources (Yu and Oldfield, 1989; Walling and Woodward, 1995; Palazón et al., 2015b; Gaspar et al., 2019b; Gateuille et al., 2019). Several studies following the methodology implemented by Collins and Walling (2002a) compare the range between the sources and the sediment mixtures for each fingerprint tracer. However, by using the most widespread tracer selection methodologies, some not conservative tracers could be selected while informative tracers removed. Furthermore, the addition of tracers with redundant information does not deliver essential data for unmixing. Besides, the inclusion of only redundant tracers likely creates underdetermined systems where the model solution could be erroneous Lizaga et al., (under review).

In order to select the best set of tracers for fingerprinting studies we applied the novel consensus-based method, a novel ensemble technique composed by the CI and CR methods for sediment fingerprinting tracer selection proposed by Lizaga et al. (under review). CI is a conservativeness index that uses the predictions of single-tracer models to identify non-conservative tracers and creates a ranking that indicates how conservative each tracer is. The CR method is a scoring function based on several random debates between tracers, in which the tracer that prevents consensus is discarded. Both, CR and CI methods represent a novel attempt that fills the gap created by the previous methodologies that are user-dependent and do not use the mixture information after the mass conservation test. The method extracts the individual information and the signal that each tracer could introduce into unmixing models. To further check this new methodology, the 21 mixture samples were individually tested and their results compared. Furthermore, to avoid user-dependent decisions after applying the CI and CR method, the final tracer selection was accomplished by using the Discriminant Function Analysis (DFA) test with a niveau of 0.1 after to remove the tracers with redundant information.

To explore the behaviour of each element and the possible element depletion or enrichment due to pollution, we created a timeline scatter plot with the seven SSM seasonal samples values for each tracer together with the mean values of each source (Fig. 2).

3. Results

3.1. Spatio-temporal variations of sediment properties and mixtures tracers

The statistics of grain size, radionuclides and elemental composition for the potential sediment sources presented in Table 1 shows that the four sediment sources had similar contents of clay and sand, with mean values between 14-17% and 16-19% for clay and sand, respectively. However, the silt contents were lower in AG and RG than in the other sources, with the highest contents in CB and SS. The means of ^{40}K, B, Bi, Ca, Li, Mg, Na, Ni, Sr, Tl and V were significantly higher in SS than in the other sources (AG, CB, RG) ($p \leq 0.05$). Besides, AG showed higher values of P and As while RG had higher values of ^{137}Cs and χLF. Apart from P, major elements such as Al, Ca, Mg, K, Ti, Fe and Mn were not significantly different between sources.

The timeline of the properties in the SSM showed similar trends for some elements (Fig. 2). Most elements that were significantly correlated with the fine fraction paralleled the clay trends during the study period. Only Ca, Mn, S, Sb, Tl and partially ^{238}U did not show related trends with the clay fraction (Fig. 2).

The SSM sample weights and the accumulated rainfall were directly and significantly correlated ($r > 0.9$) in ST2 though correlations were not significant in ST1 and in the catchment outlet (CO) (Table 2). The differences between subcatchments could be caused by the temporal or partial blocking of the mixture collector in ST2 during the 3rd seasonal campaign as it only accumulated 17 g in comparison with 159 g and 622 g collected in ST1 and CO in this campaign. However, the amount of sediment collected in ST1 and CO was remarkably high for the scarce rain fallen during the 3rd seasonal campaign (100 mm) (Fig. 3). By removing this outlier campaign, the correlations significantly increased in the three subcatchments (Table 2).

	SSM Weights		
All campaigns	**SBC1**	**SBC2**	**SBC3**
precipitation (mm)	0.12	0.91	0.31
Campaign 3 removed	**SBC1**	**SBC2**	**SBC3**
precipitation (mm)	0.81	0.91	0.68

Table 2. Correlations between the SSM sample weights and the accumulated rainfall.

According to the analysed tracers in the sediment mixtures, the subcatchments showed slightly different behaviour with the largest differences in SBC2. Most SSM tracers were significantly and directly correlated with the clay fraction, but all tracers were inversely correlated with the silt and sand fractions and with rainfall. The tracers that were enriched in some campaigns such as As, Cu, Ni, ^{226}Ra, S, Sr, ^{238}U and Zn were also strongly correlated between them.

The mean concentrations of Al, As, Be, Cd, Cr, Cu, Li, Mg, Ni, Pb, Rb, V, and Zn in the SSM were the highest in ST1 at the headwaters but the lowest in the CO (Fig. 2). However, the sample weights were more than four times higher in CO than in ST1 and ST2. Thus, even with less concentration, the total contents of the referred elements in CO were more than two times higher than in ST1 and ST2. Besides, As, Co, Li, Mn, Zn and ^{238}U were enriched and out of the sources range for most study seasons in the three subcatchments. Moreover, Be, Cd, Cu and Pb also were enriched though only in some seasons. Phosphorus showed high concentrations for all study seasons with slightly higher values in CO. P contents were out of range for all the source samples except for the agricultural samples.

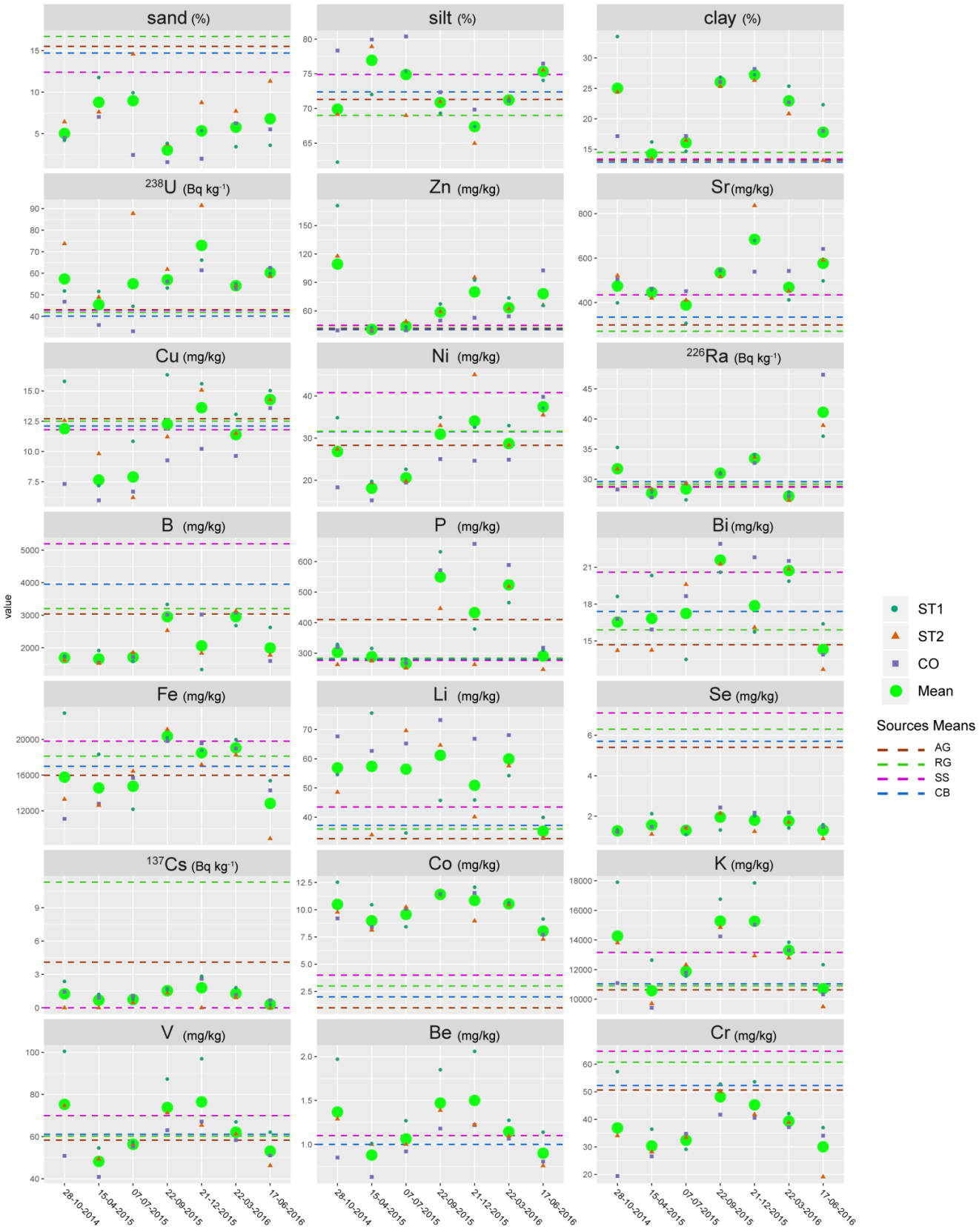

Fig. 2a. Timeline plot of the tracer values analysed in the suspended sediment mixtures (SSM) for the seven seasonal campaigns and the mean values of each source represented with dash lines.

The sample weight increases were paralleled with silt percentage increases, thus, elements with high negative correlations with silt such us ^{238}U, Zn, Cu, Ni, Pb, As, ^{232}Th showed strong negative correlations with weight. Overall, there were some elements frequently enriched in the SSM

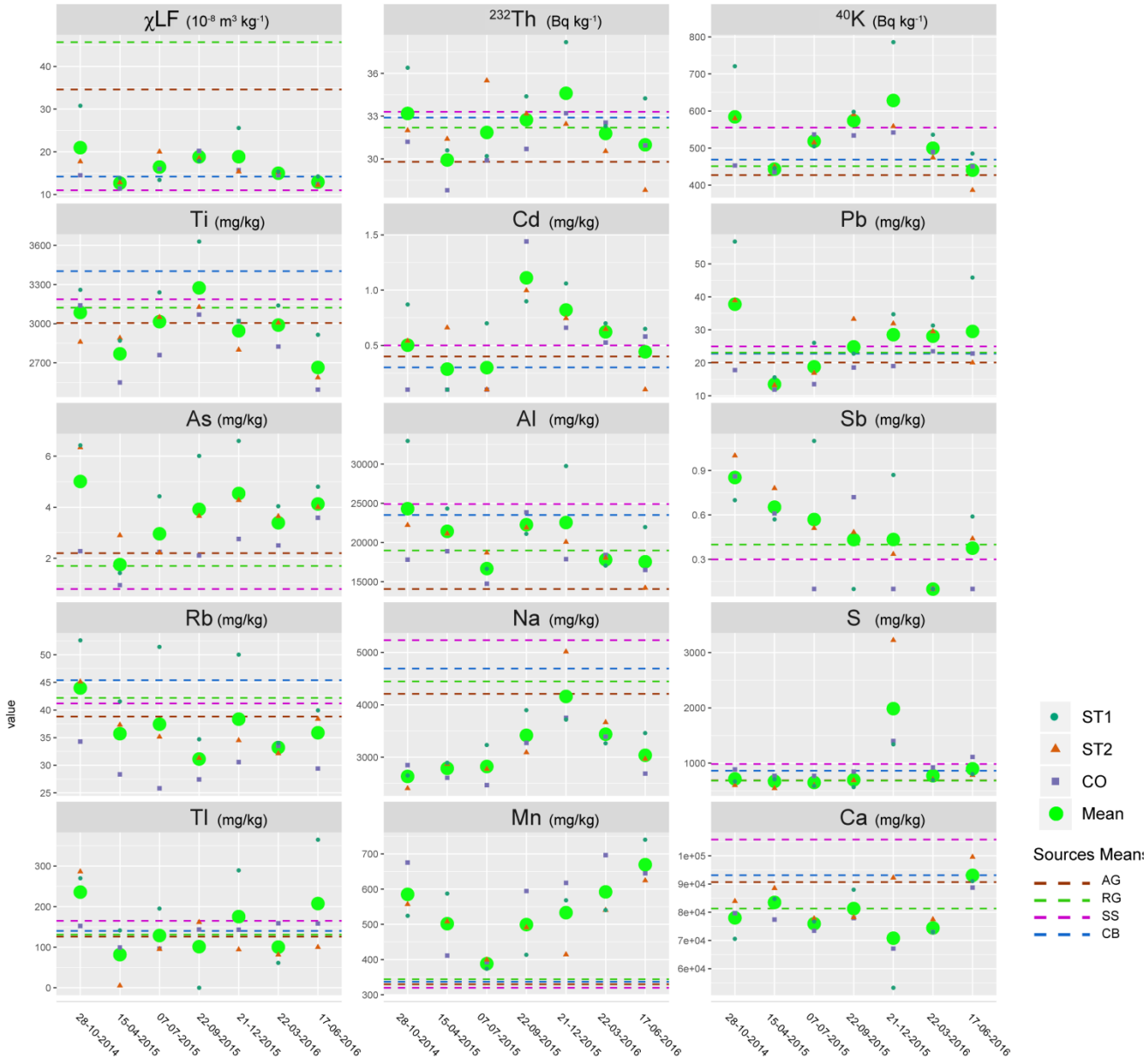

Fig. 2b. Timeline plot of the tracer values analysed in the suspended sediment mixtures (SSM) for the seven seasonal campaigns and the mean values of each source represented with dash lines.

such as ^{238}U, Sb, Mn, Zn, Li, Co and As while others as Rb, Na, Se, B and Cr were depleted. Between autumn and spring campaigns, it was detected an increase in the concentrations of elements positive and significantly correlated with the clay fraction. Besides, some elements with low positive correlation with clay also showed a high increase during the autumn campaign such as ^{238}U, Na and S. During these campaigns it was found that ^{238}U, P, S, Li, Mn and As were clearly above the sources range, indicating an increase of these elements during the sowing season.

3.2. Agricultural cycle and sediment exports

season campaign. Image 7 represents the period from 2016-03-22 to 2016-05-01 when the fallow fields in SBC3 and SBC2 were ploughed and left bare until sowing. Image

The calculation through satellite images of the bare soil surface generated by the agricultural cycle (Fig. 3) displayed the evolution of plant cover during the agricultural cycle and the area of bare soil surface in AG close to each of the seven seasonal campaigns. Although each image only shows the cropland stage when the SSM samples were collected, they are also representative of the cropland stages between campaigns except from the time-lapse between images, 1-2 and 7-8. Between images 1-2 the time-lapse was seven months and the cropland stages moved from autumn-winter bare soil to fully-grown spring plants. For images 7-8 the time-lapse was within the same 8 was taken by the sensor one week after the sampling campaign when most crops were harvested. However, the lower part of the catchment was not harvested until one to

two weeks before sampling. Thus, as much as 90% of the catchment's lower part remained unharvested for most of the seasonal campaigns or it was harvested after sampling.

The temporal evolution of the accumulated rainfall and the surface of bare soils during the study period compared with the weights of the SSM samples (Fig. 4) showed two sharp increases in SSM weights in the 2nd and 3rd seasonal campaigns. The other five seasonal campaigns followed a similar trend with that of both the bare soil surface and the accumulated rainfall.

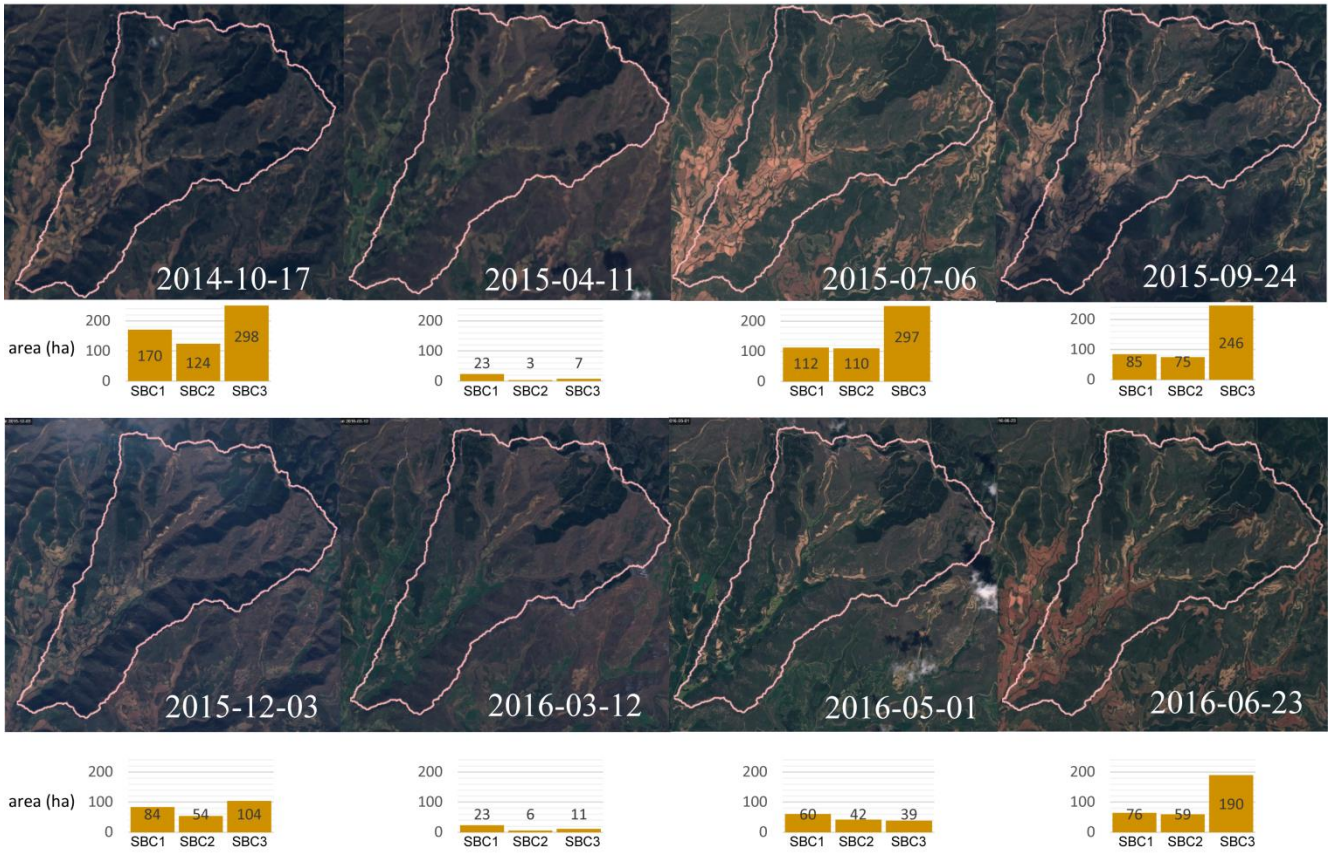

Fig. 3. Satellite images and AG bare soil area graphs for the three subcatchments during the seven seasonal campaigns

3.3. Evaluating tracers reliability: the new Consensus method

To assess the spatial variations in source apportionments from headwaters to the lower part of the catchment, it was required to create a set of optimum tracers for each SSM sample. The newly proposed tracer selection method includes several advantages in comparison with the existing ones. On the one hand, the conservativeness index (CI) method included in this method provides information about how conservative is a tracer with a realistic approach that uses the mixture information in the procedure and not only graphically or spatially as it was previously done with the mixing polygon approaches. Secondly, the Consensus Ranking (CR) method informs of which tracers are leading the model to a consensual solution and which ones are introducing dissenting messages in the unmixing model. The dissenting tracers do not deliver valuable information to models but increase uncertainty generating erroneous results if they are used together with the remaining tracers in the dataset. Thus, one of the major advantages of this new method is that it allows the removal of non-conservative and non-consensual tracers showing the individual messages of each tracer.

Applying the Consensus-based method for the different SSM and sources for each ST, CI and CR methods results extracted from the 21 SSM samples were compared and used for selecting the tracers (Table 3). There were more tracers that fulfilled the requirements of the method than selected tracers to be part of the optimum set of tracers to be used for unmixing (bold numbers). However, the messages of the non-selected tracers that passed the requirements of the method were redundant with some of the selected ones. Then, once the tracer selection that defined a well-determined system was accomplished, the inclusion of tracers with the same message only provided repetitive information without significantly modifying the model results but increasing uncertainty.

As seen in Table 3 after the harvesting period corresponding to the 4th seasonal campaign, the enriched tracer P clearly showed non-conservative and non-consensual behaviour as indicated by the important change in the average values of CI and CR during the 4th seasonal campaigns. Moreover, during the sowing season, the 5th seasonal campaign both S and P showed non-conservative and non-consensual behaviour.

However, P was the tracer that best discriminated AG from the other sediment sources. The enrichment of P lead

the tracer out of the CI and CR methods requirements during specific campaigns what might difficult discriminate AG in the unmixing procedure.

3.4 Assessing the spatio-temporal variability of sources apportionment

Channel banks were the largest contributing source in the three subcatchments ranging from 35% to 47% (Fig. 5). The second and third largest contributing sources were AG and SS with 25% and 25%, respectively, while rangeland contributed the less (7% - 10%). At the catchment outlet (CO), a large increment of SSM sample weights was recorded along with an increase in AG percentage apportionment.

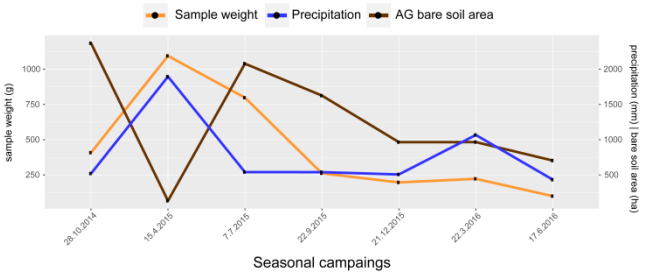

Fig. 4. Line graph of the mixture sample weights, precipitation and AG bare soil area for the seven seasonal sampling campaigns.

At a temporal scale, each subcatchment showed different but related results (Fig. 6). The main contributing source in the three sampling stations was CB being slightly higher in ST1. The CB contributions were directly and significantly correlated with the accumulated rainfall and sample weights.

On the contrary, the AG sediment contributions were negatively correlated with the accumulated rainfall and sample weights being only significant in CO. Thus, when CB contribution increased the AG contribution decreased being SS and RG mostly residual contributing sources. The AG sediment export response followed similar trends in ST1 and CO except for the 6th seasonal campaign in ST1. On the other hand, ST2 showed independent behaviour with higher CB contribution and lower AG contributions. The general trends in ST1 and CO followed the general crop stages with slightly higher AG contributions during the sowing seasons (1st and 5th seasonal campaigns) that gradually decreased as the crops grown-up. However, the increase in AG sediment exports expected after the harvest season is only significant in CO. In ST2 the SSM samples showed significant AG contributions only immediately after the harvest seasons (3rd and 7th seasonal campaigns) with an increasing trend from the 5th to 7th campaigns contrary to what it was observed in CO that showed decreasing AG apportions during the last three sampling campaigns.

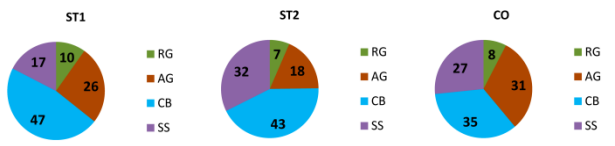

Fig. 5. Pie chart of the mean total apportions of the different sediment sources for each sampling station.

4. Discussion

4.1. The spatio-temporal variability in sediment exports

The differences in the provenance of sediment exported are mainly produced by the agricultural practices and the vegetation cover over the different soil sources. Thus, due to the protection capacity of rangelands, the main driver of sediment exports is the agricultural cycle and the agricultural practices what agrees with highest soil erosion found in the study catchment (Lizaga et al., 2018b) as well as in other nearby catchments of the south Pyrenean region (Navas et al., 2013, Gaspar et al., 2013). The low correlation between the SSM samples weights and the accumulated rainfall due to the sharp increase in sediment exports after the harvesting period, points out to an external affection in the sediment export cycle in SBC1 and SBC3. The high increase in sediment mobilised during the 3rd seasonal campaign is likely a consequence of agricultural practices during harvest increasing compaction and rendering soil more prone to erosion (Hamza and Anderson, 2005). Further increased sediment mobilisation is likely caused by machinery operations at harvest (Schuller et al., 2013) or when crossing the streams disturbing and mobilising the channel bed sediments. Thus, a lower correlation with rainfall and the high increase in the coarse sediment fraction indicates that sediment was not only naturally generated but that other factors related to agricultural practices have an important influence. Furthermore, the processes after harvesting such as erosion by raindrop impact (Beguería et al., 20015) sheet wash erosion and rilling due to the absence of cover protection and the loosening of soil could also increase the sediment export rates (Ruiz-Colmenero et al., 2013; Quijano et al., 2016, 2019, 2020). However, this pattern is not observed in the last campaign because most of the SBC3 remained unharvested one to two weeks before sampling. The low precipitation rates during the 3rd and the 7th seasonal campaigns could have prevented the eroded or mobilised sediment from the harvested fields reaching the STs before sampling. The anomalous values in the 2nd seasonal campaign (2015-04-15) are associated with the longest period that doubled the sediment amount accumulated in the other seasonal regular campaigns.

The relative enrichment in the clay fraction and depletion in the sand fraction in the suspended sediment mixtures compared to the sources suggests that fine sediment is reaching the streams and preferentially exported out of the catchment. Similar results were found by Lizaga et al. (2019b) during an extreme storm event that happened in the study area in 2012. The low sand content transported determines that most tracers' positively correlated with the clay fraction have weak negative correlations with sand. The temporal variation of the clay fraction follows the crop stages as supported by the higher clay contents present during sampling campaigns between July and December when fields have non-vegetation cover to protect soil surface from erosion.

Table 3 CI and CR values for the three sampling (SST1, SST2 and CO) stations during the seven seasonal campaigns. Bold numbers represent the tracers selected for unmixing.

	SST1													
	CR1	**CI1**	**CR 2**	**CI2**	**CR3**	**CI3**	**CR4**	**CI4**	**CR5**	**CI5**	**CR6**	**CI6**	**CR7**	**CI7**
^{137}Cs	**99.68**	**-0.03**	**96.78**	**-0.15**	**98.18**	**-0.15**	**99.30**	**-0.08**	**99.90**	**-0.14**	**98.92**	**-0.16**	**95.70**	**-0.18**
^{40}K	28.28	-0.89	**95.24**	**-0.09**	**95.04**	**-0.12**	77.20	-0.39	11.86	-1.48	91.54	-0.13	**96.44**	**-0.10**
^{226}Ra	37.62	-2.67	95.00	-0.31	84.50	-0.48	74.04	-0.76	49.68	-2.04	96.62	-0.31	7.54	-3.63
^{232}Th	89.88	-0.30	89.70	-0.16	75.60	-0.18	95.42	-0.30	64.64	-0.60	93.50	-0.13	94.32	-0.29
^{238}U	82.28	-0.89	57.68	-0.81	**96.42**	**-0.18**	51.42	-1.05	19.82	-3.12	28.90	-1.28	15.90	-2.15
χLF	**98.06**	**-0.21**	90.22	-0.27	95.20	-0.32	**97.96**	**-0.15**	**99.58**	**-0.17**	**95.24**	**-0.20**	93.98	-0.16
Al	47.46	-0.63	91.30	-0.17	89.04	-0.12	**98.08**	**-0.10**	75.26	-0.52	89.20	-0.27	**97.34**	**-0.20**
As	0.72	-3.48	**97.48**	**-0.10**	0.70	-1.85	0.44	-3.10	0.86	-3.64	1.86	-1.60	0.40	-2.17
Be	14.18	-1.79	**97.06**	**-0.07**	85.66	-0.41	17.42	-1.50	8.58	-2.04	88.22	-0.41	**96.22**	**-0.20**
Bi	**98.26**	**-0.15**	71.88	-0.28	13.36	-0.38	77.08	-0.32	**96.04**	**-0.24**	91.30	-0.17	90.46	-0.20
B	9.14	-0.92	2.70	-0.78	0.86	-1.03	75.40	-0.23	4.50	-1.15	21.32	-0.43	31.56	-0.44
Ca	68.46	-0.73	92.80	-0.14	66.02	-0.41	94.06	-0.22	20.88	-1.58	43.76	-0.65	**97.50**	**-0.07**
Cd	27.22	-0.86	5.68	-1.18	76.24	-0.44	9.30	-0.98	8.95	-1.70	78.94	-0.44	89.98	-0.27
Co	0.00	-32.70	0.00	-27.01	0.00	-21.50	0.00	-29.66	0.00	-31.44	0.00	-27.53	0.00	-23.42
Cr	**97.88**	**-0.06**	1.30	-0.79	0.98	-1.20	86.16	-0.15	**97.34**	**-0.14**	6.08	-0.55	4.44	-0.77
Cu	31.88	-2.23	4.98	-3.43	69.68	-0.72	11.34	-2.76	38.06	-2.06	90.48	-0.40	33.82	-1.60
Fe	79.12	-0.47	**97.46**	**-0.09**	5.10	-0.88	95.22	-0.30	**99.36**	**-0.10**	**95.26**	**-0.22**	53.16	-0.43
K	23.20	-1.13	86.84	-0.19	**95.40**	**-0.19**	32.52	-0.82	22.14	-1.19	83.78	-0.37	93.54	-0.16
Li	19.52	-1.09	0.74	-3.05	94.12	-0.09	70.02	-0.40	73.66	-0.42	16.10	-1.07	92.72	-0.21
Mg	51.14	-1.25	73.72	-0.36	93.54	-0.31	39.54	-0.83	74.06	-0.69	23.44	-0.88	73.94	-0.47
Mn	1.66	-3.95	0.02	-5.45	60.52	-0.60	14.30	-1.33	1.20	-5.00	0.32	-4.34	0.30	-9.20
Na	3.10	-3.69	1.50	-3.24	2.02	-2.37	36.68	-0.91	44.12	-1.21	3.18	-2.23	8.16	-1.88
Ni	**97.80**	**-0.23**	1.10	-0.61	2.70	-0.42	**95.68**	**-0.17**	**99.16**	**-0.20**	**94.46**	**-0.16**	88.18	-0.33
Pb	1.16	-8.21	6.94	-1.21	81.62	-0.50	**97.62**	**-0.16**	7.68	-2.29	11.40	-1.54	0.86	-5.25
P	95.28	-0.49	92.54	-0.51	**98.72**	**-0.24**	0.22	-6.50	66.16	-1.17	0.90	-2.90	**95.68**	**-0.16**
Rb	79.30	-1.99	97.52	-0.28	54.86	-1.71	95.44	-0.34	89.24	-1.51	92.92	-0.58	**98.56**	**-0.12**
Sb	48.44	-1.07	44.44	-0.87	2.40	-2.47	96.54	-0.28	20.56	-1.71	95.82	-0.28	58.44	-0.78
Se	3.06	-2.18	0.12	-1.75	0.24	-2.35	0.90	-2.18	3.82	-1.82	0.68	-2.14	0.80	-2.05
S	**95.80**	**-0.15**	**94.34**	**-0.11**	79.68	-0.24	81.18	-0.25	84.02	-0.47	90.52	-0.15	**96.32**	**-0.08**
Sr	**96.96**	**-0.15**	72.88	-0.60	**95.82**	**-0.14**	59.58	-0.83	37.84	-1.85	92.10	-0.28	70.20	-0.58
Ti	98.32	-0.23	67.98	-0.61	**96.60**	**-0.15**	37.80	-1.27	98.56	-0.33	**96.34**	**-0.25**	77.14	-0.51
Tl	2.74	-3.92	**94.98**	**-0.13**	19.52	-1.40	1.24	-4.20	2.04	-4.66	4.26	-2.02	0.32	-7.15
V	15.20	-1.42	83.00	-0.25	91.78	-0.13	41.46	-0.72	19.18	-1.16	**95.10**	**-0.11**	**96.60**	**-0.13**
Zn	0.04	-14.81	**97.56**	**-0.17**	**96.96**	**-0.07**	3.30	-2.11	0.54	-5.12	1.34	-2.73	3.28	-2.01

	SST2													
	CR1	**CI1**	**CR 2**	**CI2**	**CR3**	**CI3**	**CR4**	**CI4**	**CR5**	**CI5**	**CR6**	**CI6**	**CR7**	**CI7**
^{137}Cs	**96.14**	**-0.16**	**97.50**	**-0.16**	**96.20**	**-0.14**	**98.82**	**-0.14**	**95.94**	**-0.16**	**97.54**	**-0.12**	**94.70**	**-0.16**
^{40}K	97.56	-0.30	58.94	-0.20	**96.62**	**-0.11**	85.60	-0.26	**97.92**	**-0.22**	82.46	-0.25	14.32	-0.64
^{226}Ra	**95.48**	**-0.17**	96.54	-0.50	**96.78**	**-0.16**	95.90	-0.38	88.02	-0.72	80.46	-0.89	35.64	-2.21
^{232}Th	85.96	-0.41	88.28	-0.59	**96.66**	**-0.15**	**96.98**	**-0.18**	95.02	-0.36	77.72	-0.78	57.20	-1.32
^{238}U	6.60	-1.79	98.44	-0.28	2.32	-3.00	10.74	-1.09	1.72	-3.28	70.68	-0.45	68.28	-0.65
χLF	98.06	-0.27	95.72	-0.45	**95.50**	**-0.22**	96.32	-0.41	94.24	-0.19	86.70	-0.20	86.42	-0.25
Al	**98.34**	**-0.11**	**98.78**	**-0.10**	**98.14**	**-0.11**	**98.50**	**-0.15**	**99.18**	**-0.09**	**98.54**	**-0.08**	**98.60**	**-0.25**
As	1.08	-1.49	91.74	-0.19	**96.16**	**-0.21**	8.38	-0.64	23.44	-0.60	67.34	-0.41	68.02	-0.53
Be	**97.90**	**-0.16**	69.28	-0.36	60.06	-0.36	63.12	-0.37	**98.44**	**-0.05**	93.40	-0.30	16.90	-1.27
Bi	65.60	-0.15	78.76	-0.14	93.22	-0.25	91.52	-0.22	**95.56**	**-0.14**	75.92	-0.36	58.46	-0.22
B	10.78	-0.42	15.64	-0.44	16.72	-0.36	24.02	-0.26	23.50	-0.37	**95.06**	**-0.08**	24.54	-0.38
Ca	94.70	-0.16	**98.64**	**-0.23**	**97.46**	**-0.10**	90.20	-0.10	96.06	-0.26	**96.80**	**-0.10**	86.98	-0.22
Cd	**98.30**	**-0.09**	**97.86**	**-0.21**	59.22	-0.73	54.08	-0.42	81.48	-0.57	90.52	-0.17	72.82	-0.73
Co	0.00	-18.32	0.00	-15.22	0.00	-19.23	0.00	-21.37	0.00	-16.84	0.00	-19.64	0.06	-13.44
Cr	16.70	-1.00	16.32	-1.24	8.68	-1.04	79.66	-0.11	49.44	-0.82	24.48	-0.81	8.50	-1.80
Cu	**98.08**	**-0.20**	52.86	-1.94	5.10	-4.78	92.70	-0.15	70.38	-1.44	87.20	-0.81	93.56	-0.76
Fe	26.48	-0.65	28.46	-0.59	90.26	-0.16	91.12	-0.27	**95.50**	**-0.09**	**98.08**	**-0.11**	5.74	-1.25
K	**97.26**	**-0.21**	48.68	-0.48	**97.04**	**-0.13**	72.66	-0.54	**98.36**	**-0.08**	**96.58**	**-0.05**	59.62	-0.64
Li	83.14	-0.45	86.80	-0.11	1.52	-2.11	5.72	-1.35	97.50	-0.26	8.24	-1.23	91.52	-0.19
Mg	**95.30**	**-0.23**	92.40	-0.19	34.62	-0.51	35.92	-0.55	74.20	-0.37	7.46	-1.12	**99.00**	**-0.09**
Mn	2.14	-5.03	4.06	-3.61	33.28	-1.05	9.94	-1.95	38.12	-1.56	1.26	-4.56	1.16	-6.61
Na	4.34	-0.98	12.36	-0.66	3.42	-0.71	5.98	-0.59	94.24	-0.18	64.18	-0.34	15.38	-0.74
Ni	55.32	-0.26	18.80	-0.81	7.52	-0.79	93.80	-0.17	78.42	-0.38	80.78	-0.20	**99.04**	**-0.12**
Pb	1.84	-2.09	8.82	-1.31	21.36	-0.69	0.80	-2.44	25.88	-0.83	51.48	-0.58	90.54	-0.25
P	83.12	-0.29	**97.50**	**-0.15**	70.86	-0.42	43.34	-0.42	89.44	-0.29	2.02	-2.13	87.20	-0.43
Rb	95.44	-0.30	96.64	-0.50	83.14	-0.89	67.74	-1.17	87.34	-0.96	69.98	-1.24	97.88	-0.35
Sb	16.26	-1.18	74.08	-0.48	**97.88**	**-0.04**	**96.28**	**-0.23**	**98.06**	**-0.22**	80.62	-0.52	**98.76**	**-0.20**
Se	6.58	-2.48	5.54	-2.60	3.26	-2.41	2.84	-2.12	9.22	-2.50	4.14	-2.24	5.00	-2.69
S	83.42	-0.11	85.22	-0.11	93.10	-0.11	82.40	-0.12	0.20	-4.59	**96.98**	**-0.14**	**98.22**	**-0.21**
Sr	84.20	-0.50	97.18	-0.32	90.64	-0.16	85.12	-0.31	0.38	-1.36	74.26	-0.38	32.50	-0.65
Ti	77.40	-0.83	90.26	-0.70	91.48	-0.39	91.38	-0.23	81.50	-0.98	90.54	-0.47	78.28	-1.30
Tl	0.34	-4.24	0.68	-3.40	12.46	-0.73	40.40	-0.55	21.90	-0.82	4.00	-1.05	45.78	-0.64
V	**97.92**	**-0.15**	29.26	-0.82	48.86	-0.40	**95.16**	**-0.22**	**95.66**	**-0.12**	88.20	-0.33	28.88	-0.88
Zn	0.42	-11.44	75.44	-0.54	**97.12**	**-0.15**	5.86	-2.01	0.46	-7.55	18.12	-1.74	21.32	-2.37

	CO													
	CR1	**CI1**	**CR 2**	**CI2**	**CR3**	**CI3**	**CR4**	**CI4**	**CR5**	**CI5**	**CR6**	**CI6**	**CR7**	**CI7**
^{137}Cs	**98.54**	**-0.11**	**99.80**	**-0.07**	**99.90**	**-0.15**	**99.64**	**-0.09**	**99.80**	**-0.17**	**99.18**	**-0.09**	**99.10**	**-0.20**
^{40}K	**97.82**	**-0.07**	**97.40**	**-0.19**	96.00	-0.35	94.96	-0.46	95.50	-0.39	**97.82**	**-0.23**	**99.00**	**-0.17**
^{226}Ra	96.92	-0.26	95.10	-1.47	98.70	-0.33	87.84	-1.17	75.70	-2.94	85.24	-1.15	2.90	-18.06
^{232}Th	**97.60**	**-0.21**	63.60	-1.18	91.20	-0.65	93.72	-0.23	99.60	-0.28	**99.30**	**-0.17**	98.20	-0.26
^{238}U	72.72	-0.84	93.50	-1.30	64.30	-2.06	11.50	-3.50	7.10	-5.16	16.90	-2.52	8.90	-5.52
χLF	91.18	-0.10	99.00	-0.30	**99.80**	**-0.20**	**99.50**	**-0.20**	**99.50**	**-0.13**	**97.70**	**-0.10**	97.60	-0.36
Al	**96.32**	**-0.19**	**97.80**	**-0.16**	83.60	-0.57	98.06	-0.25	**97.30**	**-0.17**	**95.48**	**-0.23**	97.70	-0.43
As	49.44	-0.48	99.20	-0.29	78.40	-0.46	67.28	-0.45	33.40	-0.92	25.78	-0.65	4.60	-1.84
Be	22.00	-1.12	6.70	-3.04	90.30	-0.72	93.10	-0.58	94.70	-0.86	**98.68**	**-0.11**	51.50	-1.57
Bi	**97.78**	**-0.14**	**98.40**	**-0.11**	99.00	-0.26	19.22	-1.02	65.00	-0.78	42.60	-0.65	73.50	-0.39
B	2.04	-1.06	3.80	-1.17	5.30	-1.06	68.86	-0.34	89.60	-0.34	78.16	-0.28	14.30	-1.18
Ca	81.16	-0.58	89.80	-0.53	80.60	-0.75	72.20	-0.64	67.00	-1.20	58.12	-0.78	**99.10**	**-0.13**
Cd	24.52	-1.62	65.70	-1.62	66.60	-1.62	2.50	-6.49	94.80	-0.78	**98.50**	**-0.22**	98.80	-0.38
Co	0.00	-32.36	0.00	-29.30	0.00	-35.60	0.00	-40.73	0.00	-41.07	0.00	-37.36	0.00	-26.69
Cr	0.48	-3.67	6.30	-2.88	18.90	-1.85	47.88	-1.23	70.00	-1.17	14.40	-1.52	20.20	-1.92
Cu	10.98	-7.25	11.30	-9.51	9.90	-8.32	31.70	-3.97	74.90	-2.43	33.30	-3.41	88.50	-1.38
Fe	0.98	-2.41	21.24	-1.73	90.90	-0.35	93.48	-0.59	98.40	-0.49	**97.12**	**-0.22**	59.00	-0.87
K	98.24	**-0.24**	66.50	-0.67	**99.50**	**-0.25**	43.50	-1.11	28.80	-1.64	77.96	-0.62	93.50	-0.34
Li	0.56	-4.16	6.40	-3.39	2.00	-3.85	0.44	-5.04	1.50	-4.03	0.40	-4.23	88.90	-0.28
Mg	11.16	-0.85	5.80	-1.33	5.10	-1.47	2.96	-2.02	12.60	-1.58	2.14	-1.57	43.70	-0.83
Mn	0.62	-18.78	47.00	-3.81	62.00	-2.89	1.90	-14.18	2.50	-15.55	0.88	-20.00	2.20	-16.99
Na	0.52	-2.36	0.10	-2.76	0.20	-2.95	9.16	-1.77	45.60	-1.02	6.22	-1.58	1.70	-2.63
Ni	1.78	-1.39	2.70	-1.86	11.20	-1.24	48.14	-0.53	72.50	-0.53	39.70	-0.71	93.80	-0.57
Pb	9.08	-1.31	1.90	-3.66	3.10	-2.75	46.36	-1.05	75.50	-0.92	**98.82**	**-0.05**	**99.00**	**-0.08**
P	**98.82**	**-0.17**	**99.60**	**-0.10**	**99.10**	**-0.16**	8.32	-2.36	2.90	-3.42	1.84	-2.56	**99.60**	**-0.08**
Rb	66.68	-1.02	80.90	-2.39	59.70	-2.79	44.68	-2.50	79.00	-1.83	71.06	-1.10	71.30	-2.16
Sb	5.72	-3.11	89.70	-1.30	61.70	-1.52	30.82	-2.02	74.20	-1.52	37.78	-1.52	62.70	-1.52
Se	0.84	-4.16	2.80	-3.91	3.50	-3.96	10.94	-3.02	17.40	-3.26	3.88	-3.24	5.20	-3.91
S	**95.90**	**-0.09**	**99.30**	**-0.04**	**98.10**	**-0.23**	**98.60**	**-0.23**	16.70	-2.04	97.12	-0.31	80.10	-0.81
Sr	27.14	-1.23	92.60	-0.68	94.10	-0.70	33.94	-1.46	56.80	-1.45	22.16	-1.46	8.60	-2.37
Ti	**98.82**	**-0.15**	77.90	-2.05	86.40	-1.17	**98.12**	**-0.21**	**98.70**	**-0.19**	67.38	-0.97	64.70	-2.31
Tl	90.26	-0.30	6.00	-1.12	4.50	-1.32	**98.32**	**-0.09**	**99.10**	**-0.20**	90.52	-0.35	94.80	-0.46
V	19.18	-1.10	6.60	-2.40	84.50	-0.57	98.16	-0.25	98.90	-0.25	91.54	-0.20	66.60	-1.08
Zn	88.82	-0.30	94.80	-0.76	96.00	-0.30	50.66	-1.58	43.10	-2.35	9.98	-2.81	0.30	-17.34

On the contrary, the highest silt contents during the sampling campaigns when fields are fully covered by crops suggest that less fine sediment is reaching the streams and that the sediment mobilised is coarser likely related with the higher rainfall amounts (Fig. 6). Most of the croplands are distributed surrounding the main stream, thus full plant covered fields likely minimise the sediment exported by other sources in the areas that are not directly connected with the streams that store sediments during these periods. The lower clay contents and the significantly higher silt content at the CO also indicate that higher discharge and transport capacity downstream increase the transport of coarser fractions and associated elements. Besides, the presence of heavy metals along with As, S, P and ^{238}U in the SSM with contents above the range of the sources and following the agricultural cycle points out to the anthropogenic origin of these pollutants. Furthermore, the overall decrease in the fine fraction while sample weight increases suggest a possible scenario of clay and related elements export and the subsequent downstream pollution (Karageorgis et al., 2003) favoured by the association of lithogenic radionuclides such as ^{238}U with the clay fractions (Navas et al., 2002b, 2011) and the radionuclide mobility observed in similar environments (Navas et al., 2005).

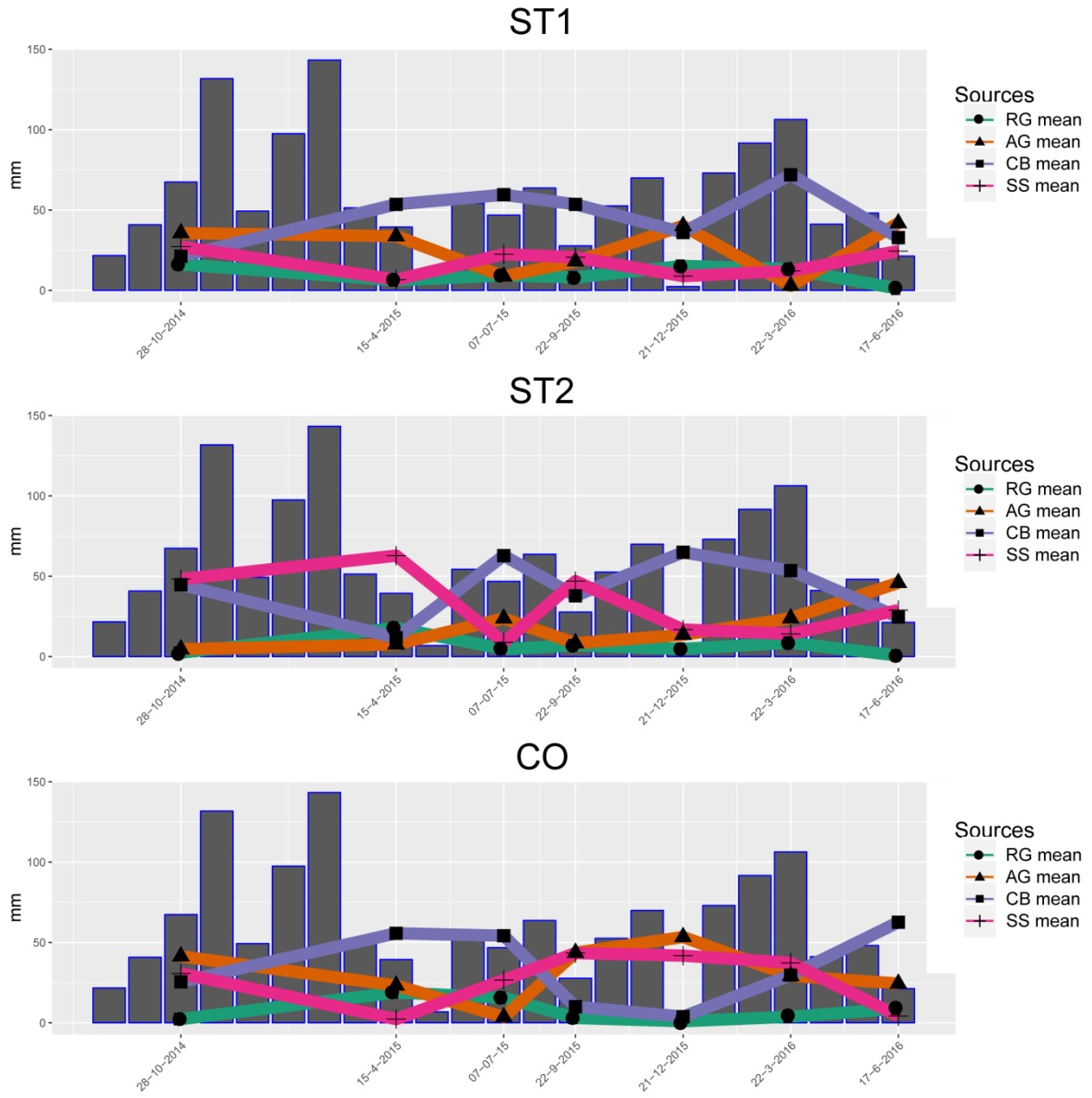

Fig. 6. Mean sediment source contributions modelled with FingerPro for the three sampling stations during the seven seasonal campaigns.

4.2. Conservativeness and consensus message of the studied tracers

As it can be seen in Table 3, the conservativeness and consensus method shows how the tracers unusually enriched or depleted are classified as low consensual and non-conservative tracers. First, the tracers unusually enriched or depleted show a lower value of CI than the assumed limits of this study. Thus, these tracers are not selected for the unmixing modelling. Secondly, the tracers that are in the appropriate range, but did not fit the

consensus standards are assumed as dissenting tracers and excluded to avoid uncertainties and likely erroneous model results. The high contents of P in the 4th seasonal campaign at ST1 lead to exclude P as tracer for unmixing. Then, the lack of tracers that clearly discriminate the agricultural land likely produced in this mixture reduces AG source apportions. Thus, the increase of bare soil surface in croplands along with the agricultural management that mobilise sediment during the 3rd seasonal campaign and the important increases in P, As and fine fraction contents likely suggest that the AG contribution is underestimated by the model in this campaign highlighting the impact of pollutants in the unmixing modelling.

	Seasonal campaign	RG		AG		CB		SS		GOF	
ST 1		mean	sd	mean	sd	mean	sd	mean	sd	mean	sd
	1st	0.161	0.129	0.356	0.182	0.212	0.147	0.272	0.089	0.898	0.034
	2nd	0.062	0.066	0.337	0.165	0.535	0.133	0.066	0.071	0.934	0.040
	3rd	0.093	0.114	0.087	0.079	0.595	0.145	0.225	0.128	0.893	0.054
	4th	0.080	0.054	0.180	0.100	0.535	0.152	0.206	0.097	0.951	0.022
	5th	0.152	0.091	0.401	0.166	0.360	0.149	0.088	0.059	0.912	0.025
	6th	0.132	0.038	0.028	0.073	0.719	0.129	0.121	0.104	0.977	0.021
	7th	0.010	0.026	0.418	0.155	0.328	0.200	0.244	0.151	0.866	0.055
ST 2											
	1st	0.024	0.034	0.046	0.066	0.447	0.165	0.482	0.136	0.938	0.052
	2nd	0.178	0.103	0.076	0.069	0.117	0.108	0.628	0.115	0.866	0.036
	3rd	0.047	0.067	0.237	0.096	0.628	0.191	0.088	0.107	0.930	0.050
	4th	0.070	0.021	0.083	0.069	0.378	0.102	0.469	0.087	0.995	0.012
	5th	0.048	0.077	0.136	0.093	0.649	0.157	0.168	0.080	0.890	0.041
	6th	0.086	0.065	0.238	0.099	0.535	0.130	0.141	0.053	0.914	0.032
	7th	0.006	0.024	0.459	0.100	0.246	0.136	0.289	0.096	0.929	0.042
CO											
	1st	0.023	0.037	0.414	0.060	0.255	0.210	0.307	0.175	0.885	0.039
	2nd	0.189	0.091	0.232	0.067	0.557	0.111	0.023	0.052	0.835	0.027
	3rd	0.156	0.062	0.036	0.069	0.542	0.237	0.266	0.188	0.874	0.060
	4th	0.030	0.053	0.436	0.110	0.100	0.124	0.434	0.113	0.917	0.039
	5th	0.010	0.027	0.534	0.066	0.038	0.080	0.418	0.088	0.873	0.039
	6th	0.038	0.067	0.292	0.107	0.297	0.201	0.373	0.150	0.871	0.030
	7th	0.088	0.069	0.244	0.077	0.626	0.131	0.042	0.067	0.901	0.032

Table 4. Mean and standard deviation percentages source contributions from the FingerPro model for rangeland (RG), agricultural (AG), subsoil (SS) and channel bank (CB) to the mixture samples.

By applying the new consensus method, it is possible to detect atypical enriched tracers and ascertain a likely underestimation of AG apportion in SCB1. Therefore, careful attention must be paid during unmixing modelling, especially for the tracer selection. The new method offers great potential for the quality information that delivers for each tracer in each mixture. As seen in Table 3 during the sowing period the enriched tracers S and P clearly show non-conservative and non-consensual behaviour as indicated by the important change in average values of CI and CR during the seasonal campaigns. With this complementary information it appears that these tracers were unnaturally enriched during these campaigns in comparison with other elements that do not show such large variations in their CR values. However, the exclusion of tracers that efficiently discriminate one of the sources could influence the results and mislead the models by reducing or increasing the underrepresented source.

4.3. Main drivers of sediment source contribution

Channel banks are the main contributing source due to its proximity to the active water flow. Despite that stream talus are deeper and steeper at the lower part of the catchment close to the outlet, the increase of cropland surface and the location of most crops surrounding the principal and secondary streams produce significant AG sediment inputs, especially when crops remain unprotected due to the absence of vegetation cover. Thus, the high concordance between the SSM sample weights, the accumulated rainfall and the surface area of the bare soil in croplands during the seven seasonal campaigns suggest that the main drivers of sediment export are both the stages of vegetation cover in croplands and rainfall. On the other hand, the lowest AG contribution during most seasonal campaigns recorded in ST2 agrees with the lowest surface of bare soil in croplands. Lizaga et al. (2019a), found SS as one of the main contributing sources in this part of the catchment due to the proximity of steep slopes with highly disturbed areas and the predominance of bare soils as it can be seen in Fig. 1. Besides, most of the cultivated fields in SBC2 are located at the headwaters instead of surrounding the main streams as in SBC1 and SBC3. Furthermore, during the second agricultural cycle several fields in SBC2 were left fallow. However, a slight increase in AG source contribution was observed during the 7th seasonal campaign. This increase coincides with the plough of the fields surrounding the main streams that were left fallow in SBC2 during the previous agricultural cycle. For this reason, instead of a progressive decreasing trend in AG

sediment contributions due to vegetation growth as in SBC3, a progressive increasing trend in AG sediment contributions occurs. Finally, ST1 shows a progressive decreasing trend in AG contribution in the first agricultural cycle from the 1st to the 3th seasonal campaigns that coincide with the vegetation growth while an increase from the 3th to the 5th campaigns occurs when the highest surface of bare soil in croplands happen. Similar behaviour than in ST2 was observed during the 7th seasonal campaign coinciding with the plough of the fields that were left fallow.

5. Conclusions

The study of a medium-size catchment during two hydrological years with fingerprinting methods has emphasised the great impact of agricultural activities and the agricultural cycle in the suspended sediment and pollutants exported to the streams. The positive correlation between the cropland area and the sediment mixture weights confirm the influence of the agricultural practices as the primary driver of rising sediment exports rates. The enrichment above sources ranges detected in the suspended sediment mixtures of some elements such as As, Co, Li, Mn, Zn, ^{238}U and P, and their higher increase during sowing and after harvest periods points to the important impact of agricultural activities on supplying sediment and pollutants to the streams.

This work has revealed that the consensus method ensures the exclusion of non-conservative and dissenting tracers. CI and CR methods were successful in detecting the optimum set of tracers in the 21 unmixing runs. The consensus-based method highlighted the elements with similar behaviour and the ones occasionally enriched or depleted. The method provides a broader and easier application in fingerprinting studies creating an agreement in tracer selection methodologies. The results of the unmixing modelling highlights the increase in AG sediment provenance during sowing and after harvest periods, underlining the lower AG contribution in the subcatchment with less bare soil area.

The evidence from this study suggests that the agricultural practices are the main drivers of the variability of sediment export in mountain agroecosystems for regular hydrological years as the ones of the study period. These findings report the effect of human activities in mountain agroecosystems and shed new light about the periods when most pollutants are supplied to streams. From these results, conservation practices are recommended to land users and policymakers to ensure the protection of cropland soils, especially in periods of absence of vegetation cover to prevent the loss of fertile soil and the export of pollutants to water bodies.

Acknowledgements
This work has been supported by project CGL2014-52986-R funded by the Spanish Ministry of Science, Innovation and Universities and the aid of a predoctoral contract (BES-2015-071780).

References

Beguería, S., Angulo-Martínez, M., Gaspar, L., Navas, A. 2015. Detachment of soil organic carbon by rainfall splash: Experimental assessment on three agricultural soils of Spain. Geoderma, 245–246:21–30. doi: 10.1016/j.geoderma.2015.01.010

Casado, J., Brigden, K., Santillo, D., Johnston, P., 2019. Screening of pesticides and veterinary drugs in small streams in the European Union by liquid chromatography high resolution mass spectrometry. Science of The Total Environment 670, 1204–1225. https://doi.org/10.1016/j.scitotenv.2019.03.207

Collins, A.L., Pulley, S., Foster, I.D.L., Gellis, A., Porto, P., Horowitz, A.J., 2017. Sediment source fingerprinting as an aid to catchment management: A review of the current state of knowledge and a methodological decision-tree for end-users. Journal of Environmental Management, Sediment source fingerprinting for informing catchment management: methodological approaches, problems and uncertainty 194, 86–108. https://doi.org/10.1016/j.jenvman.2016.09.075

Collins, A.L., Walling, D.E., 2002a. Selecting fingerprint properties for discriminating potential suspended sediment sources in river basins. Journal of Hydrology 261, 218–244. https://doi.org/10.1016/S0022-1694(02)00011-2

Collins, A.L., Walling, D.E., 2002b. Selecting fingerprint properties for discriminating potential suspended sediment sources in river basins. Journal of Hydrology 261, 218–244. https://doi.org/10.1016/S0022-1694(02)00011-2

Estrany, J., Garcia, C., Walling, D.E., 2010. An investigation of soil erosion and redistribution in a Mediterranean lowland agricultural catchment using caesium-137. International Journal of Sediment Research 25, 1–16. https://doi.org/10.1016/S1001-6279(10)60023-6

Evrard, O., Poulenard, J., Némery, J., Ayrault, S., Gratiot, N., Duvert, C., Prat, C., Lefèvre, I., Bonté, P., Esteves, M., 2013. Tracing sediment sources in a tropical highland catchment of central Mexico by using conventional and alternative fingerprinting methods. Hydrol. Process. 27, 911–922. https://doi.org/10.1002/hyp.9421

Gaspar, L., Navas, A., Walling, D.E., Machín, J. Gómez Arozamena, J. 2013. Using 137Cs and 210Pbex to assess soil redistribution on slopes at different temporal scales. Catena, 102: 46-54. DOI: 10.1016/j.catena.2011.01.004

Gaspar, L., Blake, W.H., Smith, H.G., Lizaga, I., Navas, A., 2019a. Testing the sensitivity of a multivariate mixing model using geochemical fingerprints with artificial mixtures. Geoderma 337, 498–510. https://doi.org/10.1016/j.geoderma.2018.10.005

Gaspar, L., Lizaga, I., Blake, W.H., Latorre, B., Quijano, L., Navas, A., 2019b. Fingerprinting changes in source contribution for evaluating soil response during an exceptional rainfall in Spanish pre-pyrenees. Journal of Environmental Management 240, 136–148. https://doi.org/10.1016/j.jenvman.2019.03.109

Gaspar, L., Quijano, L., Lizaga, I., Navas, A., 2019c. Effects of land use on soil organic and inorganic C and N at 137Cs traced erosional and depositional sites in mountain agroecosystems. Catena 181, 104058. https://doi.org/10.1016/j.catena.2019.05.004

Gateuille, D., Owens, P.N., Petticrew, E.L., Booth, B.P., French, T.D., Déry, S.J., 2019. Determining contemporary and historical sediment sources in a large drainage basin impacted by cumulative effects: the regulated Nechako River, British Columbia, Canada. J Soils Sediments 19, 3357–3373. https://doi.org/10.1007/s11368-019-02299-2

Gómez, J.A., Guzmán, M.G., Giráldez, J.V., Fereres, E., 2009. The influence of cover crops and tillage on water and sediment yield, and on nutrient, and organic matter losses in an olive orchard on a sandy loam soil. Soil and Tillage Research 106, 137–144. https://doi.org/10.1016/j.still.2009.04.008

Hamza, M.A., Anderson, W.K., 2005. Soil compaction in cropping systems: A review of the nature, causes and possible solutions. Soil and Tillage Research 82, 121–145. https://doi.org/10.1016/j.still.2004.08.009

Karageorgis, A.P., Nikolaidis, N.P., Karamanos, H., Skoulikidis, N., 2003. Water and sediment quality assessment of the Axios River and its coastal environment. Continental Shelf Research, European Land-Ocean Interaction 23, 1929–1944. https://doi.org/10.1016/j.csr.2003.06.009

Klages, M.G., Hsieh, Y.P., 1975. Suspended Solids Carried by the Gallatin River of Southwestern Montana: II. Using Mineralogy for Inferring Sources. Journal of Environmental Quality 4, 68–73. https://doi.org/10.2134/jeq1975.00472425000400010016x

Lizaga, I., Quijano, L., Palazón, L., Gaspar, L., Navas, A. 2018a. Enhancing connectivity index to assess the effects of land use changes in a Mediterranean catchment. Land Degradation and Development. 29: 663–675. DOI: 10.1002/ldr.2676

Lizaga, I., Quijano, L., Gaspar, L., Navas, A., 2018b. Estimating Soil Redistribution Patterns with 137Cs Measurements in a Mediterranean Mountain Catchment Affected by Land Abandonment. Land Degrad Develop, 29: 105–117. https://doi.org/10.1002/ldr.2843

Lizaga, I., Gaspar, L., Blake, W.H., Latorre, B., Navas, A., 2019a. Fingerprinting changes of source apportionments from mixed land uses in stream sediments before and after an exceptional rainstorm event. Geomorphology 341, 216–229. https://doi.org/10.1016/j.geomorph.2019.05.015

Lizaga, I., Gaspar, L., Quijano, L., Dercon, G., Navas, A., 2019b. NDVI, 137Cs and nutrients for tracking soil and vegetation development on glacial landforms in the Lake Parón Catchment (Cordillera Blanca, Perú). Science of The Total Environment 651, 250–260. https://doi.org/10.1016/j.scitotenv.2018.09.075

Lizaga, I., Quijano, L., Gaspar, L., Ramos, M.C., Navas, A., 2019c. Linking land use changes to variation in soil properties in a Mediterranean mountain agroecosystem. Catena 172, 516–527. https://doi.org/10.1016/j.catena.2018.09.019

Lizaga, I., Latorre, B., Gaspar, L., Navas, A., 2020. Consensus ranking as a method to identify non-conservative and dissenting tracers in fingerprinting studies. Science of The Total Environment.

Martínez-Carreras, N., Krein, A., Gallart, F., Iffly, J.F., Pfister, L., Hoffmann, L., Owens, P.N., 2010. Assessment of different colour parameters for discriminating potential suspended sediment sources and provenance: A multi-scale study in Luxembourg. Geomorphology 118, 118–129. https://doi.org/10.1016/j.geomorph.2009.12.013

Meusburger, K., Porto, P., Mabit, L., La Spada, C., Arata, L., Alewell, C., 2018. Excess Lead-210 and Plutonium-239+240: Two suiTable radiogenic soil erosion tracers for mountain grassland sites. Environmental Research 160, 195–202. https://doi.org/10.1016/j.envres.2017.09.020

National Research Council, 1993. Soil and Water Quality: An Agenda for Agriculture. The National Academies Press, Washington, DC. https://doi.org/10.17226/2132

Navas, A., Machín, J. 2002. Spatial distribution of heavy metals and arsenic in soils of Aragón (northeast Spain): controlling factors and environmental implications. Applied Geochemistry, 17: 961-973.

Navas, A., Soto, J., Machín, J. 2002. Edaphic and physiographic factors affecting the distribution of natural gamma-emitting radionuclides in the soils of the Arnás catchment in the Central Spanish Pyrenees. European Journal of Soil Science, 53: 629-638.

Navas, A., Valero Garcés, B., Machín, J., 2004. An approach to integrated assessement of reservoir siltation: the Joaquín Costa reservoir as a case study. Hydrology and Earth System Sciences 8, 1193–1199. https://doi.org/10.5194/hess-8-1193-2004

Navas, A., Soto, J., Machín, J. 2005. Mobility of natural radionuclides and selected major and trace elements along a soil toposequence in the central Spanish Pyrenees. Soil Science, 170 (9): 743-757.

Navas, A., Gaspar, L., López-Vicente, M., Machín, J. 2011. Spatial distribution of natural and artificial

agroecosystems (NE Spain). Science of the Total Environment, 496: 132-143. doi:10.1016/j.scitotenv.2014.07.026

Navas, A., Quine, T.A., Walling, D.E., Gaspar, L., Quijano, L., Lizaga, I., 2017. Relating Intensity of Soil Redistribution to Land Use Changes in Abandoned Pyrenean Fields Using Fallout Caesium-137. Land Degradation & Development 28, 2017–2029. https://doi.org/10.1002/ldr.2724

Owens, P.N., Blake, W.H., Gaspar, L., Gateuille, D., Koiter, A.J., Lobb, D.A., Petticrew, E.L., Reiffarth, D.G., Smith, H.G., Woodward, J.C., 2016. Fingerprinting and tracing the sources of soils and sediments: Earth and ocean science, geoarchaeological, forensic, and human health applications. Earth-Science Reviews 162, 1–23. https://doi.org/10.1016/j.earscirev.2016.08.012

Palazón, L., Gaspar, L., Latorre, B., Blake, W.H., Navas, A., 2015a. Identifying sediment sources by applying a fingerprinting mixing model in a Pyrenean drainage catchment. J Soils Sediments 15, 2067–2085. https://doi.org/10.1007/s11368-015-1175-6

Palazón, L., Latorre, B., Gaspar, L., Blake, W.H., Smith, H.G., Navas, A., 2015b. Comparing catchment sediment fingerprinting procedures using an auto-evaluation approach with virtual sample mixtures. Science of The Total Environment 532, 456–466. https://doi.org/10.1016/j.scitotenv.2015.05.003

Phillips, D.L., Gregg, J.W., 2003. Source partitioning using sTable isotopes: coping with too many sources. Oecologia 136, 261–269. https://doi.org/10.1007/s00442-003-1218-3

Phillips, J.M., Russell, M.A., Walling, D.E., 2000. Time-integrated sampling of fluvial suspended sediment: a simple methodology for small catchments. Hydrological Processes 14, 2589–2602. https://doi.org/10.1002/1099-1085(20001015)14:14<2589::AID-HYP94>3.0.CO;2-D

Prashar, P., Shah, S., 2016. Impact of Fertilizers and Pesticides on Soil Microflora in Agriculture, in: Lichtfouse, E. (Ed.), Sustainable Agriculture Reviews: Volume 19. Springer International Publishing, Cham, pp. 331–361. https://doi.org/10.1007/978-3-319-26777-7_8

Pulley, S., Foster, I., Antunes, P., 2015. The uncertainties associated with sediment fingerprinting suspended and recently deposited fluvial sediment in the Nene river basin. Geomorphology 228, 303–319. https://doi.org/10.1016/j.geomorph.2014.09.016

Quesada, S., Tena, A., Guillén, D., Ginebreda, A., Vericat, D., Martínez, E., Navarro-Ortega, A., Batalla, R.J., Barceló, D., 2014. Dynamics of suspended sediment borne persistent organic pollutants in a large regulated Mediterranean river (Ebro, NE Spain). Science of The Total Environment 473–474, 381–390. https://doi.org/10.1016/j.scitotenv.2013.11.040

Quijano, L., Kuhn, N.J., Navas, A., 2020. Effects of interrill erosion on the distribution of soil organic and inorganic carbon in different sized particles of Mediterranean Calcisols. Soil & Tillage Research, 196: 104461 https://doi.org/10.1016/j.still.2019.104461.

Quijano, L., Kuhn, N.J., Navas, A., 2019. Soil particle size distribution and induced soil carbon transport by ephemeral gully erosion in Mediterranean mountain arable land. Earth Surface Processes and Landforms. DOI: 10.1002/esp.4703

Quijano, L., Beguería, S., Gaspar, L., Navas, A., 2016. Estimating erosion rates using 137Cs measurements and WATEM/SEDEM in a Mediterranean cultivated field. CATENA 138, 38–51. https://doi.org/10.1016/j.catena.2015.11.009

Ruiz-Colmenero, M., Bienes, R., Eldridge, D.J., Marques, M.J., 2013. Vegetation cover reduces erosion and enhances soil organic carbon in a vineyard in the central Spain. CATENA 104, 153–160. https://doi.org/10.1016/j.catena.2012.11.007

Schillaci, C., Acutis, M., Lombardo, L., Lipani, A., Fantappiè, M., Märker, M., Saia, S., 2017. Spatio-temporal topsoil organic carbon mapping of a semi-arid Mediterranean region: The role of land use, soil texture, topographic indices and the influence of remote sensing data to modelling. Science of The Total Environment 601–602, 821–832. https://doi.org/10.1016/j.scitotenv.2017.05.239

Schuller, P., Walling, D.E., Iroumé, A., Quilodrán, C., Castillo, A., Navas, A., 2013. Using 137Cs and 210Pbex and other sediment source fingerprints to document suspended sediment sources in small forested catchments in south-central Chile. Journal of Environmental Radioactivity 124, 147–159. https://doi.org/10.1016/j.jenvrad.2013.05.002

Sharma, N., Singhvi, R., 2017. Effects of Chemical Fertilizers and Pesticides on Human Health and Environment: A Review. International Journal of Agriculture, Environment and Biotechnology 10, 675. https://doi.org/10.5958/2230-732X.2017.00083.3

Smith, H.G., Blake, W.H., 2014. Sediment fingerprinting in agricultural catchments: A critical re-examination of source discrimination and data corrections. Geomorphology 204, 177–191. https://doi.org/10.1016/j.geomorph.2013.08.003

Smith, J.A., Mazumder, D., Suthers, I.M., Taylor, M.D., 2013. To fit or not to fit: evaluating sTable isotope mixing models using simulated mixing polygons. Methods in Ecology and Evolution 4, 612–618. https://doi.org/10.1111/2041-210X.12048

Useya, J., Chen, S., 2019. Exploring the Potential of Mapping Cropping Patterns on Smallholder Scale Croplands Using Sentinel-1 SAR Data. Chin. Geogr. Sci. 29, 626–639. https://doi.org/10.1007/s11769-019-1060-0

Walling, D.E., Peart, M.R., Oldfield, F., Thompson, R., 1979. Suspended sediment sources identified by magnetic measurements. Nature 281, 110–113. https://doi.org/10.1038/281110a0

Walling, D.E., Woodward, J.C., 1995. Tracing sources of suspended sediment in river basins: a case study of the River Culm, Devon, UK. Marine and Freshwater Research 46, 327–336.

Wang, J., Ding, J., Yu, D., Ma, X., Zhang, Z., Ge, X., Teng, D., Li, X., Liang, J., Lizaga, I., Chen, X., Yuan, L., Guo, Y., 2019. Capability of Sentinel-2 MSI data for monitoring and mapping of soil salinity in dry and wet seasons in the Ebinur Lake region, Xinjiang, China. Geoderma 353, 172–187. https://doi.org/10.1016/j.geoderma.2019.06.040

Yu, L., Oldfield, F., 1989. A multivariate mixing model for identifying sediment source from magnetic measurements. Quaternary Research 32, 168–181. https://doi.org/10.1016/0033-5894(89)90073-2

CHAPTER 10

CSSI for tracking the provenance of sediments in a mediterranean agroecosystem under intense land cover changes

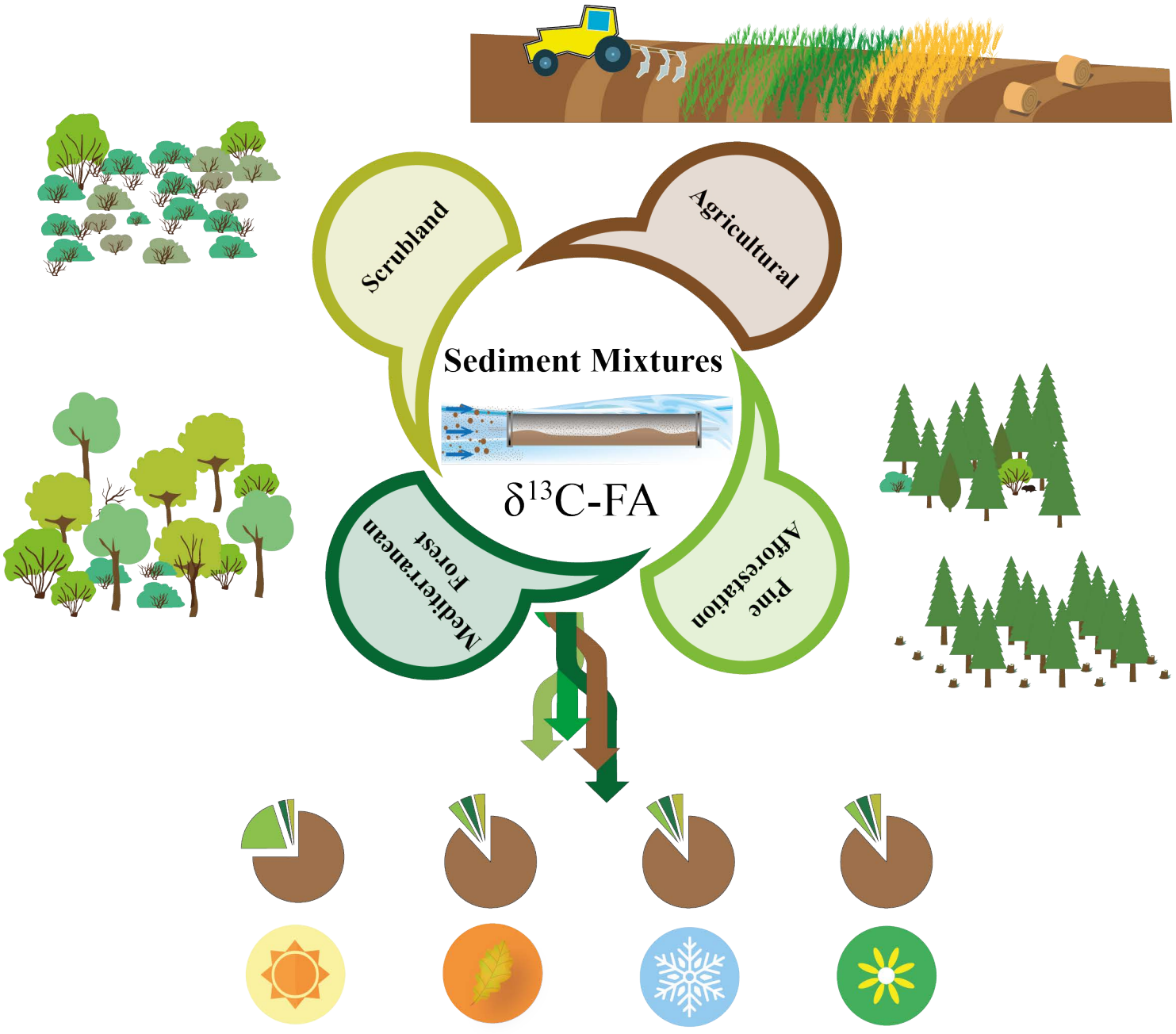

CSSI for tracking the provenance of sediments in a mediterranean agroecosystem under intense land cover changes

Ivan Lizaga [a]*, Samuel Bodé [b], Leticia Gaspar [a], Borja Latorre [a], Pascal Boeckx [b], Ana Navas [a]*

a Estación Experimental de Aula-Dei (EEAD-CSIC), Spanish National Research Council, Zaragoza, Spain. Avenida Montañana, 1005, 50059 Zaragoza (Spain).
b Isotope Bioscience Laboratory - ISOFYS, Faculty of Bioscience Engineering, Ghent University, Coupure Links 653, 9000 Gent, Belgium.

ABSTRACT

A Compound Specific Stable Isotope (CSSI) sediment tracing approach is evaluated for the first time in Mediterranean mountain agroecosystems subjected to intense land use changes in the past decades. Mediterranean mountain environments have suffered the conversion of rangelands into croplands during the previous centuries to increase agricultural production. Among side effects, conversion lands practices have increased the risk of erosion and in severe conditions have led to loss of fertile topsoil. After land abandonment the process was reversed during the middle of the XXth century, allowing the recovery of vegetation and subsequent variation in land cover and soil erosion rates.

This work aims to assess the potential of FAs to discriminate vegetation covers in complex landscapes subjected to land cover changes after generalised land abandonment. We attempt to evaluate for the first time the soil response in highly altered agroforestry systems by applying state of the art sediment fingerprinting techniques along with compound-specific stable isotopes (CSSI) as tracers. The MixSIAR model with concentration dependence is applied for unmixing CSSI in suspended sediments mixtures collected in a medium-sized Mediterranean agroforestry catchment. To this purpose, 30 composite sediment sources were collected over the four main land covers existing in the study area: cropland, Mediterranean forest, pine afforestation forest, scrubland, and two main geomorphic elements: subsoil and channel bank. To analyse the variability of source contributions from the headwaters to the outlet of the catchment during one year sampling period, three sampling points with three replicates were established for collecting suspended sediments mixtures. The fatty acids (FAs) concentrations were significantly higher at the catchment outlet than at the headwaters. Most of the mixture samples were below the sources range for the majority of FAs. The δ^{13}C-FAs were successful in discriminating between Mediterranean forest, scrubland, pine afforestation and both geomorphic elements. Overall, the unmixing model results identify agricultural land cover as the largest contributing source for most seasonal campaigns. The inclusion of prior information increases the agricultural contributions in detriment to the other sources except for subsoil. The results of this study likely suggest that additional tracers are needed to correctly assess channel bank and subsoil contributions. The high agricultural apportionments point out to the impact of human activities and the agriculture cycle in these mountain agroecosystems.

Keywords:
Compound Specific Stable Isotope (CSSI)
Fatty acids (FAs)
Sediment source fingerprinting
Concentration dependence
Land cover changes

1. Introduction

The significant increase in fine sediment transport to water bodies has been confirmed as one of the most prevalent contaminants in aquatic biomes, compromising human water supplies and being a major cause of reservoir siltation (Navas et al., 2004). Soil is a valuable natural resource that performs crucial ecosystem functions and is vital to meet the food need for the growing world population (Costanza et al., 1997). At present, soil formation is an estimated 10–40 times less than soil erosion rates what represents a main threat because the loss of fertile topsoil leads to the subsequent reduction in agricultural productivity. In turn, soil losses are directly related with increases in sediment export rates (Borrelli et al., 2017).

In order to mitigate the impacts of soil loss and the associated sediment exports to water bodies, reliable quantitative information on fine-grained sediment sources is required. Nevertheless, determining the sediment provenance in catchments is often challenging and requires expensive monitoring stations challenging to install in remote areas. In

this regard, Klages and Hsieh. (1975) and Clarke (2014) pursued preliminary studies tracking the source of sediments developing the technique known as fingerprinting. The initial fingerprinting investigations were essentially qualitative in their result, but the introduction of quantitative mixing models enabled researchers to obtain quantitative results of the relative contribution from different sediment sources (Collins et al., 1997; Walling, 2005). Since these early works, sediment source fingerprinting applications have been greatly expanding with the development of new techniques (Owens et al., 2016). To date, there are several studies on identifying source apportions by fingerprinting techniques (Gruszowski et al., 2003; Clarke, 2014; Palazón et al., 2015a). The increasing complexity of the studies promoted including additional tracers to fulfil the basics of the technique. A wide range of sediment-properties has been implemented as fingerprinting tracers such as radionuclides (Evrard et al., 2013; Palazón et al., 2015a), geochemical properties (Smith et al., 2013; Mabit et al., 2014; Wynants et al., 2020) and magnetic properties (Martínez-Carreras et al., 2010). While these tracers can provide accurate estimates of source apportionment as was proved by Gaspar et al. (2019a), they are restricted in their capability to discriminate between different land uses especially those with vegetation cover in some specific ecosystems. This is particularly evident in areas where the lithology is homogenous, and most of the variability of the sources is introduced by the type of vegetation (Gellis and Walling, 2013; Hancock and Revill, 2013).

Recent research has proposed plant-specific organic molecules that exist in sediment as a new effective isotopic fingerprinting approach for land-use-specific sediment source identification (Gibbs, 2008; Gibbs, 2013). To this purpose, the use of compound-specific stable isotope (CSSI) of very long-chain fatty acids (VLCFAs) has emerged as a suitable alternative to the previously analysed tracers (Reiffarth et al., 2016, 2019). Recent research use the CSSI signatures of soil organic biomarkers such as natural fatty acids (Blake et al., 2012; Alewell et al., 2016; Upadhayay et al., 2017; Bravo-Linares et al., 2018; Mabit et al., 2018; Lavrieux et al., 2019) to obtain the sediment export apportionments from various land uses.

The land use is usually defined by the plants growing in the land. These plants tend to modify soil properties and exude different biomarkers (Reiffarth et al., 2016). Most plant species produce a similar range of organic compounds but with different isotopic signatures $\delta^{13}C$ (Tolosa et al., 2013). Thus, for fingerprinting studies, the CSSI technique relies on the determination of the $\delta^{13}C$ signatures of particular soil organic compounds (i.e. FAs) (Mabit et al., 2018). An additional quality of the technique is the ratio conservatism. The isotopic signature is fully conservative from sources to the mixture in contrast to concentration. The CSSI technique exploits differences in the stable isotope signature of individual biotracers to recognise the areas prone to erosion and those that export high quantities of sediment to water supplies (Blake et al., 2012; Cooper et al., 2015; Alewell et al., 2016; Upadhayay et al., 2018; Reiffarth et al., 2019).

The likely limited capabilities of traditionally implemented tracers to effectively discriminate between different land covers growing on similar substrates was detected in a Mediterranean agroecosystem by Lizaga et al. (2019a). Thus, the low geochemical discrimination by the same shared lithology for pine afforestation and Mediterranean forest forced merging both sources. In this context, the present paper aims to validate for the first time the utility of CSSI as an improvement in the discrimination of land covers developed on similar lithology in an agroforestry mountain catchment subjected to highly dynamic changes in land cover and land uses.

We aim to assess the usefulness of state of the art techniques implemented for the use of CSSI in fingerprinting studies in Mediterranean landscapes. Our research evaluates the sediment provenance during one hydrological year (June 2016 to June 2017) from the headwaters to the catchment outlet in a representative agroforestry catchment. To this purpose, a total of 66 samples, including 30 sediment sources and 36 suspended sediment mixtures were collected to characterize the system, and the following four steps are carried out: i) the selection of suitable tracers by applying the within a polygon approach or mixing polygon (Phillips and Gregg, 2003); ii) evaluate the capability of $\delta^{13}C$ Fatty Acids as fingerprinting tracers; iii) apply the MixSIAR model implementing the concentration dependence; iv) evaluate the use of informative priors in the unmixing model result. Our results will contribute to gain knowledge on the main factors leading to sediment export in complex and highly dynamic landscapes.

2. METHODOLOGY

2.1 Study Area

The study catchment with a total area of 23 km^2 is drained by an ephemeral stream tributary of the Arba River located in the Pre-Pyrenean range (Fig. 1). The Barués catchment structure is dominated by the low angle dip sandstones of the Uncastillo Miocene formation bedding and the presence of a Quaternary glacis located at the Middle Eastern part. The climate is characterised by cold winters and hot and dry summers. The rainfall periods are mainly concentrated in the spring and autumn-winter seasons while the droughts take place in summer. The area is subjected to intense and localised storms during the second half of the summer period. The mean annual rainfall is nearly 500 mm and the maximum, and minimum yearly temperatures are between 30°C and -6°C, respectively.

At the start of the twentieth century, most of the catchment was cultivated, remaining as croplands nearly 60% of the area during the 1960s. However, as much as 75% of the agricultural land was abandoned during the following decade. Currently, ~16% of the catchment is still cultivated while the rangeland occupies the remaining 83.5 % (Lizaga et al., 2018a). The main land covers are cropland (AG), Mediterranean forest (MF), pine afforestation forest (PI) and scrubland (SC). Besides, most croplands are located on a Quaternary glacis and fluvial terraces with gentle slopes covering the valley floors. Rangeland occupies the upper part

of the catchment and the highest altitudes. Interspersed patches of highly disturbed areas such as bare soil (subsoil; SS) are dispersed across the catchment. The valley floor is infilled by eroded sediment from the surrounding slopes which is deeply incised, especially in the middle part of the catchment where its thickness reaches its maximum up to 4 m. The stream channel banks (CB) are mainly composed by loess type sediment characterised by steep talus without vegetation cover.

The study catchment is organised in three subcatchments (SBCs: 1, 2 and catchment outlet) with different percentages of land use/land cover (LU/LC). Thus, the agricultural land use predominates in the lower part of the catchment while Mediterranean forest and scrubland spread over the catchment occupying the East and West parts, being the pine afforestation forest the predominant land use at the headwaters. The abandonment of croplands during the recent decades was substantially greater at the headwaters due to the existence of shallow soils and more steep slopes that hinder the use of machinery (Navas et al., 2017).

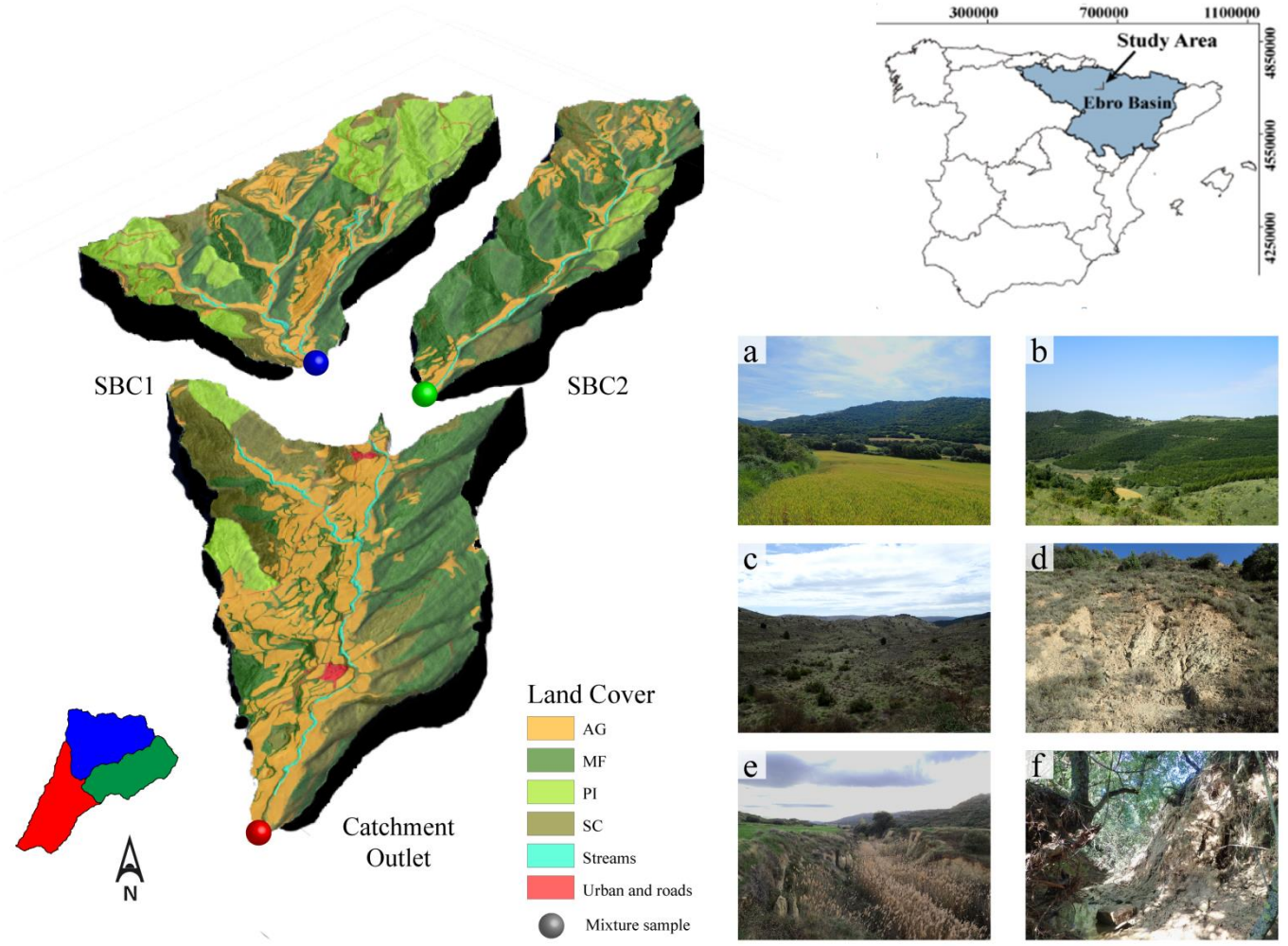

Fig.1. Location of the study catchment in the central part of the Ebro Basin (NE Spain). 3D map of the land covers: (a) cropland (AG) and Mediterranean forest (MF); (b) pine afforestation; (c) scrubland (SC) developed over abandoned cropland fields; (d) subsoil area (SS); (e) channel banks (CB), deeply incised stream and landslides (topples), and (f) view of topples in a channel bank (CB) section.

2.2. Soil sampling, analysis and clearcutting monitoring

The potential sediment sources and sediment sampling locations established in this study were selected following the information of reconnaissance surveys, connectivity maps (Lizaga et al., 2018a), soil properties (Lizaga et al., 2019b) and spatial soil redistribution rates (Lizaga et al., 2018b). The precipitation was recorded per minute at the study site with an Em50 decagon data logger connected to a tipping bucket rain gauge in order to correlate the rainfall information with the variability of sediment properties. Furthermore, to monitor the strip clearcutting in the catchment, satellite imagery data was analysed with digital image processing methods. A multitemporal Sentinel 2 satellite dataset formed the basis for monitoring the areas affected by clearcutting during the study seasons. Satellite images where selected based on the status of the strip clearcutting to track the beginning of the clearcutting and the dates when the forest recovered in terms of density cover. The selected dates when images were available without cloud cover were 2016-01-05, 2016-05-24, 2016-06-23 and 2016-10-21.

A total of 30 sampling points (5 for each source) were selected as the most representative for each sediment source. The samples were collected with a 2 cm cylindrical sampler with a total surface area of 127 cm^2. Four replicates were collected at each sampling point and later combined in the field to create a representative composite sample following Owens et al. (2016). Source samples were collected from agricultural land (AG), Mediterranean forest (MF), pine afforestation (PI), scrubland (SC), eroded subsoil (SS) and channel bank (CB). Thus, five subsoil samples were collected over the catchment, and another five samples were collected along the main streams on the channel banks.

Suspended sediment mixtures (SSC) were collected following the methodology proposed by Phillips et al. (2000) in the middle part of the channel bed along the principal streams from the headwaters to the outlet of the catchment in three sampling locations with three parallel replicates in each point. Suspended sediments samples at SBC1, SBC2 and the catchment outlet were collected during one hydrological year period, from June 2016 to June 2017 each three months to analyse the seasonal variability. The objective of the sampling schedule was to provide a close replication of sediments transported during each season for evaluating both seasonality and the effect of different crop practices such as sowing, fertilising and harvesting in the CSSI signal. Samples were air-dried, weighted, ground, homogenised and sieved to ≤63µm following the most widespread methodology (Palazón et al., 2015b; Owens et al., 2016; Collins et al., 2017). Besides, the selection of the ≤63µm particle size for sources and mixtures was related to the predominant silt texture of soils in the catchment (Lizaga et al., 2019a).

Lipids were extracted from the soil (source) and sediment (sink mixture) samples using accelerated solvent extraction (Dionex ASE 350, Thermo Scientific, Bremen Germany) with dichloromethane (DCM): MeOH (9:1 v/v) at 100ºC and 13 MPa for three cycles of 5 min (30 mL cells, 60% flush volume). For this c.a. 3 g of dried (x °C, y h) and 0.063 mm sieved sample was weighed in 22 mL stainless steel cells to which a recovery standard was added (12.5 ng C17:0FA, dissolved in 50 µL ethyl acetate). The lipid extract was dried using rotary evaporation (CentriVap, Labconco, Kansas City, USA) at 60ºC and 20 mbar. Lipid fraction was re-dissolved in DCM/Isopropanol (2:1 v/v) before being separated in neutral and acid fraction using aminopropyl solid-phase extraction columns (Bond Elute, 500mg, 6mL, Agilent Technologies) according to Blake et al. (2012). Neutral fraction was removed with DCM/Isopropanol after which the acid fraction was eluted using 2 % acetic acid in diethyl ether (Russell and Werne, 2007). After taking the acid fraction to dryness by rotary evaporation, the Fatty acids were methylated using Methanolic BF_3 (14%, 20min at 60°C).

The obtained fatty acid methyl esters (FAME) were quantified, after addition of an internal standard (C19:0 FAME), using capillary gas chromatography (GC Trace Ultra, Thermo scientific) with flame ionisation detection (FID) equipped with a 5% Phenyl Polysilphenylene-siloxane column (BPX5, 30 m x 0.25 mm x 0.25 µm, Trajan). After adapting the solvent volume for optimal concentration for compound-specific stable isotope (CSSI) analysis, the ^{13}C abundance of the individual FAME was determined using GC-isotope ratio mass spectroscopy (GC-IRMS). The GC-IRMS system used consisted out of a Trace 1310 GC equipped with the same GC column as for GC-FID connected to an ISOLINK II through a CongFlo IV to a Delta-V advantage IRMS detector (All Thermo scientific). Normalisation of the ^{13}C signal on the Vienna Pee Dee belemnite (VPDB) scale was performed by injecting a mixture of C14:0, C16:0, C18:0 C20:0 and C30 FAME, and C14:0, C16:0, C18:0 C20:0 Fatty acid ethyl ester provided by Arndt Schimmelmann (Indiana University), calibrated using NBS 19, and L-SVEC defined as exactly +1.95 and -46.6 ‰, on the VPDB scale, respectively, every five samples. Additionally, mixtures of Fatty acids (C16, C17, C19 and C20) were methylated together with the samples to correct for the contribution of the methyl group of the FAME in order to obtain the $\delta^{13}C$ of the FA.

2.3. Data processing and MixSIAR formulation

The estimation of the relative contribution of each potential sediment source to the sediment mixtures was done with the MixSIAR unmixing model and package following the recommendation of previous research using compound-specific stable isotopes (CSSI) of very-long-chain fatty acids (VLCFAs: C22-C32). To test the discrimination capacity of the selected tracers, an LDA (Linear Discriminant Analysis) was performed. A crucial requirement in fingerprint assessment is the implementation of previous statistical tests to identify individual fingerprint properties, which discriminate between potential sources to select the optimum set of fingerprint properties (Yu and Oldfield, 1989; Walling and Woodward, 1995; Collins et al., 1996; Palazón and Navas, 2017). MixSIAR is Bayesian tracer mixing model framework implemented as an open-source R package that helps to create and run Bayesian mixing models with JAGS, a program for analysis of Bayesian graphical models using Gibbs sampling (Plummer. 2003).

Before running the unmixing model with MixSIAR, the conservativeness of the tracers was tested using the mixing polygon approach as the most widespread techniques when unmixing CSSI (Upadhayay et al., 2017). The method states that the mixture samples must be within a polygon bounding the signatures of the sources as a requirement of conservativeness. The apportionment of land use sources contributing to sediment was estimated using the $\delta^{13}C$ values of the selected fatty acids. The concentration of the selected FA was included as concentration dependence in MixSIAR, using a residual error term. However, two different results were delivered by using an uninformative prior and including the prior information obtained from previous fingerprinting studies in the catchment extracted from Gaspar et al. (2019b), Lizaga et al. (2019a) and Lizaga et al. (under review) together with a geomorphological assessment pursued during fieldworks. The Markov Chain Monte Carlo (MCMC) parameters in MixSIAR were set as follows: number of chains = 3, chain length = 3,000,000 (extreme), burn = 1,500,000, thin =500. The convergence of mixing models

was evaluated using the Gelman-Rubin diagnostic, rejecting the model output if any variable was above 1.0, in which case the chain length was increased. Furthermore, a diagnostic matrix plot of posterior source contribution was used to evaluate the quality of source discrimination. Density plots are reported along with the mean, median and standard deviation proportional contributions.

Moreover, due to the previous knowledge of high sediment contribution from the CB and SS sources a second model was created by introducing an informative prior extracted from a previous fingerprinting study pursued in the catchment during two hydrological years by using radionuclides and stable elements as tracers by Lizaga et al. (under review). In this study, the overall modelled mean contributions were 24%, 44%, 8% and 24% for AG, CB, RG (MF, PI, SC) and SS, respectively.

3. Results

3.1. Sediment source discrimination

The analytical results and the LDA plot evidenced the discrimination capacity of the δ^{13}C-FAs (Table 1, Fig. 2).

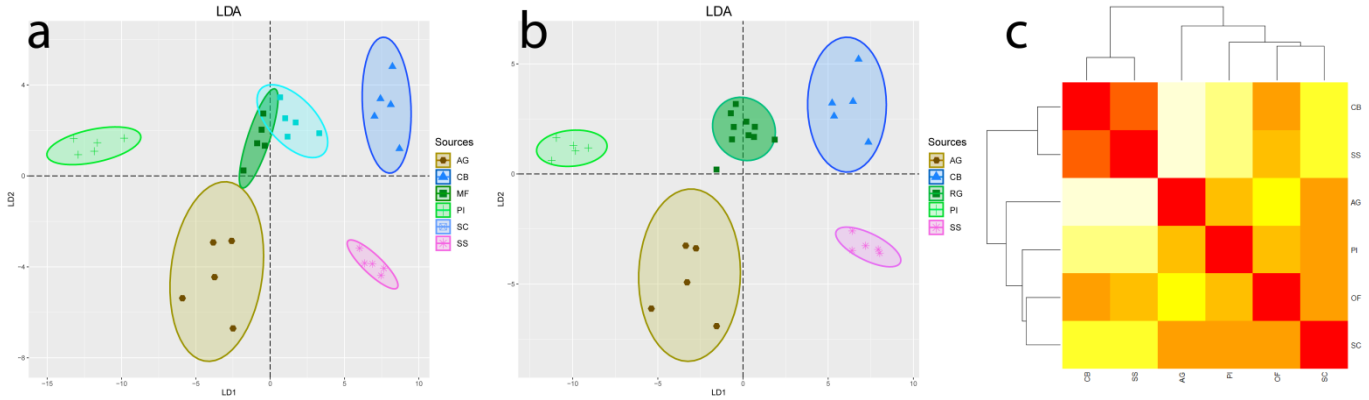

Fig.2. Linear discrimination analysis (LDA) plot of the sediment sources in the Barués catchment a) six sources; b) five sources and c) cluster analysis of the sediment sources.

The LDA plots discriminated the four land covers what was especially evident between AG and PI though with a small overlap between MF and SC. Overall, the four different land covers and both geomorphic elements were efficiently discriminated by δ^{13}C-FAs of the VLCFA. Considering the results from the LDA and cluster analyses the two natural vegetation covers (MF and SC) were merged into one source termed as rangeland (RG). After merging, the LDA plot showed significant discrimination between the five potential sediment sources.

Table 1. Mean and standard deviation of the δ13C-FAs for the sediment sources.

	C22		C24		C26		C28		C30		C32	
sources	**mean**	**sd**	**mean**	**sd**	**mean**	**sd**	**mean**	**sd**	**mean**	**sd**	**mean**	**sd**
AG	-34.26	0.49	-34.66	0.46	-35.71	0.38	-36.05	0.38	-35.50	0.47	-35.79	0.43
CB	-33.13	0.51	-33.27	0.50	-33.73	0.69	-34.04	0.31	-34.37	0.32	-33.79	0.83
OF	-32.79	0.27	-33.58	0.25	-33.93	0.42	-34.95	0.19	-35.08	0.17	-36.08	0.20
PI	-32.40	0.66	-34.26	0.53	-35.74	0.29	-35.71	0.28	-35.73	0.32	-36.05	0.41
SC	-33.47	0.18	-33.96	0.09	-34.28	0.11	-35.05	0.10	-35.45	0.25	-36.44	0.33
SS	-33.45	0.58	-33.26	0.81	-33.28	0.32	-34.72	0.61	-34.07	0.87	-32.23	2.49

There were differences in the VLCFAs concentrations between the different sediment sources (Table 2, Fig. 3). The dominant FA in the source samples was C26, whereas C32 had the lowest concentration. For all analysed FAs the highest concentrations were found in MF while the lowest were in SS. The concentrations in the suspended sediment mixtures ranged between a minimum of 0.49 µg g^{-1} soil for C32 and a maximum of 16.19 µg g^{-1} soil for C24.

3.2. Spatio - Temporal variation of FAs in the suspended sediment mixtures

The sample weights of the suspended sediment mixtures varied with the accumulated rainfall (Fig. 3). A decreasing trend in the mixture sample weights was recorded from summer to spring seasons in SBC1 and in the catchment outlet.

Table 2. Mean and standard deviation of the FAs concentration sediment sources and sediment mixture samples.

	C22		C24		C26		C28		C30		C32	
sources	**mean**	**sd**	**mean**	**sd**	**mean**	**sd**	**mean**	**sd**	**mean**	**sd**	**mean**	**sd**
AG	3.28	0.78	3.64	0.78	4.45	1.58	4.11	1.61	2.79	0.78	1.43	0.25
CB	1.93	0.61	3.13	1.52	2.87	1.36	2.87	1.14	2.66	0.75	1.47	0.36
OF	7.38	3.12	9.96	4.61	14.88	7.63	12.67	7.32	12.95	7.22	5.52	3.15
PI	10.50	6.32	12.78	7.36	19.02	14.97	11.92	7.82	11.24	7.93	5.33	3.58
SC	8.38	2.92	11.25	4.66	17.43	8.36	10.79	6.10	10.22	5.31	4.54	2.70
SS	0.84	0.34	0.74	0.34	0.60	0.25	0.84	0.35	0.85	0.38	0.49	0.21
Mixture	3.40	1.85	4.32	2.87	3.88	2.46	4.40	2.28	4.32	2.80	1.67	1.83

The sample weights in SBC 2 remained constant during summer, autumn and winter. However, a slight increase in the sample weight was recorded during spring for all three subcatchments. The accumulated rainfall presented an inverse trend with the sample weights in SBC 1 and in the catchment outlet (Fig. 4).

The mean contents of all FAs were higher in the catchment outlet than in the headwaters subcatchments being significantly higher ($p<0.05$) for C22, C24 and C30 (Fig. 5). The concentrations of the SSC in the three subcatchments had different trends though similarities were closer between SBC 1 and the catchment outlet. The mean values for the three subcatchments displayed similar temporal variation in all FAs (from C22 to C30) except for C32. Overall, the lowest concentrations were recorded in autumn in the three subcatchments.

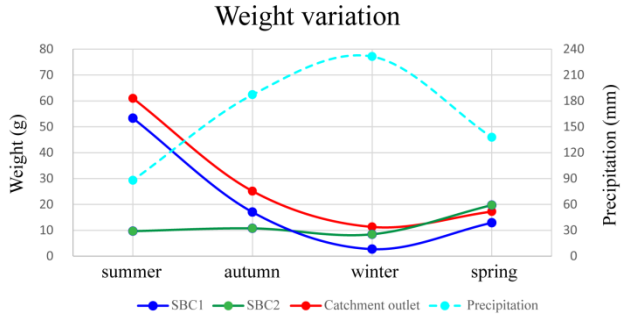

Fig.3. Line graph of the sediment mixture weights in the subcatchments and the accumulated rainfall for the four seasonal sampling campaigns.

Despite significantly higher concentrations in the catchment outlet, this pattern was not observed in the δ^{13}C-FAs values that were similar in SBC1 and in the catchment outlet but differed slightly in SBC 2 (Fig. 6).

The timeline of δ^{13}C-FAs showed two different trends for C22 to C28 and for C30 to C32 (Fig.4). Contrary to the FA concentrations, the mean δ^{13}C-FA values were similar in SBC 1 and in the catchment outlet (Fig. 5) that in turn had similar trends during the study hydrological year. However, this pattern was not observed in SBC 2. In all subcatchments, the minimum δ^{13}C-FA values from C22 to C30 were in autumn with maxima in winter.

Most δ^{13}C-FA values in the suspended sediment mixtures were out of the mean values of the sources for C22, C24, C30 and C32 (Fig. 6). Only C26 and C28 were inside the mean sources range in most mixture samples. In most seasons, δ^{13}C-FAs values of VLCFAs were little conservative for C22, C24, C30 and C32.

3.3. Source discrimination and sediment source contributions

A significant discrimination between the four different land covers was found by using the δ^{13}C isotopic signatures of the VLCFAs. The MixSIAR average means relative contributions of each potential source to the sediment mixtures indicated that overall, AG was the predominant source for the whole year (Table 3). Despite the general high contribution from AG along the year, in SBC 1 a significantly higher contribution of PI than in both SBC 2 and catchment outlet was found during summer and autumn seasons but during the spring season in SBC 2.

After the inclusion of the prior information, the results varied, increasing the AG apportions and reducing contributions from the other sources except for CB that remained almost equal (Table 3).

4. Discussion

4.1 δ^{13}C-FAs signature for land use discrimination

The concentrations and δ^{13}C-FAs values under each land cover type and for the two geomorphic elements in this study show the extent of source discrimination that might be expected from the literature. The slight differences between MF and SC are linked with their origins. Most scrubs and forests were previous croplands few decades before, and the geochemical signal of the agricultural lands likely remains in soil increasing the complexity to discriminate between land covers. For this reason, scrubland that is the early phase of the successional stages of natural revegetation, in the transition to Mediterranean forest present similar isotopic values and FAs concentrations as in MF. The effect of centuries of rainfed agriculture and the later abandonment of agricultural land in the last 60 years and its subsequent natural revegetation, as well as afforestation practices likely introduce a significant limitation to source discrimination.

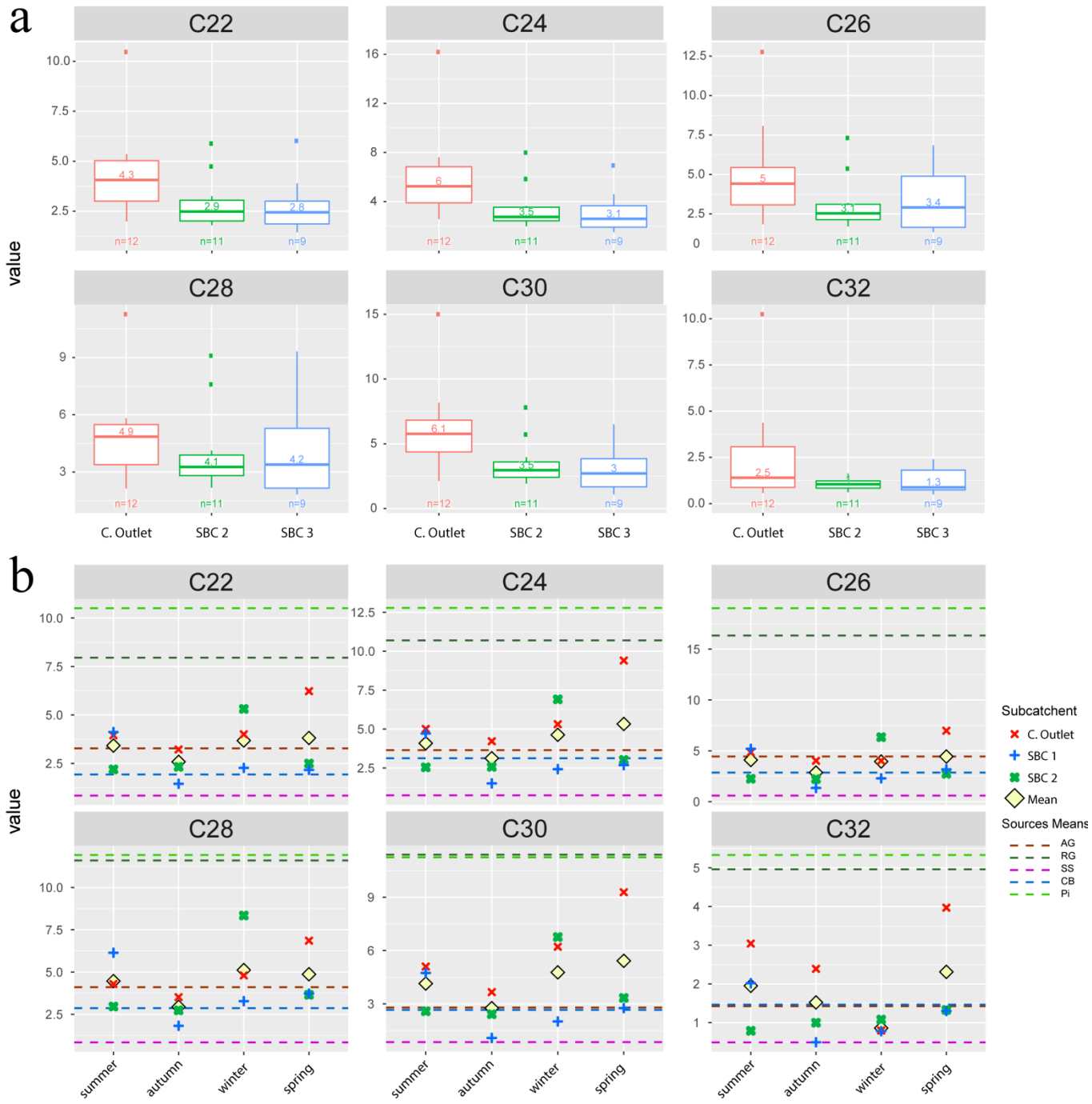

Fig.4. a) Boxplots of FAs concentrations in SBC1, SBC2 and in the catchment outlet. b) Timeline of the FAs concentration in the four seasons and mean values of the sediment sources (dash lines).

However, δ^{13}C-FAs has the ability to discriminate between the different land covers such as AG, PI and RG, which suggests in agreement with Lizaga et al. (2019b) that 60 years after land abandonment, the soils under natural revegetation and afforestation covers have recovered previous soil quality and differ from agriculture land. This implies that δ^{13}C-FAs signatures extracted from the soil surface were not extremely influenced by the past crops that occupied most of the area during the previous century.

4.2 FAs data for catchment assessment

The differences in the provenance of sediment are mainly produced by rainfall, agricultural practices and vegetation cover. Thus, due to the soil protection capacity of rangelands, the main drivers of sediment export are the quantity and intensity of rainfall but especially the agricultural practices what agrees with highest soil erosion rates found in the study catchment by Lizaga et al. (2018b) as well as in other nearby catchments of the south Pyrenean region (Gaspar et al., 2013; Navas et al., 2013).

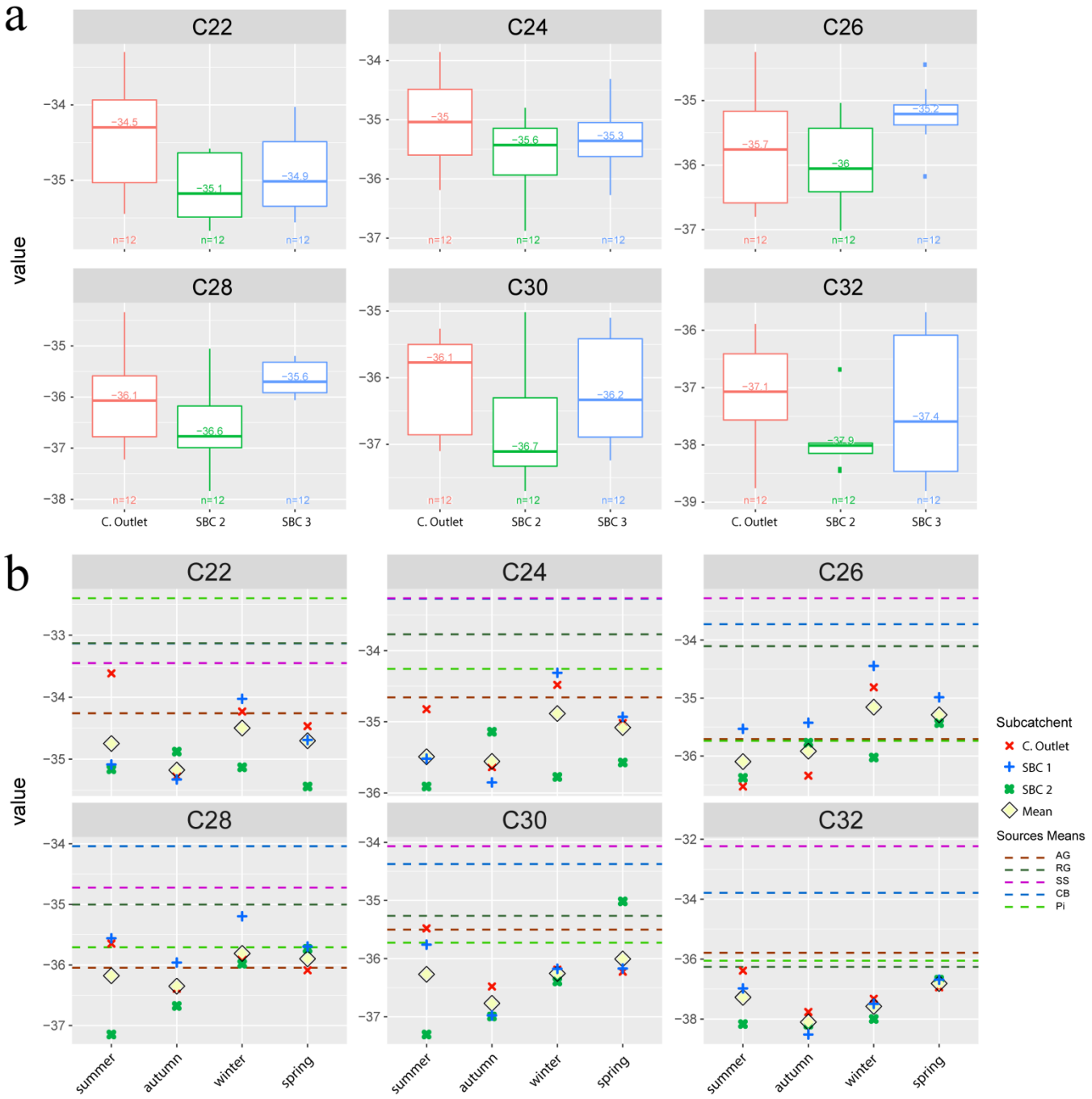

Fig.5. a) Boxplots of δ13C-FAs in SBC1, SBC2 and in the catchment outlet. b) Timeline of the δ13C-FAs in the four seasons and mean values of the sediment sources (dash lines).

The negative correlation between the mixture samples weights and the accumulated rainfall pinpoint the agricultural cycle and the farming practices as the main drivers of the variability of sediment export in the catchment. The heaviest mixture samples were collected after summer with only 88 mm of accumulated precipitation, of which 54 mm were recorded during a 3 days storm event by mid-September. Thus, localised storms after several months without precipitation along with high temperatures cause severe erosion of both dry soils and bare fields before crops planting in autumn. These interacting factors likely increase the sediment supply to streams and subsequently, the weights of the suspended sediment mixtures.

After summer the three next seasons had higher precipitation rates, but the sediment collected was lower what suggests an additional factor to rainfall. The reduction of suspended sediment weights is likely affected by two main factors; first the gradual growth of crops and the soil protection by the growth of natural vegetation favoured by more water available in soil after summer.

The headwaters subcatchments SBC1 and SBC2 showed the highest percentage areas of land uses with the highest FAs concentrations such as PI, SC and MF. Interestingly, the

sediment mixtures in SBC1 and SBC2 have similar low concentrations while the catchment outlet has the highest FAs concentrations. Thus, a difference between the three sampling points in terms of concentration can only be attributable to the stream discharge, and to relatively higher AG sediment apportions in the catchment outlet. However, the variation in the FAs concentrations through the four seasons shows a similar trend for SBC 1 and the catchment outlet indicating the influence of similar factors in both. Besides, SBC 2 shows a different temporal trend and also different sample weights than in both SBC 1 and the catchment outlet likely due to greater surfaces occupied by natural vegetation covers. Besides, most cultivated fields in SBC2 are located at the headwaters instead of surrounding main streams as in SBC1 and the catchment outlet, what would probably limit connectivity thus restraining the supply of sediments reaching the streams.

Despite similar concentrations between the different FAs, C32 shows the lowest concentration and a different temporal trend than the other FAs. Besides, C32 contents negatively correlate with the accumulated rainfall but positively with the sediment weight. This pattern is specially marked in the catchment outlet what likely suggests the sensitivity of C32 to external factors in terms of concentration. This pattern is not visible in $\delta^{13}C$ isotopic values indicating the conservatism of the isotopic signatures. However, the low conservatism between $\delta^{13}C$-C32 mixture and sources values suggest the low conservatism of this FA in this type of Mediterranean environment.

The high fluctuations found in isotope values during and between seasons are in agreement with previous results by Reiffarth et al. (2019) who attribute such fluctuations to continuously variable environmental conditions. In addition, the high variability of the different land covers in our mountain agroecosystems could also have an influence on the isotope fluctuations recorded.

4.3 Source sediment contributions

The potential of CSSI to effectively discriminate land covers document a successful discrimination between different vegetation covers for unmixing what was not possible to achieve by using only geochemical tracers (Lizaga et al., 2019a; Gaspar et al., 2019b). The sources with mature and undisturbed vegetation covers show a small contribution to total sediment apportions what agrees with previous findings in other environments (Gibbs et al. 2008; Bravo-Linares et al., 2019).

The good discrimination of vegetation covers from CSSI allows to identify pine afforestation as the main contributing source among the natural vegetation covers (SC, MF and PI). The high contribution of PI in SBC1 during summer is likely associated with the strip clearcutting also favoured by the intense and localised rainfall on dry soil conditions.

The increased contribution from PI in the SBC 1 that varies from <10% in spring to >30% in summer during clearcutting is in agreement with findings reported by Gibbs (2008) in New Zealand where the high sediment contribution came from clear cut areas of recently harvested pine forest. The pine sediment contribution increase due to clearcutting was also reported by Schuller et al. (2013) by unmixing suspended sediments using radionuclides as tracers in Chilean catchments. Moreover, further studies pursued in the same catchments using CSSI as tracers highlighted the low sediment contribution from Chilean forests before clear-cut operations (Bravo-Linares et al., 2019). With this information in mind and the low ^{137}Cs derived soil redistribution rates of the PI cover calculated by Lizaga et al. (2018b) it is likely that high PI contributions are promoted by external factors such as strip clearcutting what can be appreciated in the satellite images of Figure 6.

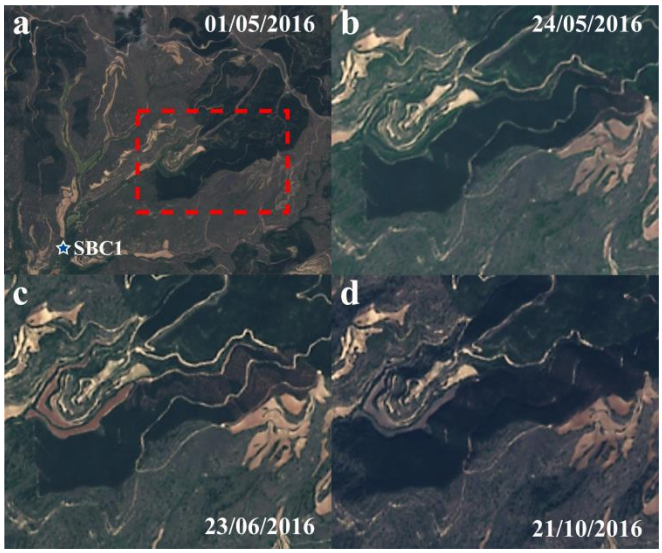

Fig.6. Sentinel 2 satellite images comparison from different months evidencing the clearcut area: a) Location of the pine afforestation submitted to strip clearcutting in the SBC1; b) pine afforestation harvest start; c) end of the clearcutting, and d) prompt recovery of the pine afforestation by October 2016.

The residual contribution of RGs is determined by the protecting capacity of the vegetation cover. Only extreme storm events have the capability to mobilise surface soil sediment from these well-protected lands to the streams. However, during extreme storm events as studied by Gaspar et al. (2019b) and Lizaga et al. (2019a) the rises of AG, CB and SS contributions mask the sediment exported from RGs. Thus, the low contributions of RGs, together with the only occasional PI apportionments, also suggest an anthropic factor for PI contribution rises. In contrast to Alewell et al. (2016), our results indicate that sediment contribution from forest does not vary substantially between base flow and high flow regime, what highlights the protection capacity of the vegetation in Mediterranean mountain agroecosystems.

Despite clearly identifying the signals of vegetation cover, it appears that the other sources from geomorphic elements such as channel banks and subsoil are probably underestimated. At this point, further research is required to determine the cause of the insignificant apportionments from the CB source and the mostly absence of SS in the overall contribution.

Furthermore, the "prior" implementation mainly affects contributions from land covers with permanent vegetation, reducing its apportionment in favour of AG while not significantly modifying the other source apportionments. Besides, the informative priors effectively remove the PI

contribution of autumn and spring seasons when no clear-cutting works occurred and the afforestation forest has recovered most of the lost density cover (Fig. 6). However, while the prior implementation significantly increases the summer SS contribution and the winter CB contribution in SBC1, these patterns are not observed in the other subcatchments and seasons. Thus, overall CB and SS sediment sources appear as residual sources of sediments in this study by using only CSSI as tracers. Furthermore, it cannot be totally discarded an anchoring problem of the model as reported by Davis et al. (2015) when using the SIAR model.

Table 3. Sediment source contributions (mean, sd) to the sediment mixtures modelled with MixSIAR by implementing: a) uninformative priors and b) informative priors. Agricultural (AG), channel bank (CB), rangeland (RG), pine forest (PI) and subsoil (SS).

a)	**AG**		**CB**		**RG**		**PI**		**SS**	
Mixture id	**mean**	**sd**	**mean**	**sd**	**mean**	**sd**	**mean**	**sd**	**mean**	**sd**
1	74.3	10.2	3.5	3.1	4.8	3.9	9.6	8.3	7.9	7.3
2	88.9	6.2	2.7	2.7	1.0	1.1	2.4	2.6	5.0	5.1
3	33.4	26.3	7.5	6.5	4.0	3.3	38.1	23.8	17	14.9
4	82.2	13.6	2.8	2.6	1.3	1.4	7.5	9.5	6.1	8.2
5	82.2	10.3	4.2	4.1	1.5	1.5	3.7	6.6	8.5	8.0
6	48.9	27.7	4.8	4.2	2.9	2.5	25.4	24.4	18	16.6
7	75.3	18.8	4.2	4.2	4.6	3.7	3.2	3.0	12.8	19.5
8	86.6	8.6	3.4	3.2	1.7	1.8	2.7	2.7	5.5	7.5
9	36.4	15.7	16.3	12.8	19.5	12.9	6.8	7.4	21.1	17.5
10	84.5	9.1	4.0	3.7	2.4	2.3	2.7	2.7	6.4	8.3
11	35.2	20.7	11.7	9.4	4.9	4.2	28.5	17.9	19.7	14.5
12	69.2	18.7	5.1	4.7	4.4	3.4	2.9	3.4	18.4	19.6
Mean	**66.4**	15.5	**5.9**	5.1	**4.4**	3.5	**11.1**	9.4	**12.2**	12.3

b)	**AG**		**CB**		**RG**		**PI**		**SS**	
Mixture id	**mean**	**sd**	**mean**	**sd**	**mean**	**sd**	**mean**	**sd**	**mean**	**sd**
1	90.9	9.0	2.7	3.3	0.9	2.4	2.1	5.9	3.4	6.2
2	96.9	3.9	1.3	2	0	0.2	0.1	0.4	1.6	3.4
3	61.9	36	8.5	8.7	0.5	1.6	20	32.8	9.2	15.4
4	96.7	3.9	1.4	2	0	0.2	0.3	1.6	1.6	3.1
5	93.3	7.7	2.6	3.6	0.1	0.4	0.2	2.6	3.7	6.7
6	83.0	20.1	4.1	5	0.2	0.9	2.8	13.2	9.9	15.4
7	88.6	18.1	3.2	4.4	0.6	1.9	0.2	1.0	7.3	18.2
8	96.4	4.9	1.8	2.7	0.1	0.4	0.1	0.6	1.6	4.1
9	42.1	17.0	29.8	19.4	5.7	12.5	0.4	2.2	22.0	27.0
10	94.4	7.8	2.7	3.8	0.2	0.7	0.2	0.6	2.5	7.0
11	63.3	24.3	14.1	11.9	0.5	1.7	6.9	17.6	15.3	18.7
12	81.1	20.6	4.7	5.9	0.5	1.7	0.1	0.6	13.5	21.4
Mean	**82.4**	14.4	**6.4**	6.1	**0.8**	2.1	**2.8**	6.6	**7.6**	12.2

The apparent lack of correlation with previous results and with the geomorphological assessment of the study area can be attributed to the low FAs concentration in CB and SS that could limit their applicability to assess the apportionment of geomorphic elements that have not vegetation cover. Furthermore, the δ^{13}C-FAs indicate high similarity between most suspended sediment mixture samples and the AG source what suggest the need for additional information. Thus, following the recommendation proposed by Reiffart et al. (2016) it would be needed to implement along with CSSI other additional tracing methods such as geochemistry or radionuclides for detecting CB and SS sources in order to complement the CSSI approach and further confirm the results from these novel tracers in geomorphological actives landscapes.

5. Conclusions

Comparison of the CSSI-derived source sediment apportions with previous unmixing results using radionuclides, magnetic properties and geochemical tracers revealed further detail about the soil mobilization dynamics from croplands and forest covers in this agroecosystem. By using CSSI of VLCFA for the first time in Mediterranean

environments, we found that exported sediments are mainly originated from agricultural lands; thus, efforts should be focused to control soil erosion in croplands.

Only C26 and C28 FAs showed conservative behaviour for most suspended sediment mixtures. The low conservativeness of some FAs such as C30 and C32 and its temporal trend coinciding with external factors likely suggest the low conservative behaviour of these VLFA in Mediterranean mountain agroecosystems.

Our results suggest that CSSI should be applied in conjunction with radionuclides and geochemical fingerprinting approaches in highly dissected landscapes, with exposed substrates drained by energetic streams and gullies that are also affected by intense rainfalls and present high sediment export dynamics. Future work will concentrate on implementing a method to combine the excellent discrimination of CSSI with geochemical data for further assessing the contribution from channel banks and subsoils.

This research has highlighted the effect of the agricultural and afforestation practices, agricultural cycle and vegetation cover in the delivery of sediment to water bodies.

Conservation practices, especially in periods of absence of vegetation cover, should be encouraged to prevent the loss of fertile topsoil. These findings report the effect of human activities in mountain agroecosystems, shed new light about the impacts of clearcutting practices in Mediterranean mountain agroecosystems and underline the benefits of natural covers to prevent soil loss.

Acknowledgements

This work has been supported by project CGL2014-52986-R funded by the Spanish Ministry of Science, Innovation and Universities and the aid of a predoctoral contract (BES-2015-071780). We would like to express our gratitude to the University of Ghent (Belgium), especially the ISOFYS group, for allowing us to do part of the analysis at their lab.

References

Alewell, C., Birkholz, A., Meusburger, K., Schindler Wildhaber, Y., Mabit, L., 2016. Quantitative sediment source attribution with compound-specific isotope analysis in a C3 plant-dominated catchment (central Switzerland). Biogeosciences 13, 1587–1596. https://doi.org/10.5194/bg-13-1587-2016

Blake, W.H., Ficken, K.J., Taylor, P., Russell, M.A., Walling, D.E., 2012. Tracing crop-specific sediment sources in agricultural catchments. Geomorphology 139, 322–329. https://doi.org/10.1016/j.geomorph.2011.10.036

Borrelli, P., Robinson, D.A., Fleischer, L.R., Lugato, E., Ballabio, C., Alewell, C., Meusburger, K., Modugno, S., Schütt, B., Ferro, V., Bagarello, V., Oost, K.V., Montanarella, L., Panagos, P., 2017. An assessment of the global impact of 21st century land use change on soil erosion. Nature Communications 8, 2013. https://doi.org/10.1038/s41467-017-02142-7

Bravo-Linares, C., Schuller, P., Castillo, A., Ovando-Fuentealba, L., Muñoz-Arcos, E., Alarcón, O., de los Santos-Villalobos, S., Cardoso, R., Muniz, M., Meigikos dos Anjos, R., Bustamante-Ortega, R., Dercon, G., 2018. First use of a compound-specific stable isotope (CSSI) technique to trace sediment transport in upland forest catchments of Chile. Science of The Total Environment 618, 1114–1124. https://doi.org/10.1016/j.scitotenv.2017.09.163

Chen, F., Fang, N., Shi, Z., 2016. Using biomarkers as fingerprint properties to identify sediment sources in a small catchment. Science of The Total Environment 557–558, 123–133. https://doi.org/10.1016/j.scitotenv.2016.03.028

Clarke, R.T., 2014. A bootstrap calculation of confidence regions for proportions of sediment contributed by different source areas in a 'fingerprinting' model. Hydrological Processes 29, 2694–2703. https://doi.org/10.1002/hyp.10397

Collins, A., Walling, D., Leeks, G.J.L., 1996. Composite fingerprinting of the spatial source of fluvial suspended sediment : a case study of the Exe and Severn river basins, United Kingdom. Géomorphologie : relief, processus, environnement 2, 41–53. https://doi.org/10.3406/morfo.1996.877

Collins, A.L., Walling, D.E., Leeks, G.J.L., 1997. Source type ascription for fluvial suspended sediment based on a quantitative composite fingerprinting technique. CATENA 29, 1–27. https://doi.org/10.1016/S0341-8162(96)00064-1

Cooper, R.J., Pedentchouk, N., Hiscock, K.M., Disdle, P., Krueger, T., Rawlins, B.G., 2015. Apportioning sources of organic matter in streambed sediments: An integrated molecular and compound-specific stable isotope approach. Science of The Total Environment 520, 187–197. https://doi.org/10.1016/j.scitotenv.2015.03.058

Davis, P., Syme, J., Heikoop, J., Fessenden-Rahn, J., Perkins, G., Newman, B., Chrystal, A.E., Hagerty, S.B., 2015. Quantifying uncertainty in stable isotope mixing models. Journal of Geophysical Research: Biogeosciences 120, 903–923. https://doi.org/10.1002/2014JG002839

Evrard, O., Poulenard, J., Némery, J., Ayrault, S., Gratiot, N., Duvert, C., Prat, C., Lefèvre, I., Bonté, P., Esteves, M., 2013. Tracing sediment sources in a tropical highland catchment of central Mexico by using conventional and alternative fingerprinting methods. Hydrol. Process. 27, 911–922. https://doi.org/10.1002/hyp.9421

Gaspar, L., Navas, A., Walling, D.E., Machín, J. Gómez Arozamena, J. 2013. Using 137Cs and 210Pbex to assess soil redistribution on slopes at different temporal scales. Catena, 102: 46-54. DOI: 10.1016/j.catena.2011.01.004

Gaspar, L., Blake, W.H., Smith, H.G., Lizaga, I., Navas, A., 2019a. Testing the sensitivity of a multivariate mixing model using geochemical fingerprints with artificial mixtures. Geoderma 337, 498–510. https://doi.org/10.1016/j.geoderma.2018.10.005

Gaspar, L., Lizaga, I., Blake, W.H., Latorre, B., Quijano, L., Navas, A., 2019b. Fingerprinting changes in source contribution for evaluating soil response during an exceptional rainfall in Spanish pre-pyrenees. Journal of

Environmental Management 240, 136–148. https://doi.org/10.1016/j.jenvman.2019.03.109

Gellis, A.C., Walling, D.E., 2013. Sediment Source Fingerprinting (Tracing) and Sediment Budgets as Tools in Targeting River and Watershed Restoration Programs, in: Stream Restoration in Dynamic Fluvial Systems. American Geophysical Union (AGU), pp. 263–291. https://doi.org/10.1029/2010GM000960

Gibbs, M.M., 2008. Identifying Source Soils in Contemporary Estuarine Sediments: A New Compound-Specific Isotope Method. Estuaries and Coasts: J CERF 31, 344–359. https://doi.org/10.1007/s12237-007-9012-9

Gibbs MM., 2013. Protocols on the use of the CSSI technique to identify and apportion soil sources from land use. Report no: HAM2013–106. National Institute of Water and Atmospheric Research Ltd, Hamilton, New Zealand.

Glaser, B., 2005. Compound-specific stable-isotope (δ13C) analysis in soil science. Journal of Plant Nutrition and Soil Science 168, 633–648. https://doi.org/10.1002/jpln.200521794

Gruszowski, K.E., Foster, I.D.L., Lees, J.A., Charlesworth, S.M., 2003. Sediment sources and transport pathways in a rural catchment, Herefordshire, UK. Hydrol. Process. 17, 2665–2681. https://doi.org/10.1002/hyp.1296

Hancock, G.J., Revill, A.T., 2013. Erosion source discrimination in a rural Australian catchment using compound-specific isotope analysis (CSIA). Hydrological Processes 27, 923–932. https://doi.org/10.1002/hyp.9466

Klages, M.G., Hsieh, Y.P., 1975. Suspended Solids Carried by the Gallatin River of Southwestern Montana: II. Using Mineralogy for Inferring Sources. Journal of Environmental Quality 4, 68–73. https://doi.org/10.2134/jeq1975.00472425000400010016x

Lavrieux, M., Birkholz, A., Meusburger, K., Wiesenberg, G.L.B., Gilli, A., Stamm, C., Alewell, C., 2019. Plants or bacteria? 130 years of mixed imprints in Lake Baldegg sediments (Switzerland), as revealed by compound-specific isotope analysis (CSIA) and biomarker analysis. Biogeosciences 16, 2131–2146. https://doi.org/10.5194/bg-16-2131-2019

Lizaga, I., Quijano, L., Palazón, L., Gaspar, L., Navas, A. 2018a. Enhancing connectivity index to assess the effects of land use changes in a Mediterranean catchment. Land Degradation and Development. 29: 663–675. DOI: 10.1002/ldr.2676

Lizaga, I., Quijano, L., Gaspar, L., Navas, A., 2018b. Estimating Soil Redistribution Patterns with 137Cs Measurements in a Mediterranean Mountain Catchment Affected by Land Abandonment. Land Degrad Develop, 29: 105–117. https://doi.org/10.1002/ldr.2843

Lizaga, I., Gaspar, L., Blake, W.H., Latorre, B., Navas, A., 2019a. Fingerprinting changes of source apportionments from mixed land uses in stream sediments before and after an exceptional rainstorm event. Geomorphology 341, 216–229. https://doi.org/10.1016/j.geomorph.2019.05.015

Lizaga, I., Gaspar, L., Quijano, L., Dercon, G., Navas, A., 2019b. NDVI, 137Cs and nutrients for tracking soil and vegetation development on glacial landforms in the Lake Parón Catchment (Cordillera Blanca, Perú). Science of The Total Environment 651, 250–260. https://doi.org/10.1016/j.scitotenv.2018.09.075

Lizaga, I., Quijano, L., Gaspar, L., Ramos, M.C., Navas, A., 2019b. Linking land use changes to variation in soil properties in a Mediterranean mountain agroecosystem. Catena 172, 516–527. https://doi.org/10.1016/j.catena.2018.09.019

Mabit, L., Benmansour, M., Abril, J.M., Walling, D.E., Meusburger, K., Iurian, A.R., Bernard, C., Tarján, S., Owens, P.N., Blake, W.H., Alewell, C., 2014. Fallout 210Pb as a soil and sediment tracer in catchment sediment budget investigations: A review. Earth-Science Reviews 138, 335–351. https://doi.org/10.1016/j.earscirev.2014.06.007

Mabit, L., Gibbs, M., Mbaye, M., Meusburger, K., Toloza, A., Resch, C., Klik, A., Swales, A., Alewell, C., 2018. Novel application of Compound Specific Stable Isotope (CSSI) techniques to investigate on-site sediment origins across arable fields. Geoderma 316, 19–26. https://doi.org/10.1016/j.geoderma.2017.12.008

Martínez-Carreras, N., Krein, A., Gallart, F., Iffly, J.F., Pfister, L., Hoffmann, L., Owens, P.N., 2010. Assessment of different colour parameters for discriminating potential suspended sediment sources and provenance: A multi-scale study in Luxembourg. Geomorphology 118, 118–129. https://doi.org/10.1016/j.geomorph.2009.12.013

Navas, A., Valero Garcés, B., Machín, J., 2004. An approach to integrated assessement of reservoir siltation: the Joaquín Costa reservoir as a case study. Hydrology and Earth System Sciences 8, 1193–1199. https://doi.org/10.5194/hess-8-1193-2004

Owens, P.N., Blake, W.H., Gaspar, L., Gateuille, D., Koiter, A.J., Lobb, D.A., Petticrew, E.L., Reiffarth, D.G., Smith, H.G., Woodward, J.C., 2016. Fingerprinting and tracing the sources of soils and sediments: Earth and ocean science, geoarchaeological, forensic, and human health applications. Earth-Science Reviews 162, 1–23. https://doi.org/10.1016/j.earscirev.2016.08.012

Palazón, L., Gaspar, L., Latorre, B., Blake, W.H., Navas, A., 2015a. Identifying sediment sources by applying a fingerprinting mixing model in a Pyrenean drainage catchment. J Soils Sediments 15, 2067–2085. https://doi.org/10.1007/s11368-015-1175-6

Palazón, L., Latorre, B., Gaspar, L., Blake, W.H., Smith, H.G., Navas, A., 2015b. Comparing catchment sediment fingerprinting procedures using an auto-evaluation approach with virtual sample mixtures. Science of The Total Environment 532, 456–466. https://doi.org/10.1016/j.scitotenv.2015.05.003

Palazón, L., Navas, A., 2017. Variability in source sediment contributions by applying different statistic test for a Pyrenean catchment. Journal of Environmental

Management, Sediment source fingerprinting for informing catchment management: methodological approaches, problems and uncertainty 194, 42–53. https://doi.org/10.1016/j.jenvman.2016.07.058

Phillips, J.M., Russell, M.A., Walling, D.E., 2000. Time-integrated sampling of fluvial suspended sediment: a simple methodology for small catchments. Hydrological Processes 14, 2589–2602. https://doi.org/10.1002/1099-1085(20001015)14:14<2589::AID-HYP94>3.0.CO;2-D

Phillips, D.L., Gregg, J.W., 2003. Source partitioning using stable isotopes: coping with too many sources. Oecologia 136, 261–269. https://doi.org/10.1007/s00442-003-1218-3

Pimentel, D., 2006. Soil Erosion: A Food and Environmental Threat. Environ Dev Sustain 8, 119–137. https://doi.org/10.1007/s10668-005-1262-8

Plummer, M., Plummer, M., Hornik, K., Leisch, F., Zeileis, A., Zeileis, A., Hornik, K., Leisch, F., 2003. JAGS: a program for analysis of Bayesian graphical models using Gibbs sampling.

Reiffarth, D.G., Petticrew, E.L., Owens, P.N., Lobb, D.A., 2019. Spatial differentiation of cultivated soils using compound-specific stable isotopes (CSSIs) in a temperate agricultural watershed in Manitoba, Canada. J Soils Sediments 19, 3411–3426. https://doi.org/10.1007/s11368-019-02406-3

Reiffarth, D.G., Petticrew, E.L., Owens, P.N., Lobb, D.A., 2016. Sources of variability in fatty acid (FA) biomarkers in the application of compound-specific stable isotopes (CSSIs) to soil and sediment fingerprinting and tracing: A review. Science of The Total Environment 565, 8–27. https://doi.org/10.1016/j.scitotenv.2016.04.137

Russell, J.M., Werne, J.P., 2007. The use of solid phase extraction columns in fatty acid purification. Organic Geochemistry 38, 48–51. https://doi.org/10.1016/j.orggeochem.2006.09.003

Schuller, P., Walling, D.E., Iroumé, A., Quilodrán, C., Castillo, A., Navas, A., 2013. Using 137Cs and 210Pbex and other sediment source fingerprints to document suspended sediment sources in small forested catchments in south-central Chile. Journal of Environmental Radioactivity 124, 147–159. https://doi.org/10.1016/j.jenvrad.2013.05.002

Smith, J.A., Mazumder, D., Suthers, I.M., Taylor, M.D., 2013. To fit or not to fit: evaluating stable isotope mixing models using simulated mixing polygons. Methods in Ecology and Evolution 4, 612–618. https://doi.org/10.1111/2041-210X.12048

Stewart, H.A., Massoudieh, A., Gellis, A., 2015. Sediment source apportionment in Laurel Hill Creek, PA, using Bayesian chemical mass balance and isotope fingerprinting. Hydrological Processes 29, 2545–2560. https://doi.org/10.1002/hyp.10364

Tolosa, I., Fiorini, S., Gasser, B., Martín, J., Miquel, J.C., 2013. Carbon sources in suspended particles and surface sediments from the Beaufort Sea revealed by molecular lipid biomarkers and compound-specific isotope analysis. Biogeosciences 10, 2061–2087. https://doi.org/10.5194/bg-10-2061-2013

Upadhayay, H.R., Bodé, S., Griepentrog, M., Huygens, D., Bajracharya, R.M., Blake, W.H., Dercon, G., Mabit, L., Gibbs, M., Semmens, B.X., Stock, B.C., Cornelis, W., Boeckx, P., 2017. Methodological perspectives on the application of compound-specific stable isotope fingerprinting for sediment source apportionment. J Soils Sediments 17, 1537–1553. https://doi.org/10.1007/s11368-017-1706-4

Upadhayay, H.R., Smith, H.G., Griepentrog, M., Bodé, S., Bajracharya, R.M., Blake, W., Cornelis, W., Boeckx, P., 2018. Community managed forests dominate the catchment sediment cascade in the mid-hills of Nepal: A compound-specific stable isotope analysis. Science of The Total Environment 637–638, 306–317. https://doi.org/10.1016/j.scitotenv.2018.04.394

Verheijen, F.G.A., Jones, R.J.A., Rickson, R.J., Smith, C.J., 2009. Tolerable versus actual soil erosion rates in Europe. Earth-Science Reviews 94, 23–38. https://doi.org/10.1016/j.earscirev.2009.02.003

Walling, D.E., 2005. Tracing suspended sediment sources in catchments and river systems. Science of The Total Environment 344, 159–184. https://doi.org/10.1016/j.scitotenv.2005.02.011

Walling, D.E., Woodward, J.C., 1995. Tracing sources of suspended sediment in river basins: a case study of the River Culm, Devon, UK. Marine and Freshwater Research 46, 327–336.

Wynants, M., Millward, G., Patrick, A., Taylor, A., Munishi, L., Mtei, K., Brendonck, L., Gilvear, D., Boeckx, P., Ndakidemi, P., Blake, W.H., 2020. Determining tributary sources of increased sedimentation in East-African Rift Lakes. Science of The Total Environment 717, 137266. https://doi.org/10.1016/j.scitotenv.2020.137266

Yu, L., Oldfield, F., 1989. A multivariate mixing model for identifying sediment source from magnetic measurements. Quaternary Research 32, 168–181. https://doi.org/10.1016/0033-5894(89)90073-2

CHAPTER 11

Conclusions

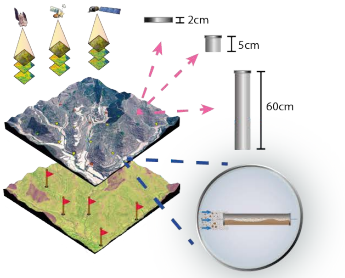

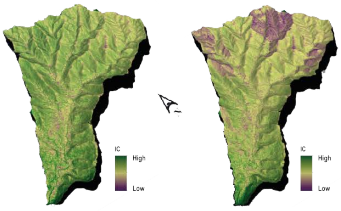

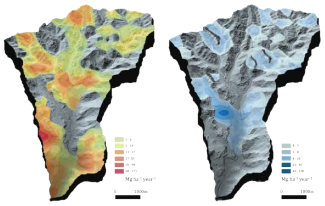

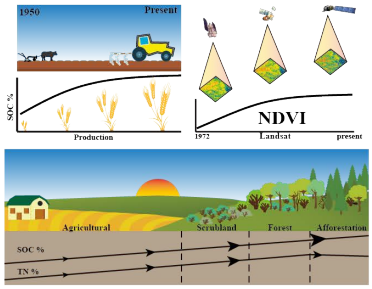

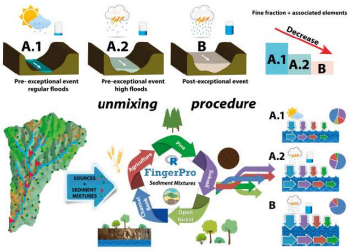

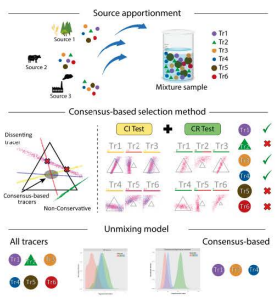

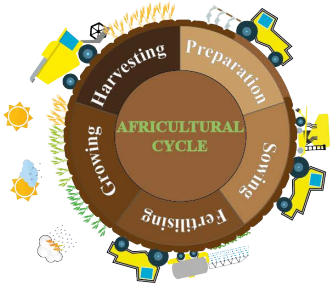

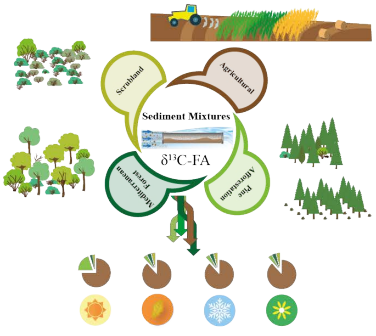

11. Conclusions

11.1 Soil properties, sediment connectivity, plant cover changes and soil redistribution rates

After decades of land abandonment that have greatly transformed the distribution of land uses in the Barués catchment a main impact is recorded in some main soil physico-chemical properties that have changed over the years resulting in significant differences among the land uses especially between those that have maintained previous agricultural uses and the afforested lands. Besides, naturally revegetated and afforested areas have been shown to be very efficient in reducing connectivity and soil redistribution rates, thus likely limiting soil erosion in present times.

On the other hand, contemporary land use and land cover changes produced by human intervention mostly agriculture practices and clearcutting, have intensified the natural geomorphological processes such as landsliding and gullying what increased sediment export. The tillage practices and the fact that soil is left bare during part of the year have contributed to increase soil mobilization resulting in important soil loss. Overall higher soil redistribution rates recorded in cultivated fields were directly linked to tillage and other agricultural practices. Higher erosion rates are associated with the loss of nutrients that result in less fertile agricultural soils. On the contrary lower erosion rates are related to the natural revegetation with an increase in the vegetation cover and its maturity what is most documented in the Mediterranean open forest.

The implementation of the SdRI roughness index and Total Aerial Biomass estimate improved both the topography and vegetation cover features, increasing the quality and adjustment of the connectivity index. The novel connectivity index proposed is probably a good approximation to the reality in this area, emphasising that anthropogenic activities are nowadays the greatest landscape modifiers. Moreover, this index represents a good estimate to the temporal connectivity variation in Mediterranean agricultural catchments and has the potential to be used for ecological purposes, soil management as well as for field geomorphological surveys, mapping and sampling.

The potential of ^{137}Cs measurements to quantify and spatialise the soil redistribution rates in the context of land use changes that occurred in last decades confirms that some of the main factors triggering erosion are related to tillage and farming practices. This method enabled to identify and discriminate the main erosion and deposition areas in the catchment. The tillage practices and the fact that soil is left bare during part of the year under the predominant agricultural use in the catchment lowlands led to the highest soil redistribution rates. The lowest soil erosion rates were found under land uses with more abundant plant cover on higher altitudes and slopes. Therefore, in this environment, land use was found to be the main controlling factor of soil redistribution rates.

Although the ^{137}Cs method has generated precise spatial distribution data, the extrapolation at the catchment scale is complex but allows gaining a better understanding of the spatial extent, the severity of soil loss over the catchment and the benefits of the natural revegetated areas in terms of soil conservation. The knowledge acquired on the relationships between the land use change and the spatial variability of soil redistribution, may help to implement erosion control practices to mitigate soil degradation and reservoir siltation.

Multitemporal satellite imagery has been a fundamental tool for the quantification of spatial and temporal vegetation changes and the effects of human intervention, which could not be accomplished through conventional mapping. The results extracted from remote sensing analysis and estimates of soil nutrient stocks indicate that in the short term, afforestation produces a faster increase in SOC than natural covers, although a similar increase is not observed in TN. After more than 50 years since land abandonment, the soil quality was similar under naturally revegetated and afforested cover. Furthermore, the abandoned land became naturally revegetated with native species 15 years after land abandonment. The use of mixtures of native and fast-growing species such as pine promotes increases in SOC and TN

and good soil recovery. It could, therefore, be a suitable alternative to cost-intensive afforestation with pine monoculture.

The first three chapters of this thesis highlight the effects of recent land use changes on the hydraulic connectivity, soil redistribution rates and soil properties. This section underlines the importance of preserving natural forests to prevent erosion and the subsequent nutrient depletion produced by intensive agricultural practices. Here, it has been shown three different approaches to analyse the soil erosion problem and detect the most vulnerable areas in order to establish effective and localised remediation practices. Besides, the results of this research suggest that the effects of recent land use changes on soil properties should be considered for rational land use planning. Overall, the knowledge gained is useful for environmental managers to take decisions about best practices to implement after land abandonment and for future afforestation programmes.

11.2 Sediment source fingerprinting and tracer selection methods

The fingerprinting approach and the application of the FingerPro® unmixing model have been proved relevant to understand source-tracer relationships and are of value for identifying sediment sources, the processes leading to increased sediment load and for providing useful information for management strategies.

During this research an open-source R package, FingerPro®, was developed. In this package, the need for using additional software' or R packages to select the best combination of sediment tracers has been eliminated by including various tests and mechanisms for tracer selection. Furthermore, the inclusion of several informative plot functions has increased the efficiency on the time-consuming fingerprinting procedure for checking if the selected tracers are suitable for the unmixing process.

Tracer selection methods are crucial in fingerprinting studies, as the use of one or another tracer could substantially modify the output of the models. It has been proved that including tracers with dissenting information produces inconsistent results in different unmixing models such as FingerPro and MixSIAR. Besides, some conservative tracers could provide unreliable information and may be erroneous. Unmixing models cannot estimate reliable contributions of sediment sources if the tracer selection procedure applied does not account for tracers with non-coherent information. Thus, in this thesis, we have devised an innovative methodology to identify non-conservative and dissenting tracers that enables to understand datasets and, likewise, the effect of each tracer. The currently used methods without CI and CR information may lead to selecting non-consensual and non-conservative tracers. Our study provides the framework for a new way to obtain individual tracer information to prevent the inclusion of erroneous information into fingerprinting studies.

The application of the new FingerPro model provided the opportunity to trace efficiently the sediment sources before and after exceptional rainstorm events. The results indicate an important input from subsoil despite its small spatial coverage in the catchment what represents a significant environmental problem with hot spots that are worth controlling. In contrast, the insignificant sediment apportionment from forests underlines the benefits of plant covers to prevent soil loss. Streambank failure induced by natural tunnelling or piping and landslides significantly contributed to sediment delivery being the channel bank the most contributing source. The magnitude of agricultural and bare soil mobilisation during the course of this exceptional rainstorm was much greater than under regular discharge regimes. The significant differences between pre- and post-storm sediment mixtures highlight the great impact of extreme events on the characteristics of channel bed sediments. Overall, our results provide evidence of the severe erosion produced by this exceptional rainstorm and reveal important variations between pre and post storm event sediment source contributions.

By implementing the novel consensus method together with FingerPro model, it has been emphasised the great impact of agricultural activities and the agricultural cycle in the suspended sediment and pollutants exported to the streams. The positive correlation between the cropland area and the sediment

mixture weights confirm the influence of the agricultural practices as the primary driver of rising sediment exports rates. The enrichment above sources ranges detected in the suspended sediment mixtures of some elements such as As, Co, Li, Mn, Zn, ^{238}U and P, and their higher increase during sowing and after harvest periods points to the important impact of agricultural activities on supplying sediment and pollutants to the streams. The results of the unmixing modelling highlight the increase in agricultural sediment provenance during sowing and after harvest periods.

The comparison of the CSSI-derived source sediment apportions with previous unmixing results using radionuclides, magnetic properties and geochemical tracers revealed further detail about the soil mobilisation dynamics from croplands and forest covers. By using CSSI of VLCFA for the first time in Mediterranean environments, we found that exported sediments are mainly originated from agricultural lands and afforested areas under clearcutting practices; thus, efforts should be focused to control soil erosion in croplands and bare soil areas during clearcuts.

Results, however, indicate that CSSI should be applied in conjunction with radionuclides and geochemical fingerprinting approaches in highly dissected landscapes affected by intense and localised rainfalls and high sediment export dynamics. Future work will concentrate on implementing a method to combine the excellent cropland and forestland discrimination by CSSI with geochemical data that effectively estimate the apportionment of channel banks and subsoils. It has been evidenced the important effect of agricultural practices in the delivery of sediment to water bodies and more importantly, in the associated pollutants exported. Besides, this study shed new light about the impacts of clearcutting practices and underlines the benefits of natural covers to prevent soil loss in Mediterranean environments.

Overall, the different methodologies implemented in this research have allowed to successfully estimate the consequences of recent land use changes and contemporary human activities on soil physico-chemical properties, soil redistribution rates and sediment delivery provenance. The three main strategies implemented to quantify and model such effects pinpoint to agricultural land and agricultural practices as main drivers of soil loss in Mediterranean mountain agroecosystems. The findings from different methodologies and approaches implemented and elaborated during this research support similar conclusions about the effect of recent and contemporary land use changes what provides additional robustness to the results obtained. Our study suggests that environmental planners and stakeholders should support conservation practices, especially in periods of absence of vegetation cover to prevent the loss of fertile soil and pollutants export.

REFERENCES

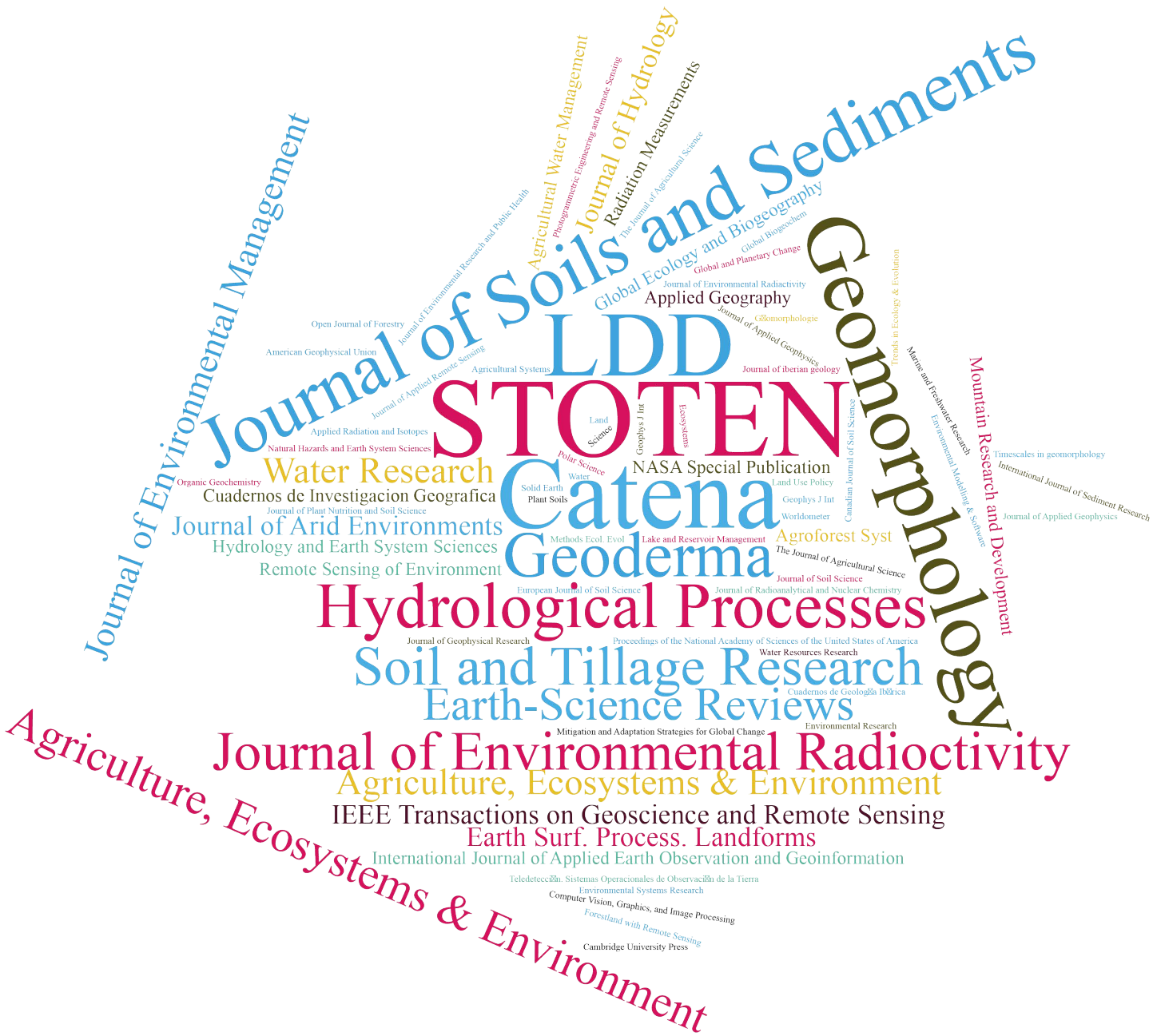
Journal of Soils and Sediments
Geomorphology
Journal of Environmental Management
Journal of Hydrology
Agricultural Water Management
Radiation Measurements
Global Ecology and Biogeography
Photogrammetric Engineering and Remote Sensing
The Journal of Agricultural Science
Global Biogeochem
Global and Planetary Change
Journal of Environmental Radioactivity
Applied Geography
Journal of Environmental Research and Public Health
Open Journal of Forestry
American Geophysical Union
Journal of Applied Remote Sensing
Agricultural Systems
LDD
Journal of Applied Geophysics
Géomorphologie
Journal of iberian geology
Trends in Ecology & Evolution
Marine and Freshwater Research
Environmental Modelling & Software
Mountain Research and Development
Timescales in geomorphology
International Journal of Sediment Research
Journal of Applied Geophysics
STOTEN
Land
Science
Ecosystems
Geophys J Int
Applied Radiation and Isotopes
Natural Hazards and Earth System Sciences
Polar Science
Water
NASA Special Publication
Water Research
Organic Geochemistry
Solid Earth
Land Use Policy
Catena
Cuadernos de Investigacion Geografica
Plant Soils
Geophys J Int
Canadian Journal of Soil Science
Worldometer
Journal of Plant Nutrition and Soil Science
Journal of Arid Environments
Methods Ecol. Evol.
Lake and Reservoir Management
Agroforest Syst
Hydrology and Earth System Sciences
The Journal of Agricultural Science
Geoderma
Remote Sensing of Environment
Journal of Soil Science
European Journal of Soil Science
Journal of Radioanalytical and Nuclear Chemistry
Hydrological Processes
Journal of Geophysical Research
Proceedings of the National Academy of Sciences of the United States of America
Water Resources Research
Soil and Tillage Research
Cuadernos de Geología Ibérica
Earth-Science Reviews
Environmental Research
Mitigation and Adaptation Strategies for Global Change
Journal of Environmental Radioctivity
Agriculture, Ecosystems & Environment
IEEE Transactions on Geoscience and Remote Sensing
Earth Surf. Process. Landforms
International Journal of Applied Earth Observation and Geoinformation
Teledetección. Sistemas Operacionales de Observación de la Tierra
Environmental Systems Research
Computer Vision, Graphics, and Image Processing
Forestland with Remote Sensing
Cambridge University Press
Agriculture, Ecosystems & Environment

References

Alewell C, Meusburger K, Juretzko G, Mabit L, Ketterer ME. 2014. Suitability of $^{239+240}$Pu and ^{137}Cs as tracers for soil erosion assessment in mountain grasslands. *Chemosphere* **103**: 274–280. DOI: 10.1016/j.chemosphere.2013.12.016

Alewell C, Birkholz A, Meusburger K, Schindler Wildhaber Y, Mabit L. 2016. Quantitative sediment source attribution with compound-specific isotope analysis in a C3 plant-dominated catchment (central Switzerland). *Biogeosciences* **13**: 1587–1596. DOI: 10.5194/bg-13-1587-2016

Alonso-Sarría F, Martínez-Hernández C, Romero-Díaz A, Cánovas-García F, Gomariz-Castillo F. 2016. Main environmental features leading to recent land abandonment in Murcia region (Southeast Spain). *Land Degradation & Development* **27**: 654–670. DOI: 10.1002/ldr.2447

Álvaro-Fuentes, J., Paustian, K., 2011. Potential soil carbon sequestration in a semiarid Mediterranean agroecosystem under climate change: Quantifying management and climate effects. *Plant Soil* 338, 261–272. https://doi.org/10.1007/s11104-010-0304-7

Andrén, O., Kätterer, T., 1997. Icbm: The Introductory Carbon Balance Model for Exploration of Soil Carbon Balances. Ecological Applications 7, 1226–1236. https://doi.org/10.1890/1051-0761(1997)007[1226:ITICBM]2.0.CO;2

Balota, E.L., Colozzi Filho, A., Andrade, D.S., Dick, R.P., 2004. Long-term tillage and crop rotation effects on microbial biomass and C and N mineralization in a Brazilian Oxisol. *Soil and Tillage Research* 77, 137–145. https://doi.org/10.1016/j.still.2003.12.003

Ben-Dor, E., Banin, A., 1995. Near-Infrared Analysis as a Rapid Method to Simultaneously Evaluate Several Soil Properties. Soil Science Society of America Journal 59, 364–372. https://doi.org/10.2136/sssaj1995.03615995005900020014x

Blake WH, Ficken KJ, Taylor P, Russell MA, Walling DE. 2012. Tracing crop-specific sediment sources in agricultural catchments. *Geomorphology* **139**: 322–329. DOI: 10.1016/j.geomorph.2011.10.036

Blake, W.H., Boeckx, P., Stock, B.C., Smith, H.G., Bodé, S., Upadhayay, H.R., Gaspar, L., Goddard, R., Lennard, A.T., Lizaga, I., Lobb, D.A., Owens, P.N., Petticrew, E.L., Kuzyk, Z.Z.A., Gari, B.D., Munishi, L., Mtei, K., Nebiyu, A., Mabit, L., Navas, A., Semmens, B.X., 2018. A deconvolutional Bayesian mixing model approach for river basin sediment source apportionment. Scientific Reports 8, 13073. https://doi.org/10.1038/s41598-018-30905-9

Boix-Fayos C, Calvo-Cases A, Imeson AC, Soriano-Soto MD, Tiemessen IR. 1998. Spatial and short-term temporal variations in runoff, soil aggregation and other soil properties along a mediterranean climatological gradient. *Catena* **33:** 123–138. DOI: 10.1016/S0341-8162(98)00048-4

Boix-Fayos, C., Martínez-Mena, M., Cutillas, P.P., de Vente, J., Barberá, G.G., Mosch, W., Navarro Cano, J.A., Gaspar, L., Navas, A., 2017. Carbon redistribution by erosion processes in an intensively disturbed catchment. *Catena*, Geoecology in Mediterranean mountain areas. Tribute to Professor José María García Ruiz 149, 799–809. https://doi.org/10.1016/j.catena.2016.08.003

Borselli L, Cassi P, Torri D. 2008. Prolegomena to sediment and flow connectivity in the landscape: A GIS and field numerical assessment. *Catena* 75: 268–277. DOI:10.1016/j.catena.2008.07.006

Bortoluzzi, E.C., dos Santos, D.R., Santanna, M.A., Caner, L., 2013. Mineralogy and nutrient desorption of suspended sediments during a storm event. *Journal of Soils and Sediments* 13, 1093–1105. https://doi.org/10.1007/s11368-013-0692-4

Borrelli, P., Robinson, D.A., Fleischer, L.R., Lugato, E., Ballabio, C., Alewell, C., Meusburger, K., Modugno, S., Schütt, B., Ferro, V., Bagarello, V., Oost, K.V., Montanarella, L., Panagos, P., 2017. An assessment of the global impact of 21st century land use change on soil erosion. Nature Communications 8, 2013. https://doi.org/10.1038/s41467-017-02142-7

Bravo-Linares, C., Schuller, P., Castillo, A., Ovando-Fuentealba, L., Muñoz-Arcos, E., Alarcón, O., de los Santos-Villalobos, S., Cardoso, R., Muniz, M., Meigikos dos Anjos, R., Bustamante-Ortega, R., Dercon, G., 2018. First use of a compound-specific stable isotope (CSSI) technique to trace sediment transport in upland forest catchments of Chile. *Science of The Total Environment* 618, 1114–1124. https://doi.org/10.1016/j.scitotenv.2017.09.163

Bracken LJ, Turnbull L, Wainwright J, Bogaart P. 2015. Sediment connectivity: a framework for understanding sediment transfer at multiple scales. *Earth Surface Processes and Landforms* **40:** 177–188. DOI:10.1002/esp.3635

Bruce, J.P., Frome, M., Haites, E., Janzen, H., Lal, R., Paustian, K., 1999. Carbon sequestration in soils. Journal of Soil and Water Conservation 54, 382–389.

Brunsden D, Thornes J. 1979. Landscape sensitivity and change. *Transactions of the Institute of British Geographers* **4**: 463–484. Bryan RB, Campbell IA. 1986

Bruun TB, Elberling B, de Neergaard A, Magid J. 2015. Organic carbon dynamics in different soil types after conversion of forest to agriculture. *Land Degradation & Development* **26**: 272–283. DOI: 10.1002/ldr.2205

Bryan RB, Campbell IA, 1986.Runoff and sediment discharge in a semiarid drainage basin. *Zeitschrift für Geomorphologie* Suppl. **58:** 121–143.

Buendia C, Batalla RJ, Sabater S, Palau A, Marcé R. 2016. Runoff Trends Driven by Climate and Afforestation in a Pyrenean Basin. *Land Degradation & Development* **27:** 823–838. DOI:10.1002/ldr.2384

Busari, M.A., Kukal, S.S., Kaur, A., Bhatt, R., Dulazi, A.A., 2015. Conservation tillage impacts on soil, crop and the environment. International Soil and Water Conservation Research 3, 119–129. https://doi.org/10.1016/j.iswcr.2015.05.002

Cammeraat ELH, Cerdà A, Imeson AC. 2010. Ecohydrological Adaptation of Soils Following Land Abandonment in a Semi-Arid Environment. *Ecohydrology* **34:** 421-430. DOI:10.1002/eco.161.

Carpenter, S. R., N. F. Caraco, D. L. Correll, R. W. Howarth, A. N. Sharpley, and V. H. Smith. 1998. Nonpoint pollution of surface waters with phosphorus and nitrogen. *Ecological Applications* **8:**559-568.

Cavalli M, Marchi L. 2008. Characterisation of the surface morphology of an alpine alluvial fan using airborne LiDAR. *Natural Hazards and Earth System Sciences* **8**: 323–333.

Cavalli M, Trevisani S, Comiti F, Marchi L. 2013. Geomorphometric assessment of spatial sediment connectivity in small Alpine catchments. *Geomorphology* **188;** 31–41. DOI:10.1016/j.geomorph.2012.05.007.

Celik, I., 2005. Land-use effects on organic matter and physical properties of soil in a southern Mediterranean highland of Turkey. *Soil and Tillage Research* 83, 270–277. https://doi.org/10.1016/j.still.2004.08.001

Cerdà A. 1998. The influence of aspect and vegetation on seasonal changes in erosion under rainfall simulation on a clay soil in Spain. *Canadian Journal of Soil Science* **78(2)**: 321–330. DOI:10.4141/S97-060.

Chauchard S, Carcaillet C, Guibal F. 2007. Patterns of land-use abandonment control tree-recruitment and forest dynamics in Mediterranean mountains. *Ecosystems* **10**: 936–948. DOI: 10.1007/s10021-007-9065-4

Chavez, J., 1996. Image-based atmospheric corrections - Revisited and improved. *Photogrammetric Engineering and Remote Sensing* 62, 1025–1036.

Chen, F., Fang, N., Shi, Z., 2016. Using biomarkers as fingerprint properties to identify sediment sources in a small catchment. *Science of The Total Environment* 557–558, 123–133. https://doi.org/10.1016/j.scitotenv.2016.03.028

Chen, J., Shi, Z., Wen, A., Yan, D., Chen, T., 2019. 137Cs-Based Variation of Soil Erosion in Vertical Zones of a Small Catchment in Southwestern China. *International Journal of Environmental Research and Public Health* 16, 1371. https://doi.org/10.3390/ijerph16081371

Clarke, R.T., 2014. A bootstrap calculation of confidence regions for proportions of sediment contributed by different source areas in a 'fingerprinting' model. *Hydrological Processes* 29, 2694–2703. https://doi.org/10.1002/hyp.10397

Colazo JC, Buschiazzo D. 2015. The impact of agriculture on soil texture due to wind erosion. *Land Degradation & Development* **26**: 62–70. DOI: 10.1002/ldr.2297

Collins, A.L., Walling, D.E., Leeks, G.J.L., 1997. Source type ascription for fluvial suspended sediment based on a quantitative composite fingerprinting technique. *Catena* 29, 1–27. https://doi.org/10.1016/S0341-8162(96)00064-1

Collins AL, Walling DE, Sichingabula HM, Leeks GJL. 2001. Using ^{137}Cs measurements to quantify soil erosion and redistribution rates for areas under different land use in the Upper Kaleya River basin, southern Zambia. *Geoderma* **104**: 299–323. DOI: 10.1016/S0016-7061(01)00087-8

Collins, A.L., Walling, D.E., 2002. Selecting fingerprint properties for discriminating potential suspended sediment sources in river basins. *Journal of Hydrology* 261, 218–244. https://doi.org/10.1016/S0022-1694(02)00011-2

Collins, A., Walling, D., Leeks, G.J.L., 1996. Composite fingerprinting of the spatial source of fluvial suspended sediment : a case study of the Exe and Severn river basins, United Kingdom. Géomorphologie : relief, processus, environnement 2, 41–53. https://doi.org/10.3406/morfo.1996.877

Collins, A.L., Pulley, S., Foster, I.D.L., Gellis, A., Porto, P., Horowitz, A.J., 2017. Sediment source fingerprinting as an aid to catchment management: A review of the current state of knowledge and a methodological decision-tree for end-users. *Journal of Environmental Management*, Sediment source fingerprinting for informing catchment management: methodological approaches, problems and uncertainty 194, 86–108. https://doi.org/10.1016/j.jenvman.2016.09.075

Cooper, R.J., Pedentchouk, N., Hiscock, K.M., Disdle, P., Krueger, T., Rawlins, B.G., 2015. Apportioning sources of organic matter in streambed sediments: An integrated molecular and compound-specific stable isotope approach. *Science of The Total Environment* 520, 187–197. https://doi.org/10.1016/j.scitotenv.2015.03.058

Davis, P., Syme, J., Heikoop, J., Fessenden-Rahn, J., Perkins, G., Newman, B., Chrystal, A.E., Hagerty, S.B., 2015. Quantifying uncertainty in stable isotope mixing models. *Journal of Geophysical Research*: *Biogeosciences* 120, 903–923. https://doi.org/10.1002/2014JG002839

Debussche, M., Lepart, J., Dervieux, A., 1999. Mediterranean Landscape Changes: Evidence from Old Postcards. Global Ecology and Biogeography 8, 3–15.

De Luna E, Laguna A, Giráldez JV. 2000. The role of olive trees in rainfall erosivity and runoff and sediment yield in the soil beneath. *Hydrology and Earth System Sciences* **4(1):** 141–153.

Domingo D, Lamelas MT, Montealegre AL, de la Riva J. 2016. Estimación de la pérdida de biomasa y de las emisiones de CO2 generadas por la combustión de masas forestales de *Pinus halepensis* Mill. en el incendio del municipio de Luna (Aragón), mediante datos LiDAR-PNOA. *Aplicaciones de las tecnologías de la información geográfica (TIG) para el desarrollo económico sostenible, Málaga, XVII Congreso Nacional TIG*. **1:** 83-88.

Dorji T, Odeh IOA, Field DJ. 2014. Vertical distribution of soil organic carbon density in relation to land use/cover, altitude and slope aspect in the Eastern Himalayas. *Land* **3**: 1232–1250. DOI: 10.3390/land3041232

Du P, Walling DE. 2011. Using ^{137}Cs measurements to investigate the influence of erosion and soil redistribution on soil properties. *Applied Radiation and Isotopes* **69**: 717–726. DOI: 10.1016/j.apradiso.2011.01.022

Dunjó G, Pardini G, Gispert M. 2004. The role of land use–land cover on runoff generation and sediment yield at a microplot scale, in a small Mediterranean catchment. *Journal of Arid Environments* **57:** 239–256. DOI:10.1016/S0140-1963(03)00097-1

Dutta, S., 2016. Soil erosion, sediment yield and sedimentation of reservoir: a review. Model. Earth Syst. Environ. 2, 123. https://doi.org/10.1007/s40808-016-0182-y

Ellis EC, Kaplan JO, Fuller DQ, Vavrus S, Klein Goldewijk K, Verburg PH. 2013. Used planet: A global history. *Proceedings of the National Academy of Sciences of the United States of America* **110**: 7978–7985. DOI: 10.1073/pnas.1217241110

Ellis EC, Klein Goldewijk K, Siebert S, Lightman D, Ramankutty N. 2010. Anthropogenic transformation of the biomes, 1700 to 2000. *Global Ecology and Biogeography* **19**: 589–606. DOI: 10.1111/j.1466-8238.2010.00540.x

Elwell HA, Stocking MA. 1976. Vegetal cover to estimate soil erosion hazard in Rhodesia. *Geoderma* **15:** 61–70. DOI:10.1016/0016-7061(76)90071-9

Estrany, J., Garcia, C., Walling, D.E., 2010. An investigation of soil erosion and redistribution in a Mediterranean lowland agricultural catchment using caesium-137. *International Journal of Sediment Research* 25, 1–16. https://doi.org/10.1016/S1001-6279(10)60023-6

Evans JS, Hudak AT. 2007. A multiscale curvature algorithm for classifying discrete return LiDAR in forested environments. *IEEE Transactions on Geoscience and Remote Sensing* **45:** 1029–1038.

Evrard O, Nord G, Cerdan O, Souchère V, Le Bissonnais Y, Bonté P. 2010. Modelling the impact of land use change and rainfall seasonality on sediment export from an agricultural catchment of the northwestern European loess belt. *Agriculture, Ecosystems & Environment* **138**: 83–94. DOI: 10.1016/j.agee.2010.04.003

Evrard, O., Poulenard, J., Némery, J., Ayrault, S., Gratiot, N., Duvert, C., Prat, C., Lefèvre, I., Bonté, P., Esteves, M., 2013. Tracing sediment sources in a tropical highland catchment of central Mexico by using conventional and alternative fingerprinting methods. *Hydrological Processes*. 27, 911–922. https://doi.org/10.1002/hyp.9421

Evrard, O., Laceby, J.P., Ficetola, G.F., Gielly, L., Huon, S., Lefèvre, I., Onda, Y., Poulenard, J., 2019. Environmental DNA provides information on sediment sources: A study in catchments affected by Fukushima radioactive fallout. *Science of The Total Environment* 665, 873–881. https://doi.org/10.1016/j.scitotenv.2019.02.191

Evrard, O., Chaboche, P.-A., Ramon, R., Foucher, A., Laceby, J.P., 2020. A global review of sediment source fingerprinting research incorporating fallout radiocesium (137Cs). *Geomorphology* 107103. https://doi.org/10.1016/j.geomorph.2020.107103

Fan, X., Liu, Y., 2017. A Generalized Model for Intersensor NDVI Calibration and Its Comparison With Regression Approaches. IEEE Transactions on Geoscience and Remote Sensing 55, 1842–1852. https://doi.org/10.1109/TGRS.2016.2635802

Fan, X., Liu, Y., 2016. A global study of NDVI difference among moderate-resolution satellite sensors. ISPRS *Journal of Photogrammetry and Remote Sensing* 121, 177–191. https://doi.org/10.1016/j.isprsjprs.2016.09.008

Fang J, Chen A, Peng C, Zhao S, Ci L. 2001. Changes in Forest Biomass Carbon Storage in China Between 1949 and 1998. *Science* **292**: 2320–2322. DOI:10.1126/science.1058629

Faulkner H. 2008. Connectivity as a crucial determinant of badland morphology and evolution. *Geomorphology* . Fluvial Systems: Dynamics, Morphology and the Sedimentary RecordSpecial Issue in honour of Adrian Harvey **100**: 91–103. doi:10.1016/j.geomorph.2007.04.039.

Favis-Mortlock, D., 2008. Soil erosion and sediment redistribution in river catchments: Measurement, modelling and management, edited by P. N. Owens and A. J. Collins. CABI, Wallingford, UK, 2006. ISBN 978 0 85199 050 7, xiv+328 pp. *Land Degradation & Development* 19, 694–694. https://doi.org/10.1002/ldr.872

Foerster S, Wilczok C, Brosinsky A, Segl K. 2014. Assessment of sediment connectivity from vegetation cover and topography using remotely sensed data in a dryland catchment in the Spanish Pyrenees. *Journal of Soils Sediments* **14:** 1982–2000. doi:10.1007/s11368-014-0992-3

Foley JA, DeFries R, Asner GP, Barford C, Bonan G, Carpenter SR, Chapin FS, Coe MT, Daily GC, Gibbs HK, Helkowski JH, Holloway T, Howard EA, Kucharik CJ, Monfreda C, Patz JA, Prentice IC, Ramankutty N, Snyder PK. 2005. Global consequences of land use. *Science* **309:** 570–574. DOI:10.1126/science.1111772

Fornes WL, Whiting PJ, Wilson CG, Matisoff G. 2005. Caesium-137-derived erosion rates in an agricultural setting: the effects of model assumptions and management practices. *Earth Surface Processes and Landforms* **30:** 1181–1189. DOI:10.1002/esp.1269

Fox DM, Witz E, Blanc V, Soulié C, Penalver-Navarro M, Dervieux A. 2012. A case study of land cover change (1950–2003) and runoff in a Mediterranean catchment. *Applied Geography* **32:** 810–821. DOI:10.1016/j.apgeog.2011.07.007

Francaviglia, R., Coleman, K., Whitmore, A.P., Doro, L., Urracci, G., Rubino, M., Ledda, L., 2012. Changes in soil organic carbon and climate change – Application of the RothC model in agro-silvo-pastoral Mediterranean systems. *Agricultural Systems* 112, 48–54. https://doi.org/10.1016/j.agsy.2012.07.001

Fryirs KA. 2016. River sensitivity: a lost foundation concept in fluvial geomorphology. *Earth Surf. Process. Landforms* doi:10.1002/esp.3940

García-Ruiz, J.M., Martí-Bono, C., Lorente, A., Beguería, S., 2002. Geomorphological consequences of fraquent and infrequent rainfall and hydrological events in Pyrennez Mountains of Spain. *Mitigation and Adaptation Strategies for Global Change* 7, 303–320. https://doi.org/10.1023/A:1024479630433

García-Ruiz JM. 2010. The effects of land uses on soil erosion in Spain: A review. *Catena* **81:** 1–11. DOI:10.1016/j.catena.2010.01.001

García-Ruiz JM, Lasanta T, Ortigosa L, Ruiz-Flaño P, Martí C, González C. 1995. Sediment Yield under Different Land Uses in the Spanish Pyrenees. *Mountain Research and Development* **15**: 229–240. DOI:10.2307/3673930

Gao, L., Becker, E., Liang, G., Houssou, A.A., Wu, H., Wu, X., Cai, D., Degré, A., 2017. Effect of different tillage systems on aggregate structure and inner distribution of organic carbon. *Geoderma* 288, 97–104. https://doi.org/10.1016/j.geoderma.2016.11.005

Gaspar L, Navas A. 2013. Vertical and lateral distributions of ^{137}Cs in cultivated and uncultivated soils on Mediterranean hillslopes. *Geoderma* **207**–**208**: 131–143. DOI: 10.1016/j.geoderma.2013.04.034

Gaspar, L., Navas, A., Walling, D.E., Machín, J., Gómez Arozamena, J., 2013. Using ^{137}Cs and $^{210}Pb_{ex}$ to assess soil redistribution on slopes at different temporal scales. *Catena*, Scales in Soil Erosion 102, 46–54. https://doi.org/10.1016/j.catena.2011.01.004

Gaspar L, Webster R, Navas A. 2017. Fallout $^{210}Pb_{ex}$ and its relation with soil properties in soil profiles under forest and scrubland of the central Spanish Pre-Pyrenees. *European Journal of Soil Science.* DOI: 10.1111/ejss.12427.

Gaspar, L., Quijano, L., Lizaga, I., Navas, A., 2019a. Effects of land use on soil organic and inorganic C and N at 137Cs traced erosional and depositional sites in mountain agroecosystems. *Catena* 181, 104058. https://doi.org/10.1016/j.catena.2019.05.004

Gaspar, L., Blake, W.H., Smith, H.G., Lizaga, I., Navas, A., 2019b. Testing the sensitivity of a multivariate mixing model using geochemical fingerprints with artificial mixtures. *Geoderma* 337, 498–510. https://doi.org/10.1016/j.geoderma.2018.10.005

Gaspar, L., Lizaga, I., Blake, W.H., Latorre, B., Quijano, L., Navas, A. 2019c. Fingerprinting changes in source contribution for evaluating soil response during an exceptional rainfall in Spanish Pre-Pyrenees. *Journal of Environmental Management*, https://doi.org/10.1016/j.jenvman.2019.03.109

Gaspar, L., Mabit, L., Lizaga, I., Navas, A., 2020. Lateral mobilization of soil carbon induced by runoff along karstic slopes. *Journal of Environmental Management* 260, 110091. https://doi.org/10.1016/j.jenvman.2020.110091

Gellis, A.C., Walling, D.E., 2013. Sediment Source Fingerprinting (Tracing) and Sediment Budgets as Tools in Targeting River and Watershed Restoration Programs, in: Stream Restoration in Dynamic Fluvial Systems. *American Geophysical Union* (AGU), pp. 263–291. https://doi.org/10.1029/2010GM000960

Gharibreza M, Raj JK, Yusoff I, Othman Z, Tahir WZWM, Ashraf MA. 2013. Land use changes and soil redistribution estimation using ^{137}Cs in the tropical Bera Lake catchment, Malaysia. *Soil and Tillage Research* 131: 1–10. DOI: 10.1016/j.still.2013.02.010

Gibbs, M.M., 2008. Identifying Source Soils in Contemporary Estuarine Sediments: A New Compound-Specific Isotope Method. Estuaries and Coasts: J CERF 31, 344–359. https://doi.org/10.1007/s12237-007-9012-9

Gibbs MM., 2013. Protocols on the use of the CSSI technique to identify and apportion soil sources from land use. Report no: HAM2013–106. National Institute of Water and Atmospheric Research Ltd, Hamilton, New Zealand.

Glaser, B., 2005. Compound-specific stable-isotope (δ13C) analysis in soil science. *Journal of Plant Nutrition and Soil Science* 168, 633–648. https://doi.org/10.1002/jpln.200521794

Gómez, J.A., Guzmán, M.G., Giráldez, J.V., Fereres, E., 2009. The influence of cover crops and tillage on water and sediment yield, and on nutrient, and organic matter losses in an olive orchard on a sandy loam soil. *Soil and Tillage Research* 106, 137–144. https://doi.org/10.1016/j.still.2009.04.008

Grodek, T., Jacoby, Y., Morin, E., Katz, O., 2012. Effectiveness of exceptional rainstorms on a small Mediterranean basin. *Geomorphology* 159–160, 156–168. https://doi.org/10.1016/j.geomorph.2012.03.016

Grohmann CH, Smith MJ, Riccomini C. 2011. Multiscale Analysis of Topographic Surface Roughness in the Midland Valley, Scotland. *IEEE Transactions on Geoscience and Remote Sensing* **49:** 1200–1213. DOI:10.1109/TGRS.2010.2053546

Gruszowski, K.E., Foster, I.D.L., Lees, J.A., Charlesworth, S.M., 2003. Sediment sources and transport pathways in a rural catchment, Herefordshire, UK. *Hydrological Processes*. 17, 2665–2681. https://doi.org/10.1002/hyp.1296

Gutiérrez, F., Gutiérrez, M., Sancho, C., 1998. Geomorphological and sedimentological analysis of a catastrophic flash flood in the Arás drainage basin (Central Pyrenees, Spain). *Geomorphology* 22, 265–283. https://doi.org/10.1016/S0169-555X(97)00087-1

Gutiérrez F, Lizaga I. 2016. Sinkholes, collapse structures and large landslides in an active salt dome submerged by a reservoir: The unique case of the Ambal ridge in the Karun River, Zagros Mountains, Iran. *Geomorphology* **254**: 88–103. DOI:10.1016/j.geomorph.2015.11.020

Haddadchi, A., Ryder, D. S., Evrard, O., & Olley, J. 2013. Sediment fingerprinting in fluvial systems: review of tracers, sediment sources and mixing models **28(4)**: 560-578. *International Journal of Sediment Research*. https://doi.org/10.1016/S1001-6279(14)60013-5

Hancock, G.J., Revill, A.T., 2013. Erosion source discrimination in a rural Australian catchment using compound-specific isotope analysis (CSIA). *Hydrological Processes* 27, 923–932. https://doi.org/10.1002/hyp.9466

Harvey AM. 2001. Coupling between hillslopes and channels in upland fluvial systems: implications for landscape sensitivity, illustrated from the Howgill Fells, northwest England. *Catena* **42:** 225–250. DOI:10.1016/S0341-8162(00)00139-9

Harvey AM. 2002. Effective timescales of coupling within fluvial systems. *Geomorphology* **44**: 175–201. DOI:10.1016/S0169-555X(01)00174-X

Heckmann T, Schwanghart W. 2013. Geomorphic coupling and sediment connectivity in an alpine catchment — Exploring sediment cascades using graph theory. *Geomorphology* **182**: 89–103. DOI:10.1016/j.geomorph.2012.10.033

Heckmann, T., Cavalli, M., Cerdan, O., Foerster, S., Javaux, M., Lode, E., Smetanová, A., Vericat, D., Brardinoni, F., 2018. Indices of sediment connectivity: opportunities, challenges and limitations. *Earth-Science Reviews* 187, 77–108. https://doi.org/10.1016/j.earscirev.2018.08.004

Henry, R., Schang, C., Coutts, S., Kolotelo, P., Prosser, T., Crosbie, N., Grant, T., Cottam, D., O'Brien, P., Deletic, A., McCarthy, D., 2016. Into the deep: Evaluation of SourceTracker for assessment of faecal contamination of coastal waters. *Water Research* 93, 242–253. https://doi.org/10.1016/j.watres.2016.02.029

Hubble TCT, Docker BB, Rutherfurd ID. 2010. The role of riparian trees in maintaining riverbank stability: A review of Australian experience and practice. *Ecological Engineering* **36**: 292–304. DOI:10.1016/j.ecoleng.2009.04.006

Jacobs, A., Rauber, R., Ludwig, B., 2009. Impact of reduced tillage on carbon and nitrogen storage of two Haplic Luvisols after 40 years. *Soil and Tillage Research* 102, 158–164. https://doi.org/10.1016/j.still.2008.08.012

Johansen, B., Tømmervik, H., 2014. The relationship between phytomass, NDVI and vegetation communities on Svalbard. *International Journal of Applied Earth Observation and Geoinformation*, Special Issue on Polar Remote Sensing 2013 27, 20–30. https://doi.org/10.1016/j.jag.2013.07.001

Kawabata D, Bandibas J. 2009. Landslide susceptibility mapping using geological data, a DEM from ASTER images and an Artificial Neural Network (ANN). *Geomorphology* **113:** 97–109. DOI:10.1016/j.geomorph.2009.06.006

Keesstra S, Pereira P, Novara, A, Brevik, EC, Azorin-Molina, C, Parras-Alcántara L, Jordán A, Cerdà A. 2016. Effects of Soil Management Techniques on Soil Water Erosion in Apricot Orchards. *Science of the Total Environment* **551-552:** 357-366. doi:10.1016/j.scitotenv.2016.01.182.

Klages, M.G., Hsieh, Y.P., 1975. Suspended Solids Carried by the Gallatin River of Southwestern Montana: II. Using Mineralogy for Inferring Sources. Journal of Environmental Quality 4, 68–73. https://doi.org/10.2134/jeq1975.00472425000400010016x

Kim Y, Cho S, Kang H-D, Kim W, Lee H-R, Doh S-H, Kim K, Yun S-G, Kim D-S, Jeong GY. 2006. Radiocesium reaction with illite and organic matter in marine sediment. *Marine Pollution Bulletin* **52**: 659–665. DOI: 10.1016/j.marpolbul.2005.10.017

Koiter, A.J., Owens, P.N., Petticrew, E.L., Lobb, D.A., 2013. The behavioural characteristics of sediment properties and their implications for sediment fingerprinting as an approach for identifying sediment sources in river basins. *Earth-Science Reviews* 125, 24–42. https://doi.org/10.1016/j.earscirev.2013.05.009

Koiter, A.J., Owens, P.N., Petticrew, E.L., Lobb, D.A., 2018. Assessment of particle size and organic matter correction factors in sediment source fingerprinting investigations: An example of two contrasting watersheds in Canada. *Geoderma* 325, 195–207. https://doi.org/10.1016/j.geoderma.2018.02.044

Korkanç, S.Y., 2014. Effects of afforestation on soil organic carbon and other soil properties. *Catena* 123, 62–69. https://doi.org/10.1016/j.catena.2014.07.009

Kosmas C, Danalatos N, Cammeraat LH, Chabart M, Diamantopoulos J, Farand R, Gutierrez L, Jacob A, Marques H, Martinez-Fernandez J, Mizara A, Moustakas N, Nicolau JM, Oliveros C, Pinna G, Puddu R, Puigdefabregas J, Roxo M, Simao A, Stamou G, Tomasi N, Usai D, Vacca A. 1997. The effect of land use on runoff and soil erosion rates under Mediterranean conditions. *Catena* **29:** 45–59. DOI:10.1016/S0341-8162(96)00062-8

Kokaly, R.F., Clark, R.N., Swayze, G.A., Livo, K.E., Hoefen, T.M., Pearson, N.C., Wise, R.A., Benzel, W.M., Lowers, H.A., Driscoll, R.L., Klein, A.J., 2017. USGS Spectral Library Version 7 (USGS Numbered Series No. 1035), Data Series. U.S. Geological Survey, Reston, VA.

Krishnaswamy, J., Bawa, K.S., Ganeshaiah, K.N., Kiran, M.C., 2009. Quantifying and mapping biodiversity and ecosystem services: Utility of a multi-season NDVI based Mahalanobis distance surrogate. *Remote Sensing of Environment* 113, 857–867. https://doi.org/10.1016/j.rse.2008.12.011

Kruk, M.K., Mayer, B., Nightingale, M., Laceby, J.P., 2020. Tracing nitrate sources with a combined isotope approach (δ15NNO3, δ18ONO3 and δ11B) in a large mixed-use watershed in southern Alberta, Canada. *Science of The Total Environment* 703, 135043. https://doi.org/10.1016/j.scitotenv.2019.135043

Laceby, J.P., Olley, J., 2015. An examination of geochemical modelling approaches to tracing sediment sources incorporating distribution mixing and elemental correlations. *Hydrological Processes*. 29 (6), 1669–1685.

Laceby, J.P., Gellis, A.C., Koiter, A.J., Blake, W.H., Evrard, O., 2019. Preface—evaluating the response of critical zone processes to human impacts with sediment source fingerprinting. J. Soil. Sediment. 19, 3245–3254. https://doi.org/10.1007/s11368-019-02409-0.

Lana-Renault, N., Nadal-Romero, E., Serrano-Muela, M.P., Alvera, B., Sánchez-Navarrete, P., Sanjuan, Y., García-Ruiz, J.M., 2013. Comparative analysis of the response of various land covers to an exceptional rainfall event in the central Spanish Pyrenees, October 2012. Earth Surface Processes and Landforms 39, 581–592. https://doi.org/10.1002/esp.3465

Lasanta T, Nadal-Romero E, Errea P, Arnáez J. 2016. The Effect of Landscape Conservation Measures in Changing Landscape Patterns: A Case Study in Mediterranean Mountains. *Land Degradation & Development* **27 (2):** 373-386. DOI:10.1002/ldr.2359.

Lavrieux, M., Birkholz, A., Meusburger, K., Wiesenberg, G.L.B., Gilli, A., Stamm, C., Alewell, C., 2019. Plants or bacteria? 130 years of mixed imprints in Lake Baldegg sediments (Switzerland), as

revealed by compound-specific isotope analysis (CSIA) and biomarker analysis. Biogeosciences 16, 2131–2146. https://doi.org/10.5194/bg-16-2131-2019

Lecce, S.A., 2013. Stream power, channel change, and channel geometry in the Blue River, Wisconsin. Physical Geography 34, 293–314. https://doi.org/10.1080/02723646.2013.847311

Li, J., Lewis, J., Rowland, J., Tappan, G., Tieszen, L.L., 2004. Evaluation of land performance in Senegal using multi-temporal NDVI and rainfall series. Journal of Arid Environments, Land Cover, Biomass and Soil Carbon Trends in Senegal: Mnagemnet Options and Climate Sensitivity 59, 463–480. https://doi.org/10.1016/j.jaridenv.2004.03.019

Li, X.-G., Li, F.-M., Zed, R., Zhan, Z.-Y., Bhupinderpal-Singh, 2007. Soil physical properties and their relations to organic carbon pools as affected by land use in an alpine pastureland. *Geoderma* 139, 98–105. https://doi.org/10.1016/j.geoderma.2007.01.006

Li, M., Yao, W., Ding, W., Yang, J., Chen, J., 2009. Effect of grass coverage on sediment yield in the hillslope-gully side erosion system. J. Geogr. Sci. 19, 321–330. https://doi.org/10.1007/s11442-009-0321-8

Li J, Wong DWS. 2010. Effects of DEM sources on hydrologic applications. Computers, Environment and Urban Systems 34: 251–261. DOI:10.1016/j.compenvurbsys.2009.11.002

Liu, S., An, N., Yang, J., Dong, Y., Wang, C., 2015. Effects of different land-use types on soil organic carbon and its prediction in the mountainous areas in the middle reaches of Lancang River. Ying Yong Sheng Tai Xue Bao 26, 981–988.

Liu, G., Zhang, Y., van der Mark, E., Magic-Knezev, A., Pinto, A., van den Bogert, B., Liu, W., van der Meer, W., Medema, G., 2018. Assessing the origin of bacteria in tap water and distribution system in an unchlorinated drinking water system by SourceTracker using microbial community fingerprints. *Water Research* 138, 86–96. https://doi.org/10.1016/j.watres.2018.03.043

Lizaga, I., Quijano, L., Palazón, L., Gaspar, L., Navas, A., 2018a. Enhancing Connectivity Index to Assess the Effects of Land Use Changes in a Mediterranean Catchment. *Land Degradation & Development*. 663–675. https://doi.org/10.1002/ldr.2676

Lizaga,I., Quijano, L., Gaspar, L., Navas, A., 2018b. Estimating Soil Redistribution Patterns with 137cs Measurements in a Mediterranean Mountain Catchment Affected by Land Abandonment. Land Degrad Develop 105–117. https://doi.org/10.1002/ldr.2843

Lizaga, I., Latorre, B., Gaspar, L., Navas, A., 2018b. fingerPro: An R Package for SedimentSource Tracing. CRAN https://doi.org/10.5281/zenodo.1402029.

Lizaga, I, Quijano, L., Gaspar, L., Ramos, M.C., Navas, A., 2019a. Linking land use changes to variation in soil properties in a Mediterranean mountain agroecosystem. *Catena* 172, 516–527. https://doi.org/10.1016/j.catena.2018.09.019

Lizaga, I, Gaspar, L., Blake, W.H., Latorre, B., Navas, A., 2019b. Fingerprinting changes of source apportionments from mixed land uses in stream sediments before and after an exceptional rainstorm event. *Geomorphology* 341, 216–229. https://doi.org/10.1016/j.geomorph.2019.05.015

Lizaga, I, Gaspar, L., Quijano, L., Dercon, G., Navas, A., 2019c. NDVI, 137Cs and nutrients for tracking soil and vegetation development on glacial landforms in the Lake Parón Catchment (Cordillera

Blanca, Perú). *Science of The Total Environment* 651, 250–260. https://doi.org/10.1016/j.scitotenv.2018.09.075

Lizaga, I., Latorre, B., Gaspar, L., Navas, A., 2020. Consensus ranking as a method to identify non-conservative and dissenting tracers in fingerprinting studies. *Science of The Total Environment* 720, 137537. https://doi.org/10.1016/j.scitotenv.2020.137537

Llena, M., Vericat, D., Cavalli, M., Crema, S., Smith, M.W., 2019. The effects of land use and topographic changes on sediment connectivity in mountain catchments. *Science of The Total Environment* 660, 899–912. https://doi.org/10.1016/j.scitotenv.2018.12.479

Llorens P. 1997. Rainfall interception by a Pinus sylvestris forest patch overgrown in a Mediterranean mountainous abandoned area II. Assessment of the applicability of Gash's analytical model. *Journal of Hydrology* **199:** 346–359. DOI:10.1016/S0022-1694(96)03335-5

Lloyd, C.E.M., Johnes, P.J., Freer, J.E., Carswell, A.M., Jones, J.I., Stirling, M.W., Hodgkinson, R.A., Richmond, C., Collins, A.L., 2019. Determining the sources of nutrient flux to water in headwater catchments: Examining the speciation balance to inform the targeting of mitigation measures. *Science of The Total Environment* 648, 1179–1200. https://doi.org/10.1016/j.scitotenv.2018.08.190

López-Moreno JI, Vicente-Serrano SM, Moran-Tejeda E, Zabalza J, Lorenzo-Lacruz J, García-Ruiz JM. 2011. Impact of climate evolution and land use changes on water yield in the Ebro basin. *Hydrology and Earth Systems sciences* **15:** 311–322. DOI:10.5194/hess-15-311-2011

López-Tarazón, J.A., Batalla, R.J., Vericat, D., Francke, T., 2009. Suspended sediment transport in a highly erodible catchment: The River Isábena (Southern Pyrenees). *Geomorphology* 109, 210–221. https://doi.org/10.1016/j.geomorph.2009.03.003

Lorenzo-Lacruz J, Vicente-Serrano SM, López-Moreno JI, Morán-Tejeda E, Zabalza J. 2012. Recent trends in Iberian streamflows (1945–2005). *Journal of Hydrology* 414–415, 463–475. DOI:10.1016/j.jhydrol.2011.11.023

Mabit L, Bernard C, Laverdiere MR. 2002. Quantification of soil redistribution and sediment budget in a Canadian watershed from fallout caesium-137 (^{137}Cs) data. *CanadianJournal of Soil Science*

Mabit L, Bernard C. 2007. Assessment of spatial distribution of fallout radionuclides through geostatistics concept. *Journal of Environmental Radioactivity* **97**: 206–219. DOI: 10.1016/j.jenvrad.2007.05.008

Mabit L, Bernard C, Makhlouf M, Laverdière MR. 2008. Spatial variability of erosion and soil organic matter content estimated from ^{137}Cs measurements and geostatistics. *Geoderma* **145**: 245–251. DOI: 10.1016/j.geoderma.2008.03.013

Mabit L, Chhem-Kieth S, Toloza A, Vanwalleghem T, Bernard C, Amate JI, González de Molina M, Gómez JA. 2012. Radioisotopics and physicochemical background indicators to assess soil degradation affecting olive orchards in southern Spain. *Agriculture, Ecosystems & Environment* 159: 70–80.

Mabit L, Benmansour M, Abril JM, Walling DE, Meusburger K, Iurian AR, Bernard C, Tarján S, Owens PN, Blake WH, Alewell C. 2014. Fallout 210Pb as a soil and sediment tracer in catchment

sediment budget investigations: A review. *Earth-Science Reviews* 138: 335–351. DOI: 10.1016/j.earscirev.2014.06.007

Mabit, L., Gibbs, M., Mbaye, M., Meusburger, K., Toloza, A., Resch, C., Klik, A., Swales, A., Alewell, C., 2018. Novel application of Compound Specific Stable Isotope (CSSI) techniques to investigate on-site sediment origins across arable fields. *Geoderma* 316, 19–26. https://doi.org/10.1016/j.geoderma.2017.12.008

MacDonald D, Crabtree JR, Wiesinger G, Dax T, Stamou N, Fleury P, Gutierrez Lazpita J, Gibon A. 2000. Agricultural abandonment in mountain areas of Europe: Environmental consequences and policy response. *Journal of Environmental Management* **59**: 47–69. DOI: 10.1006/jema.1999.0335

Marchamalo M, Hooke JM, Sandercock PJ. 2016. Flow and Sediment Connectivity in Semi-Arid Landscapes in SE Spain: Patterns and Controls. *Land Degradation & Development* **27 (4):** 1032-1044. DOI:10.1002/ldr.2352.

Mariani, L., Parisi, S.G., 2014. Exceptional Rainfalls in the Mediterranean Area, in: Storminess and Environmental Change, Advances in Natural and Technological Hazards Research. Springer, Dordrecht, pp. 17–37. https://doi.org/10.1007/978-94-007-7948-8_2

Martínez-Carreras, N., Krein, A., Udelhoven, T., Gallart, F., Iffly, J.F., Hoffmann, L., Pfister, L., Walling, D.E., 2010. A rapid spectral-reflectance-based fingerprinting approach for documenting suspended sediment sources during storm runoff events. *Journal of Soils and Sediments* 10, 400–413. https://doi.org/10.1007/s11368-009-0162-1

Martínez-Casasnovas JA, Ramos MC, Ribes-Dasi M. 2002. Soil erosion caused by extreme rainfall events: mapping and quantification in agricultural plots from very detailed digital elevation models. *Geoderma* **105**: 125–140. DOI: 10.1016/S0016-7061(01)00096-9

Martínez-Fernández J, Sánchez N, Herrero-Jiménez CM. 2013. Recent trends in rivers with near-natural flow regime: The case of the river headwaters in Spain. *Progress in Physical Geography* **37:** 685–700. DOI:10.1177/0309133313496834

Martínez-Mena, M., Alvarez Rogel, J., Castillo, V., Albaladejo, J., 2002. Organic carbon and nitrogen losses influenced by vegetation removal in a semiarid mediterranean soil. Biogeochemistry 61, 309–321. https://doi.org/10.1023/A:1020257208048

Martins, A.A.A., Madeira, M.V., Refega, A.A.G., 1995. Influence of rainfall on properties of soils developed on granite in Portugal. Arid Soil Research and Rehabilitation 9, 353–366. https://doi.org/10.1080/15324989509385904

Masselink RJH, Keesstra SD, Temme AJAM, Seeger M, Giménez R, Casalí J. 2016. Modelling Discharge and Sediment Yield at Catchment Scale Using Connectivity Components. *Land Degradation & Development* **27:** 933–945. DOI:10.1002/ldr.2512

Masselink, R.H., Temme, A.J. a. M., Giménez Díaz, R., Casalí Sarasíbar, J., Keesstra, S.D., 2017. Assessing hillslope-channel connectivity in an agricultural catchment using rare-earth oxide tracers and random forests models. https://doi.org/10.18172/cig.3169

McCarthy, D.T., Jovanovic, D., Lintern, A., Teakle, I., Barnes, M., Deletic, A., Coleman, R., Rooney, G., Prosser, T., Coutts, S., Hipsey, M.R., Bruce, L.C., Henry, R., 2017. Source tracking

usingmicrobial community fingerprints:method comparisonwith hydrodynamic modelling. *Water Research* 109, 253–265. https://doi.org/10.1016/j.watres.2016.11.043.

Melendez-Pastor, I., Hernández, E.I., Navarro-Pedreño, J., Gómez, I., Koch, M., 2016. Multitemporal Analysis in Mediterranean *Forestland with Remote Sensing*. https://doi.org/10.5772/63721

Mesrar H, Sadiki A, Faleh A, Quijano L, Gaspar L, Navas A. 2017. Vertical and lateral distribution of fallout ^{137}Cs and soil properties along representative toposequences of central Rif, Morocco. *Journal of Environmental Radioactivity* **169**–**170**: 27–39. DOI: 10.1016/j.jenvrad.2016.12.012

Meusburger K, Mabit L, Ketterer M, Park J-H, Sandor T, Porto P, Alewell C. 2016. A multi-radionuclide approach to evaluate the suitability of $^{239+240}$Pu as soil erosion tracer. *Science of The Total Environment* 566–567: 1489–1499. DOI:10.1016/j.scitotenv.2016.06.035

Meusburger, K., Porto, P., Mabit, L., La Spada, C., Arata, L., Alewell, C., 2018. Excess Lead-210 and Plutonium-239+240: Two suitable radiogenic soil erosion tracers for mountain grassland sites. *Environmental Research* 160, 195–202. https://doi.org/10.1016/j.envres.2017.09.020

Meyer WB, BL Turner, II. (Eds). 1994. Changes in land use and land cover: a global perspective. *Cambridge University Press*. 537 pp.

Micheli ER, Kirchner JW. 2002. Effects of wet meadow riparian vegetation on streambank erosion. 2. Measurements of vegetated bank strength and consequences for failure mechanics. *Earth Surface Processes and Landforms* **27:** 687–697. DOI:10.1002/esp.340.

Mitchell, A.W., Bramley, R.G.V., Johnson, A.K.L., 1997. Export of nutrients and suspended sediment during a cyclone-mediated flood event in the Herbert River catchment, Australia. Mar. Fresh *Water Research* 48, 79–88. https://doi.org/10.1071/mf96021

Mohammad AG, Adam MA. 2010. The impact of vegetative cover type on runoff and soil erosion under different land uses. *Catena* **81**: 97–103. DOI:10.1016/j.catena.2010.01.008.

Mohawesh Y, Taimeh A, Ziadat F. 2015. Effects of land use changes and soil conservation intervention on soil properties as indicators for land degradation under a Mediterranean climate. *Solid Earth*, **6(3):** 857-868. DOI: doi:10.5194/se-6-857-2015.

Montealegre A, Lamelas T, de la Riva J, Fernández-Renau González-Anleo A, de Miguel Llanes E. 2013. Evaluación de Métodos de Filtrado Para la Clasificación de la Nube de Puntos del Vuelo LiDAR PNOA. *Teledetección. Sistemas Operacionales de Observación de la Tierra*. 184–187.

MOP-CHE. 1976. Memoria 1946-1975. Zaragoza, Ministerio de Obras públicas (DGOH) y Confederación Hidrográfica del Ebro.

Morán-Tejeda E, Ceballos-Barbancho A, Llorente-Pinto JM. 2010. Hydrological response of Mediterranean headwaters to climate oscillations and land-cover changes: the mountains of Duero River basin (Central Spain). *Global and Planetary Change* **72**: 39–49. DOI:10.1016/j.gloplacha.2010.03.003

Moore, J.W., Semmens, B.X., 2008. Incorporating uncertainty and prior information into stable isotope mixing models. Ecology Letters 11, 470–480. https://doi.org/10.1111/j.1461-0248.2008.01163.x

Muñoz-Rojas, M., Abd-Elmabod, S.K., Zavala, L.M., De la Rosa, D., Jordán, A., 2017. Climate change impacts on soil organic carbon stocks of Mediterranean agricultural areas: A case study in Northern Egypt. *Agriculture, Ecosystems & Environment*, Quantification and mitigation of

greenhouse gas emissions in Mediterranean cropping systems 238, 142–152. https://doi.org/10.1016/j.agee.2016.09.001

Nadal-Romero, E., Martínez, T.L., González-Hidalgo, J.C., Luis, M. de, García-Ruiz, J.M., 2013. The effect of intense rainstorm events on the suspended sediment response under various land uses : the Aísa Valley experimental station. *Cuadernos de Investigación Geográfica* 38, 27–47. https://doi.org/10.18172/cig.1274

Nadal-Romero, E., Cammeraat, E., Pérez-Cardiel, E., Lasanta, T., 2016. Effects of secondary succession and afforestation practices on soil properties after cropland abandonment in humid Mediterranean mountain areas. *Agriculture, Ecosystems & Environment* 228, 91–100. https://doi.org/10.1016/j.agee.2016.05.003

Nadal-Romero, E., Khorchani, M., Lasanta, T., García-Ruiz, J.M., 2019. Runoff and Solute Outputs under Different Land Uses: Long-Term Results from a Mediterranean Mountain Experimental Station. *Water* 11, 976. https://doi.org/10.3390/w11050976

Navas A, Walling DE. 1992. Using caesium-137 to assess sediment movement on slopes in a semiarid upland environment in Spain. *Erosion, debris flows and environment in mountain regions*. *Proc. international symposium, Chengdu, 1992* 129–138

Navas, A., Valero-Garcés, B.L., Machín, J. 2004. An approach to integrated assessement of reservoir siltation: the Joaquín Costa reservoir as case study. *Hydrology and Earth System Sciences*, 8 (6): 1193-1199.

Navas A, Machín J, Soto J. 2005. Assessing soil erosion in a Pyrenean mountain catchment using GIS and fallout ^{137}Cs. *Agriculture, Ecosystems & Environment* **105**: 493–506. DOI: 10.1016/j.agee.2004.07.005

Navas, A., Machín, J., Beguería, S., López-Vicente, M., Gaspar, L., 2007a. Soil properties and physiographic factors controlling the natural vegetation re-growth in a disturbed catchment of the Central Spanish Pyrenees. *Agroforestry Systems* 72, 173–185. https://doi.org/10.1007/s10457-007-9085-2

Navas A, Walling DE, Quine T, Machín Gayarre J, Soto J, Domenech S, López-Vicente M, López-Vicente M. 2007b. Variability in ^{137}Cs inventories and potential climatic and lithological controls in the central Ebro valley, Spain. *Journal of Radioanalytical and Nuclear Chemistry* **274:** 331. DOI: 10.1007/s10967-007-1119-8

Navas A, Machín J, Beguería S, López-Vicente M, Gaspar L. 2008. Soil properties and physiographic factors controlling the natural vegetation re-growth in a disturbed catchment of the Central Spanish Pyrenees. *Agroforestry Systems* **72:** 173–185. DOI:10.1007/s10457-007-9085-2

Navas A, Valero-Garcés B, Gaspar L, Machín J. 2009. Reconstructing the history of sediment accumulation in the Yesa reservoir: an approach for management of mountain reservoirs. *Lake and Reservoir Management* **25**: 15–27. DOI: 10.1080/07438140802714304

Navas, A., Gaspar, L., López-Vicente, M., Machín, J., 2011. Spatial distribution of natural and artificial radionuclides at the catchment scale (South Central Pyrenees). *Radiation Measurements* 46, 261–269. https://doi.org/10.1016/j.radmeas.2010.11.008

Navas, A, Valero-Garcés B., Gaspar, L., Palazón, L. 2011. Radionuclides and stable elements in the sediments of the Yesa Reservoir, Central Spanish Pyrenees. *Journal of Soils and Sediments* **11:** 1082. doi:10.1007/s11368-011-0401-0

Navas, A., Gaspar, L., Quijano, L., López-Vicente, M., Machín, J., 2012. Patterns of soil organic carbon and nitrogen in relation to soil movement under different land uses in mountain fields (South Central Pyrenees). https://doi.org/10.1016/j.catena.2011.05.012

Navas A, López-Vicente M, Gaspar L, Machín J. 2013. Assessing soil redistribution in a complex karst catchment using fallout ^{137}Cs and GIS. *Geomorphology* **196**: 231–241. DOI: 10.1016/j.geomorph.2012.03.018

Navas A, López-Vicente M, Gaspar L, Palazón L, Quijano L. 2014. Establishing a tracer-based sediment budget to preserve wetlands in Mediterranean mountain agroecosystems (NE Spain). *Science of The Total Environment* **496**: 132–143. DOI: 10.1016/j.scitotenv.2014.07.026

Navas A, Quine TA, Walling DE, Gaspar L, Quijano L, Lizaga I. 2017. Relating intensity of soil redistribution to land use changes in abandoned Pyrenean fields using fallout caesium-137. *Land Degradation & Development* n/a-n/a. DOI: 10.1002/ldr.2724

Navas, A., Oliva, M., Ruiz-Fernández, J., Gaspar, L., Quijano, L., Lizaga, I., 2017. Radionuclides and soil properties as indicators of glacier retreat in a recently deglaciated permafrost environment of the Maritime Antarctica. *Science of The Total Environment* 609, 192–204. https://doi.org/10.1016/j.scitotenv.2017.07.115

Navas, A., Serrano, E., López-Martínez, J., Gaspar, L., Lizaga, I. 2018. Interpreting environmental changes from radionuclides and soil characteristics in different landform contexts of Elephant Island (Maritime Antarctica). *Land Degradation & Development*, 29: 3141-3158. DOI: 10.1002/ldr.2987

Novara, A., Artemi, C., Carmelo, D., Giuseppe, L.P., Antonino, S., Luciano, G., 2015. Effectiveness of carbon isotopic signature for estimating soil erosion and deposition rates in Sicilian vineyards. *Soil and Tillage Research* 152, 1–7. doi:10.1016/j.still.2015.03.010

Novara A, Keesstra S, Cerdà A, Pereira P, Gristina L. 2016. Understanding the role of soil erosion on co2-c loss using 13c isotopic signatures in abandoned Mediterranean agricultural land. *Science of the Total Environment.* **550:** 330-336. DOI: 10.1016/j.scitotenv.2016.01.095, 2016.

Nunes AN, de Almeida AC, Coelho COA. 2011. Impacts of land use and cover type on runoff and soil erosion in a marginal area of Portugal. *Applied Geography* **31:** 687–699. DOI:10.1016/j.apgeog.2010.12.006

O'Callaghan JF, Mark DM. 1984. The extraction of drainage networks from digital elevation data. *Computer Vision, Graphics, and Image Processing* **28:** 323–344. DOI:10.1016/S0734-189X(84)80011-0

Ortigosa LM, Garcia-Ruiz JM, Gil E. 1990. Land Reclamation by Reforestation in the Central Pyrenees. *Mountain Research and Development* **10:** 281–288. doi:10.2307/3673607

Ohtsuka T, Hirota M, Zhang X, Shimono A, Senga Y, Du M, Yonemura S, Kawashima S, Tang Y. 2008. Soil organic carbon pools in alpine to nival zones along an altitudinal gradient (4400–5300 m) on the Tibetan Plateau. *Polar Science* **2**: 277–285. DOI: 10.1016/j.polar.2008.08.003

Owens, P.N., Caley, K.A., Campbell, S., Koiter, A.J., Droppo, I.G., Taylor, K.G., 2011. Total and size-fractionated mass of road-deposited sediment in the city of Prince George, British Columbia, Canada: implications for air and water quality in an urban environment. *Journal of Soils and Sediments* 11, 1040–1051. https://doi.org/10.1007/s11368-011-0383-y

Owens, P.N., Blake, W.H., Gaspar, L., Gateuille, D., Koiter, A.J., Lobb, D.A., Petticrew, E.L., Reiffarth, D.G., Smith, H.G., Woodward, J.C., 2016. Fingerprinting and tracing the sources of soils and sediments: Earth and ocean science, geoarchaeological, forensic, and human health applications. *Earth-Science Reviews* 162, 1–23. https://doi.org/10.1016/j.earscirev.2016.08.012

Palazón L, Navas A. 2014. Modeling sediment sources and yields in a Pyrenean catchment draining to a large reservoir (Ésera River, Ebro Basin). *Journal of Soils and Sediments* **14**: 1612–1625. DOI:10.1007/s11368-014-0911-7

Palazón, L., Gaspar, L., Latorre, B., Blake, W.H., Navas, A., 2015a. Identifying sediment sources by applying a fingerprinting mixing model in a Pyrenean drainage catchment. *Journal of Soils and Sediments* 15, 2067–2085. https://doi.org/10.1007/s11368-015-1175-6

Palazón, L., Latorre, B., Gaspar, L., Blake, W.H., Smith, H.G., Navas, A., 2015b. Comparing catchment sediment fingerprinting procedures using an auto-evaluation approach with virtual sample mixtures. *Science of The Total Environment* 532, 456–466. https://doi.org/10.1016/j.scitotenv.2015.05.003

Palazón L, Navas A. 2016. Land use sediment production response under different climatic conditions in an alpine–prealpine catchment. *Catena* 137: 244–255. DOI: 10.1016/j.catena.2015.09.025

Panagos P, Borrelli P, Meusburger C, Alewell C, Lugato E, Montanarella L. 2015. Estimating the soil erosion cover-management factor at European scale. *Land Use Policy*. **48C:** 38-50. DOI:10.1016/j.landusepol.2015.05.021

Pardo G, Arenas C. 1996. Late Oligocene-Early Miocene syntectonk fluvial sedimentation in the Aragonese Pyrenean domain of the Ebro basin: facies models and structural controls. *Journal of iberian geology: an international publication of earth sciences* **21**: 277-298.

Parras-Alcántara, L., Lozano-García, B., Brevik, E.C., Cerdá, A., 2015. Soil organic carbon stocks assessment in Mediterranean natural areas: A comparison of entire soil profiles and soil control sections. *Journal of Environmental Management* 155, 219–228. https://doi.org/10.1016/j.jenvman.2015.03.039

Pennock, D. 2019. Soil erosion: The greatest challenge for sustainable soil management. Rome: *FAO–Food and Agriculture Organization of the United Nations*.

Pettorelli, N., Vik, J.O., Mysterud, A., Gaillard, J.-M., Tucker, C.J., Stenseth, N.C., 2005. Using the satellite-derived NDVI to assess ecological responses to environmental change. *Trends in Ecology & Evolution* 20, 503–510. https://doi.org/10.1016/j.tree.2005.05.011

Phillips, J.M., Russell, M.A., Walling, D.E., 2000. Time-integrated sampling of fluvial suspended sediment: a simple methodology for small catchments. *Hydrological Processes* 14, 2589–2602. https://doi.org/10.1002/1099-1085(20001015)14:14<2589::AID-HYP94>3.0.CO;2-D

Phillips, D.L., Gregg, J.W., 2003. Source partitioning using stable isotopes: coping with too many sources. Oecologia 136, 261–269. https://doi.org/10.1007/s00442-003-1218-3

Pimentel, D., 2006. Soil Erosion: A Food and Environmental Threat. Environ Dev Sustain 8, 119–137. https://doi.org/10.1007/s10668-005-1262-8

Pistocchi, A., Dorati, C., Aloe, A., Ginebreda, A., Marcé, R., 2019. River pollution by priority chemical substances under the Water Framework Directive: A provisional pan-European assessment. *Science of The Total Environment* 662, 434–445. https://doi.org/10.1016/j.scitotenv.2018.12.354

Plummer, M., Plummer, M., Hornik, K., Leisch, F., Zeileis, A., Zeileis, A., Hornik, K., Leisch, F., 2003. JAGS: a program for analysis of Bayesian graphical models using Gibbs sampling.

Porto P, Walling DE, Ferro V, di Stefano C. 2003. Validating erosion rate estimates provided by caesium-^{137} measurements for two small forested catchments in Calabria, southern Italy. *Land Degradation & Development* **14**: 389–408. DOI: 10.1002/ldr.561

Porto P, Walling DE, Callegari G. 2011. Using ^{137}Cs measurements to establish catchment sediment budgets and explore scale effects. *Hydrological Processes* **25**: 886–900. DOI: 10.1002/hyp.7874

Porto P, Walling DE, Capra A. 2014. Using ^{137}Cs and ^{210}Pbex measurements and conventional surveys to investigate the relative contributions of interrill/rill and gully erosion to soil loss from a small cultivated catchment in Sicily. *Soil and Tillage Research* **135**: 18–27. DOI: 10.1016/j.still.2013.08.013

Porto P, Walling DE, Cogliandro V, Callegari G. 2016. Exploring the potential for using 210Pbex measurements within a re-sampling approach to document recent changes in soil redistribution rates within a small catchment in southern Italy. *Journal of Environmental Radioactivity* **164**: 158–168. DOI: 10.1016/j.jenvrad.2016.06.026

Puigdefabregas J, Sole A, Gutierrez L, del Barrio G, Boer M. 1999. Scales and processes of water and sediment redistribution in drylands: results from the Rambla Honda field site in Southeast Spain. *Earth-Science Reviews* **48**: 39–70. DOI:10.1016/S0012-8252(99)00046-X

Pulley, S., Foster, I., Antunes, P., 2015. The uncertainties associated with sediment fingerprinting suspended and recently deposited fluvial sediment in the Nene river basin. *Geomorphology* 228, 303–319.

Pulley, S., Collins, A.L., 2018. Tracing catchment fine sediment sources using the new SIFT (SedIment Fingerprinting Tool) open source software. *Science of The Total Environment* 635, 838–858. https://doi.org/10.1016/j.scitotenv.2018.04.126

Quesada, S., Tena, A., Guillén, D., Ginebreda, A., Vericat, D., Martínez, E., Navarro-Ortega, A., Batalla, R.J., Barceló, D., 2014. Dynamics of suspended sediment borne persistent organic pollutants in a large regulated Mediterranean river (Ebro, NE Spain). *Science of The Total Environment* 473–474, 381–390. https://doi.org/10.1016/j.scitotenv.2013.11.040

Quijano, L., Chaparro, M.A.E., Marié, D.C., Gaspar, L., Navas, A., 2014. Relevant magnetic and soil parameters as potential indicators of soil conservation status of Mediterranean agroecosystems. *Geophys J Int* 198, 1805–1817. https://doi.org/10.1093/gji/ggu239

Quijano L, Gaspar L, Navas A. 2016a. Spatial patterns of SOC, SON, ^{137}Cs and soil properties as affected by redistribution processes in a Mediterranean cultivated field (Central Ebro Basin). *Soil and Tillage Research* **155**: 318–328. DOI: 10.1016/j.still.2015.09.007

Quijano L, Gaspar L, Navas A. 2016b. Lateral and depth patterns of soil organic carbon fractions in a mountain Mediterranean agrosystem. *The Journal of Agricultural Science* **154**: 287–304. DOI: 10.1017/S002185961400135X

Quijano L, Beguería S, Gaspar L, Navas A. 2016c. Estimating erosion rates using ^{137}Cs measurements and WATEM/SEDEM in a Mediterranean cultivated field. *Catena* 138: 38–51. DOI:10.1016/j.catena.2015.11.009.

Quijano, L., Van Oost, K., Nadeu, E., Gaspar, L., Navas, A., 2017. Modelling the Effect of Land Management Changes on Soil Organic Carbon Stocks in a Mediterranean Cultivated Field. *Land Degradation & Development*. 28, 515–523. https://doi.org/10.1002/ldr.2637

Quine TA, Navas A, Walling DE, Machin J. 1994. Soil erosion and redistribution on cultivated and uncultivated land near las bardenas in the central Ebro river Basin, Spain. *Land Degradation & Development* **5**: 41–55. DOI: 10.1002/ldr.3400050106

Quiquerez, A., Brenot, J., Garcia, J.-P., Petit, C., 2008. Soil degradation caused by a high-intensity rainfall event: Implications for medium-term soil sustainability in Burgundian vineyards. *Catena* 73, 89–97. https://doi.org/10.1016/j.catena.2007.09.007

Rahimi, M.R., Ayoubi, S., Abdi, M.R., 2013. Magnetic susceptibility and Cs-137 inventory variability as influenced by land use change and slope positions in a hilly, semiarid region of west-central Iran. *Journal of Applied Geophysics* 89, 68–75. https://doi.org/10.1016/j.jappgeo.2012.11.009

Reiffarth, D.G., Petticrew, E.L., Owens, P.N., Lobb, D.A., 2019. Spatial differentiation of cultivated soils using compound-specific stable isotopes (CSSIs) in a temperate agricultural watershed in Manitoba, Canada. *Journal of Soils and Sediments* 19, 3411–3426. https://doi.org/10.1007/s11368-019-02406-3

Reiffarth, D.G., Petticrew, E.L., Owens, P.N., Lobb, D.A., 2016. Sources of variability in fatty acid (FA) biomarkers in the application of compound-specific stable isotopes (CSSIs) to soil and sediment fingerprinting and tracing: A review. *Science of The Total Environment* 565, 8–27. https://doi.org/10.1016/j.scitotenv.2016.04.137

Renard, K.G., Yoder, D.C., Lightle, D.T., Dabney, S.M., 2011. Universal Soil Loss Equation and Revised Universal Soil Loss Equation, in: Handbook of Erosion Modelling. Wiley-Blackwell, pp. 135–167. https://doi.org/10.1002/9781444328455.ch8

Reyes O, Delia A. 2014. Estimación de variables dasométricas mediante tecnología LiDAR. In: *Tésis doctoral*. Montecillo.Texcoco, Edo de Mexico.

Rigol A, Vidal M, Rauret G. 2002. An overview of the effect of organic matter on soil–radiocaesium interaction: implications in root uptake. *Journal of Environmental Radioactivity* **58**: 191–216. DOI: 10.1016/S0265-931X(01)00066-2

Romanyà J, Rovira P. 2011. An appraisal of soil organic C content in Mediterranean agricultural soils. *Soil Use and Management* **27:** 321–332. DOI:10.1111/j.1475-2743.2011.00346.x

Rouse Jr., J.W., Haas, R.H., Schell, J.A., Deering, D.W., 1974. Monitoring Vegetation Systems in the Great Plains with Erts. 351. *NASA Special Publication*, pp. 309.

Rovira, A., Alcaraz, C., Ibáñez, C., 2012. Spatial and temporal dynamics of suspended load at-a-cross-section: The lowermost Ebro River (Catalonia, Spain). *Water Research* 46, 3671–3681. https://doi.org/10.1016/j.watres.2012.04.014

Royo M, Longares LA, de Luis M. 2015. Efecto de la gestión forestal post-incendio en la dinámica regenerativa de Quercus ilex subsp. ballota en la Sierra del Moncayo. *XXIV Congreso de la Asociación de Geógrafos Españoles: Análisis espacial y representación geográfica: innovación y aplicación*. Zaragoza 2015.

Ruiz LA. 2012. Assessment of factors affecting shrub volume estimations using airborne discrete-return LiDAR data in Mediterranean areas. *Journal of Applied Remote Sensing* **6:** 63544. DOI:10.1117/1.JRS.6.063544

Russell, J.M., Werne, J.P., 2007. The use of solid phase extraction columns in fatty acid purification. *Organic Geochemistry* 38, 48–51. https://doi.org/10.1016/j.orggeochem.2006.09.003

Ryan, M., O'Donoghue, C., Phillips, H., 2015. Modelling Financially Optimal Afforestation and Forest Management Scenarios Using a Bio-Economic Model. *Open Journal of Forestry* 06, 19. https://doi.org/10.4236/ojf.2016.61003

Saadi, S., Todorovic, M., Tanasijevic, L., Pereira, L.S., Pizzigalli, C., Lionello, P., 2015. Climate change and Mediterranean agriculture: Impacts on winter wheat and tomato crop evapotranspiration, irrigation requirements and yield. *Agricultural Water Management*: Priorities and Challenges 147, 103–115. https://doi.org/10.1016/j.agwat.2014.05.008

Sadiki A, Faleh A, Navas A, Bouhlassa S. 2007. Assessing soil erosion and control factors by the radiometric technique in the Boussouab catchment, Eastern Rif, Morocco. *Catena* **71**: 13–20. DOI: 10.1016/j.catena.2006.10.003

Sandercock PJ, Hooke JM. 2011. Vegetation effects on sediment connectivity and processes in an ephemeral channel in SE Spain. *Journal of Arid Environments* **75:** 239–254. DOI:10.1016/j.jaridenv.2010.10.005

Sarmast, M., Farpoor, M.H., Esfandiarpour Boroujeni, I., 2017. Magnetic susceptibility of soils along a lithotoposequence in southeast Iran. *Catena* 156, 252–262. https://doi.org/10.1016/j.catena.2017.04.019

Sawhney BL. 1970. Potassium and cesium ion selectivity in relation to clay mineral structure. *Clays and Clay Minerals* **18**: 47–52

Schmidt, S., Meusburger, K., de Figueiredo, T., Alewell, C., 2017. Modelling Hot Spots of Soil Loss by Wind Erosion (SoLoWind) in Western Saxony, Germany. *Land Degradation & Development*. 28, 1100–1112. https://doi.org/10.1002/ldr.2652

Schoorl JM, Boix Fayos C, de Meijer RJ, van der Graaf ER, Veldkamp A. 2004. The ^{137}Cs technique applied to steep Mediterranean slopes (Part I): the effects of lithology, slope morphology and land use. *Catena* **57**: 15–34. DOI: 10.1016/j.catena.2003.08.003

Schillaci, C., Acutis, M., Lombardo, L., Lipani, A., Fantappiè, M., Märker, M., Saia, S., 2017. Spatio-temporal topsoil organic carbon mapping of a semi-arid Mediterranean region: The role of land use, soil texture, topographic indices and the influence of remote sensing data to modelling.

Science of The Total Environment 601–602, 821–832. https://doi.org/10.1016/j.scitotenv.2017.05.239

Schuller, P., Walling, D.E., Iroumé, A., Quilodrán, C., Castillo, A., Navas, A. 2013. Using ^{137}Cs and $^{210}Pb_{ex}$ and other sediment source fingerprints to document suspended sediment sources in small forested catchments in south-central Chile. *Journal of Environmental Radiactivity*, 124: 147-159. doi: 10.1016/j.jenvrad.2013.05.002

Serrano-Muela MP, Nadal-Romero E, Lana-Renault N, González-Hidalgo JC, López-Moreno JI, Beguería S, Sanjuan Y, García-Ruiz JM. 2015. An exceptional rainfall event in the central western Pyrenees: spatial patterns in discharge and impact. *Land Degradation & Development* **26**: 249–262.

Serrano-Notivoli, R., Mora, D., Ollero, A., Sánchez-Fabre, M., Sanz, P., Saz, M.Á., 2017. Floodplain occupation and flooding in the Central Pyrenees. *Cuadernos de Investigación Geográfica* 43, 309–328. https://doi.org/10.18172/cig.3057

Selassie, Y.G., Anemut, F., Addisu, S., 2015. The effects of land use types, management practices and slope classes on selected soil physico-chemical properties in Zikre watershed, North-Western Ethiopia. *Environmental Systems Research* 4, 3. https://doi.org/10.1186/s40068-015-0027-0

Shang, Z.H., Cao, J.J., Degen, A.A., Zhang, D.W., Long, R.J., 2019. A four year study in a desert land area on the effect of irrigated, cultivated land and abandoned cropland on soil biological, chemical and physical properties. *Catena* 175, 1–8. https://doi.org/10.1016/j.catena.2018.12.002

Smith, J.A., Mazumder, D., Suthers, I.M., Taylor, M.D., 2013. To fit or not to fit: evaluating stable isotope mixing models using simulated mixing polygons. *Methods Ecol. Evol*. 4, 612–618. https://doi.org/10.1111/2041-210X.12048.

Smith, L.C., Olyphant, G.A., 1994. Within-storm variations in runoff and sediment export from a rapidly eroding coal-refuse deposit. Earth Surface Processes and Landforms 19, 369–375. https://doi.org/10.1002/esp.3290190407

Smith, H.G., Blake, W.H., 2014. Sediment fingerprinting in agricultural catchments: A critical re-examination of source discrimination and data corrections. *Geomorphology* 204, 177–191. https://doi.org/10.1016/j.geomorph.2013.08.003

Smith, H.G., Karam, D.S., Lennard, A.T., 2018. Evaluating tracer selection for catchment sediment fingerprinting. *Journal of Soils and Sediments* 18, 3005–3019. https://doi.org/10.1007/s11368-018-1990-7

Sole J, Del Valle J, Ramírez J. 1972. Mapa Geológico de España escala 1:50,000. Instituto Geologico y Minero. *Hoja MAGNA 207 26-10 Sos del Rey Católico*.

Soto J, Navas A. 2004. A model of ^{137}Cs activity profile for soil erosion studies in uncultivated soils of Mediterranean environments. *Journal of Arid Environments* **59**: 719–730. DOI: 10.1016/j.jaridenv.2004.02.003

Soto J, Navas A. 2008. A simple model of Cs-^{137} profile to estimate soil redistribution in cultivated stony soils. *Radiation Measurements* **43**: 1285–1293. DOI: 10.1016/j.radmeas.2008.02.024

Staunton S, Dumat C, Zsolnay A. 2002. Possible role of organic matter in radiocaesium adsorption in soils. *Journal of Environmental Radioactivity* **58**: 163–173. DOI: 10.1016/S0265-931X(01)00064-9

Stewart, H.A., Massoudieh, A., Gellis, A., 2015. Sediment source apportionment in Laurel Hill Creek, PA, using Bayesian chemical mass balance and isotope fingerprinting. *Hydrological Processes* 29, 2545–2560. https://doi.org/10.1002/hyp.10364

Tarboton DG, 1997. A new method for the determination of flow directions and upslope areas in grid digital elevation models. *Water Resources Research* **33**: 309–319. DOI:10.1029/96WR03137

Taylor, A., Blake, W.H., Iurian, A.R., Millward, G.E., Mabit, L., 2019. The Use of Be-7 as a Soil and Sediment Tracer, in: Mabit, L., Blake, W. (Eds.), Assessing Recent Soil Erosion Rates through the Use of Beryllium-7 (Be-7). *Springer International Publishing*, Cham, pp. 1–13. https://doi.org/10.1007/978-3-030-10982-0

Teixel A, Montes M, Arenas C, Garrido E. 1992. Mapa Geológico de España escala 1:50,000. Instituto Geologico y Minero. *Hoja MAGNA 207 27-10 Uncastillo*.

Tirapu GP, Arenas C. 1996. Late Oligocene - Early Miocene syntectonic fluvial sedimentation in the Aragonese Pyrenean domain of the Ebro Basin: facies models and structural controls. *Cuadernos de Geología Ibérica* **21**: 277–296. DOI: 10.5209/rev_CGIB.1996.v21.2532

Tolosa, I., Fiorini, S., Gasser, B., Martín, J., Miquel, J.C., 2013. Carbon sources in suspended particles and surface sediments from the Beaufort Sea revealed by molecular lipid biomarkers and compound-specific isotope analysis. Biogeosciences 10, 2061–2087. https://doi.org/10.5194/bg-10-2061-2013

Upadhayay HR, Bodé S, Griepentrog M, Huygens D, Bajracharya RM, Blake WH, Dercon G, Mabit L, Gibbs M, Semmens BX, Stock BC, Cornelis W, Boeckx P. 2017. Methodological perspectives on the application of compound-specific stable isotope fingerprinting for sediment source apportionment. *Journal of Soils and Sediments* **17**: 1537–1553. DOI: 10.1007/s11368-017-1706-4

Upadhayay, H.R., Smith, H.G., Griepentrog, M., Bodé, S., Bajracharya, R.M., Blake, W., Cornelis, W., Boeckx, P., 2018. Community managed forests dominate the catchment sediment cascade in the mid-hills of Nepal: A compound-specific stable isotope analysis. *Science of The Total Environment* 637–638, 306–317. https://doi.org/10.1016/j.scitotenv.2018.04.394

Useya, J., Chen, S., 2019. Exploring the Potential of Mapping Cropping Patterns on Smallholder Scale Croplands Using Sentinel-1 SAR *Data. Chin. Geogr. Sci*. 29, 626–639. https://doi.org/10.1007/s11769-019-1060-0

Vågen, T.-G., Winowiecki, L.A., Abegaz, A., Hadgu, K.M., 2013. Landsat-based approaches for mapping of land degradation prevalence and soil functional properties in Ethiopia. *Remote Sensing of Environment* 134, 266–275. https://doi.org/10.1016/j.rse.2013.03.006

Vågen, T.-G., Winowiecki, L.A., Tondoh, J.E., Desta, L.T., Gumbricht, T., 2016. Mapping of soil properties and land degradation risk in Africa using MODIS reflectance. *Geoderma* 263, 216–225. https://doi.org/10.1016/j.geoderma.2015.06.023

Valero-Garces B, Navas A, Machin J. (Estacion E de AD. 1997. Sediment deposition in the Barasona reservoir (central Pyrenees, Spain): temporal and spatial variability of sediment yield and land use

impacts. *AHS Publications-Series of Proceedings and Reports-Intern Assoc Hydrological Sciences*, vol. 245, p. 241-250.

Valverde, P., de Carvalho, M., Serralheiro, R., Maia, R., Ramos, V., Oliveira, B., 2015. Climate change impacts on rainfed agriculture in the Guadiana river basin (Portugal). *Agricultural Water Management* 150, 35–45. https://doi.org/10.1016/j.agwat.2014.11.008

Van Oost, K., Govers, G., Quine, T.A., Heckrath, G., Olesen, J.E., De Gryze, S., Merckx, R., 2005. Landscape-scale modeling of carbon cycling under the impact of soil redistribution: The role of tillage erosion. *Global Biogeochem*. Cycles 19, GB4014. https://doi.org/10.1029/2005GB002471

Van Oost, K., Govers, G., Van Muysen, W., 2003. A process-based conversion model for caesium-137 derived erosion rates on agricultural land: an integrated spatial approach. *Earth Surf. Process. Landforms Landforms* 28, 187–207. https://doi.org/10.1002/esp.446

Vaze J, Teng J, Spencer G. 2010. Impact of DEM accuracy and resolution on topographic indices. *Environmental Modelling & Software* **25:** 1086–1098. DOI:10.1016/j.envsoft.2010.03.014

Verheijen, F.G.A., Jones, R.J.A., Rickson, R.J., Smith, C.J., 2009. Tolerable versus actual soil erosion rates in Europe. *Earth-Science Reviews* 94, 23–38. https://doi.org/10.1016/j.earscirev.2009.02.003

Vigiak O, Borselli L, Newham L, McInnes J, Roberts A. 2012. Comparison of conceptual landscape metrics to define hillslope-scale sediment delivery ratio. *Geomorphology* **138:** 74-88

Walling, D.E., Peart, M.R., Oldfield, F., Thompson, R., 1979. Suspended sediment sources identified by magnetic measurements. Nature 281, 281110a0. https://doi.org/10.1038/281110a0

Walling DE, Quine TA. 1991. Use of ^{137}Cs measurements to investigate soil erosion on arable fields in the UK: potential applications and limitations. *Journal of Soil Science* **42**: 147–165. DOI: 10.1111/j.1365-2389.1991.tb00099.x

Walling, D.W., Woodward, J.C., Nicholas, A.P., 1993. A multi-parameter approach to fingerprinting suspended-sediment sources. Tracers in Hydrology. *Proc. International Symposium*, Yokohama. 1993, pp. 329–338.

Walling, D.E., Woodward, J.C., 1995. Tracing sources of suspended sediment in river basins: a case study of the River Culm, Devon, UK. *Marine and Freshwater Research* 46, 327–336.

Walling, D.E., Collins, A.L., 2008. The catchment sediment budget as a management tool. Environmental Science & Policy, Monitoring and modelling diffuse pollution from agriculture for policy support: UK and European experience. 11, 136–143. https://doi.org/10.1016/j.envsci.2007.10.004

Wang, J., Ding, J., Yu, D., Ma, X., Zhang, Z., Ge, X., Teng, D., Li, X., Liang, J., Lizaga, I., Chen, X., Yuan, L., Guo, Y., 2019. Capability of Sentinel-2 MSI data for monitoring and mapping of soil salinity in dry and wet seasons in the Ebinur Lake region, Xinjiang, China. *Geoderma* 353, 172–187. https://doi.org/10.1016/j.geoderma.2019.06.040

White, S., García-Ruiz, J.M., Martí, C., Valero, B., Errea, M.P., Gómez-Villar, A., 1997. The 1996 Biescas campsite disaster in the Central Spanish Pyrenees, and its temporal and spatial context. *Hydrological Processes* 11, 1797–1812. https://doi.org/10.1002/(SICI)1099-1085(199711)11:14<1797::AID-HYP605>3.0.CO;2-7

Winowiecki, L., Vågen, T.-G., Huising, J., 2016. Effects of land cover on ecosystem services in Tanzania: A spatial assessment of soil organic carbon. *Geoderma* 263, 274–283. https://doi.org/10.1016/j.geoderma.2015.03.010

Winston, W.E., Criss, R.E., 2002. Geochemical variations during flash flooding, Meramec River basin, May 2000. Journal of Hydrology 265, 149–163. https://doi.org/10.1016/S0022-1694(02)00105-1

Wise SM. 1980. Caesium-137 and lead-210: a review of the techniques and some applications in geomorphology. *Timescales in geomorphology* 109–127

Worldometer - real time world statistics [WWW Document], 2020. *Worldometer*. URL http://www.worldometers.info/ (accessed 4.2.20).

Wynants, M., Solomon, H., Ndakidemi, P., Blake, W.H., 2018. Pinpointing areas of increased soil erosion risk following land cover change in the Lake Manyara catchment, Tanzania. *International Journal of Applied Earth Observation and Geoinformation* 71, 1–8. https://doi.org/10.1016/j.jag.2018.05.008

Wynants, M., Millward, G., Patrick, A., Taylor, A., Munishi, L., Mtei, K., Brendonck, L., Gilvear, D., Boeckx, P., Ndakidemi, P., Blake, W.H., 2020. Determining tributary sources of increased sedimentation in East-African Rift Lakes. *Science of The Total Environment* 717, 137266. https://doi.org/10.1016/j.scitotenv.2020.137266

Yu, L., Oldfield, F., 1989. A multivariate mixing model for identifying sediment source from magnetic measurements. Quaternary Research 32, 168–181. https://doi.org/10.1016/0033-5894(89)90073-2

Zhang Y, Long Y, Yu X, An J. 2014. A comparison of measured ^{137}Cs and excess 210Pb levels in the cultivated brown and cinnamon soils of the Yimeng Mountain area. *Chinese Journal of Geochemistry* **33**: 155–162. DOI: 10.1007/s11631-014-0671-5

Zhang, X.C. (John), Liu, B.L., 2016. Using multiple composite fingerprints to quantify fine sediment source contributions: a new direction. *Geoderma* 268, 108–118. https://doi.org/10.1016/j.geoderma.2016.01.031.

Zhang, J., Yang, M., Zhang, F., Zhang, W., Zhao, T., Li, Y., 2017. Fingerprinting Sediment Sources After an Exceptional Rainstorm Event in a Small Catchment on the Loess Plateau, PR China. *Land Degradation & Development* 28, 2527–2539. https://doi.org/10.1002/ldr.2803

Zhang, H., Fan, J., Cao, W., Harris, W., Li, Y., Chi, W., Wang, S., 2018. Response of wind erosion dynamics to climate change and human activity in Inner Mongolia, China during 1990 to 2015. *Science of The Total Environment* 639, 1038–1050. https://doi.org/10.1016/j.scitotenv.2018.05.082

Zuazo VHD, Pleguezuelo CRR. 2008. Soil-erosion and runoff prevention by plant covers. A review. *Agronomy for Sustainable Development* **28:** 65–86. DOI:10.1051/agro:2007062

GOBIERNO DE ESPAÑA
MINISTERIO DE CIENCIA E INNOVACIÓN

CSIC
Consejo Superior de Investigaciones Científicas

EEAD
Estación Experimental de AulaDei

Universidad Zaragoza
1542

Facultad de Ciencias
Universidad Zaragoza

Departamento de Ciencias de la Tierra
Universidad Zaragoza
1542

"In memory of all those, who have been persecuted for defending science"